UNCLASSIFIED

LA - 1004

[redacted]

October 28, 1946

This document contains 163 pages

VOL. I EXPERIMENTAL TECHNIQUES

Part II Ionization Chambers and Counters

Section B

Written By:

Bruno Rossi
Hans Staub

NOTE: IT IS PROPOSED THAT THIS DOCUMENT WILL BE ISSUED IN AN EDITED FORM AS PART OF THE LOS ALAMOS SECTION OF THE MANHATTAN PROJECT TECHNICAL SERIES AT A SUBSEQUENT DATE.

UNCLASSIFIED

UNCLASSIFIED

LOS ALAMOS TECHNICAL SERIES

This is Copy___of____Copies

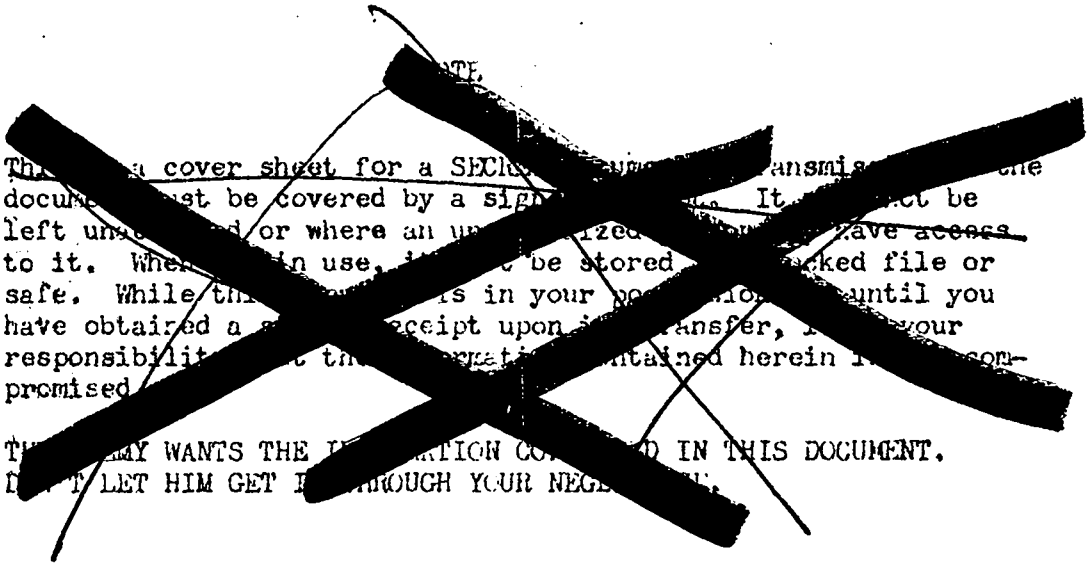

This is a cover sheet for a SECRET document transmitted herein must be covered by a signed receipt. It must not be left unattended or where an unauthorized person may have access to it. When not in use, it must be stored in a locked file or safe. While this document is in your possession until you have obtained a signed receipt upon its transfer, it is your responsibility that the information contained herein is not compromised.

THE ENEMY WANTS THE INFORMATION CONTAINED IN THIS DOCUMENT. DON'T LET HIM GET IT THROUGH YOUR NEGLIGENCE.

UNCLASSIFIED

UNCLASSIFIED

MANHATTAN PROJECT TECHNICAL SERIES

CONTRIBUTION OF

LOS ALAMOS PROJECT

The following material may be subject to certain minor revisions in the event that factual errors are discovered previous to final publications of this part of the Technical Series. Any such changes will be submitted for patent clearance and declassification in the usual manner.

UNCLASSIFIED

LOS ALAMOS TECHNICAL SERIES

VOLUME I

EXPERIMENTAL TECHNIQUES

PART II

CHAPTER 13

ALPHA PARTICLE DETECTORS

by

BRUNO ROSSI AND HANS STAUB

UNCLASSIFIED

APPROVED FOR PUBLIC RELEASE

CHAPTER 13

ALPHA PARTICLE DETECTORS

13.1 ALPHA PARTICLE SPECTROSCOPY

In most cases of interest the source of α-particles is used in solid form. Consequently the material under investigation is deposited as a thin film. If one is interested in the energy distribution, the detector has to be constructed so that, regardless of their energy, all of the particles spend their entire range in the detector and also that the height of the pulses has a known relation to the particle energy. Suppose a thin film of active material is deposited on one of the electrodes of a plane parallel plate chamber, such that no α - particle escapes from the counting volume. If the chamber is operated as an ion pulse chamber, the voltage rise of the collecting electrode resulting from every particle will be directly proportional to its energy, regardless of the direction of emission (assuming, of course, constancy of the value of the average energy spent per ion pair). If the chamber is operated as an electron pulse chamber, the pulse height is proportional to Q_o^-.

For α-particles originating at the negative electrode Q_o^- is given by the equation:

$$Q_o^- = N_o e\left(1 - \frac{\bar{x}}{d}\cos\Theta\right) \qquad (1)$$

where N_o is the total number of ion pairs produced by an α-particle, $\bar{x}$ is the distance of the center of gravity of ionization from the origin of the track and Θ the angle between the track and the perpendicular electrode (See Section 10.5). Since for an isotropically emitting source, the number of particles emitted between Θ and $\Theta + d\Theta$ is proportional to $\sin\Theta\, d\Theta$, the number of pulses with height between P and $P + dP$ is given by:

$$f(P)\ dP = (\text{const.}) \sin\Theta\ d\Theta$$

Θ and P are connected by (1) considering that P is proportional to Q_o^-. Therefore

$$dP = (\text{const.})\ d(\cos\Theta)$$

and
$$f(P) = (\text{const.}) \qquad (2)$$

The curve representing f(P) is called the differential pulse height distribution. Equation 2 shows that for the case under consideration f(P) is a constant between P_{max} and P_{min} where:

$$P_{min}/P_{max} = Q_{o\ min}^-/Q_{o\ max}^- = 1 - \bar{x}/d \qquad (3)$$

The pulses of size P_{min} correspond to particles emitted perpendicularly to the electrode; those of size P_{max} to particles emitted parallel to the electrode. The relative spread of the pulse sizes depends only on the ratio of electrode separation to particle range and the stopping power of the gas used.

In Section A.1 (see Appendix to Part II) the value of $\bar{x}$ is given as a function of the α-particle energy for various gases. In Figure 1 two experimental distributions measured with α-particles from polonium are shown, together with the theoretically expected curves. The finite differential resolution of the detector was taken into account. This is the reason for the finite slope of the theoretical curves at P_{max} and P_{min}.

From the foregoing, it is obvious that the use of plane parallel chambers with electron collection for α-particle spectroscopy would offer great difficulties in the interpretation of the result, since every monochromatic α-line would show up as a square distribution of pulses. To avoid this difficulty, one can insert a screening grid electrode between the collecting and high voltage electrodes. As described in Section 10.2, the grid electrode, which is placed so far from the negative electrode (carrying the α-particle

Figure 1

Differential pulse height distribution for monoenergetic α-particles of polonium in an electron pulse chamber. Active material on negative electrode. Data taken with stopping powers of 3.1 and 4.8 respectively to show effect of different values of $\bar{x}/R$. Curves are calculated and corrected for finite channel width of detecting instrument.

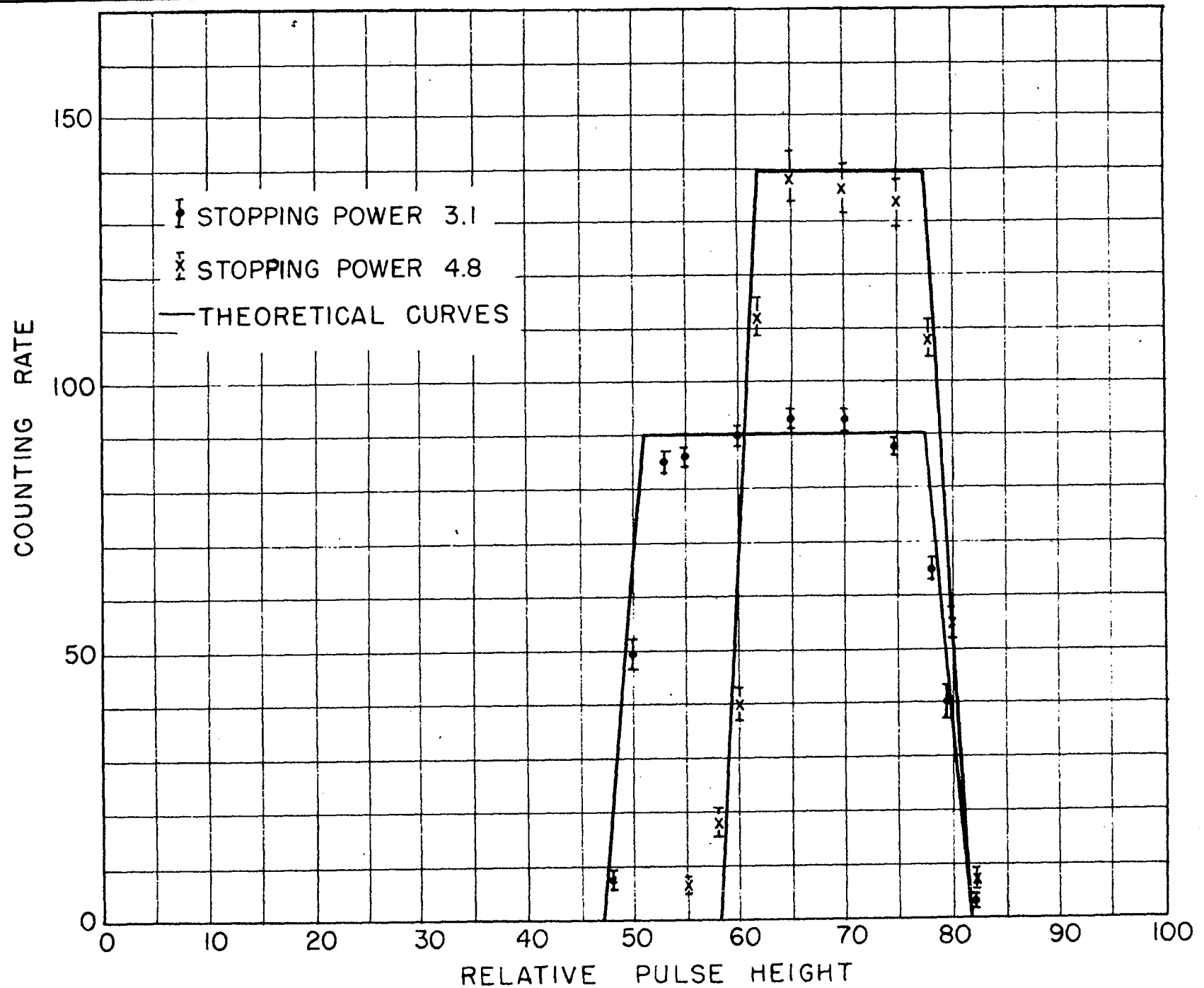

APPROVED FOR PUBLIC RELEASE

source) that it is not reached by the α-particles, shields the collecting electrode from the field of the positive ions remaining after the complete collection of the electrons. Consequently, the pulses observed are all equal and proportional to N_0. The construction of a grid chamber used for α-particles is shown in Figure 15.12. The negative electrode, carrying the thin deposit of the α-source was kept at -2500 V with respect to the collector, and the grid electrode at -1250 V. It is rather important for good resolution that the grid is at a relatively high negative potential with respect to the collector. The voltage between grid and negative electrode can be small. It should only be high enough to prevent recombination or attachment of the electrons. The high voltage between grid and positive electrode tends to reduce the spread in the sizes of the α-particle pulses since the higher field in the neighborhood of the grid lowers the probability for capture of the electrons by the wires. The grid is constructed so as to give a maximum of transparency in order to make the fraction of electrons captured by the wires as small as possible. It consists of 3 mil diameter parallel steel wires, spaced 1/16 inch apart.

With a chamber filling of 7.5 Atm. argon, and a normal sample of uranium (U-234 in equilibrium with U-238), the differential pulse height distribution given in Figure 2 was obtained. It shows the two groups of α-particles well resolved and of about the same intensity. The width of the peaks is only slightly larger than the channel width of the detector as indicated in the figure.

It may be pointed out that spectral distributions could also quite conveniently be determined by accurate range measurements. However, it was found that the results obtained by the above described pulse height method showed considerably better resolution, since the straggling in range has no effect on the pulse size.

Figure 2

Differential pulse height distribution for α-particles of normal uranium (U-234 and U-238 in equilibrium) in an electron pulse chamber with grid.

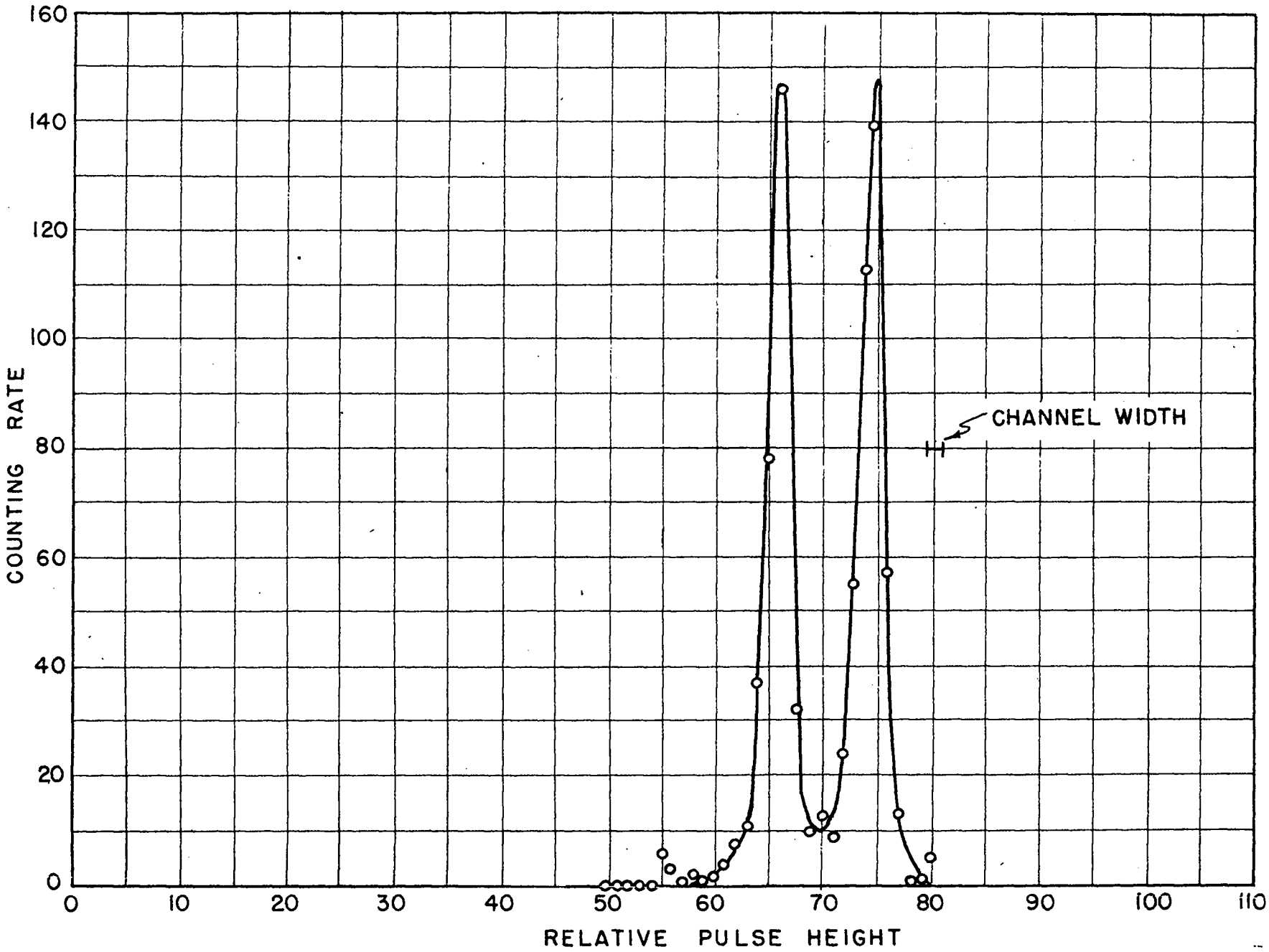

APPROVED FOR PUBLIC RELEASE

13.2 ABSOLUTE COUNTERS

Very often it is desired to measure the α activity of a sample for determination of half lives or of the amount of α active material. In this case the size of a pulse produced by the particle is of minor importance. It is, however, necessary to determine accurately the number of α -particles emitted within an accurately known solid angle per unit time.

If the material is present in the form of a thin deposit (thin compared to the range of the α -particles in the material) backed by a heavy plate, the arrangement is called a "2 π detector". Usually it is built in the form of a simple plane parallel plate chamber with such dimensions, that any α -particle traversing the counting volume produces a pulse large enough to be counted . Ideally the solid angle subtended for every nucleus of the sample is 2π . Therefore, the detection efficiency defined as the number of counts divided by the number of disintegrations should be:

$$F = 1/2.$$

However, two corrections have to be applied. The first arises from the finite thickness t of the active material. Particles emerging under an almost grazing angle with respect to the foil surface may have undergone such a high energy loss on their long path in the material that they cannot produce a pulse of sufficient height to be counted. This results in a reduction of the efficiency which now depends on the bias energy B. The quantity B is defined as the minimum pulse height which is detected. As shown in Section A.6, F(B) is given by the equation:

$$F(B) = 1/2 \left(1 - \frac{t}{2[R_o - R(B)]} \right) \qquad (4)$$

where R_o is the range of the α -particles in the material of the source, and R(B) is the range of an α -particle of energy B. F(B) represents also the so-called integral pulse height distribution:

$$F(B) = \int_{B}^{\infty} f(P)\, dP$$

where f(P) is normalized so that $\int_{0}^{\infty} f(P)\, dP$ is equal to the ratio of the number of particles penetrating the chamber to the total number of disintegrations.

The second correction is due to the back scattering of the α-particles by the plate supporting the active material and the material itself. The back scattering of an α-particle travelling in the material in a direction away from the counting volume will give rise to an increased counting rate. The number of α-particles moving toward the counting volume and being scattered toward the backplate is obviously smaller than the number of those scattered into the counter by the backplate, since the former ones traverse only a small amount of material. From Rutherford's formula it follows that the back scattering, due to a single scattering process, is extremely small on account of the small probability for scattering under a large angle. However, a noticeable increase of particles in the counter volume is caused by a large number of multiple scattering processes under small angles. The problem was treated theoretically at the Metallurgical Laboratory. It is assumed that if an initially narrow and parallel beam of α-particles has travelled through a sufficient layer of material, the density of particles in a radial direction in the plane perpendicular to the beam will show a Gaussian distribution. Under this assumption the counting efficiency is given by the expression:

$$F(B) = 1/2 \left[1 - \frac{t}{2[R_o - R(B)]} + .201\, \Phi(B)\right]$$

where the second term is the thickness correction as before, and the term $.201\, \Phi(B)$ is the back scattering correction. The quantity Φ is a function of the initial range R_o of the α-particle, the residual range R(B), and depends on the material in which back scattering takes place. Numerical values of Φ are given in Section A.13. It may be pointed out that for a

Figure 3

Parallel plate type 2π counter for absolute measurement of the number of α-particles emitted by a source.

1. Polystyrene insulator.
2. Collecting electrode.
3. Amphenol insulator.
4. Guard electrode.
5. High voltage electrode
6. Holder for plate carrying the source.

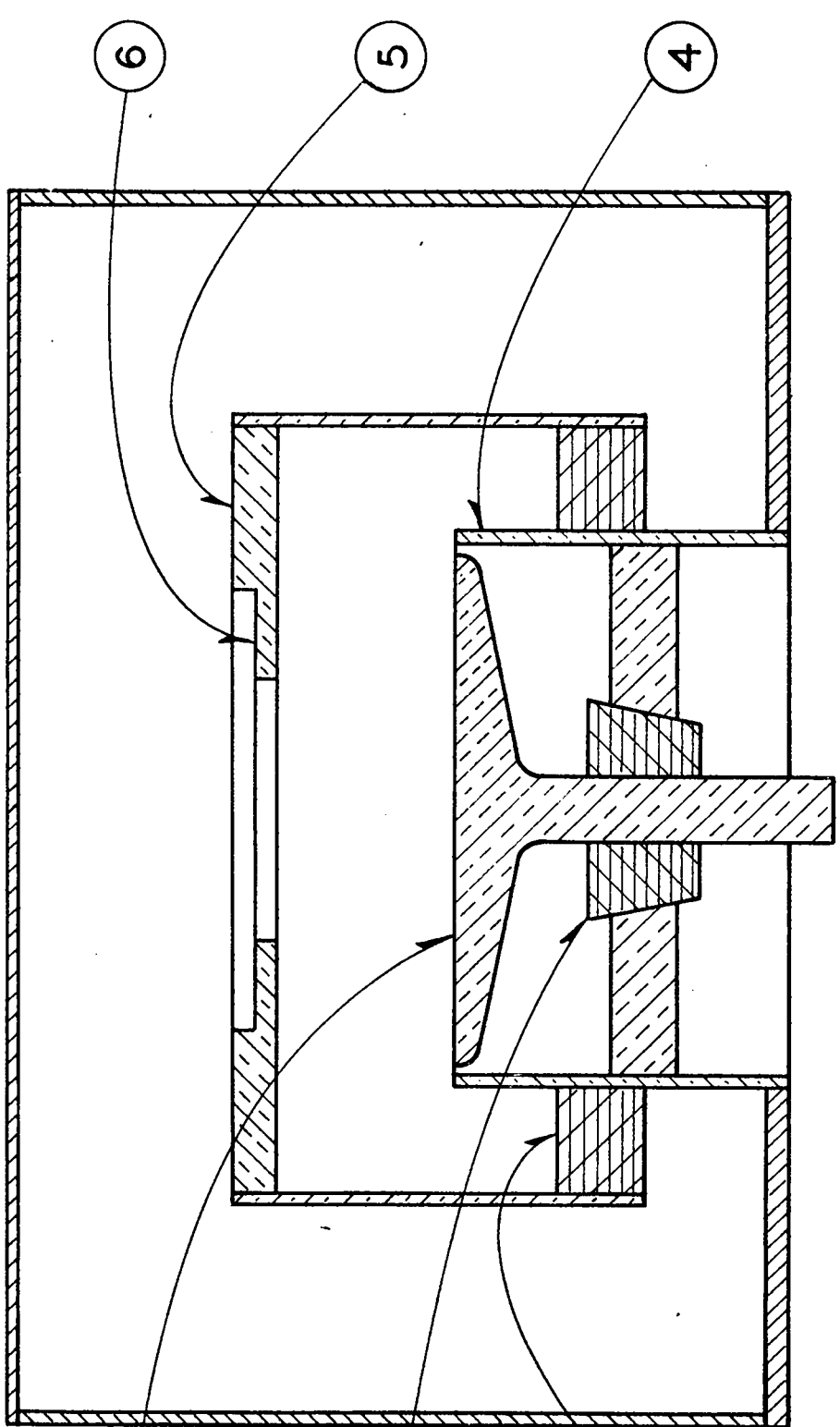

Figure 4

4π proportional counter for absolute measurement of the number of α-particles emitted by a source.

1. Gas inlet.
2. Kovar-glass seal.
3. Holder for foil.
4. Collecting electrodes (.004" platinum wire).
5. Lucite discs supporting the collecting electrodes.

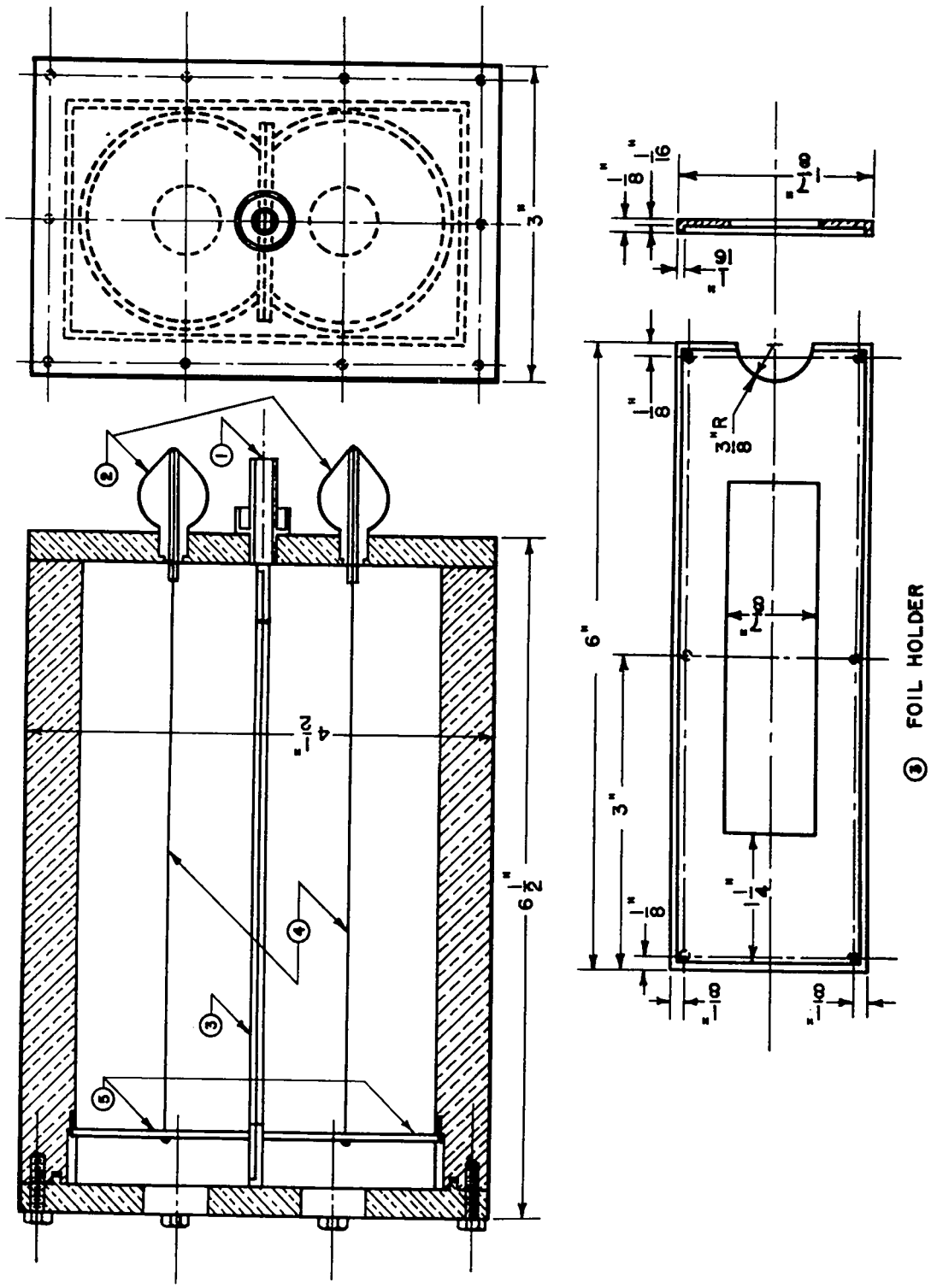

thin layer of α-active material, backed by a solid thick plate, the back scattering does not depend on the thickness t of the active layer.

An example of a 2π counter is shown in Figure 3. The active material is spread over a circle of 3.1 cm diameter on a platinum foil, which is mounted on the negative electrode of the chamber. The separation of the electrodes is 1.2 cm. The chamber is filled with 1.5 Atm. of argon. The back scattering for a uranium source was determined experimentally and theoretically with the results:

$$.201 \left\{ \begin{matrix} \\ \end{matrix} \right. = .613 \text{ (experimentally)}$$

$$.201 \left\{ \begin{matrix} \\ \end{matrix} \right. = .616 \text{ (theoretically)}$$

An arrangement known as a "4π counter", which allows quantitative counting of α-particles and avoids the effect of back scattering is shown in Figure 4. It consists of a brass block in which two overlapping cylindrical openings have been drilled. Two thin wires are mounted along the axes of the two cylinders, thus forming two proportional counters. They are supported on one side by metal glass seals, on the other by lucite disks. The α-active material is deposited on a very thin collodion foil which is mounted over the window of the foil holder (see detail). The foil holder is inserted into a slot between the two counters. In this way all the α-particles emitted over the full solid angle 4π are detected. The counting rate is not affected by back scattering and only the thickness correction has to be applied. It was found to be unnecessary to insure conductibility on both sides of the collodion. The counters are filled with 1 Atm. of argon and operated with a voltage of -700 volts at the wall. A bias curve is shown in Figure 5.

13.3 RANGE MEASUREMENTS

A very simple arrangement for the measurement of the range of α-particles is shown in Figure 6. The ionization chamber, of the parallel plate type, and the foils carrying a thin layer of the α-active material are supported by a

Figure 5

Bias curve of 4π counter (shown in Figure 4), thin collodion foil with thin uranium coating. The ordinate represents the sum of the counting rates of both counters.

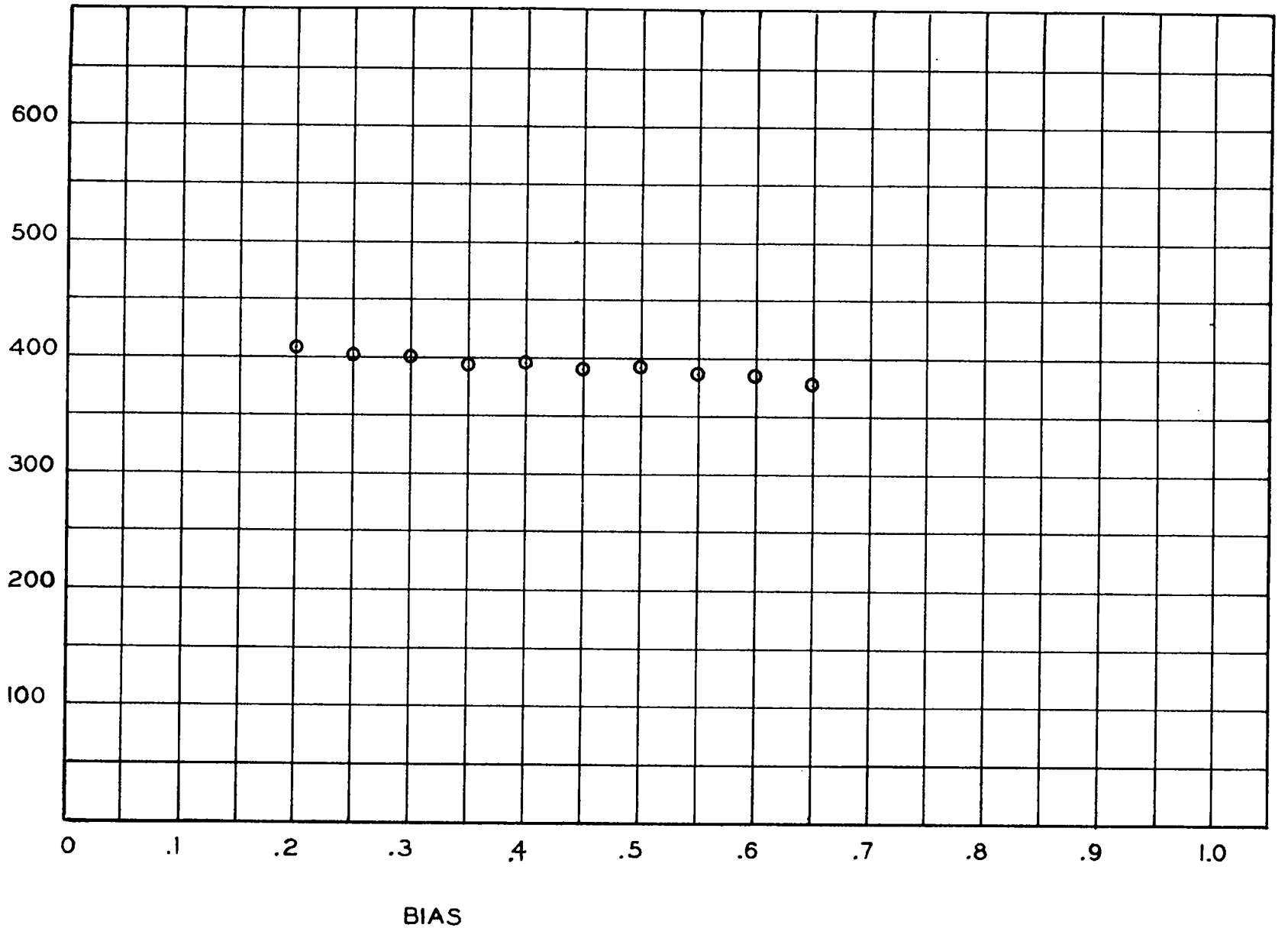

APPROVED FOR PUBLIC RELEASE

Figure 6

Arrangement of source and ionization chamber for range measurements.

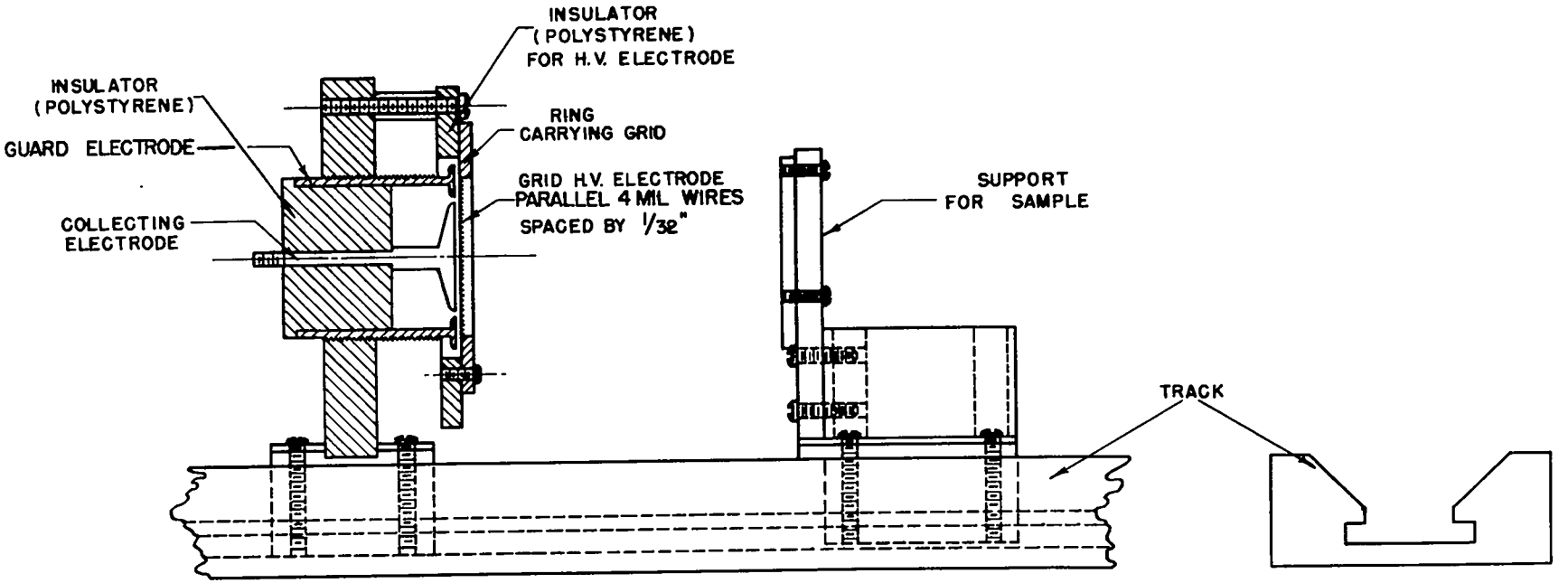

APPROVED FOR PUBLIC RELEASE

track. This allows an exact reproduction of their relative distance. The whole arrangement is placed in an airtight container filled with argon at approximately 1 Atm. pressure. An accurate manometer is used to measure the pressure. In order to determine the range, the number of counts is measured as a function of the pressure in the container with the sample a fixed distance from the chamber. This distance should be rather large in order to avoid excessive variations in the path length of the various particles if absolute range measurements are desired. The chamber is very shallow (0.1 cm). The front electrode is formed by a grid of parallel wires of 14 mil. diameter and spaced 1/32" apart. The chamber is operated at 400 volts. The bias of the detecting equipment has to be set so low that any α-particle traversing the chamber at the lowest pressure in the container is counted.

A typical number versus pressure curve obtained with this apparatus is shown in Figure 7. The most simple procedure to obtain accurate values of the range consists in comparing the unknown sample with a standard, such as polonium. If the unknown sample and the standard are both thin (layer thickness very small compared to the range) and are spread over the same area, the mean range R_x in standard air of the unknown sample is

$$R_x = R_o + d \cdot \left(\frac{\Delta p}{76}\right)_{15^\circ} \cdot s$$

In this equation R_o is the mean range in standard air (see Livingston, Bethe: Rev. Mod. Phys. 9,281,1937) of the standard, d the distance of the samples from the chamber, s the stopping power of the gas for an energy of the α-particle corresponding to a range $\frac{R_x + R_o}{2}$, and Δ p the pressure difference for corresponding points of the number versus pressure curves for the unknown and the standard source. As corresponding points of the two curves, one can, for instance, take those at which the counting rates are one-half of the maximum. The value of d is obtained from the measurement with the standard. If the α-particles were collimated, the pressure at which half maximum counting rate occurs would be re-

Figure 7

Counting rate versus pressure taken with apparatus of Figure 6 with a polonium sample. Distance of source to chamber: 2.84 centimeters.

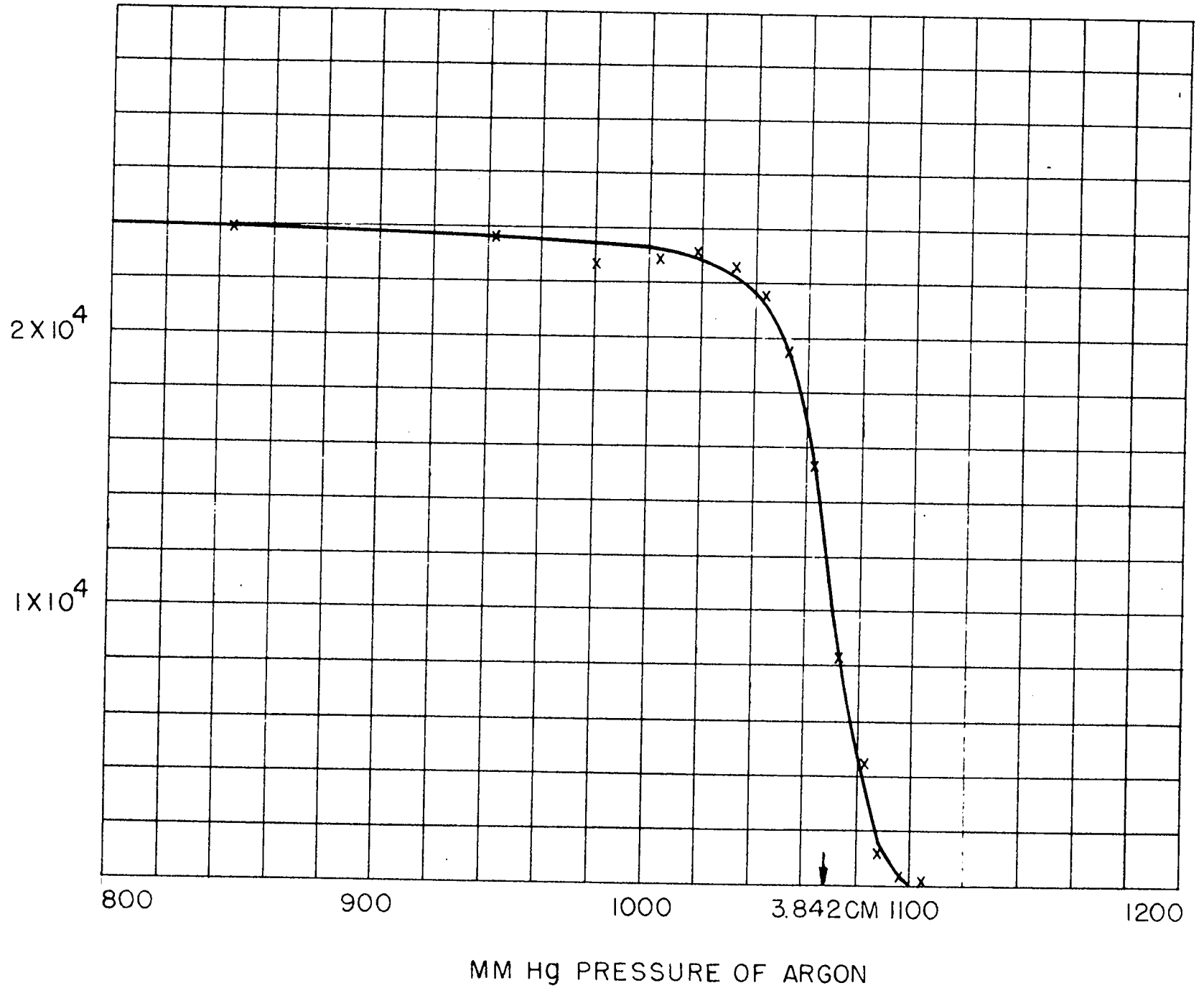

lated to the mean range R_0 and the distance d by the equation

$$d = \left(\frac{760}{P_{\frac{1}{2}}}\right)_{15^\circ} \cdot \frac{R_0}{S}$$

where s is the stopping power for α-particles of mean range R_0. This procedure is not quite correct since the lack of collimation results in the abscissa at half maximum counting rate being slightly smaller than the mean range. The error, however, enters only in the computation of the difference in range between standard and unknown samples and is therefore small.

The data shown in Figure 7 were obtained with a thin sample of polonium spread over a circle of 1 cm diameter at a distance of 2.84 cm. It may be pointed out that argon is particularly suitable as a gas filling, since its stopping power is very nearly independent of the α-particle energy.

For range measurements of samples with several ranges, differential ionization chambers have been used. The arrangement is schematically shown in Figure 8. The ions produced by α-particles which cross both sections of the chamber induce on the collecting electrode opposite and nearly equal charges. Therefore they give rise to small pulses which can be biased off, and only particles ending in the front half of the two chambers are recorded. With polonium samples differential α-particle distributions with a width at half maximum of 0.3 cm air at N. T. P. were obtained. This width is considerably more than the one observed with grid chambers using the pulse height method, where (see Figure 3) the width at half maximum corresponds to about 0.13 cm.

Figure 8

Differential chamber for range measurements of α-particles (Schematic).

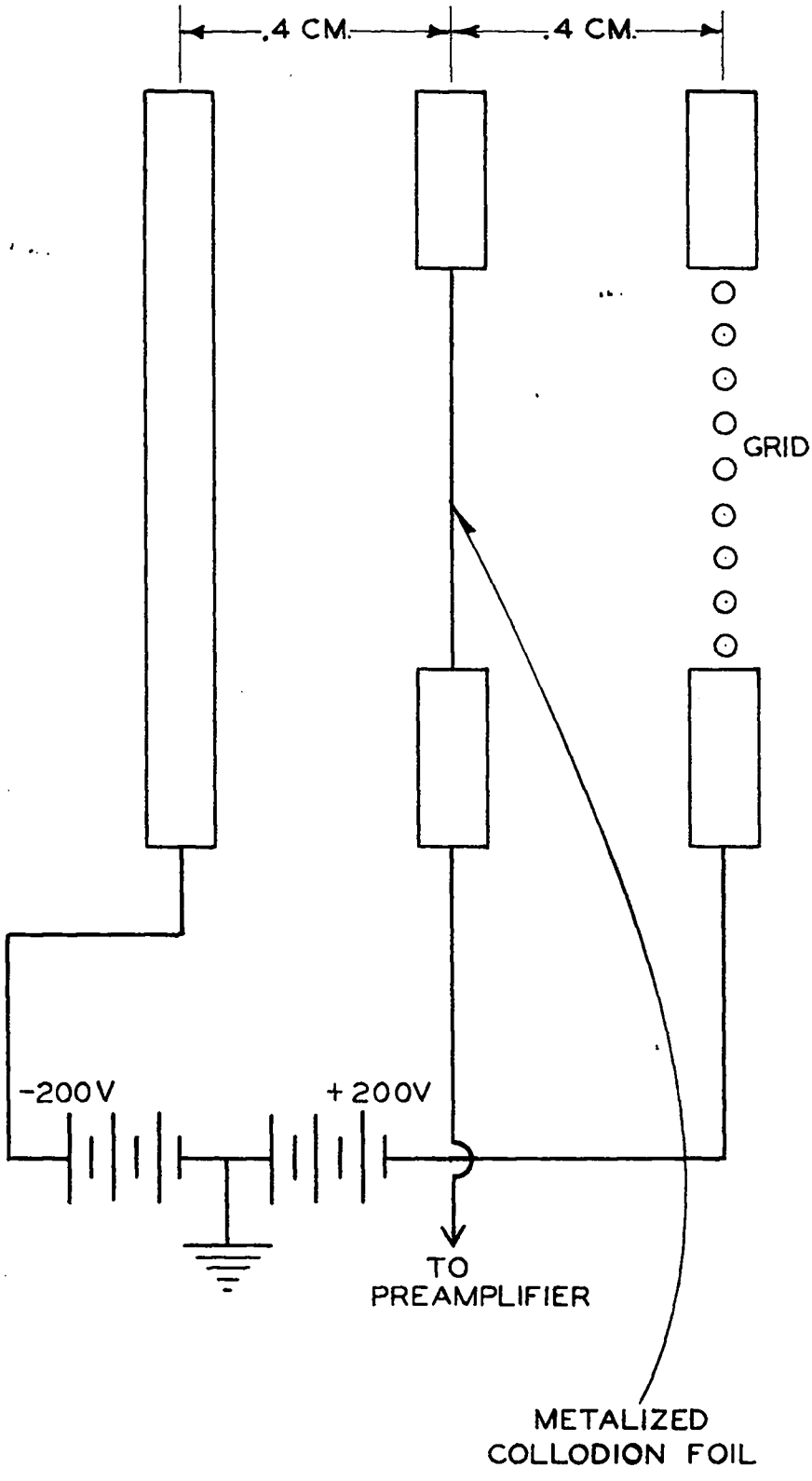

LOS ALAMOS TECHNICAL SERIES

VOLUME I

EXPERIMENTAL TECHNIQUES

PART II

CHAPTER 14

DETECTORS FOR NEUTRON RECOILS

by

BRUNO ROSSI AND HANS STAUB

CHAPTER 14

DETECTORS FOR NEUTRON RECOILS

14.1 INTRODUCTORY CONSIDERATIONS

The chambers described in the present section are designed for the purpose of detecting recoils produced when neutrons collide elastically with atomic nuclei.

In the laboratory system, let E_n be the energy of the neutron before the collision and θ the angle between the lines of flight of the incoming neutron and of the recoil nucleus. From the principles of conservation of energy and momentum, one obtains for the energy E of the recoil the following expression:

$$E = \frac{4A}{(1+A)^2} E_n \cos^2\theta \qquad (1)$$

where A is the mass number of the nucleus. The recoil energy E is a maximum for a head-on collision ($\theta = 0$), in which case it has the following value:

$$E_{max} = \frac{4A}{(1+A)^2} E_n \qquad (2)$$

Another useful relation is that connecting the recoil energy E with the angle of scattering φ of the neutron in the frame of reference where the center of gravity of the neutron and the nucleus is at rest. This relation can be easily shown to be as follows:

$$E = \frac{2A}{(1+A)^2} E_n (1 - \cos\varphi) \qquad (3)$$

Let σ_s be the integral scattering cross section, $\sigma(\varphi)$ the differential scattering cross section in the center of gravity system, so that $\frac{\sigma(\varphi)\,dw}{\sigma_s}$ represents the probability that in a collision the neutron be scattered through the angle φ, into the element of solid angle dw, φ and dw being measured in the center of gravity system. The probability $p(E)\,dE$ for the nucleus to acquire in a collision a recoil energy between E and $E + dE$ is then given by:

$$p(E)\,dE = \frac{\sigma(\varphi)}{\sigma_s}\,2\pi \sin\varphi\, d\varphi$$

where φ is the function of E defined by Equation 3. It follows:

$$p(E) = \frac{\sigma(\varphi)}{\sigma_s}\,\frac{\pi}{E_n}\,\frac{(A+1)^2}{A} \qquad (4)$$

Equation 4 expresses a simple relation between the energy distribution of the recoil nuclei in the laboratory system and the angular distribution of the scattered neutrons in the center of gravity system.

It may be pointed out that the maximum recoil energy decreases as the mass number increases. Hence the recoils of highest energy always arise from the elements of lowest mass number present in the gas or the walls of the chambers. In order to interpret the observations quantitatively, one generally sees to it that one of the elements present in the active volume of the chamber is considerably lighter than all the others, and one arranges the experiment in such a way as to detect only the recoils of higher energy arising from this lighter element.

Recoil chambers may be classified according to the nature of the light element from which the recoils are produced, and according to whether this element is part of the gas or is present as a film on the walls of the chamber. In the latter case one may further distinguish between thin radiators, namely radiators of a thickness small compared

with the range of the fastest recoils, and thick radiators, namely radiators of a thickness larger than the range of the fastest recoils. Moreover, recoil chambers differ according to their geometry (parallel plate, cylindrical, spherical, etc.) and according to the method of detection of the ionization (electron pulse chamber, ion pulse chamber, proportional counter, irtegrating chamber).

14.2 GENERAL PROPERTIES OF HYDROGEN RECOIL CHAMBERS

Hydrogen stands out among other elements as a radiator for recoil chambers because at most energies its scattering cross section is appreciably larger than that of other light nuclei and is well known, at least in the energy region, from about 0.4 to 5.0 million electron volts (see Section A.4). Also, the cross section is a smooth function of the energy (no resonances), and the energy of hydrogen recoils is larger than that of recoils from any other element.

For hydrogen, Equations 1 and 2 become:

$$E = E_n \cos^2 \theta \tag{5}$$

$$E_{max} = E_n \tag{6}$$

For energies below 10 million electron volts, the scattering of neutrons on protons is spherically symmetric in the center of gravity system, namely:

$$\frac{\sigma(\phi)}{\sigma_s} = \frac{1}{4\pi}$$

It then follows from Equation 4 that the probability p(E) dE of a hydrogen recoil of energy (E, dE) being produced in a collision is given by:

$$p(E) = \frac{1}{E_n} = \text{const} \qquad \text{for } E < E_n$$
$$p(E) = 0 \qquad \text{for } E > E_n \tag{7}$$

Range, R, and energy loss per centimeter, $-dE/dx$, as a function of energy for protons in various substances are given in Section A.1. The energy loss per centimeter divided by the energy per ion pair (see Section A.2) gives the specific ionization; i.e., the number of ion pairs per centimeter. A fairly good approximation for the energy-range relation in the high energy region is the following:

$$R = \alpha E^{3/2} \tag{8}$$

where α is a constant. From this equation one obtains for the energy loss the expression:

$$-\frac{dE}{dx} = \frac{1}{\frac{dR}{dE}} = \frac{2}{3\alpha} E^{-1/2} \tag{9}$$

Both expressions, Equations 8 and 9, are grossly inaccurate for low energies (< 0.4 million electron volts). In this region, a better approximation is given by the equations:

$$R = \alpha E^{3/2} + \beta E \tag{8'}$$

$$-\frac{dE}{dx} = \frac{1}{3/2\alpha E^{1/2} + \beta} \tag{9'}$$

where α and β are two constants.

The following sections (Sections 3 and following) describe the distribution in size of the ionization pulses produced in hydrogen recoil chambers of different design by monoenergetic neutrons. The funtions representing the differential pulse height distributions will be normalized so as to give the number of pulses per unit pulse height interval divided by the total number of recoil protons produced in the radiator. Correspondingly, the functions representing the integral pulse high distributions will be normalized to give the number of pulses larger than a certain amount, relative to the total number of recoils. With this normalization, the value of the integral pulse height distribution function corresponding to a given value P of the pulse height coincides with the detection efficiency for a bias energy B = P. The detection efficiency is here defined as the ratio of the number of counts to the number of secondary processes produced in the radiator.

It is convenient to measure pulse heights in terms of the neutron energy E_n, rather than in eV (see Section 10.3); i.e., to express the differential and integral pulse height distributions by means of functions of the ratio P/E_n or $f\ (P/E_n)$ and $F\ (P/E_n)$, respectively. If P is a function of the recoil energy alone, $f\ (P/E_n)$ is related to the probability p(E) defined previously by the equation

$$f\ (P/E_n) = E_n\ p(E)\ \frac{dE}{dP} \qquad (10)$$

The efficiency of a radiator, $\mathcal{E}$, defined as the average number of hydrogen recoils produced when a neutron traverses the chamber has, for monoenergetic neutrons, the following expression:

$$\mathcal{E}(E_n) = t\nu\sigma_s\ (E_n) \qquad (11)$$

where t is the thickness of the radiator for the neutron beam under consideration in micrograms per square centimeter (γ/cm^2), ν is the number of hydrogen atoms per microgram in the radiator, and $\sigma_s(E_n)$ is the neutron scattering cross section for hydrogen. Table 14.2-1 gives the efficiency as a function of energy for a film of glycerol-tristearate ($C_{57}H_{110}O_6$) of 100 micrograms per square centimeter.

Table 14.2-1

Efficiency $\mathcal{E}$ of a glycerol tristearate radiator of 100 γ per square centimeter as a function of neutron energy E_n.

E_n (Mev)	0.1	0.5	2	8
$\mathcal{E} \times 10^5$	9.56	4.94	2.23	0.97

In the case of monoenergetic neutrons, the counting yield η (i.e., the number of counts per neutron traversing the chamber) is given by the equation:

$$\eta = \mathcal{E}(E_n)\ F(B/E_n) = t\nu\sigma_s(E_n)\ F(B/E_n) \qquad (1)$$

where B is the bias energy.

14.3 INFINITELY THIN SOLID RADIATOR: ION PULSE CHAMBER, OR ELECTRON PULSE CHAMBER WITH GRID, OR PROPORTIONAL COUNTER: NO WALL CORRECTION

In this case no appreciable amount of energy is dissipated by the recoil protons in the radiator, and the chamber is supposed to be sufficiently deep so that none of the protons hits the walls. Hence, the energy

dissipated by each proton in the chamber is equal to its original recoil energy. Moreover, on account of the specified method of detection, the pulse height P is equal to the energy dissipated. Therefore,

$$P = E = E_n \cos^2 \Theta \tag{13}$$

If we now assume that the chamber is irradiated with neutrons all of the same energy E_n, the differential pulse height distribution, according to Equations 7 and 10, is given by

$$\begin{aligned} f\ (P/E_n) &= 1 \qquad \text{for } P/E_n < 1 \\ f\ (P/E_n) &= 0 \qquad \text{for } P/E_n > 1 \end{aligned} \tag{14}$$

The corresponding integral pulse height distribution is

$$F\ (P/E_n) = \int_{P/E_n}^{1} f(P'/E_n)\, d\ (P'/E_n) = 1 - P/E_n \tag{15}$$

The counting yield of the chamber for a bias energy B (see Equation 12) can be written as follows:

$$\eta = t\nu\sigma_s\ (E_n)\ (1 - B/E_n) \tag{16}$$

On a first approximation, in the energy region between 0.05 and 3 million electron volts, the scattering cross section of hydrogen may be assumed to be inversely proportional to the square root of the energy, so that we may write

$$\sigma_s\ (E_n) = \sigma_0\, E_n^{-1/2} \tag{17}$$

where σ_0 = constant. With this expression for σ_s, Equation 16 becomes

$$\eta = \varepsilon_B \left(\frac{E_n}{B}\right)^{-1/2} \left(1 - \frac{B}{E_n}\right) \tag{16'}$$

Figure 1

Ion pulse, parallel plate chamber with infinitely thin radiator or ion pulse gas recoil chamber with negligible wall effects. Counting yield η in terms of the efficiency ε_B at the bias energy, as a function of the ratio E_n/B of the neutron energy to the bias energy.

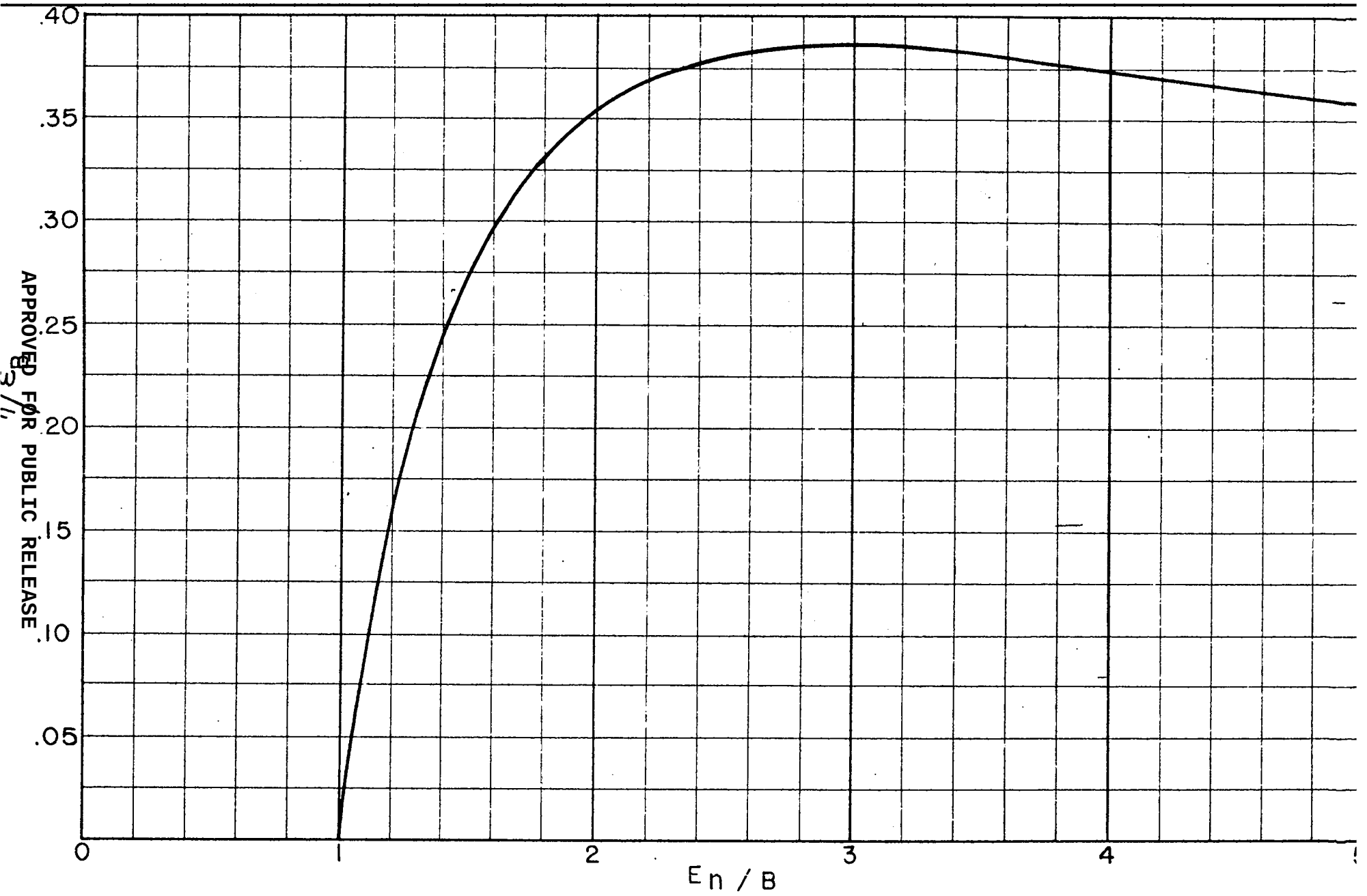

where

$$\varepsilon_B = t\nu\sigma_c B^{-1/2}$$

represents the efficiency of the radiator for neutrons of energy $E_n = B$ (see Equation 11). One sees that the counting yield is a function of the ratios of the neutron energy to the bias energy. The behavior of this function is shown in Figure 1. The yield η is obviously zero for $E<B$. It reaches a maximum for a value of E_n (which by differentiation of Equation 18' may be shown to be $E_n = 3B$) and then decreases very slowly.

14.4 INFINITELY THIN RADIATOR: PARALLEL PLATE, ELECTRON PULSE CHAMBER: NO WALL CORRECTIONS

The energy loss of the recoil protons in the radiator is still negligible, and the protons are supposed to dissipate all of their energy in the sensitive volume of the chamber. However, the pulse height is no longer equal to the energy dissipated in the chamber but is given by this energy multiplied by the distance of the "center of gravity" of the ionization from the positive electrode and divided by the separation of the electrodes. Let us assume that the radiator is placed on the negative electrode and that the neutrons are incident perpendicularly upon it, as shown in Figure 2. Let d be the separation of the electrodes and p the pressure of the gas in atmospheres.

Let us consider a recoil of energy E emitted from the radiator under an angle θ, and let $\bar{x}/p$ be the distance from the origin of the recoil track to the center of gravity of the ionization. The pulse height produced by the recoil under consideration is then given by the equation:

$$P = \left(1 - \frac{\bar{x}\cos\theta}{pd}\right) E \qquad (18)$$

Figure 2

Parallel plate recoil chamber with solid radiator.

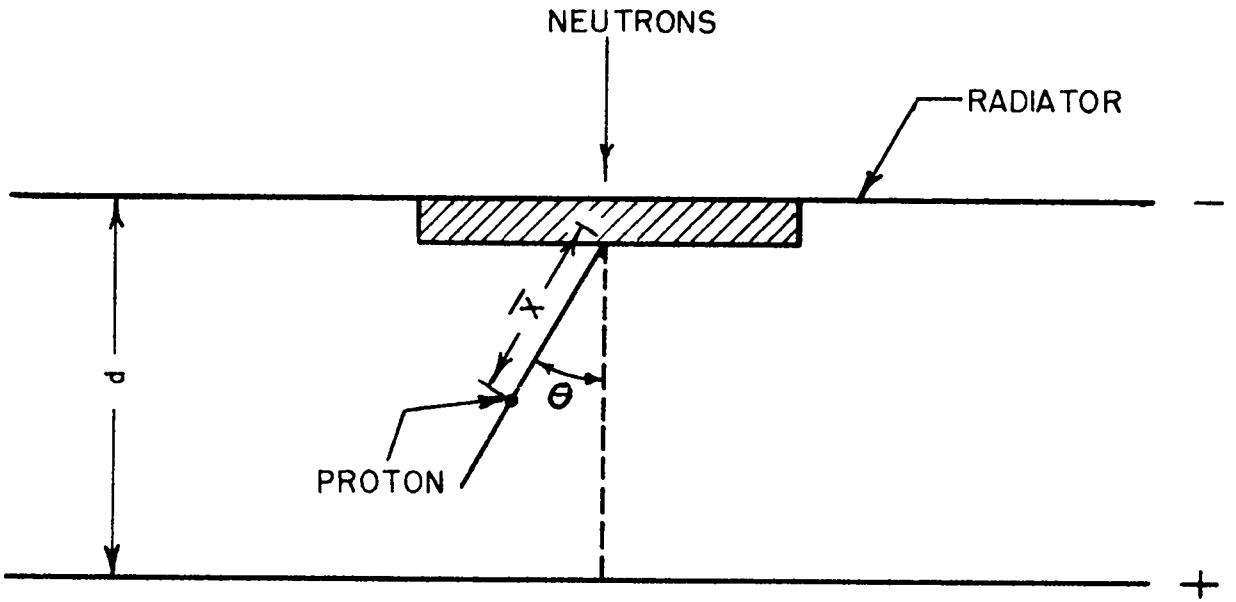

APPROVED FOR PUBLIC RELEASE

Since the specific ionization is proportional to the energy loss, the quantity $\bar{x}$ has the following general expression

$$\bar{x} = \frac{1}{E} \int_0^R \left(-\frac{dE}{dx}\right) x \, dx \qquad (19)$$

where energy losses and ranges are relative to the gas under consideration at one atmosphere pressure. The value of $\bar{x}$ for various gases is given, as a function of energy, in Section A.1. For sufficiently large recoil energies, one can use for R and $-\frac{dE}{dx}$ the expressions Equations 8 and 9 and one obtains:

$$\bar{x} = 3/5 \, R = 3/5 \alpha E^{3/2} \qquad (20)$$

If one remembers Equation 5, Equation 18 becomes

$$P = \left(1 - \frac{3}{5} \frac{R}{pd} \sqrt{\frac{E}{E_n}}\right) E \qquad (21)$$

which can also be written as

$$\frac{P}{E_n} = \frac{E}{E_n} - \frac{3}{5} \frac{R_o}{pd} \left(\frac{E}{E_n}\right)^3 \qquad (21')$$

where $R_o = \alpha E_n^{3/2}$ is the maximum range of the recoil protons.

By differentiating Equation 21' one obtains

$$\frac{dP}{dE} = \frac{d\,(P/E_n)}{d\,(E/E_n)} = 1 - \frac{9}{5} \frac{R_o}{pd} \left(\frac{E}{E_n}\right)^2 \qquad (21'')$$

Now E is a single valued function of P only if dP/dE never changes sign. According to the equation written above, this is the case if the following condition is satisfied:

$$R_o \leq 5/9 \; pd \qquad (22)$$

If, however, $R > 5/9$ pd, there are recoils of two different energies, emerging from the radiator at two correspondingly different angles, which give rise to pulses of the same size.

When Equation 22 is satisfied, the maximum pulse size corresponds to the maximum recoil energy, namely:

$$\frac{P_{max}}{E_n} = 1 - \frac{3}{5}\,\frac{R_o}{pd} \tag{23}$$

When Equation 22 is not satisfied, the maximum pulse size is that for which dP/dE vanishes, namely:

$$\frac{P_{max}}{E_n} = \frac{2}{9}\left(\frac{5\ pd}{R_o}\right)^{1/2} \tag{23'}$$

If Equation 22 is satisfied, the differential pulse height distribution $f(P/E_n)$, according to Equations 7, 10 and 21'', can be written as follows:

$$f\,(P/E_n) = \frac{1}{1 - \frac{9}{5}\,\frac{R_o}{pd}\left(\frac{E}{E_n}\right)^2} \quad \text{for } P \leqslant P_{max} \tag{24}$$

$$= 0 \quad \text{for } P > P_{max}$$

where E is given as a function of P by Equation 21'.

Graphs of $f(P/E_n)$ for various values of the parameter $\frac{R_o}{pd}$ are given in Figure 3. The area under all curves is 1, since all the recoil protons produced in the radiator penetrate the active volume of the chamber. For $\frac{R_o}{pd} = 0$, the function $f(P/E_n)$ reduces to a constant as in the case discussed in the preceding section. For $\frac{R_o}{pd} = \frac{5}{9}$, $f(P/E_n)$ becomes infinity at $P = P_{max}$. For $\frac{R_o}{pd} > \frac{5}{9}$, the function exhibits peculiarities on account of the multiple valued relation between E and P. The function $f(P/E_n)$ for the case under

Figure 3

Electron pulse, parallel plate chamber with infinitely thin hydrogenous radiator on one plate. Differential pulse height distributions of hydrogen recoils produced by monoenergetic neutrons falling perpendicularly upon the radiator, for different values of the ratio between the maximum range R_o/p of the recoils in the gas and the depth d of the chamber.

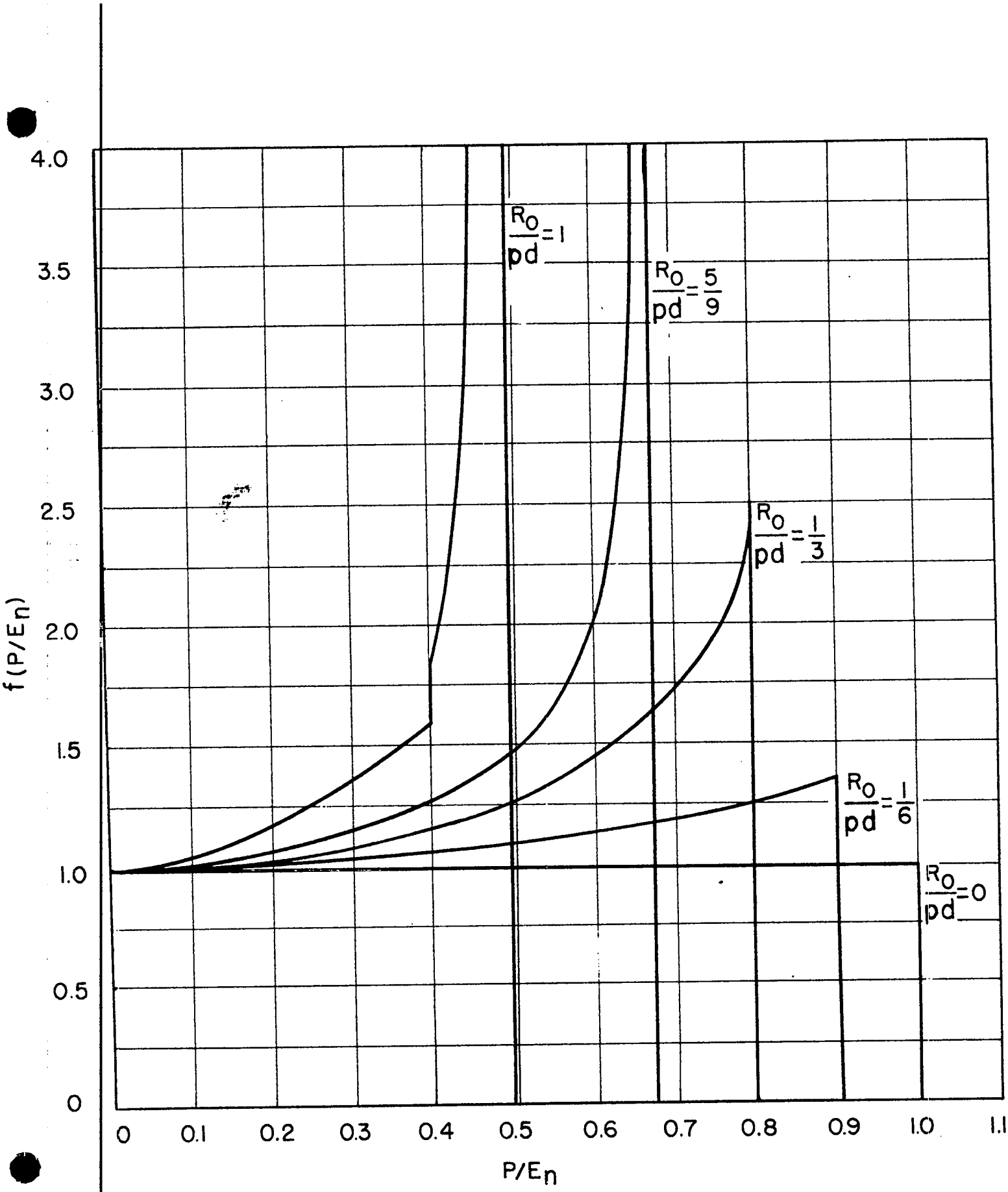

consideration, has also been calculated by using the energy range relation given in Section A.1, instead of the $E^{3/2}$ law. The results are summarized in Table 14.5-1.

14.5 THIN RADIATOR: PARALLEL PLATE: ION PULSE CHAMBER: ELECTRON PULSE CHAMBER WITH GRID OR PROPORTIONAL COUNTER: NO WALL CORRECTION

This case is similar to that discussed in Section 3 except that the thickness of the radiator, even though smaller than the maximum range of the recoil protons in the radiator itself, is not negligible compared with this range. We shall assume that the radiator is placed on one of the plates of the chamber and that monoenergetic neutrons of energy E_n fall perpendicularly upon it, as indicated in Figure 2. The recoil protons which give a pulse larger than P are those which emerge from the radiator with an energy larger than P. If R'(E) represents the range in the material of the radiator of protons of energy E, it follows that a proton, generated at a depth x in the radiator, at an angle θ, and with an energy E, will produce a pulse larger than P if $x \leqslant X$, where X satisfies

$$R'(E) - \frac{X}{\cos \theta} = R'(P) \qquad (25)$$

or

$$R'(E) - X\sqrt{\frac{E_n}{E}} = R'(P)$$

Hence, the total number of pulses larger than P, relative to the total number of recoils generated in the radiator, is given by the following expression:

$$F = \frac{1}{t\,E_n} \int_P^{E_n} X\,(E)\,dE \qquad (26)$$

where X is either the thickness, t, of the radiator or the function of E defined by Equation 25, whichever is smaller. If we assume that R'(E) is proportional to $E^{3/2}$, Equation 25 becomes:

$$X = R_o' \sqrt{\frac{E}{E_n}} \left[\left(\frac{E}{E_n}\right)^{3/2} - \left(\frac{P}{E_n}\right)^{3/2} \right] \qquad (25')$$

where R_o' is the range in the radiator of protons of energy E_n. Equation 26 can then be written as follows:

$$F\left(\frac{P}{E_n}\right) = \int_{P/E_n}^{1} (1/t)\, X \left(\frac{E}{E_n}, \frac{P}{E_n}\right) d\left(\frac{E}{E_n}\right) \qquad (26')$$

Since X/t is either 1 or a function of $\frac{R_o'}{t}$, E/E_n and P/E_n. Equation 26' shows that, under the assumption made, the function F depends only on the ratios P/E_n and $\frac{R_o'}{t}$. The same is true for the differential pulse height distribution, which is obtained by differentiating F with respect to P/E_n.

The functions $f(P/E_n)$ and $F(P/E_n)$ have been calculated, under the assumption of R' proportional to $E^{3/2}$, and the results are given in Figure 4.

It may be noted that the areas under the curves for $f(P/E_n)$ corresponding to different thicknesses of the radiator are not equal. The reason is that as the radiator becomes thicker, an increasing fraction of the recoils produced in the radiator are absorbed by the radiator itself before they reach the active volume of the chamber.

14.6 THIN RADIATOR: PARALLEL PLATE, ELECTRON PULSE CHAMBER: NO WALL CORRECTION

This case is similar to that discussed in Section 4, except for a finite thickness of the radiator. The differential and integral pulse height distributions for this case were calculated, on the basis of the energy range relations given in Section A.1. for radiators of glycerol-tristearate ($C_{57}H_{110}O_6$) and argon filled chambers.

These results are summarized in Table 14.6-1, where f and F are given as a function of P/E_n for various values of the neutron energy E_n, of the

Figure 4

Ion pulse, parallel plate chamber with thin hydrogenous radiator on one plate. (A) Differential and (B) integral pulse height distributions of hydrogen recoils produced by monoenergetic neutrons falling perpendicularly upon the radiator, for different values of the ratio t/R_0, between the thickness of the radiator and the maximum range of the recoils in the radiator.

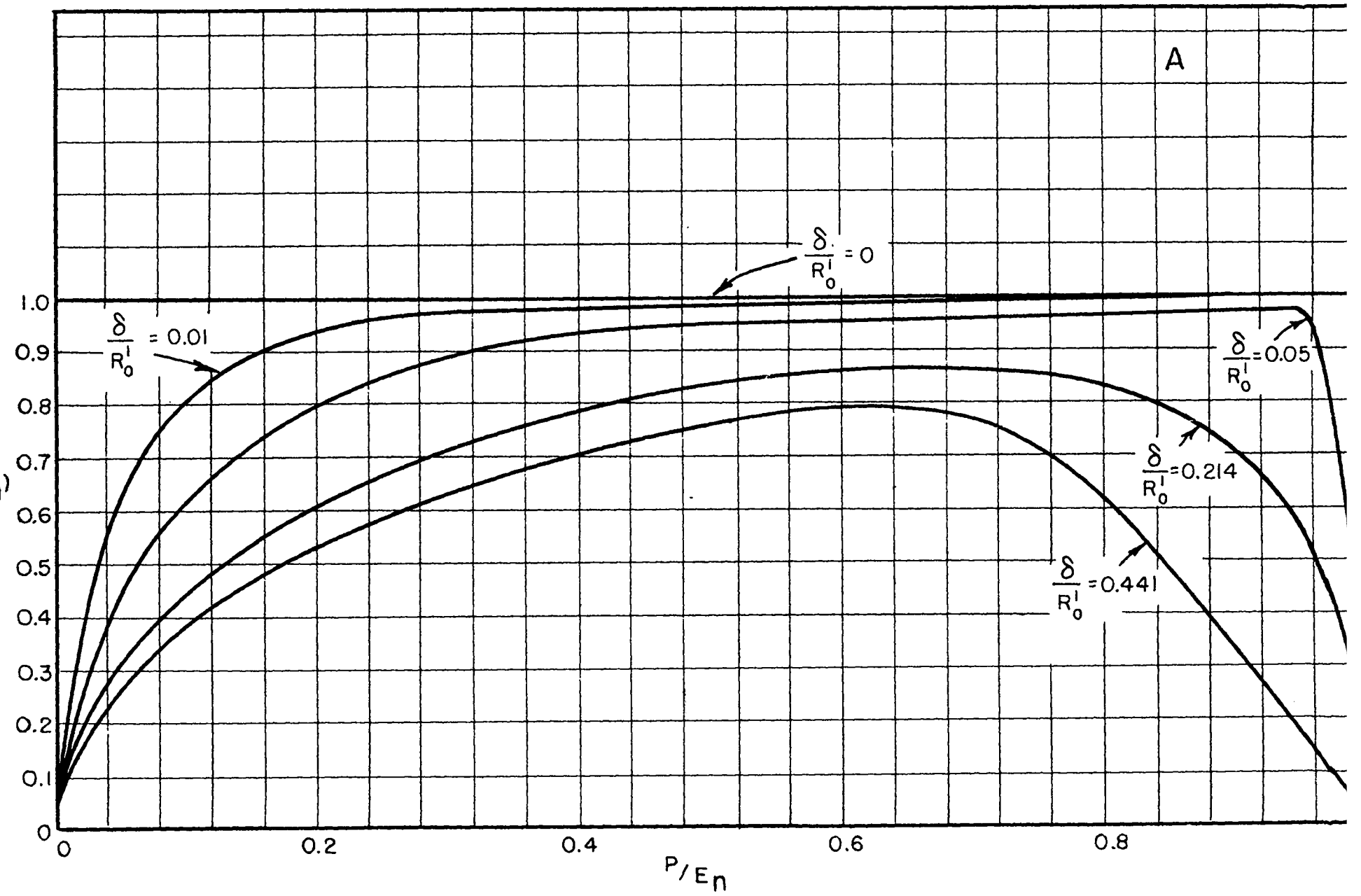

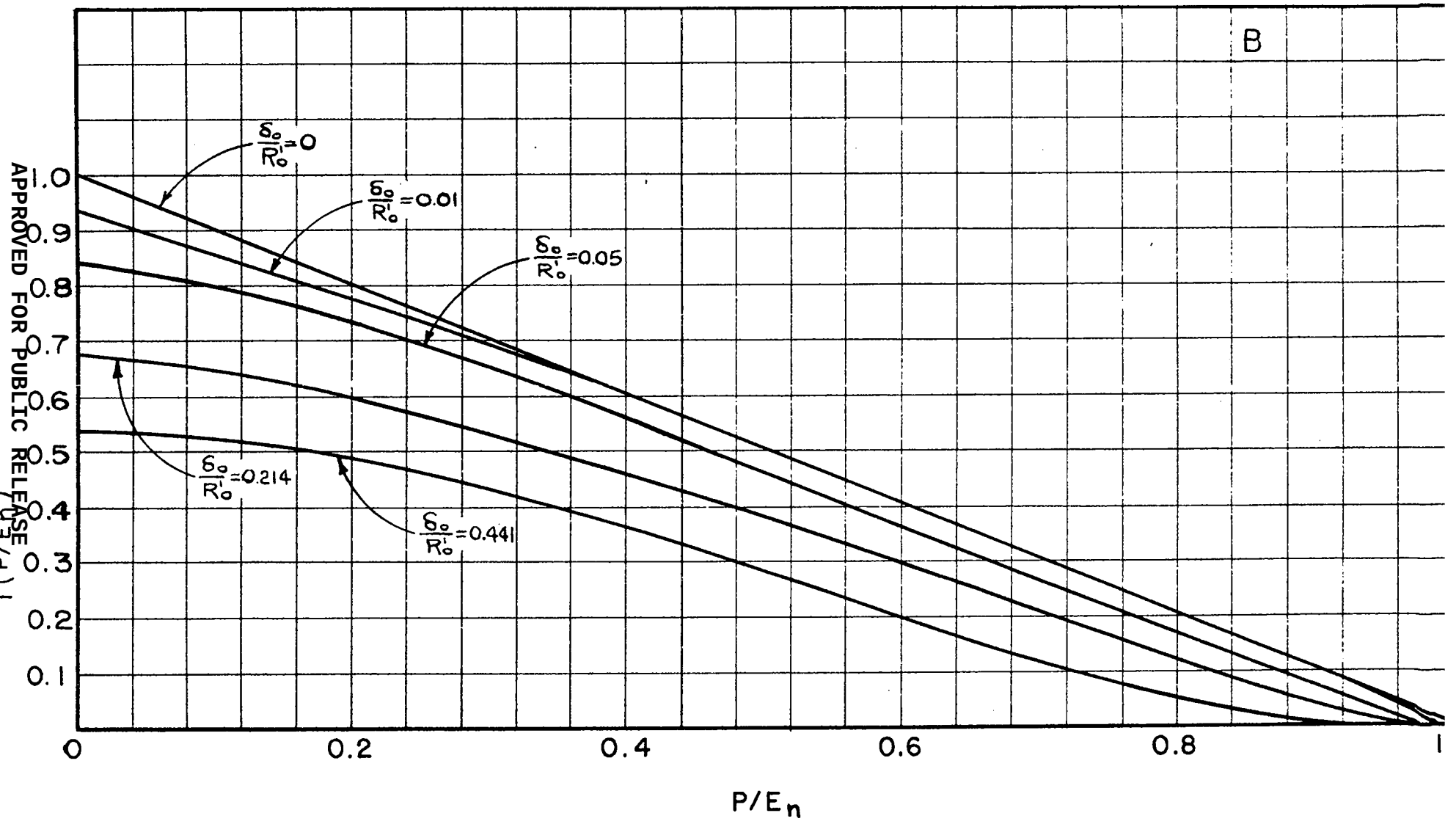

APPROVED FOR PUBLIC RELEASE

APPROVED FOR PUBLIC RELEASE

Table 14.6-1

Differential and Integral Pulse Height Distributions for Argon Filled, Parallel Plate, Electron Pulse Chambers with Glycerol Tristearate Radiators

E_n = 0.3 Mev pd = 4.02 atm. cm

P/E_n	t = 0	t = 25 γ / cm^2		t = 50 γ / cm^2		t = 75 γ / cm^2	
	f	f	F	f	F	f	F
0.1666	1.0083	0.8430	0.7410	0.7449	0.5622	0.5864	0.6045
0.3333	1.0122	0.8935	0.5960	0.8159	0.5337	0.7642	0.4853
0.5000	1.0476	0.9557	0.4420	0.8931	0.3945	0.8485	0.3531
0.6000	1.0695	1.0004	0.3425	0.9444	0.3007	0.9020	0.2644
0.6666	1.0874	1.0260	0.2735	0.9773	0.2355	0.9396	0.2024
0.7000	1.0979	1.0393	0.2385	0.9952	0.2022	0.9613	0.1701
0.7333	1.1088	1.0562	0.2050	1.0166	0.1697	0.9854	0.1383
0.7666	1.1203	1.0742	0.1700	1.0375	0.1362	1.0082	0.1055
0.7848	1.1278	1.0850	0.1500	1.0496	0.1168	1.0216	0.0864
0.8386	1.1508	1.1145	0.0915	1.0830	0.0605	0.7220	0.0400
0.8909	1.1773	1.1467	0.0300	0.5733	0.0150	0.3822	0.0100
0.9423	1.2040	0.0000	0.0000	0.0000	0.0000	0.0000	0.0000

APPROVED FOR PUBLIC RELEASE

Table 14.6-1 Continued

E_n = 0.4 Mev pd = 4.02 atm. cm

P/E_n	t = 0	t = 25 γ/cm^2		t = 50 γ/cm^2		t = 75 γ/cm^2	
	f	f	F	f	F	f	F
0.1250	1.0073	0.8151	0.8005	0.7117	0.7358	0.6568	0.3990
0.2500	1.0201	0.8835	0.6910	0.7990	0.6393	0.7449	0.5990
0.3750	1.0414	0.9471	0.5760	0.8818	0.5348	0.8343	0.5006
0.5000	1.0735	1.0084	0.4545	0.9582	0.4218	0.9188	0.3933
0.6250	1.1262	1.0776	0.3220	1.0385	0.2967	1.0063	0.2731
0.7500	1.2015	1.1564	0.1820	1.1358	0.1618	1.1099	0.1425
0.7750	1.2219	1.1898	0.1530	1.1606	0.1330	1.1360	0.1140
0.8000	1.2434	1.2133	0.1235	1.1866	0.1037	1.1640	0.0845
0.8204	1.2622	1.2341	0.0985	1.2095	0.0790	1.1885	0.0594
0.8513	1.2926	1.2676	0.0605	1.2458	0.0407	0.8306	0.0271
0.8829	1.3292	1.3064	0.0190	0.6532	0.0095	0.4355	0.0063
0.9117	1.3624	0.0000	0.0000	0.0000	0.0000	0.0000	0.0000

E_n = 0.5 Mev pd = 4.02 atm. cm

P/E_n	t = 0	t = 25 γ/cm^2	t = 50 γ/cm^2	t = 75 γ/cm^2
	f	f	f	f
0.4000	1.0649	0.9963	0.9424	0.9004
0.5000	1.1088	1.0591	1.0173	0.9822
0.6000	1.1733	1.1364	1.1033	1.0748
0.7000	1.2702	1.2438	1.2188	1.1959
0.7600	1.3533	1.3308	1.3071	1.2854
0.8000	1.4250	1.4016	1.3827	1.3653
0.8208	1.4691	1.4479	1.4295	1.4132
0.8396	1.5146	1.4947	1.4771	0.9847
0.8581	1.5652	1.5464	0.7727	0.5151
0.8756	1.6090	0.0000	0.0000	0.0000

APPROVED FOR PUBLIC RELEASE

Table 14.6-1 Continued

E_n = 0.6 Mev pd = 4.02 atm. cm

P/E_n	t = 25 γ/cm^2	t = 50 γ/cm^2		t = 75 γ/cm^2		t = 100 γ/cm^2	t = 175 γ/cm^2	
	f	f	F	f	F	F	f	F
0.1666	0.8507	0.7576	0.7488	0.7103	0.7181	----	----	----
0.2500	0.9228	0.8491	0.8798	0.7995	0.6538	0.6303	0.6826	0.5710
0.3333	0.9825	0.9246	0.6067	0.8818	0.5843	0.5634	0.7740	0.5101
0.4166	1.0447	1.0001	0.5258	0.9634	0.5076	0.4904	0.8651	0.4429
0.5000	1.1141	1.0805	0.4408	1.0502	0.4246	0.4095	0.9660	0.3665
0.5833	1.2004	1.1756	0.3482	1.1534	0.3336	0.3194	1.0823	0.2812
0.6666	1.3329	1.3151	0.2440	1.2968	0.2313	0.2192	1.2351	0.1652
0.7000	1.4087	1.3772	0.1998	1.3569	0.1876	0.1762	1.3082	0.1434
0.7333	1.5083	1.4889	0.1507	1.4692	0.1401	0.1295	1.4144	0.0982
0.7524	1.5686	1.5485	0.1223	1.5329	0.1111	0.1008	1.4782	0.0720
0.7649	1.6113	1.5934	0.1027	1.5794	0.0962	0.0822	------	0.0530
0.7770	1.6631	1.6491	0.0837	1.6357	0.0736	0.0631	------	0.0377
0.7892	1.7306	1.7169	0.0623	1.7030	0.0520	0.0414	------	0.0237
0.8010	1.7951	1.7806	0.0425	1.7654	0.0321	0.0241	------	0.0138
0.8126	1.8619	1.8471	0.0220	------	0.0147	0.0110	------	0.0063
0.8243	1.9375	------	0.0050	------	0.0033	0.0025	------	0.0014
0.8351	0.0000	0.0000	0.0000	------	0.0000	0.0000	------	0.0000

Table 14.6-1 Continued

E_n = 0.6 Mev pd = 8.98 atm. cm

P/E_n	t = 0	t = 175 γ/ cm²	
	f	f	F
0.1666	1.0077	------	0.6231
0.2500	1.0149	0.6668	0.5732
0.3333	1.0255	0.7416	0.5141
0.4167	1.0405	0.8098	0.4501
0.5000	1.0591	0.8746	0.3790
0.5873	1.0821	0.9347	0.3038
0.6666	1.1125	0.9927	0.2231
0.7500	1.1594	1.0555	0.1377
0.8000	1.1935	1.0966	0.0832
0.8160	1.2049	1.1112	0.0681
0.8480	1.2257	0.8293	0.0359
0.8796	1.2530	0.5209	0.0121
0.9260	1.2937	0.0000	0.0000

E_n = 1.0 Mev pd = 8.98 atm. cm

P/E_n	t = 0	t = 175 γ/ cm²	
	f	f	F
0.10	------	------	0.7527
0.15	------	------	0.7217
0.20	1.0188	0.70387	0.6884
0.25	1.0311	0.76750	0.6524
0.30	1.0456	0.82845	0.6120
0.35	1.0652	0.88625	0.5692
0.40	1.0872	0.93923	0.5244
0.45	1.1179	0.99250	0.4750
0.50	1.1526	1.0479	0.4241
0.55	1.1979	1.1089	0.3705
0.60	1.2597	1.1819	0.3123
0.65	1.3319	1.2652	0.2545
0.70	1.4412	1.3802	0.1870
0.75	1.5988	1.5452	0.1131
0.78	1.7188	1.6859	0.0645
0.8017	1.8499	1.8004	0.0322
0.8109	1.9046	1.3360	0.0161
0.8201	2.0576	0.8350	0.0058
0.8336	2.0685	0.0000	0.0000

Table 14.6-1 Continued

E_n = 1.6 Mev pd= 8.98 atm. cm

P/E_n	t = 175 γ/cm^2
	F
0.1250	0.7928
0.1562	0.7713
0.1875	0.7467
0.2187	0.7217
0.2500	0.6948
0.2812	0.6658
0.3125	0.6360
0.3437	0.6068
0.3750	0.5705
0.4062	0.5359
0.4375	0.4988
0.4687	0.4588
0.5000	0.4185
0.5312	0.3719
0.5625	0.3180
0.5937	0.2565
0.6250	0.1730
0.6375	0.1180
0.6469	0.0000

E_n = 1.6 Mev pd= 12.70 atm. cm

P/E_n	t = 175 γ/cm^2	
	f	F
0.1250	------	0.7942
0.1875	------	0.7512
0.2500	0.6634	0.6949
0.3125	0.9415	0.6391
0.3750	1.0204	0.5775
0.4375	1.1064	0.5110
0.5000	1.2101	0.4393
0.5625	1.3554	0.3604
0.5937	1.4539	0.3155
0.6250	1.5978	0.2685
0.6562	1.7768	0.2180
0.6875	2.1253	0.1575
0.7187	2.6720	0.0840
0.7250	2.8800	0.0670
0.7312	3.1360	0.0485
0.7375	3.4720	0.0280
0.7404	3.8803	0.0190
0.7416	3.9782	0.0137
0.7429	2.9136	0.0093
0.7441	2.3936	0.0061
0.7454	1.8432	0.0032
0.7468	1.2621	0.0014
0.7477	0.6485	0.0004
0.7489	0.0000	0.0000

APPROVED FOR PUBLIC RELEASE

radiator thickness, t, and of the product, pd, of the gas pressure times the depth of the chamber.

In Figure 5 the function $f(P/E_n)$, corresponding to t = 0 and t = 175 γ per square centimeter and calculated for the same value of E_n (1 million electron volt) and pd (8.98 atmospheres times centimeters), is represented graphically in order to illustrate the influence of a finite radiator thickness on the pulse height distribution curves. The differential pulse height distribution for t = 0, calculated on the basis of the $R \propto E^{3/2}$ approximation, is also represented in the same figure. The difference between this curve and that calculated on the basis of the more accurate energy range relation is very small.

14.7 THICK RADIATOR: PARALLEL PLATE, ION PULSE CHAMBER, ELECTRON PULSE CHAMBER WITH GRID, OR PROPORTIONAL COUNTER; NO WALL CORRECTION

The radiator is again placed on the negative plate of the chamber, and the neutrons are incident perpendicularly on it, as shown in Figure 2. The thickness of the radiator is now supposed to be larger than the range R_o' of the fastest recoil protons in the radiator itself.

The integral pulse height distribution in the case of monoenergetic neutrons striking the chamber is given by Equation 26 or 26' where now $X(E_n, P, E)$ is always defined by Equation 25; i.e., it never becomes equal to the thickness t of the radiator. If we assume the range to be proportional to $E^{3/2}$, then Equation 25' holds and one obtains

$$F(P/E_n) = \int_{P/E_n}^{1} \frac{R_o'}{t} \left[\left(\frac{E}{E_n} \right)^{3/2} - \left(\frac{P}{E_n} \right)^{3/2} \right] \sqrt{\frac{E}{E_n}} \; d\left(\frac{E}{E_n} \right)$$

Figure 5

Electron pulse parallel plate chamber with glycerol-tristearate radiator on one plate. Plate separation d = 1.33 centimeters; gas filling 6.7 atmospheres of argon. Differential pulse height distributions for hydrogen recoils produced by neutrons of 1 million electron volt energy falling perpendicularly upon the radiator.

(A) Infinitely thin radiator($t = 0$), calculated by assuming R proportional to $E^{3/2}$.

(B) Infinitely thin radiator($t = 0$), calculated on the basis of the energy range relation given in Section A.1.

(C) "Thin" radiator ($t = 175 \gamma/cm^2$), calculated on the basis of the energy range relation given in Section A.1.

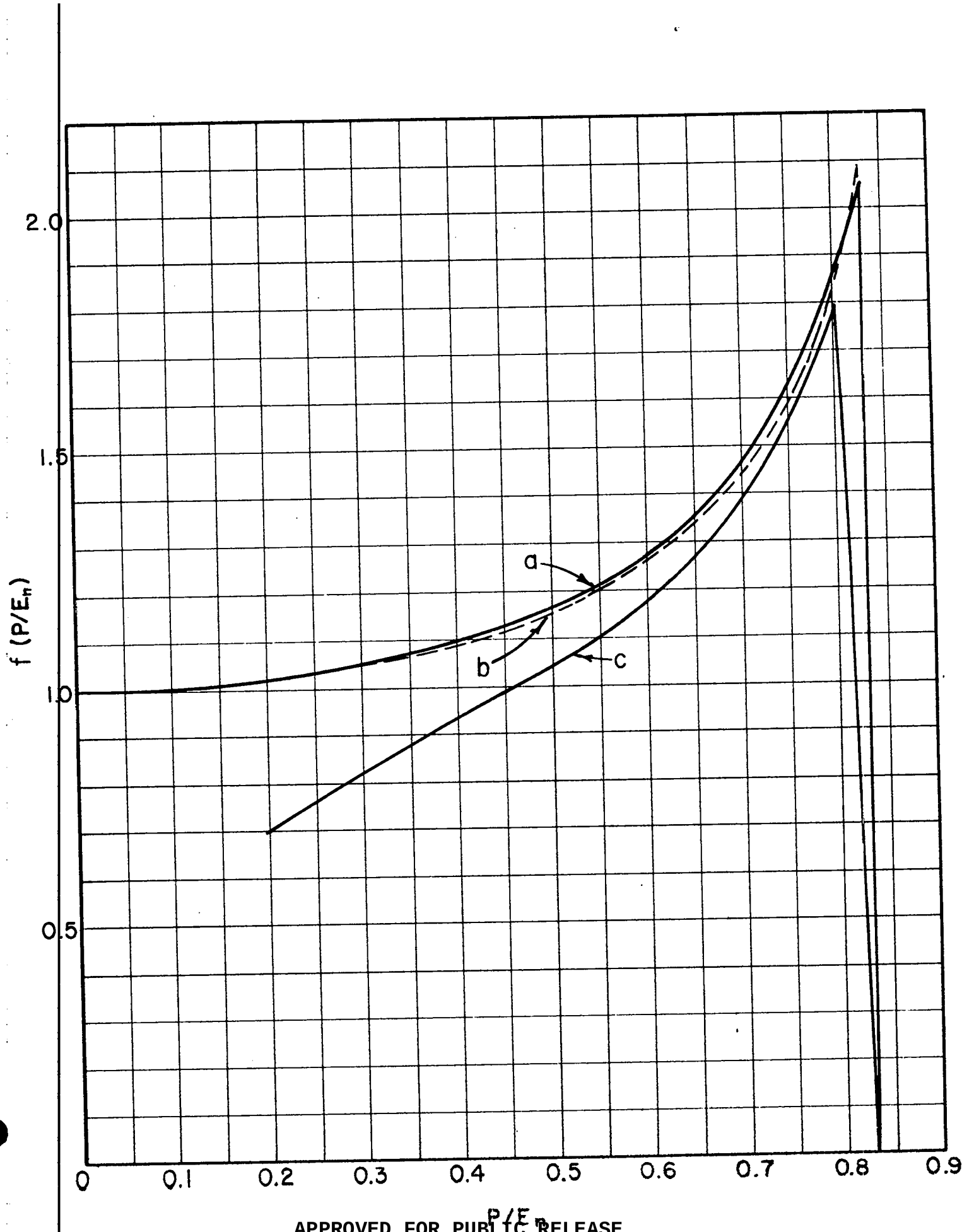

or

$$F\left(\frac{P}{E_n}\right) = \frac{R_o'}{3t}\left[1 - \left(\frac{P}{E_n}\right)^{3/2}\right]^2 \qquad (27)$$

The counting yield of the chamber for a bias energy B (see Equation 12) has the expression:

$$\eta = 1/3\, \nu \sigma_s (E_n)\, R_o' \left[1 - \left(\frac{B}{E_n}\right)^{3/2}\right]^2 \qquad (28)$$

or, if one assumes R' to be proportional to $E^{3/2}$ and σ_s proportional to $E_n^{-1/2}$:

$$\eta = 1/3\, \zeta_B \frac{E_n}{B}\left[1 - \left(\frac{B}{E_n}\right)^{3/2}\right]^2 \qquad (28')$$

In the above equation

$$\zeta_B = R'(B)\, \nu \sigma_c\, B^{-1/2}$$

represents the average number of recoils per incident neutron of energy $E_n = B$ produced in a thickness of the radiator equal to the range of protons of energy B. Equation 28' indicates that η is a function of E_n/B. A graph of this function is given in Figure 6, from which one can see that the counting yield of a recoil chamber with thick radiator increases rapidly and continuously with increasing neutron energy.

14.6 GAS RECOIL CHAMBER: NO WALL EFFECTS

We shall assume now that the chamber is filled with hydrogen, a hydrogen compound, or a hydrogen containing moisture, and that the linear dimensions of the chamber are very large compared with the range of the fastest recoil protons, so that wall effects can be disregarded.

Figure 6

Ion pulse parallel plate chamber with thick radiator. Counting yield η in terms of $\zeta_B = \nu\sigma_o B^{-1/2} R'(B)$ as a function of the ratio E_n/B of the neutron energy to the bias energy.

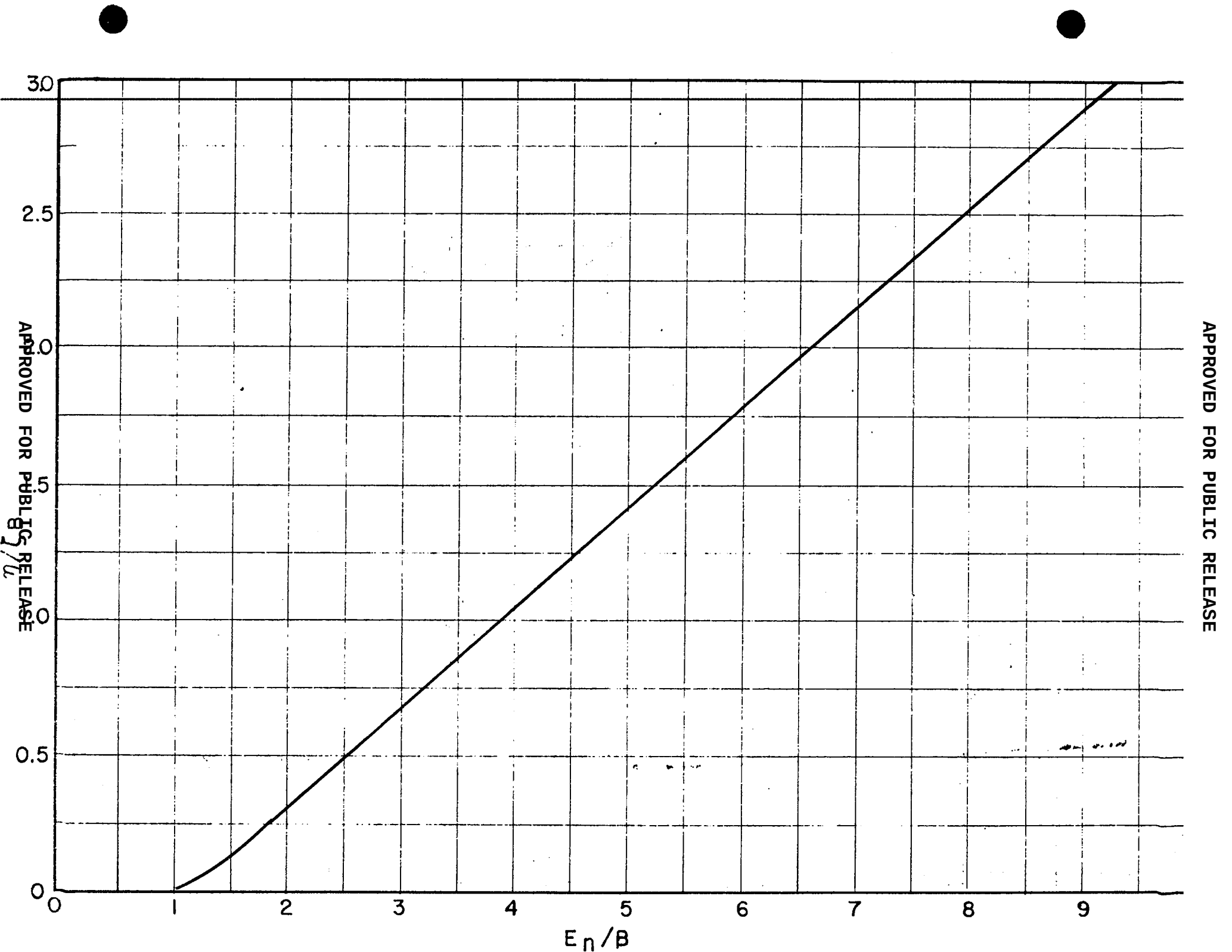

APPROVED FOR PUBLIC RELEASE

If the chamber is used as an ion pulse chamber, then P = E and the differential and integral pulse height distribution for monoenergetic neutrons are the same as in Section 3 (see Equations 14 and 15). If the chamber is used as an electron pulse chamber, the pulse height distribution depends on the geometry.

If the chamber is used as an integrating chamber and is filled with pure hydrogen, then the intensity I of the ionization current is given by

$$I = H \frac{E_n}{2} \frac{e}{W_o} \tag{29}$$

where H is the number of recoils per second produced in the chamber, e is the electron charge, W_o is the energy per ion pair, and $\frac{E_n}{2}$ represents the average energy of the hydrogen recoils.

14.9 GAS RECOIL, ION PULSE CHAMBER, COMPUTATION OF WALL EFFECTS

Let us consider the two following types of ionization chambers:

(A) Parallel plate chamber, with a circular collecting electrode, surrounded by a guard ring as shown in Figure 7.

(B) Cylindrical chamber with axial collecting electrode supported by guard electrodes as shown in Figure 8.

In both cases the active volumes are supposed to be sharply defined and in the shape of cylinders with flat ends. The direction of the incoming neutrons is parallel to the axis of the cylinder, as shown by the arrows. In the case of (A), the wall effects are caused: (1) by recoils hitting the electrode at the far end of the chamber; (2) by recoils produced in the active volume, but going out of the active volume through its lateral boundary; and (3) by recoils produced outside the active volume and entering the active volume through its lateral boundary.

Figure 7

Wall effects in a gas recoil parallel plate chamber with circular electrodes.

Figure 8

Wall effects in a gas recoil cylindrical chamber.

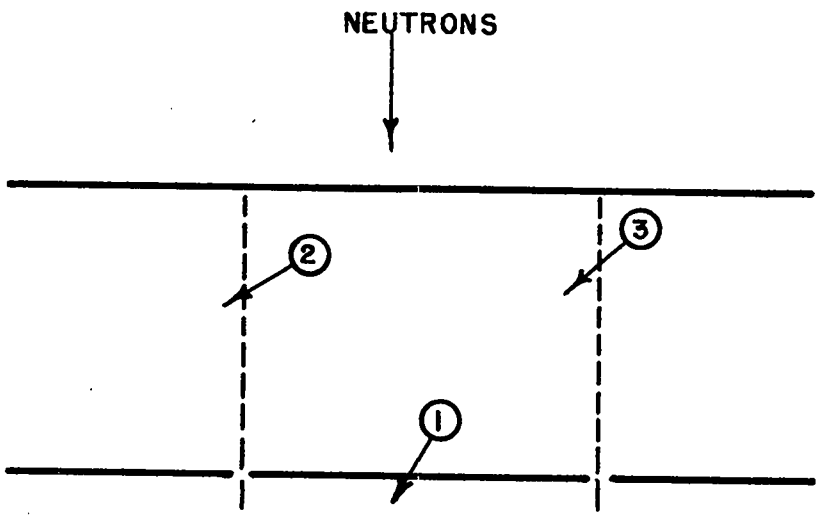

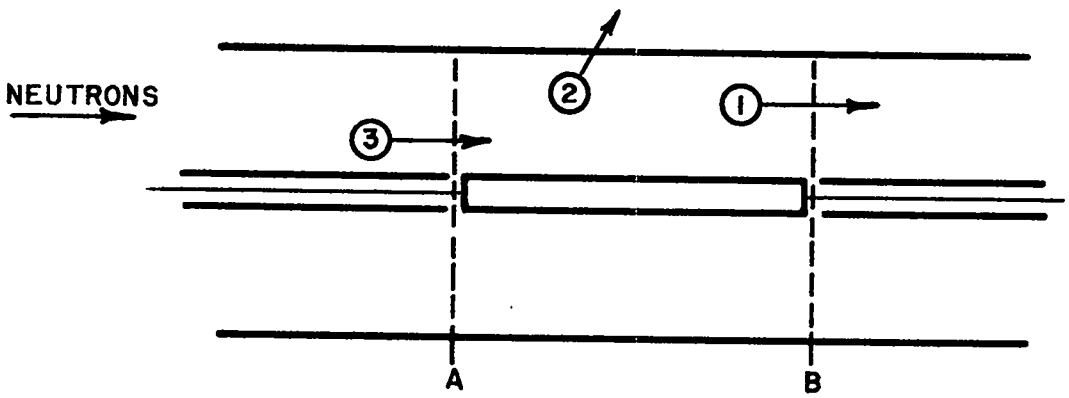

In the case of (B), the wall effects are caused:(1) by recoils produced in the active volume and crossing the boundary B (see Figure 8); (2) by recoils hitting the lateral wall; and (3) by recoils produced outside of the active volume and entering the active volume through the boundary A. The recoils hitting the central electrode are neglected .

A general computation of the wall effects for the two types of chambers described was carried out under the assumption $R = \propto E^{3/2}$.

In these calculations, edge effects (see Section 10.7) are neglected, and accordingly the pulse height for a particle which crosses the boundary of the sensitive volume is computed by considering only the ionization produced by the particle in the sensitive volume. This procedure is justified if the conditions for an "ideal" ion pulse chamber are fulfilled; i.e., if the decay time of the detecting equipment is very long compared with the time of collection of the positive ions (see Section 10.6). In the practical cases, the peculiarities in the shape of pulses produced by the motion of ions near the boundary of the active volume may have an appreciable influence on the observed pulse height distribution.

The results of the calculations are expressed by the following equations, in which b represents the radius of the cylindrical sensitive volume and a its length (a is the spacing of the plates in case (A) and the length of the collecting electrode in case (B)).These results apply to chambers of any dimensions, provided that the maximum range R_o of the recoil protons is smaller than a.

Case (A) (see Figure 7)

$$f\left(\frac{P}{E_n}\right) = 1 + \frac{R_o}{a} A\left(\frac{P}{E_n}\right) + \frac{R_o^2}{ab} B\left(\frac{P}{E_n}\right) + \frac{R_o}{b} C\left(\frac{P}{E_n}\right)$$

$$F\left(\frac{P}{E_n}\right) = \left(1 - \frac{P}{E_n}\right) + \frac{R_o}{a} D\left(\frac{P}{E_n}\right) + \frac{R_o^2}{ab} G\left(\frac{P}{E_n}\right) + \frac{R_o}{b} H\left(\frac{P}{E_n}\right) \qquad (30)$$

Table 14. 9-1

Functions entering in equations 9-30 and 9-31

P/E_n	A	B	C	D	G	H	L	M	N	Q	S	T
0	.750	+.0879	+.187	0	−.0273	.125	.750	.0439	.1875	.3333	−.01367	0
.1	.659	0	+.296	−.0707	−.0311	.0964	.965	0	.1419	.242	−.0149	−.01653
.2	.542	−.0485	+.295	−.131	−.0286	.0647	.949	−.0434	.0944	.1454	−.01209	−.0284
.3	.4025	−.0785	+.252	−.178	−.0224	.0373	.861	−.0607	.0481	.0544	−.00688	−.0355
.4	.243	−.0826	+.190	−.211	−.0139	.0152	.344	−.0640	.00506	−.0248	−.000590	−.0381
.5												
.6	−.1286	−.0637	+.0608	−.223	+.00277	−.0101	.286	−.0318	−.0637	−.1278	+.00985	−.0318
.7												
.8	−.554	+.0155	−.0436	−.156	+.00801	−.0110	−.300	+.0345	−.0945	−.1287	+.00975	−.0152
.9												
1.0	−1.000	0	0	0	0	0	−1.000	0	0	0	0	0

APPROVED FOR PUBLIC RELEASE

Case (B) (see Figure 8)

$$f\left(\frac{P}{E_n}\right) = 1 + \frac{R_o}{a} L\left(\frac{P}{E_n}\right) + \frac{R_o^2}{ab} M\left(\frac{P}{E_n}\right) + \frac{R_o}{b} N\left(\frac{P}{E_n}\right)$$

$$F\left(\frac{P}{E_n}\right) = \left(1 - \frac{P}{E_n}\right) + \frac{R_o}{a} Q\left(\frac{P}{E_n}\right) + \frac{R_o^2}{ab} S\left(\frac{P}{E_n}\right) + \frac{R_o}{b} T\left(\frac{P}{E_n}\right) \quad (31)$$

The functions A, B, C, D, G, H, L, M, N, Q, S, T are given in Table 14.9-1.

14.10 USES OF RECOIL CHAMBERS

Recoil chambers are used for the following purposes:

(A) Relative flux measurements for neutron beams with the same energy distribution.

(B) Absolute flux measurement for monoenergetic neutron beams.

(C) Determination of the energy distribution of neutrons.

(D) Investigation of neutron scattering on light atomic nuclei.

For (A), (B) and (C) hydrogen recoil chambers are generally used.

No special precautions are needed in the construction of a chamber for relative measurements of neutron flux. High sensitivity, small physical size and directionality may be desirable features. Examples of chambers designed in order to satisfy one or the other of the above requirements will be found below.

The problem of building a chamber for absolute flux measurements is a much more difficult one. In the first place it is necessary to know the efficiency ε of the radiator. In the case of a gas recoil chamber, this implies an accurate knowledge of the sensitive volume, of the total gas pressure and of the concentration of hydrogen in the gas of the chamber. In the case of a solid radiator, the mass of the foil and its chemical

composition must be known accurately. The radiator is generally prepared by distillation in a vacuum, and if it is made of a material containing different chemical species (like ordinary paraffin), the composition of the foil may be different from that of the bulk material. Mainly for this reason, the radiators for quantitative flux measurements were prepared with glycerol-tristearate, which is a definite chemical compound, rather than with paraffin.

In the second place, one must determine the fractional number of recoils produced in the chamber which are detected with the specific experimental arrangement. If no collimation of the recoil protons is used (see below), the pulses obtained range in size all the way from zero to a maximum. Only pulses above a certain size, B, are detected, where B is determined by the bias setting. It is necessary to first know B in absolute value, i.e., in terms of energy, and then to evaluate the quantity $F(B/E_n)$ which represents the fractional number of recoils giving pulses larger than B. This requires a simple geometrical design of the chamber, so that $F(B/E_n)$ may be calculated theoretically. Also, it requires an experimental check of the calculated pulse height distribution. The experimental check is necessary for the following reasons:

(A) It provides the only reliable method for the calibration of the bias setting in terms of energy; i.e., for the absolute determination of B.

(B) It determines the lowest bias at which only hydrogen recoils are detected. In addition to hydrogen recoils, one usually has in the chamber recoils of other light nuclei (argon, carbon, etc.), and also secondary electrons produced by γ-rays. If the resolving time of the detecting equipment is not small compared with the average time separation of the spurious pulses, these latter will

"pile up" and give rise to pulses larger than those which an individual recoil or secondary electron could produce (see Section A.12). The bias at which spurious pulses of the type described above start being counted is generally characterized by a sudden departure of the experimental from the theoretical pulse height distribution curve.

(C) Finally, in many cases it is found that the experimental pulse height distribution curves do not agree with the calculated ones, even for bias energies at which one would not expect to detect pulses due to spurious recoils or to secondary electrons from γ-rays. One can think of many reasons which may explain discrepancies between experiment and theory, such as:(1) lack of monochromaticity of the neutrons, either inherent in the neutron source or produced by inelastic scattering of the neutrons in the material of the chamber; incorrect evaluation of the edge effects (see Section 10.7); range straggling or error in the evaluation of the energy-range relation (only likely in the low energy region); lack of proportionality between number of ions and pulse height; or spread in pulse height when chambers with gas multiplication are used (see Section 11.6). Often it is not possible to determine what the source of the trouble actually is, but it is clear that no chamber should be used for absolute neutron flux measurements unless the theoretical and experimental pulse height distribution curves agree.

It may be pointed out that the measurement of the differential pulse height distribution provides a much more rigorous check on the behavior of the chamber than the determination of the integral pulse height distribution. It may also be pointed out that for accurate results one must be able to set the bias

sufficiently low to count a large fraction of the recoils produced in the radiator.

Another possible method for determining the ratio of the number of recoils detected to the total number of recoils produced is to collimate the recoil protons in such a way that only protons ejected within a certain angle, θ_o, with respect to the direction of the incoming neutrons, enter the chamber. These protons have energies above $E_n \cos^2 \theta_o$, and if this value is sufficiently large, one can adjust the bias so that all of the protons are detected. In this way, the fractional number of recoils detected is determined by the geometrical arrangement rather than by the bias setting. An example of a detector based on this principle will be discussed in Section 19.

Finally, one may use a gas recoil, integrating, ionization chamber (see Section 8) for absolute measurements of neutron flux. An instrument of this type will be described in Section 18.

The chambers used as neutron spectrometers must satisfy requirements somewhat different from those laid down for the chambers used for absolute flux measurements. Only the energy dependence of the efficiency, but not its absolute value, needs to be known. On the other hand, the pulse height distribution for monoenergetic neutrons must be accurately known, and, also, it must be of a sufficiently simple shape so that the neutron spectrum may be calculated from the observed distribution of recoil pulses.

In principle, one could make an ideal neutron spectrometer by using a very thin radiator and by having both the incident neutrons and the recoil protons well collimated. In such a way, one would obtain pulses of a single size for each neutron energy. The drawback to this scheme is a low sensitivity caused by the double collimation, and for this reason no detectors of the type described were built at the Los Alamos Laboratories, even though they may be useful for some specific applications.

The next best choice for a neutron spectrometer is a chamber in which a monoenergetic neutron beam gives a constant differential pulse height distribution (infinitely thin radiator, ion pulse chamber; gas recoil, ion pulse chamber of very large dimensions, etc.). In this case, if $N(E_n)\,dE_n$ represents the number of incident neutrons with energy between En and $E_n + dE_n$, and $\psi(P)dP$ represents the number of pulses observed with the height between P and P + dP, the following equation holds (see Equation 14):

$$\psi(P)dP = \text{constant} \int_{E_n=P}^{\infty} N(E_n)\ \sigma_s(E_n)dE_n \left(\frac{dP}{E_n}\right)$$

From this it follows: (32)

$$N(E_n) = \text{constant}\ \frac{E_n}{\sigma_s(E_n)} \left(\frac{d\psi}{dP}\right)_{P=E_n}$$

Chambers approaching this type were built and used successfully (see Sections 11 and 12).

With regard to the chambers to be used for the investigation of scattering cross-sections, it will suffice to note that they must be of sufficiently simple design so that from the observed pulse height distribution one may be able to deduce the energy distribution of the recoils. Equation 4 shows that the energy distribution of recoils in the laboratory system gives the differential scattering cross-section in the center of gravity system.

14.11 HIGH PRESSURE, GAS RECOIL ION PULSE CHAMBER

Figure 9 shows the construction of a chamber used as a neutron spectrometer. This chamber is similar in its design to one described by Barschall and Kanner in Physical Review, 58, 590 (1940). The sensitive volume is a cylinder 8.5 centimeter

in diameter and 8.5 centimeters high. In order to obtain a sufficiently high field through the large sensitive volume, the latter is divided into six sections by means of metal grids made of annealed copper wire of 0.008 inch diameter, the mesh width being 1/8 inch. The transparency of each grid is thus about 87 per cent. The solid plates, which limit the sensitive volume at the top and at the bottom, as well as grids (2) and (4), are connected together and form the high voltage electrode. Grids (1), (3) and (5) are similarly connected together and form the collecting electrode. Each of the three grids which forms the collecting electrode is mounted on a thin brass ring. This is supported by a wider brass ring, the guard electrode, by means of two small amber beads. Each of the three also carries a tongue which protrudes through a slot of the guard electrode into a grounded brass tubing containing the connecting lead for the three collecting grids (see detail). The capacity of the collecting electrode assembly is approximately 60 micromicrofarads.

The chamber was used with pressures up to 26 atmospheres of pure hydrogen or of hydrogen-argon mixtures. Before admitting it into the chamber the gas was freed from organic vapors and from water. A small amount of oxygen (0.01 per cent) was added in order to produce negative ions and thus avoid the fast part of the pulse due to the motion of free electrons. The chamber was usually operated at 6000 volts. The pulse amplifier had a rise time of 0.5 milliseconds and a decay time of 2.0 milliseconds. This small band width was used in order to minimize the noises. The chamber, despite its sturdy construction, is very sensitive to microphonic disturbances. It is also very sensitive to γ-rays because of the high pressure used. The large value of the decay time constant of the amplifier, which is required in order to avoid excessive distortion of the ion pulses, enhances the probability of large spurious pulses produced by

Figure 9

High pressure gas recoil chamber (see Section 11)

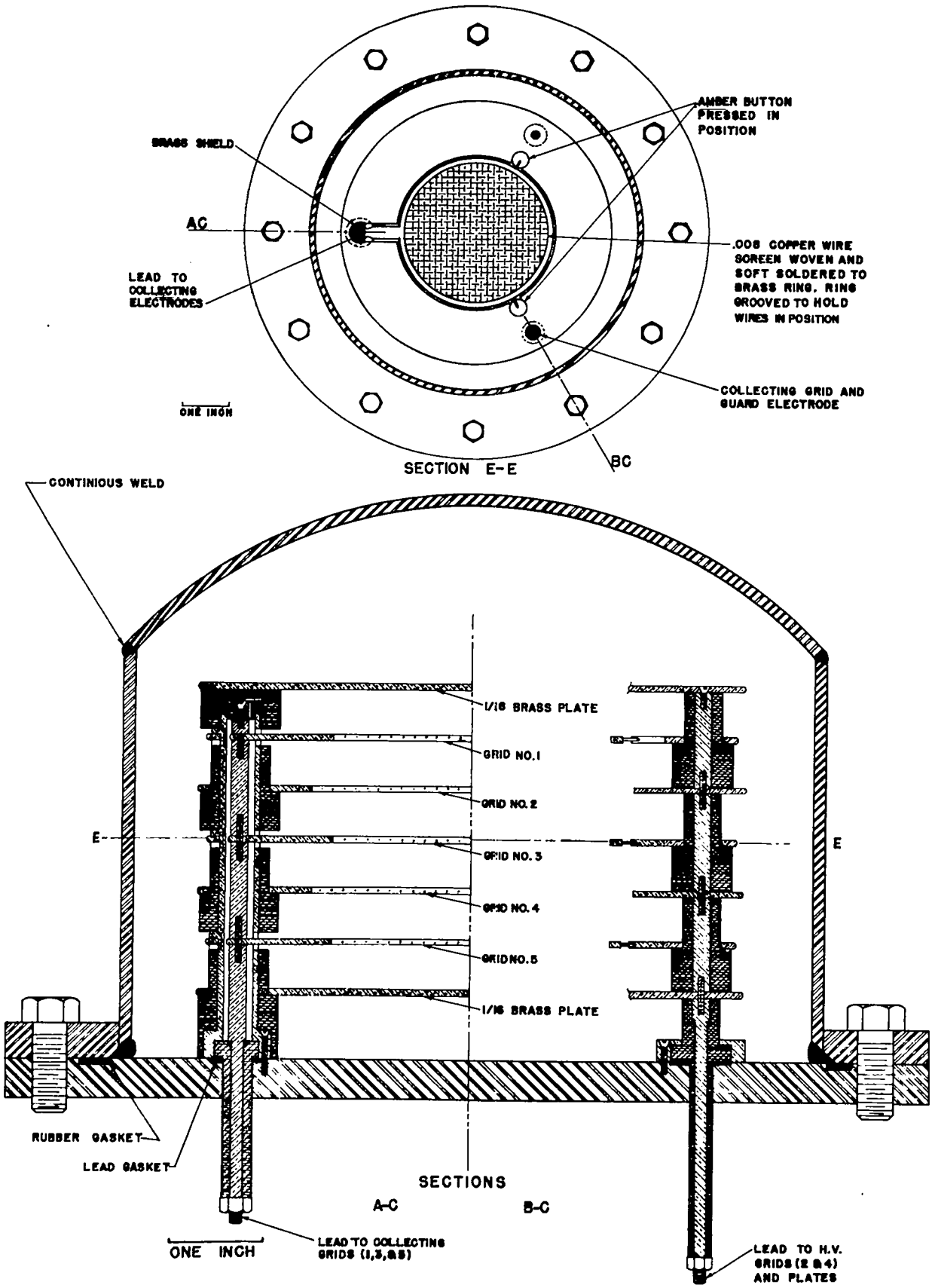

the piling up of γ-ray pulses. In the absence of γ-rays, it was found possible to record recoil protons down to an energy of about 0.6 million electron volt.

The advantages of the chamber are high counting yield (of the order of 1 or 2 per cent) and lack of directionality (except for the wall effect corrections).

The wall effect corrections can be expressed by the following equation, which gives the differential pulse height distribution:

$$f\,(P/E_n,\ E_n) = \alpha\,(E_n)\left[1 + u(E_n)\,E_n\,(1 - P/E_n)\right] \qquad (33)$$

The quantities α and u depend on the neutron energy E_n and on the gas pressure. For a sufficiently high pressure, or for a sufficiently low energy ($\alpha = 1, u \neq 0$), Equation 33 goes over into Equation 15, which represents the pulse height distribution when wall effects can be neglected (see Section 8). For a gas filling, the stopping power of which is equivalent to that of 39 atmospheres of H_2, α is represented by the curve in Figure 10, while $u(E_n)$ is approximately given by the expression

$$u(E_n) = 0.23\,(E_n - 0.6) \qquad \text{for } E_n > 0.6$$

$$u(E_n) = 0 \qquad \text{for } E_n < 0.6$$

where E_n is measured in million electron volts. The neutrons are assumed to travel in a direction perpendicular to the electrodes of the chamber.

The performance of the chamber was tested by irradiating it with monoenergetic neutrons of 2.5 million electron volts energy obtained from the D-D reaction. The observed pulse height distribution is represented by curve (a), Figure 11. Curve (b) in the same figure represents the energy spectrum of the primary neutrons, as computed from the observed recoil distribution,

Figure 10

Values of the function $\propto E_n$, which enters in Equation 33

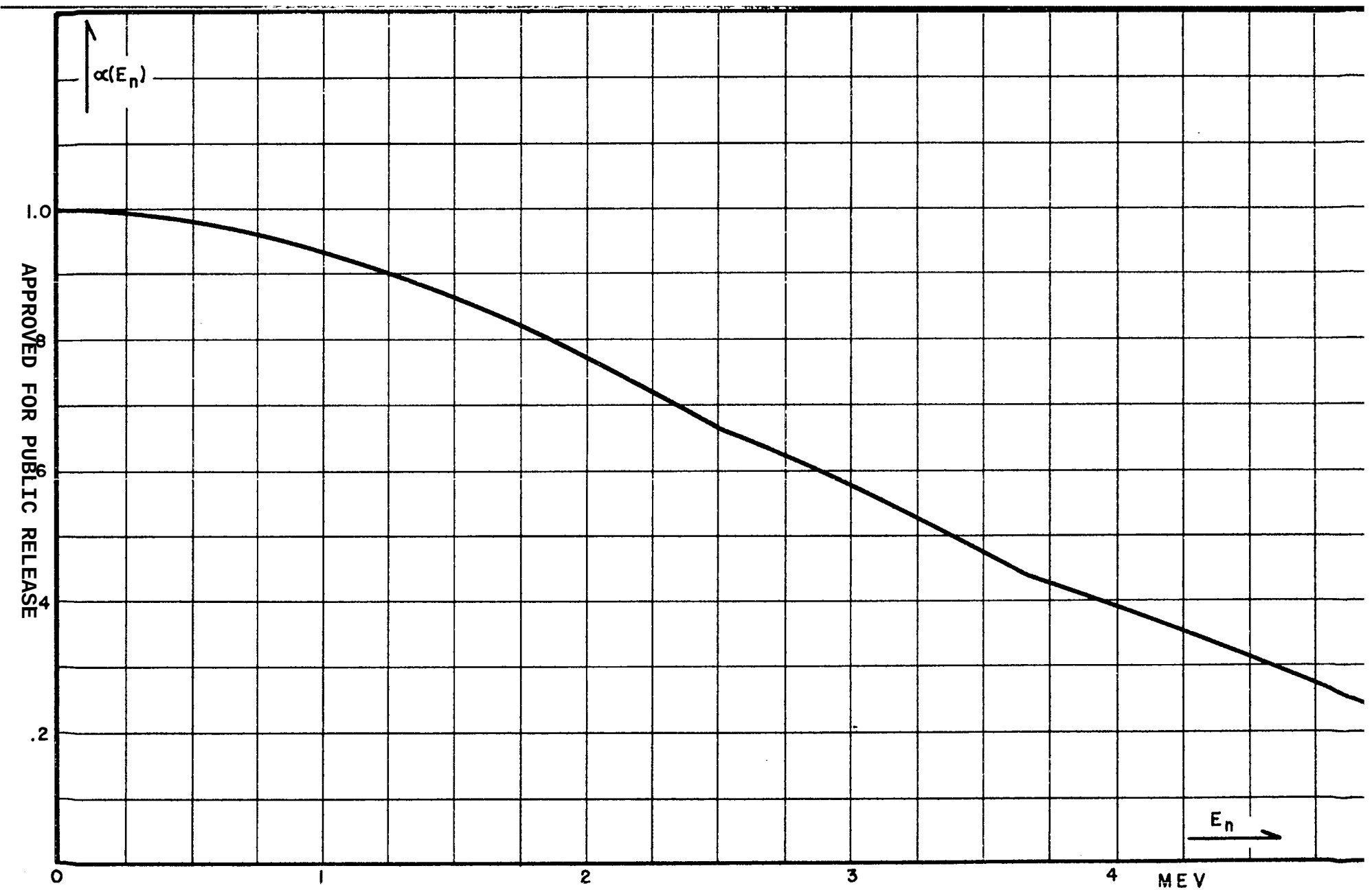

APPROVED FOR PUBLIC RELEASE

Figure 11

Differential pulse height distribution of hydrogen recoils obtained by means of the chamber described in Section 11 irradiated with monoenergetic neutrons of 2.5 million electron volts energy (curve (a)). Curve(b) represents the energy spectrum of the primary neutrons, as computed from the observed recoil distribution. Gas filling: 13.8 atmospheres of argon plus 2.73 atmospheres of hydrogen.

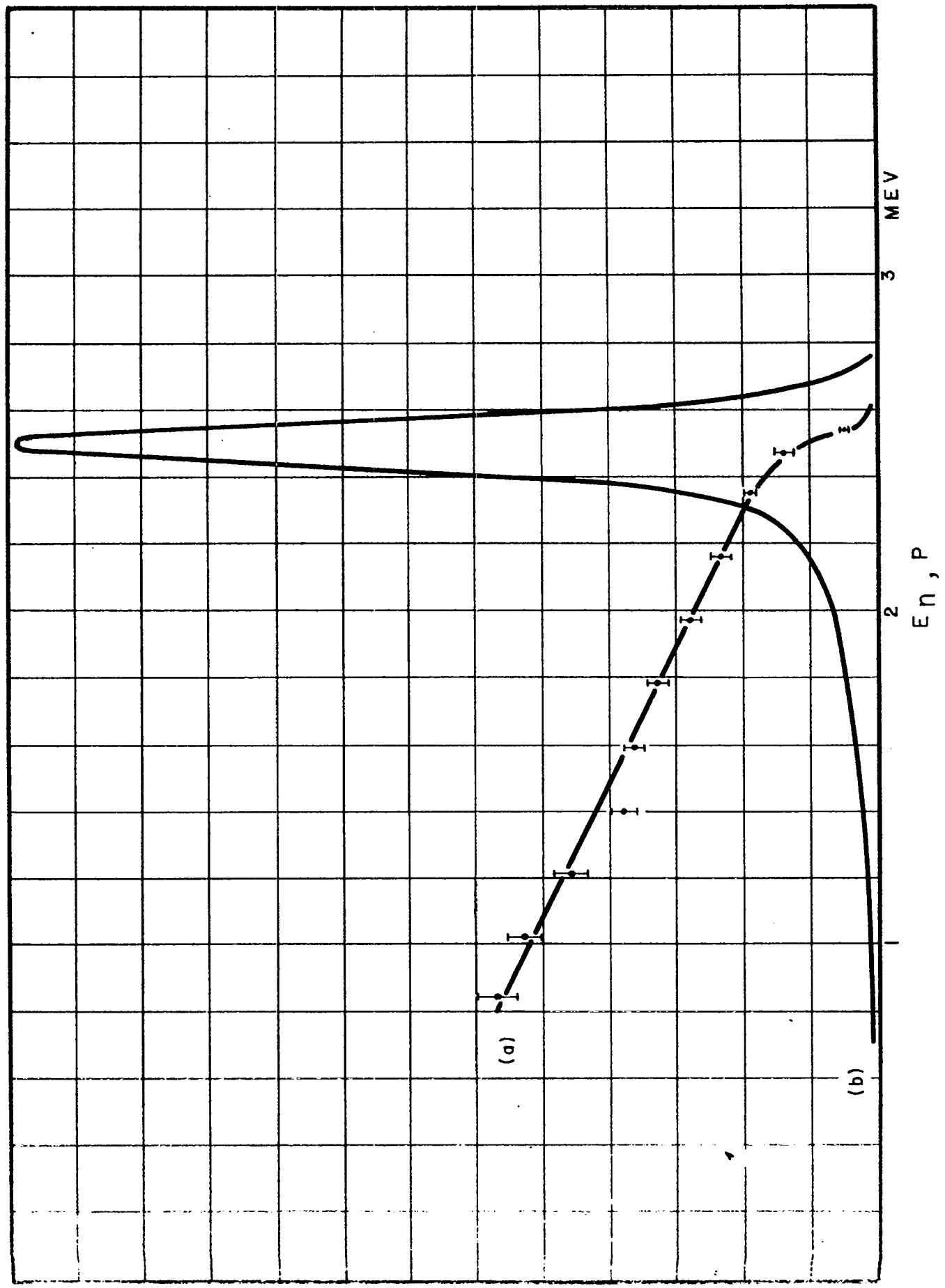

taking into account the wall corrections. The extent to which curve (b) approximates an infinitely narrow distribution gives a measure for the accuracy of the experimental method.

14.12 THIN RADIATOR, ELECTRON PULSE, PARALLEL PLATE CHAMBER

Figure 12 shows the construction of a chamber used for absolute measurements of neutron flux and as a neutron spectrometer. The chamber is filled with argon and pressures up to 7 atmospheres can be used. A hot calcium purifier is permanently connected to the chamber through two 3/8 inch steel pipes, not shown in the diagram. This makes it possible to purify the gas whenever necessary. The chamber is normally operated at -2000 volts.

The radiator is a glycerol-tristearate film of about 180 γ per square centimeter prepared by evaporation in a vacuum. It is placed on a platinum foil, which is part of the high voltage electrode. Extensive tests were made in order to make sure that the conductivity of the foil was sufficiently large to prevent accumulation of charges which might disturb the electric field and therefore distort the pulse height distribution. For this purpose, a polonium source was deposited on a platinum foil and then covered with a glycerol tristearate film. The platinum foil thus prepared was placed in the chamber in place of the radiator and the pulse height distribution of the α-particles was determined. Then a 1 gram radium source was placed near the chamber so as to produce an intense ionization of the gas. The radium source was removed and the pulse height distribution was remeasured immediately afterwards. The pulse height distributions measured before and after irradiation proved to be identical. This result was taken as a proof that, even in the presence of an ionization much heavier than that existing under normal operating conditions, the glycerol tristearate film does not acquire an amount of charge sufficient to distort the pulse height distribution.

Figure 12

Solid radiator, parallel plate chamber (see Section 12)

(1) Grid supported on brass ring.

(2) Two mil platinum foil which bears the glycerol tristearate radiator.

(3) Collecting electrode.

(4) Guard electrode.

(5) H.V. electrode.

(6) Lead to the collecting electrode insulated from the base plate with G.E. Kovar glass seal.

(7) H.V. lead insulated from the plate with a G.E. Kovar glass seal (a similar lead, not shown in the diagram, provides the connection to the grid).

(8) Sylphon bellows.

(9) Structure with keyway for lifting and rotating the radiator in or out of position. The figure shows the radiator lifted out of position. A similar structure supports a blank platinum foil which may be substituted for the radiator in order to determine the background.

(10) Soft metal gasket.

(11) Steel plate, 1/4 inch thick.

(12) Steel shell, 1/16 inch thick.

(13) Glass insulators. The ends are platinized and soldered to brass caps.

(14) Cross-section of a U-shaped yoke carrying the knurled screw.

(15) Keyway for rotating radiator.

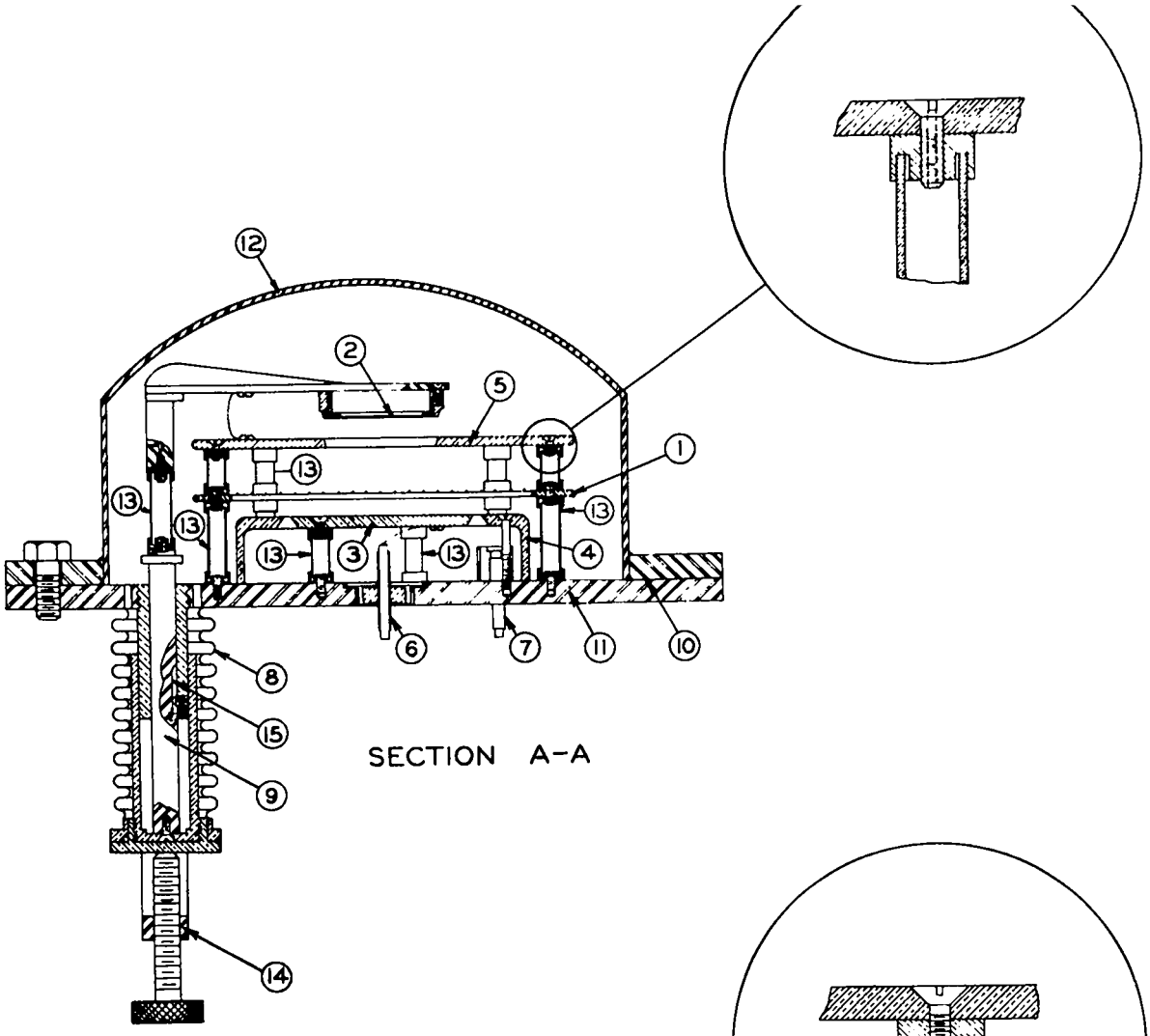

SECTION A-A

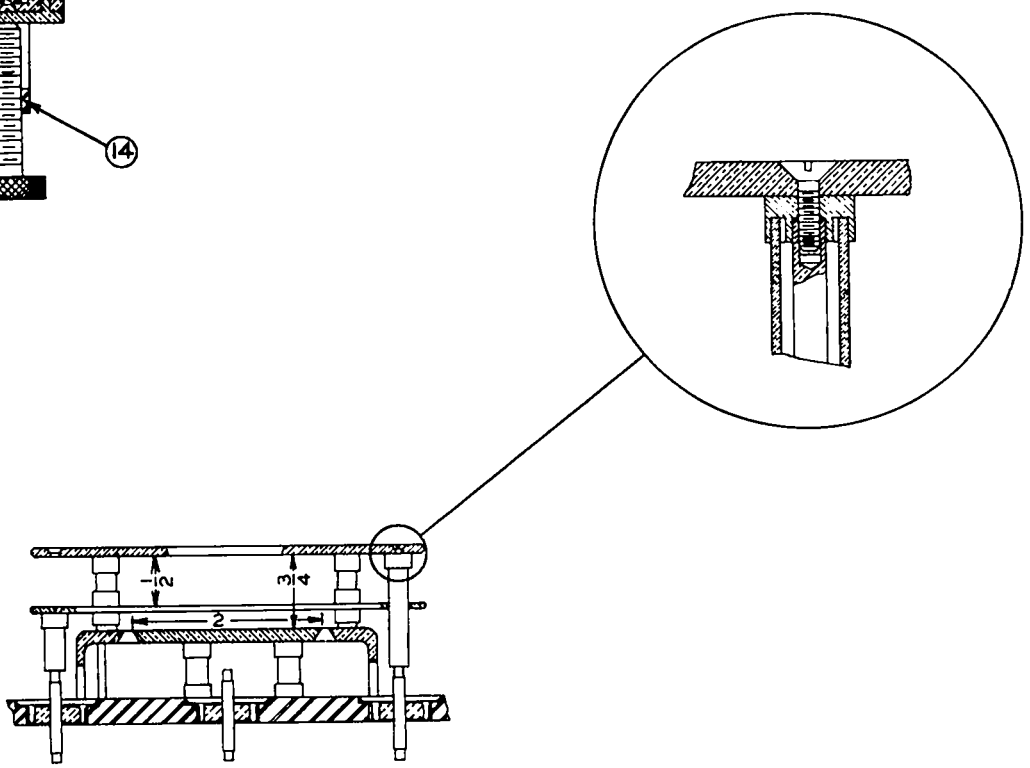

SECTION B-B

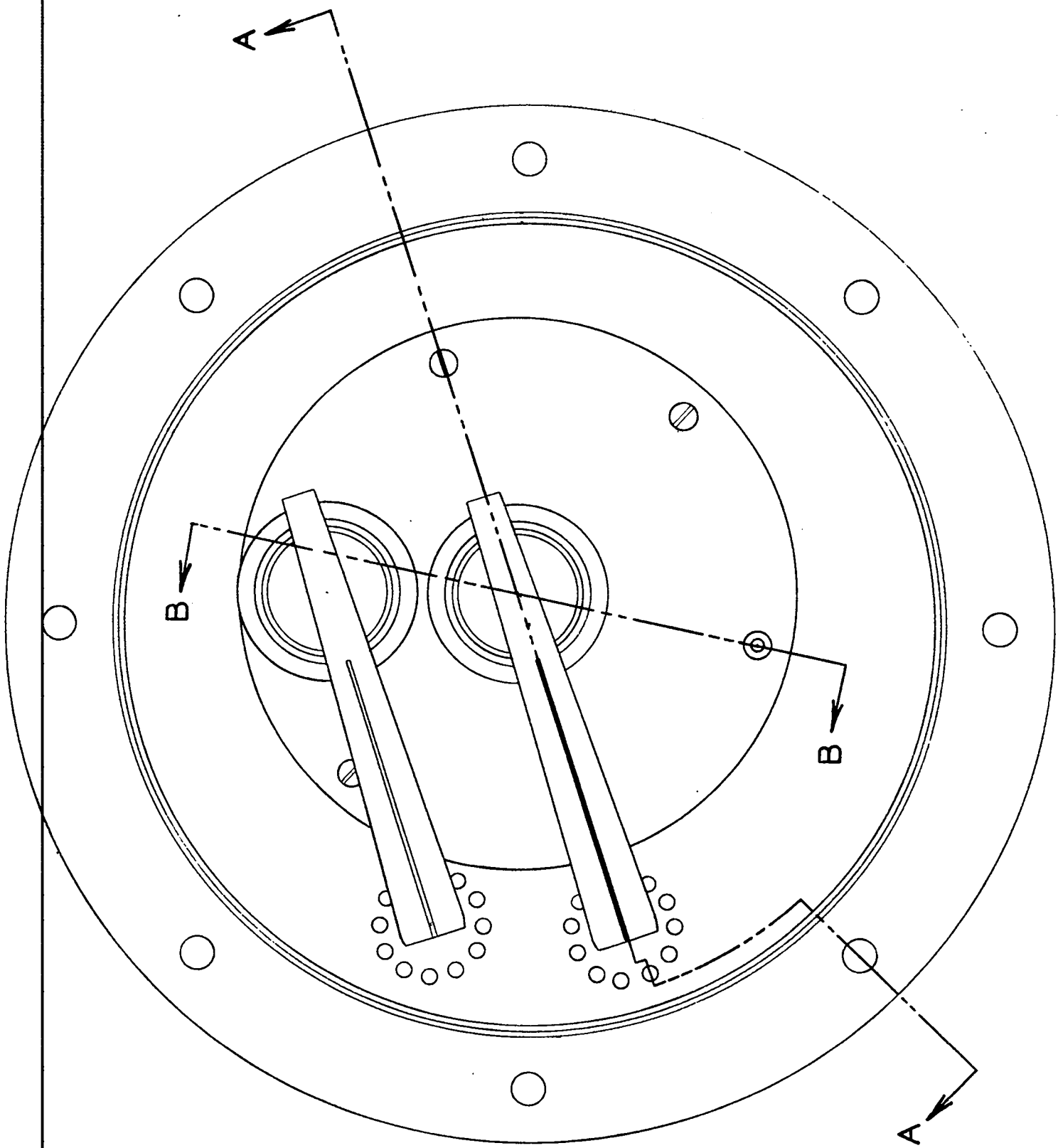

The collecting electrode and the attached lead have a capacity of 10 to 15 micromicrofarads. The chamber was used with an amplifier having a rise time of 2 microseconds and a decay time constant of 20 microseconds. The small value of the latter time constant practically eliminates microphonic disturbances and makes it possible to operate the chamber in the presence of a fairly strong γ-radiation. The minimum pulse height which can be measured safely is approximately 0.2 million electron volt. The maximum neutron energy for which the chamber can be used is determined by the condition that the maximum range of the recoil protons should be not more than 5/9 the spacing of the electrodes (see Section 4). This energy is about 2 million electron volts.

In the construction of the chamber care was taken to avoid heavy materials in the path of the incident neutrons so as to minimize the danger of inelastic scattering. All metal parts in contact with the active volume of the chamber were gold-plated and then outgassed by heating in vacuum in an effort to minimize the background caused by recoils from hydrogen absorbed in the metal. This background was experimentally determined by irradiating the chamber with neutrons after replacing the radiator with a blank platinum foil. The number of recoils recorded under these conditions was about ten per cent of the number recorded with the radiator in place.

The chamber can be used with or without the grid (1) shown in Figure 12. When used, the grid is kept at a voltage of -1400 volts with respect to the collecting electrode (the high voltage electrode being at -2000 volts). In both conditions, the operation of the chamber was tested by determining the pulse height distribution with a polonium source on a platinum foil in place of the radiator. Without any grid, one should expect a "rectangular" pulse height distribution if the measurements are taken with a channel discriminator

of infinitesimal width, or a "trapezoidal" pulse height distribution if a channel discriminator of finite width is used (see Section 13.1).

With the grid, one should expect all the α-particle pulses to be of the same size (see Sections 10.2 and 13.1). The experimental curves obtained confirm this prediction (see Figures 13.1 and 13.2).

The chamber was also tested, again with and without the grid, by determining the pulse height distribution of the hydrogen recoils when the chamber is placed in a monoenergetic neutron beam, falling normally upon the radiator. The curves obtained were of the expected shape. As an example, Figure 13 gives the results of measurements taken with the grid in position, in which case, if an infinitely narrow channel were used and if the radiator were infinitely thin, one should obtain a "constant" pulse height distribution as described in Section 3.

14.13 THIN RADIATOR, ELECTRON PULSE, PARALLEL PLATE DOUBLE CHAMBER

This chamber, based on the same principle as that described in Section 12, was designed primarily for the purpose of measuring fission cross-sections. It consists essentially of a fission chamber and a recoil chamber in the same case, the latter being used as a neutron flux meter. The fissionable material and the thin layer of hydrogenous material are deposited on two thin platinum foils which are placed back to back and constitute the common high voltage electrode of the two chambers. Thus the two samples are almost exactly in the same plane and are separated by an amount of material which does not produce any appreciable amount of scattering or absorption of the neutron beam. The neutron flux is therefore the same for both samples and the ratio of the cross-sections is simply equal to the ratio of the number of processes per gram atom of the active material.

Figure 13

Differential pulse height distributions obtained with the chamber with grid shown in Figure 12 irradiated with monoenergetic neutrons of two different energies.

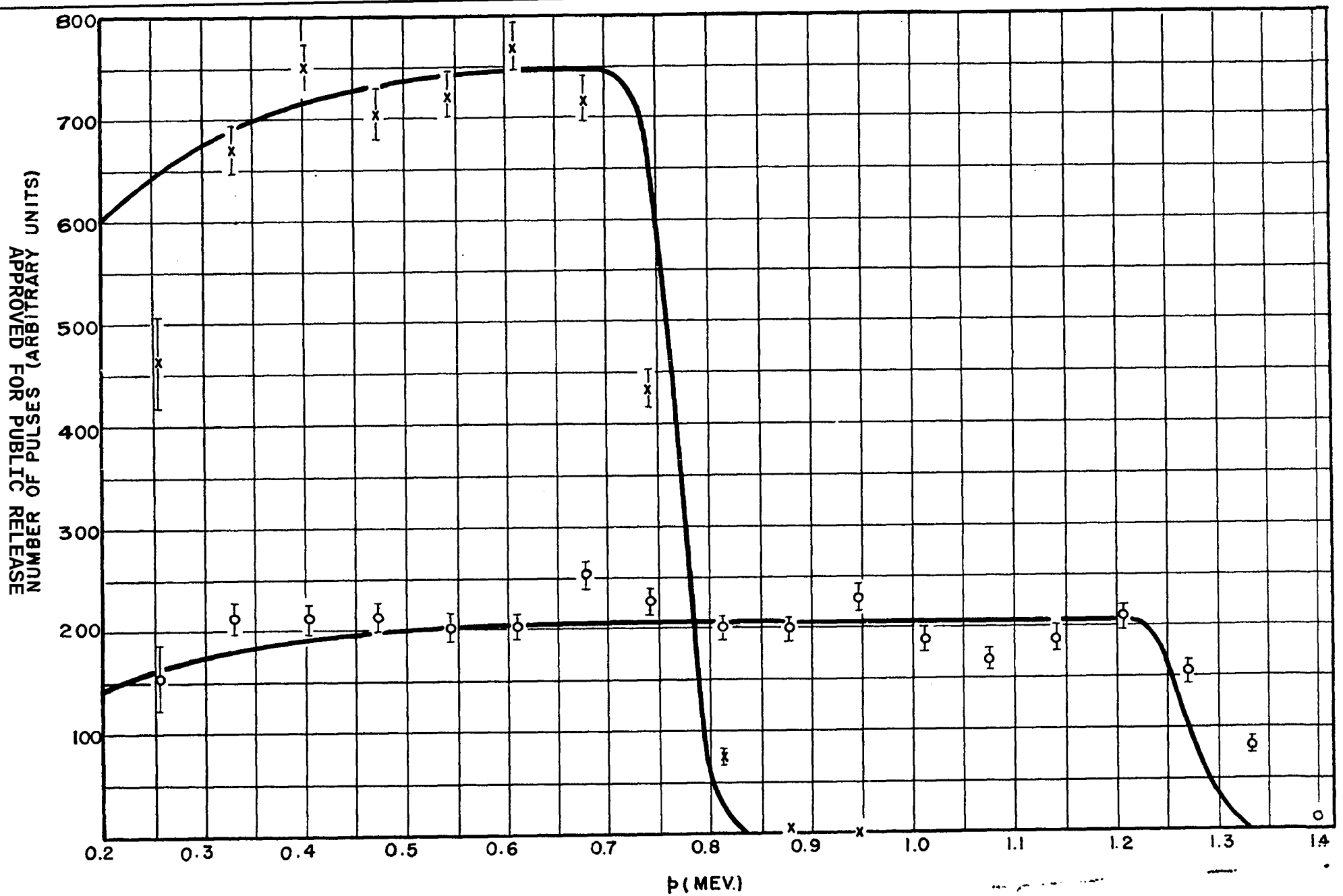

APPROVED FOR PUBLIC RELEASE

The construction details of the chamber are shown in Figure 14. Extreme care was taken to avoid any heavy material along the path of the neutron beam, so as to minimize the danger of scattering and absorption of neutrons. The chamber walls were made as thin as suitable for the pressure they had to withstand. Only glass insulators were used inside the chamber. The seal between brass cap and the base plate was made gas-tight by means of a fuse wire gasket, so that no other materials but metal and glass are in contact with the gas. The leads to the collecting electrodes and to the high voltage electrode were shielded from each other by the brass tubes supporting the chamber (see Figure 14).

Both argon and xenon, at pressures up to about 9.5 atmospheres, were used as gas fillings. A hot calcium purifier was permanently attached to the chamber. The chamber was operated at a voltage between 2000 and 3000 volts, depending on the pressure, with the high voltage electrode negative.

As hydrogenous radiators, glycerol tristearate films of various thicknesses were used. In order to avoid edge effects (see Section 10.7), the diameters of the hydrogenous foil and of the fission foil were chosen so that the ranges of all hydrogen recoils and fission fragments were well within the sensitive volumes of the chambers.

The amplifier used with the recoil chamber had a rise time of 0.5 microseconds and a decay time of 20 microseconds. The pulses were analysed with an electronic channel discriminator.

The operation of the chamber was tested with polonium α-particles, as described in Section 12. In addition, the pulse height distribution of hydrogen recoils was measured for a number of neutron energies. In these measurements, the plates of the chamber were perpendicular to the neutron beam with the glycerol tristearate film facing away from the

Figure 14

Double recoil and fission chamber (see Section 13)

APPROVED FOR PUBLIC RELEASE

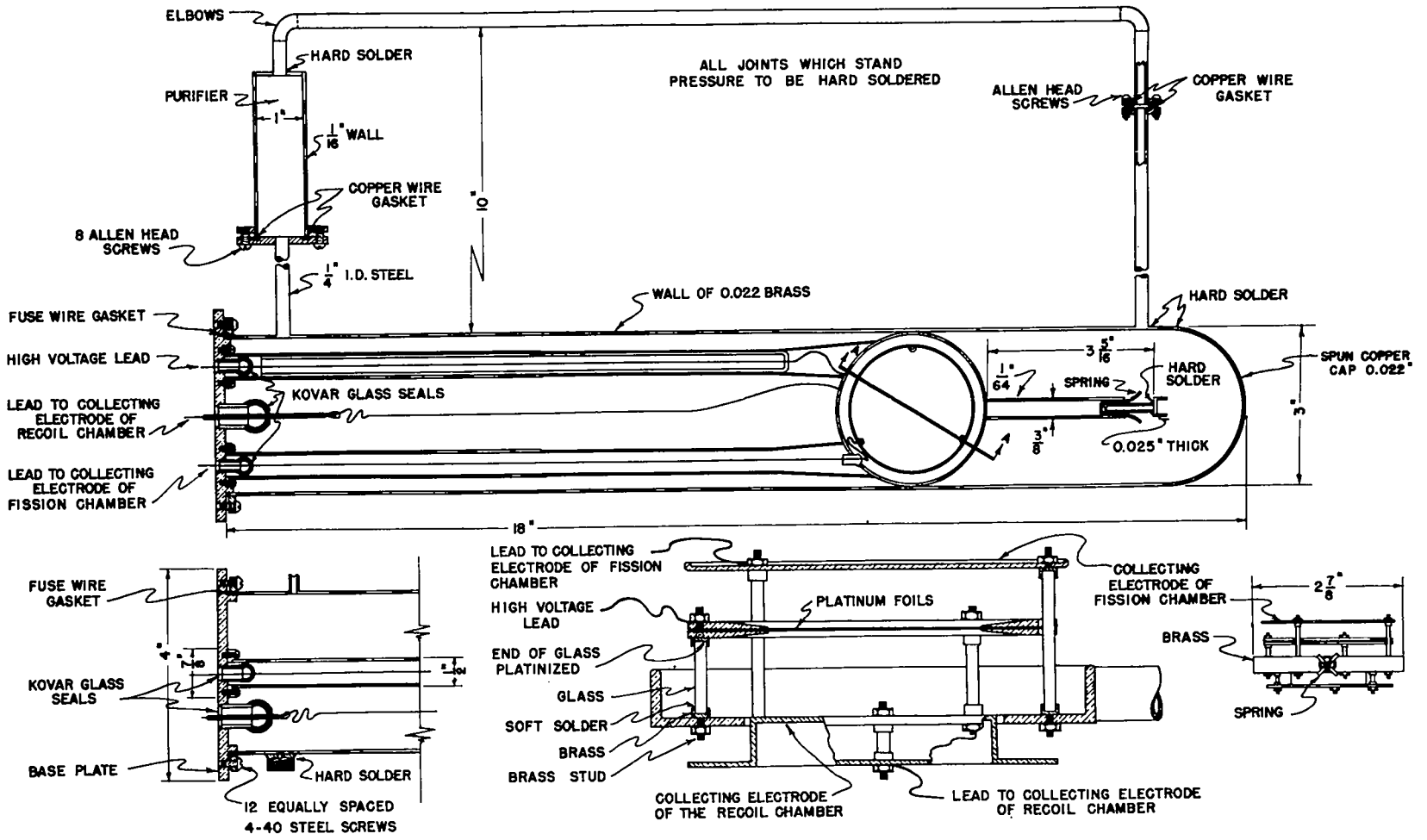

SECTION A-A

Figure 15

Differential pulse height distribution curves of hydrogen recoils obtained with the chamber described in Section 13 by using monoenergetic neutron beams perpendicular to the radiator. The channel shapes are indicated in each graph. Experimental results are represented by dots, circles or crosses. The vertical bars give the standard statistical errors. Points differently marked refer to different sets of measurements. The dotted lines are theoretical curves without channel correction. The solid lines are theoretical curves with channel corrections.

Graph A E_n = 0.457 Mev; t = 67 γ/cm^2; 3 atmospheres argon.

Graph B E_n = 0.57 Mev; t = 67 γ/cm^2; 3 atmospheres argon.

Graph C E_n = 1.0 Mev; t = 173 γ/cm^2; 6.7 atmospheres argon.

Graph D E_n = 1.6 Mev; t = 173 γ/cm^2; 9.5 atmospheres argon.

Graph E E_n = 2.6 Mev; t = 173 γ/cm^2; 9.0 atmospheres xenon.

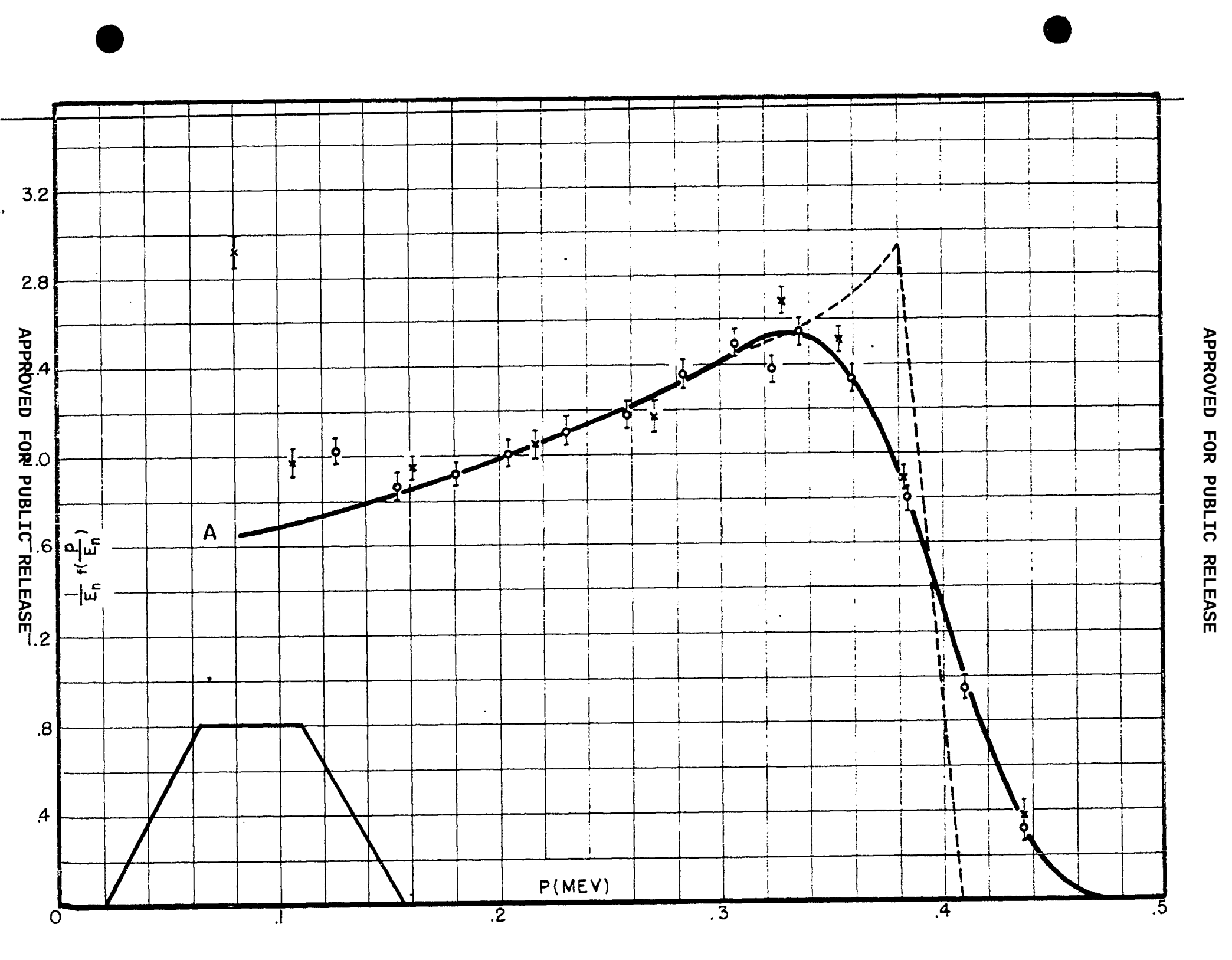

APPROVED FOR PUBLIC RELEASE

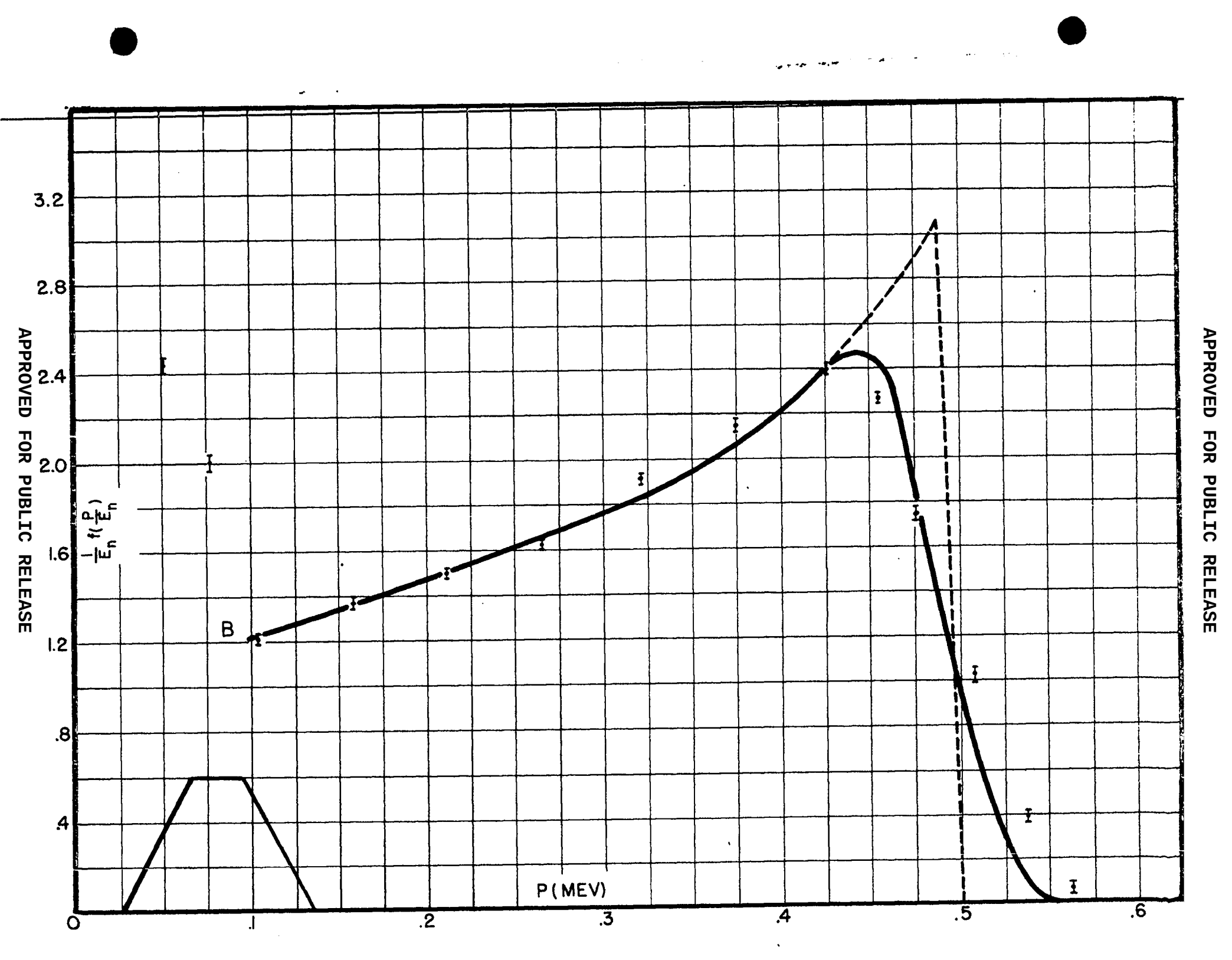

APPROVED FOR PUBLIC RELEASE

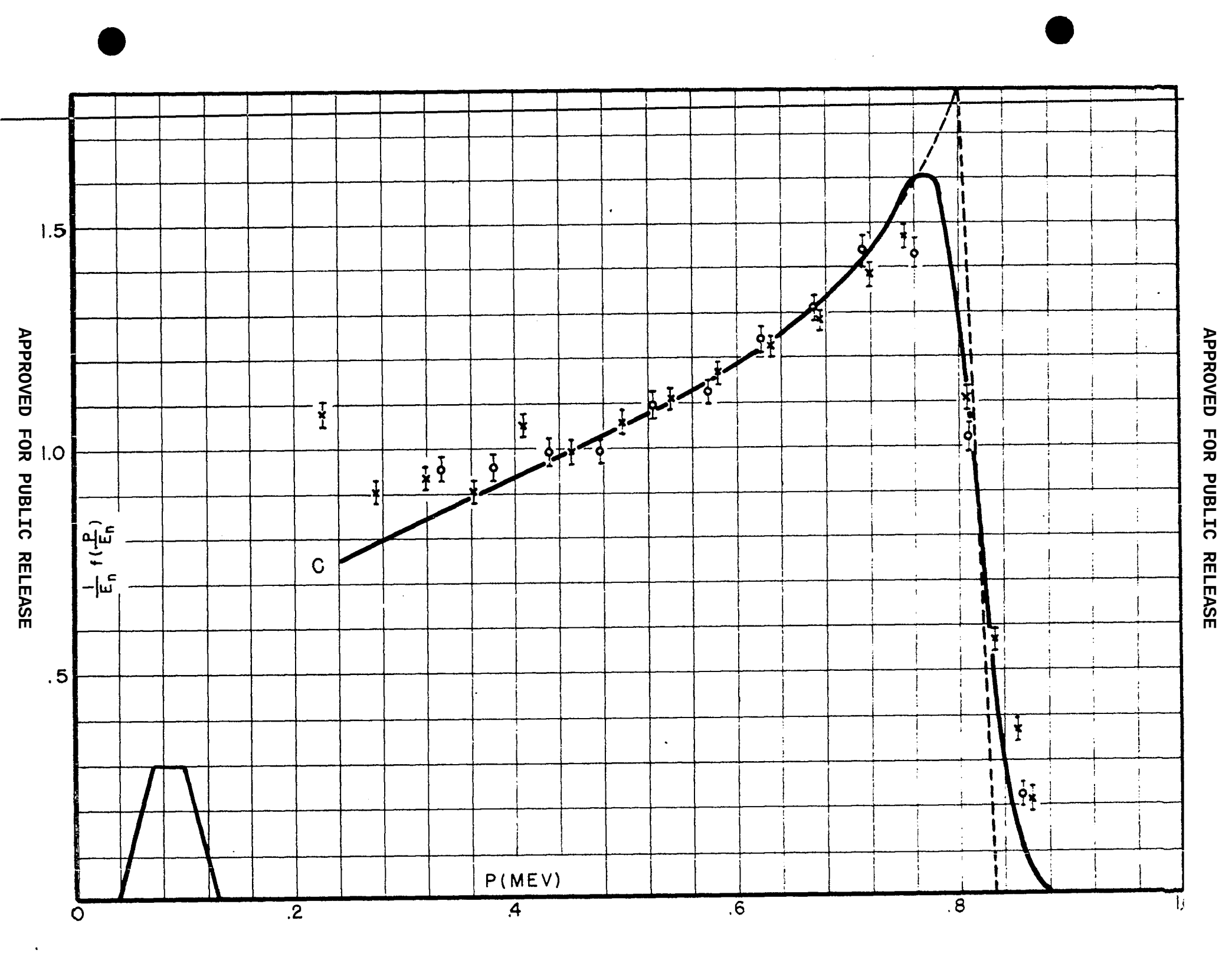

APPROVED FOR PUBLIC RELEASE

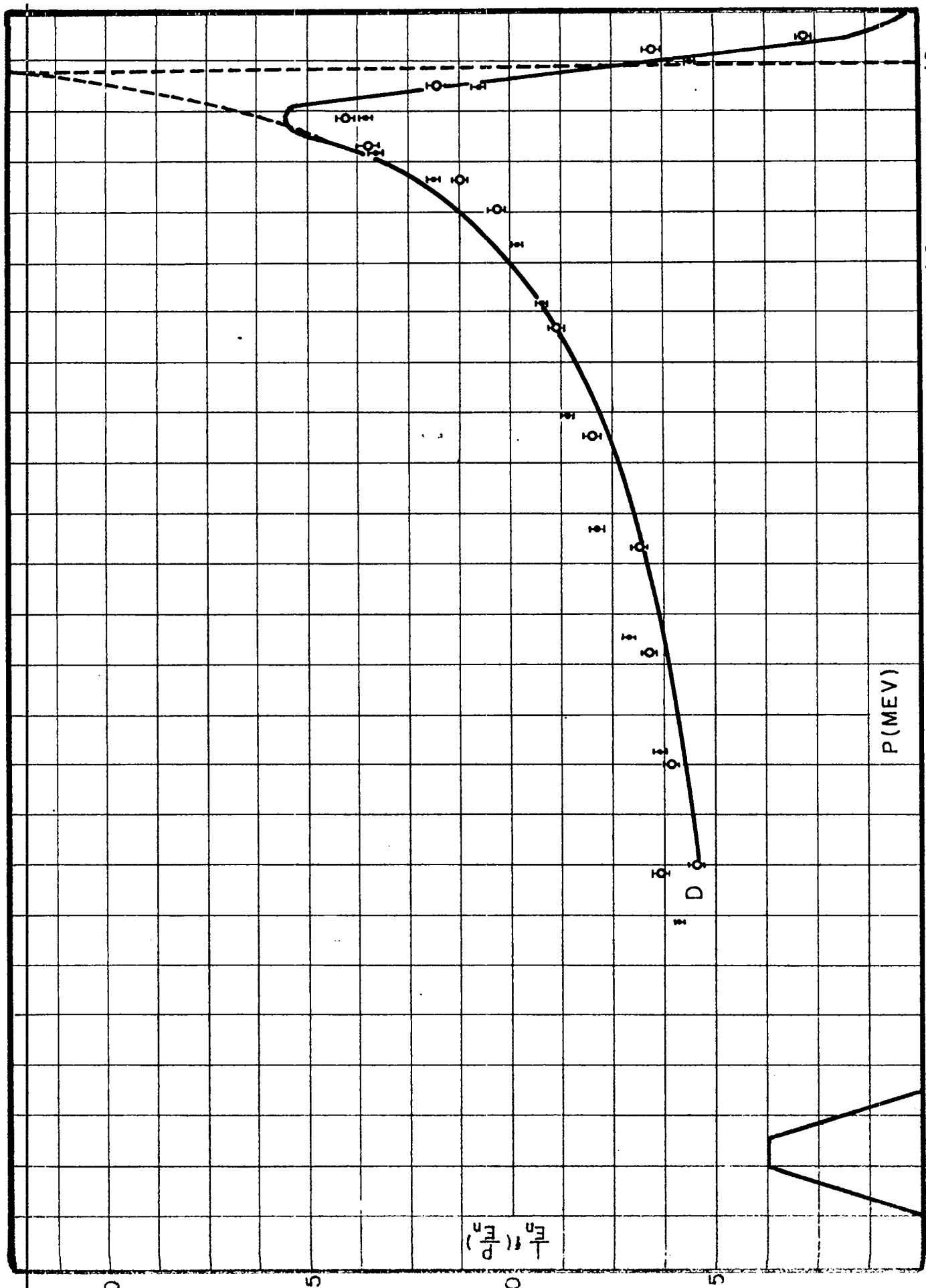

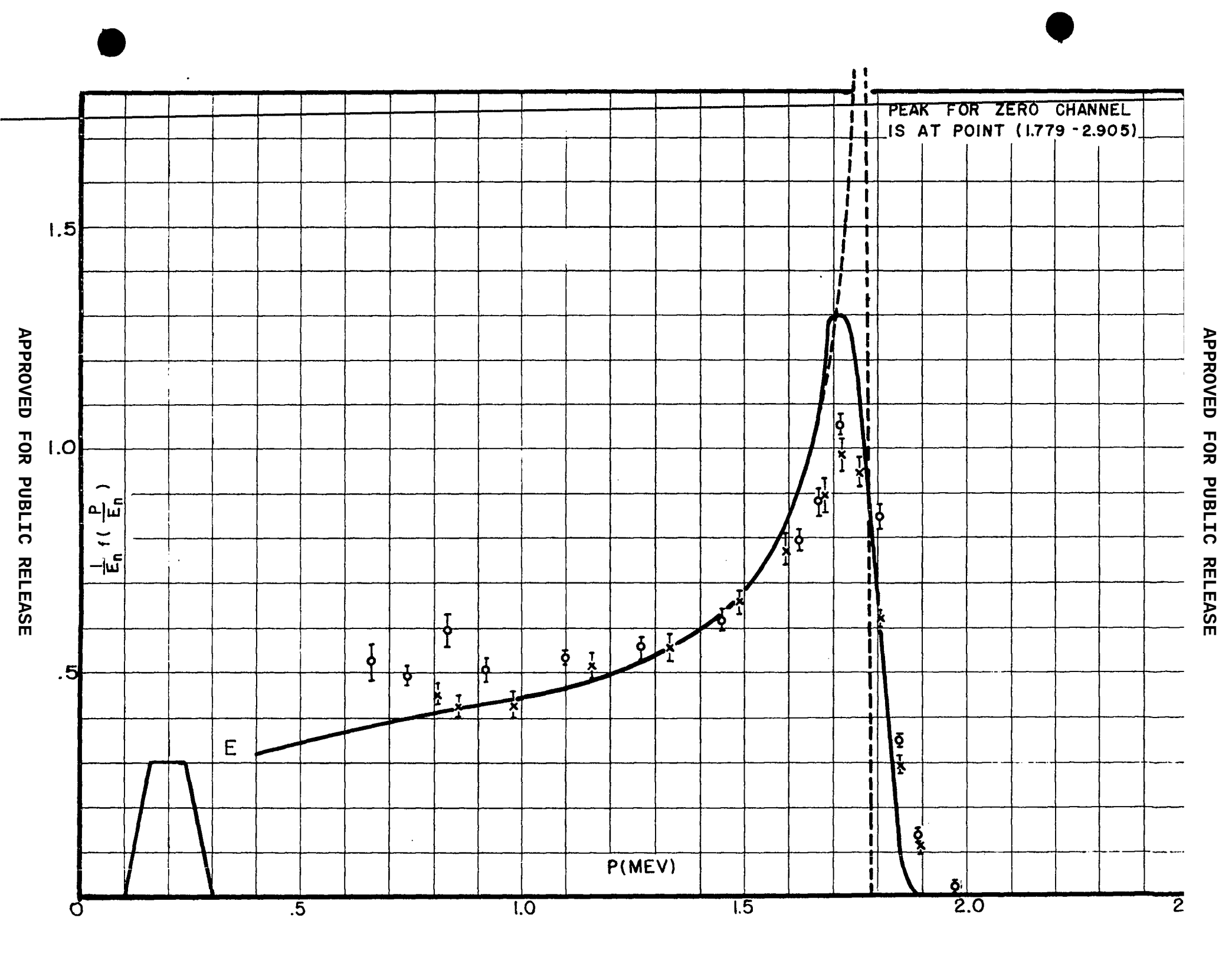

APPROVED FOR PUBLIC RELEASE

neutron source. Some of the results obtained are reproduced in Figure 15, where the corresponding theoretical curves (see Section 6) are also given. A channel correction was applied to the theoretical curves. This correction was determined experimentally by means of artificial pulses. The shape of the channel which is indicated in each curve was found to be approximately trapezoidal, the deviation from a rectangle, of course, being due to noises. The abscissae of the experimental and theoretical curves were matched at the high energy end near the point of steepest descent, where the influence of the channel correction is a minimum. The ordinates were matched a little below the peaks of the curves.

It appears from an inspection of the figures that the agreement between theoretical and experimental pulse height distribution curves is excellent. The deviations at the low energy end are caused by spurious pulses produced by piling-up of argon recoils or of electron recoils from γ-rays. The energy at which these effects set in depends, of course, on the experimental conditions. The directionality of the chamber was tested by taking counts with the chamber inverted; i.e., with the glycerol tristearate film perpendicular to the beam but facing the neutron source. Under these conditions, and with neutron energies around 1 million electron volt, the counting rate was found to be about 3 per cent of that recorded in the same neutron beam with the chamber in normal position. The per cent counting rate increases somewhat with increasing energy and is about 5 per cent around 1.8 million electron volts. Tests were also made with a blank platinum foil in place of the radiator. In most cases, the counting rate with the blank was about 2 per cent of that recorded with a radiator of 173 γ per square centimeter thickness.

14.14 GAS RECOIL, CYLINDRICAL CHAMBER

Figure 16 shows the construction of a chamber which was used for measuring differential scattering cross-sections of light nuclei. The chamber is cylindrical in shape with a thin wire as the collecting electrode. It is built as light as possible in order to minimize inelastic scattering and absorption of neutrons. The chamber can be used both with and without gas multiplication and in either case the outer cylinder is kept negative with respect to the wire. The recoils under investigation arise from the gas. In order to reduce the wall effects it is advisable to use a sufficiently high gas pressure so that the maximum range of the recoils is a small fraction of the diameter of the chamber (2.5 centimeters).

The operation of the chamber was tested by using the N^{14} $(n,p)C^{14}$ reaction, which with thermal neutrons gives rise to monoenergetic protons of about 0.6 million electron volt energy. For this test the chamber was filled with 0.5 atmospheres of nitrogen and 1.5 atmospheres of argon. Under these conditions the range of the 0.6 million electron volt protons is about 0.5 centimeter. Measurements were taken both without gas multiplication and with a gas multiplication of about 35. The pulse amplifier had a rise time of about 0.5 microsecond and a decay time of about 20 microseconds so that, when used without gas multiplication, the chamber was operated as an electron pulse chamber. However, because of the very small diameter of the wire not much spread in pulse height was produced by the fact that only the fast part of the pulse was recorded (see Section 10.6). Figure 17 represents the differential pulse height distributions as measured with a channel discriminator of the width indicated in the diagram. A theoretical pulse height distribution curve for electron pulses was calculated by considering the proton tracks as infinitely short, which involves (a) neglecting the wall effects and (b) assuming, in the calculation of the electron pulse,

Figure 16

Cylindrical chamber (see Section 14)

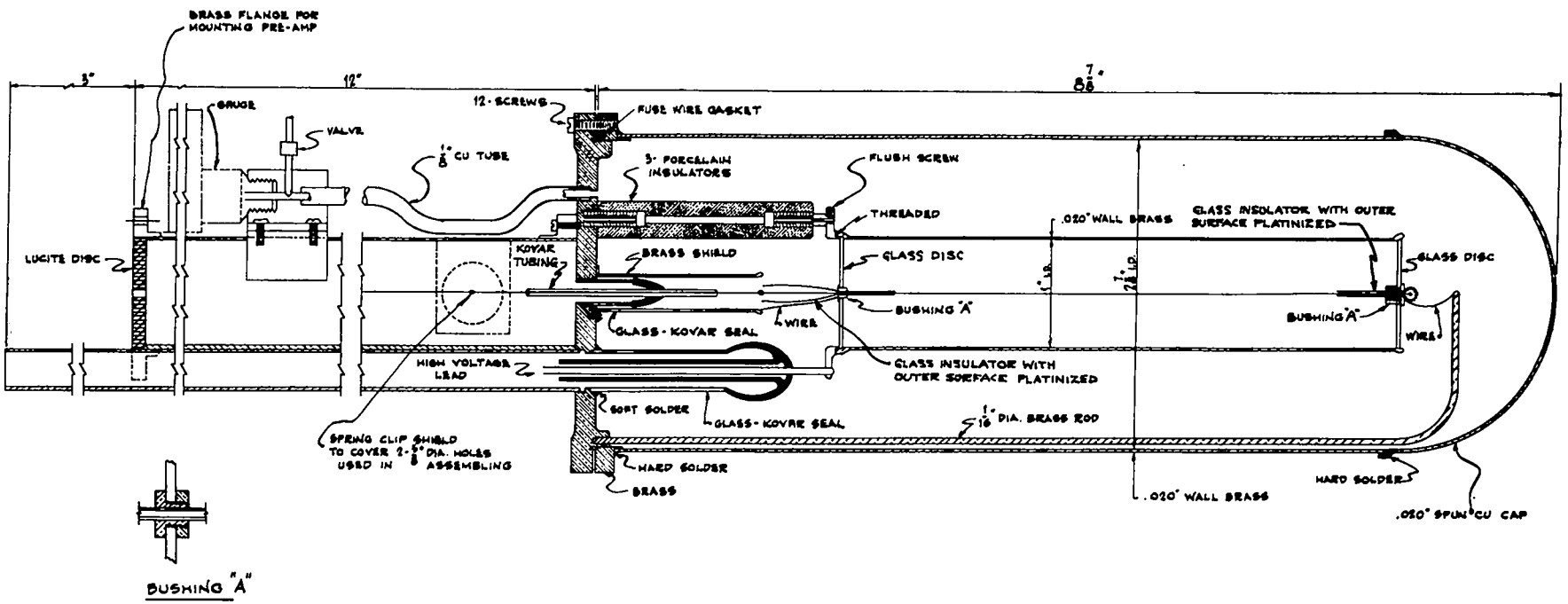

APPROVED FOR PUBLIC RELEASE

Figure 17

Differential pulse height distribution curves from the $N^{14}(n,p)C^{14}$ reaction in the cylindrical chamber described in Figure 16. Gas filling, 0.5 atmospheres of N_2, 1.5 atmospheres of argon.

(a) No gas multiplication

(b) Gas multiplication of about 35

(c) Theoretical curve for operation as an electron pulse chamber (corrected for channel width)

(Channel width indicated by the rectangle in the figure)

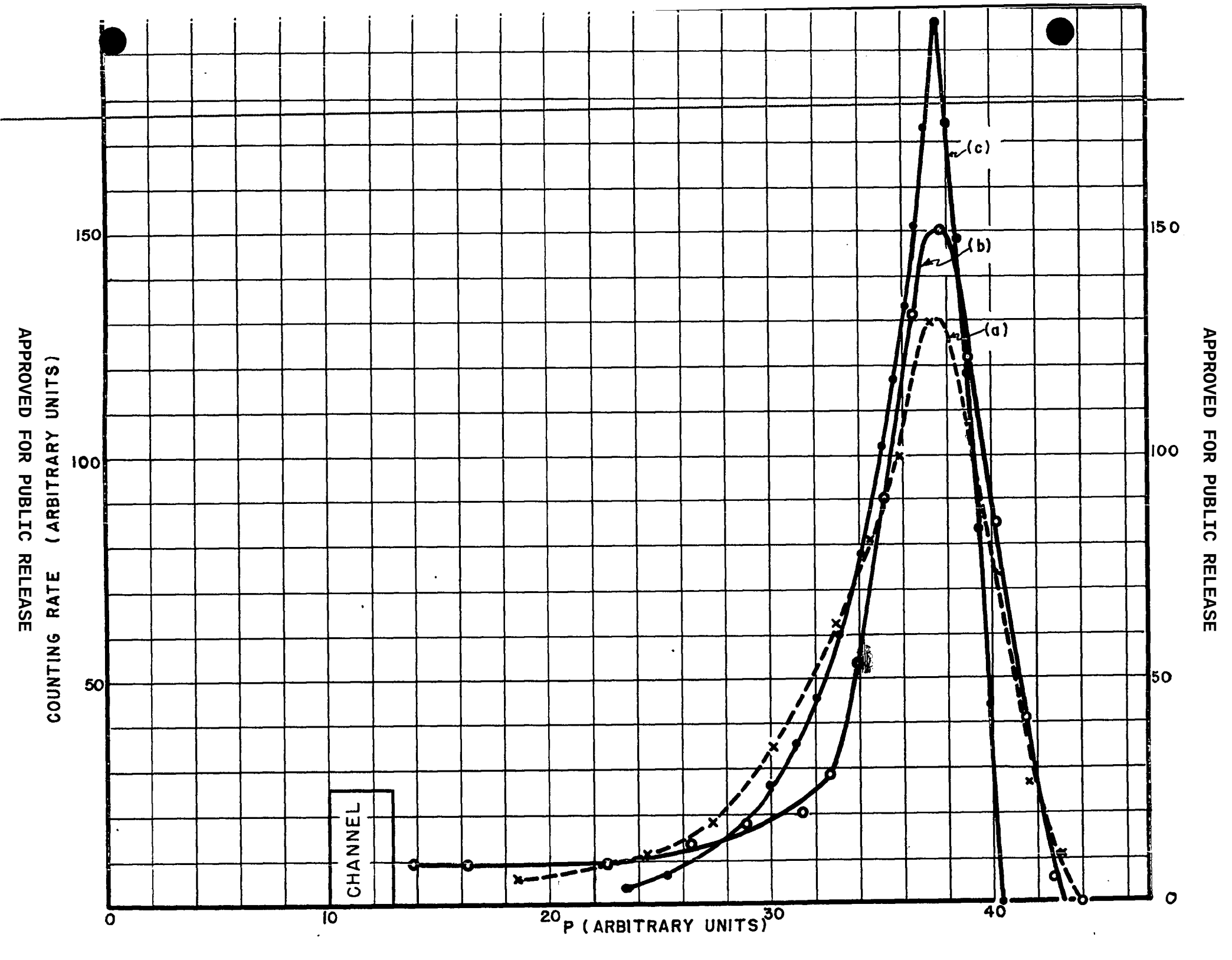
APPROVED FOR PUBLIC RELEASE
COUNTING RATE (ARBITRARY UNITS)
150
100
50
0
10
20
30
40
P (ARBITRARY UNITS)
CHANNEL
(c)
(b)
(a)
APPROVED FOR PUBLIC RELEASE

that the ionization of each track is concentrated in one point. This theoretical curve, corrected for the channel width, is also represented in Figure 17.

Both of the experimental pulse height distributions appear to be somewhat wider than one might have anticipated. The departure of the curve taken without gas multiplication from the corresponding theoretical curve may possibly be accounted for by wall effects. In the case of the measurements taken with gas multiplication there was probably some spread in pulse height due to lack of uniformity of the wire, end effects, or to a small amount of capture since the gas was not purified. The measurements with gas multiplication were repeated, after rebuilding the central wire assembly, with a higher pressure in the chamber (0.5 atmospheres of nitrogen, 4 atmospheres of argon). The pulses were analyzed photographically. The pulse height distribution thus obtained is represented in Figure 18. This curve is considerably narrower than the corresponding curve (b) in Figure 17. The difference is probably due partly to a decrease in the wall effects and partly to an improvement in the uniformity of the gas multiplication.

The chamber was used successfully for measuring the differential scattering cross-section of helium and of nitrogen.

A chamber of similar design operated as a proportional counter was also used as a neutron flux meter. For the measurements at the lowest neutron energies (0.03 million electron volt) the chamber was filled with pure hydrogen at a pressure of 10 centimeters Hg and the voltage was adjusted so as to obtain a gas multiplication of about 50. For the measurements at higher energies, higher pressures of hydrogen or hydrogen-argon mixtures were used. It may be noted that for each neutron energy the pressure should be adjusted in such a way as to strike the most favorable compromise between the γ-ray background, which increases with increasing pressure, and the wall effects, which decrease with increasing pressure. For a counter of the proportions shown in Figure 16 with the neutron beam parallel to the axis, the best condition is reached when the maximum range

Figure 18

Differential pulse height distribution curve obtained from the N^{14} $(n,p)C^{14}$ reaction in the cylindrical chamber described in Figure 16. Gas filling 0.5 atmospheres of N_2, 4 atmospheres of argon. Gas multiplication about 15. Pulses analyzed photographically.

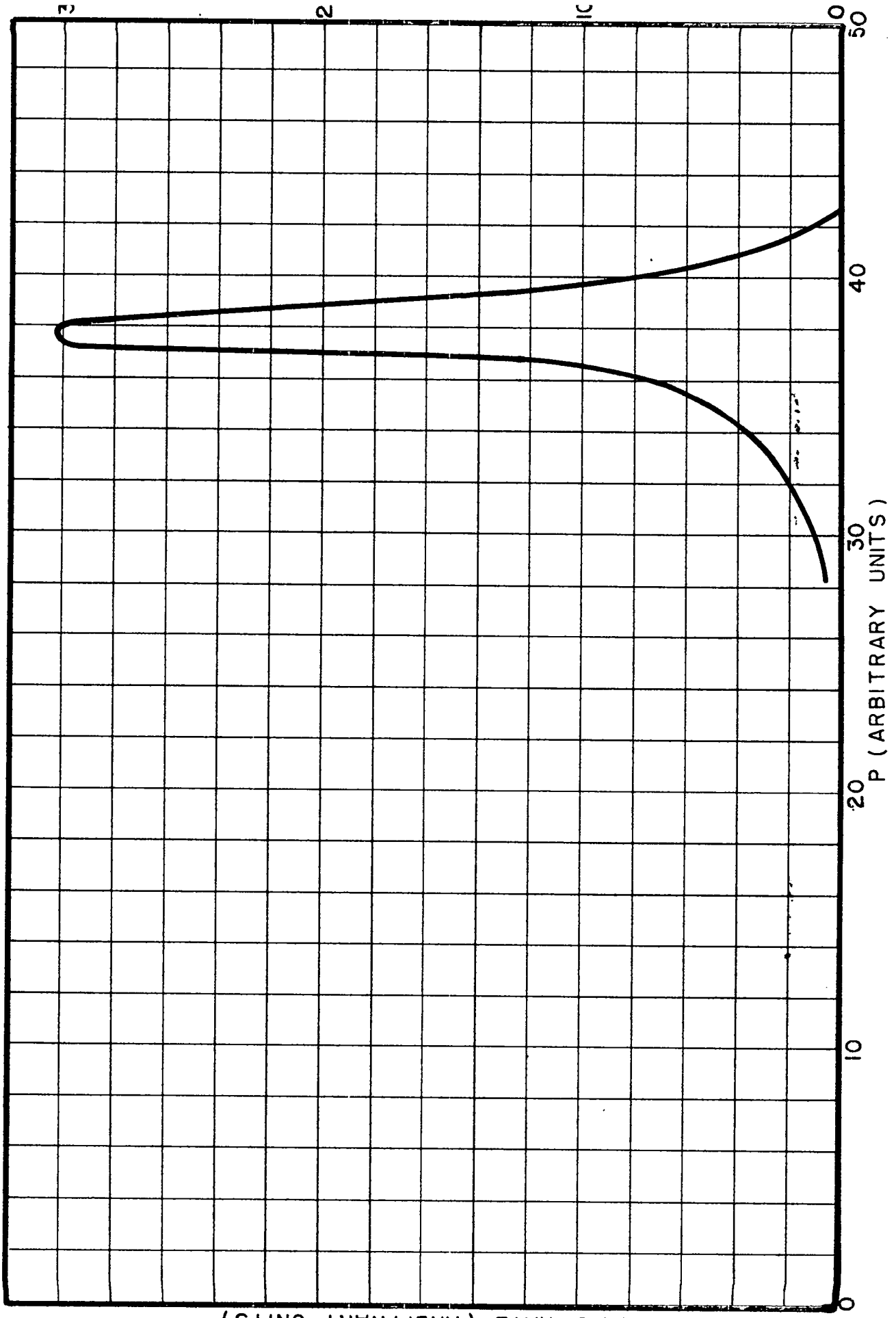

APPROVED FOR PUBLIC RELEASE

of the recoil protons in the center is of the order of the radius of the counter. Also, in order to minimize the γ-ray background, it is advisable to use, wherever possible, pure hydrogen rather than a hydrogen-argon mixture.

A number of pulse height distribution curves were measured by exposing the counter to monoenergetic neutrons traveling parallel to the axis. The results obtained with neutrons of 0.5 million electron volt energy are represented in Figure 19, curve (c). The pressure was chosen so that the maximum range R of the recoil protons was 1.2 times the radius b of the counter. The differential pulse height distribution curve, derived theoretically as described in Section 9 for R = b, is also shown in Figure 19, curve (a). In computing this curve, the gradual decrease of the gas multiplication towards the ends of the wires (see Section 11.5) was neglected. A calculation which takes into account this effect was carried out under certain simplifying assumptions for R = b. The results are given by curve (b) in Figure 19. If one considers the uncertainties in the theoretical calculations and the finite width of the channel discriminator used for the analysis of the pulses, one concludes that the agreement between the experimental and theoretical results, curves (c) and (b), is reasonably good. It may be noted that the pulse height distribution curves are not very sensitive to the ratio R/b. Hence, the comparison between the theoretical and experimental curves is not seriously invalidated by the fact that the value of this ratio was slightly different in the two cases.

At lower energies, the experimental curves depart from the theoretical ones and the discrepancy becomes more pronounced as the energy decreases. The reason for such a discrepancy has not been cleared up. It is not impossible that it may be caused, in part or completely, by lack of monochromaticity of the neutron beams used.

Figure 19

Differential pulse height distribution curves of hydrogen recoils for a proportional counter of the type shown in Figure 16. Neutron beam parallel to the axis.

(a) Calculated for $R_0 = b$, by neglecting the change in gas multiplication near the ends of the wire.

(b) Calculated for $R_0 = b$, by taking into account the change in gas multiplication near the ends of the wire.

(c) Observed with 0.5 million electron volt neutrons ($R_0 = 1.2$ b).

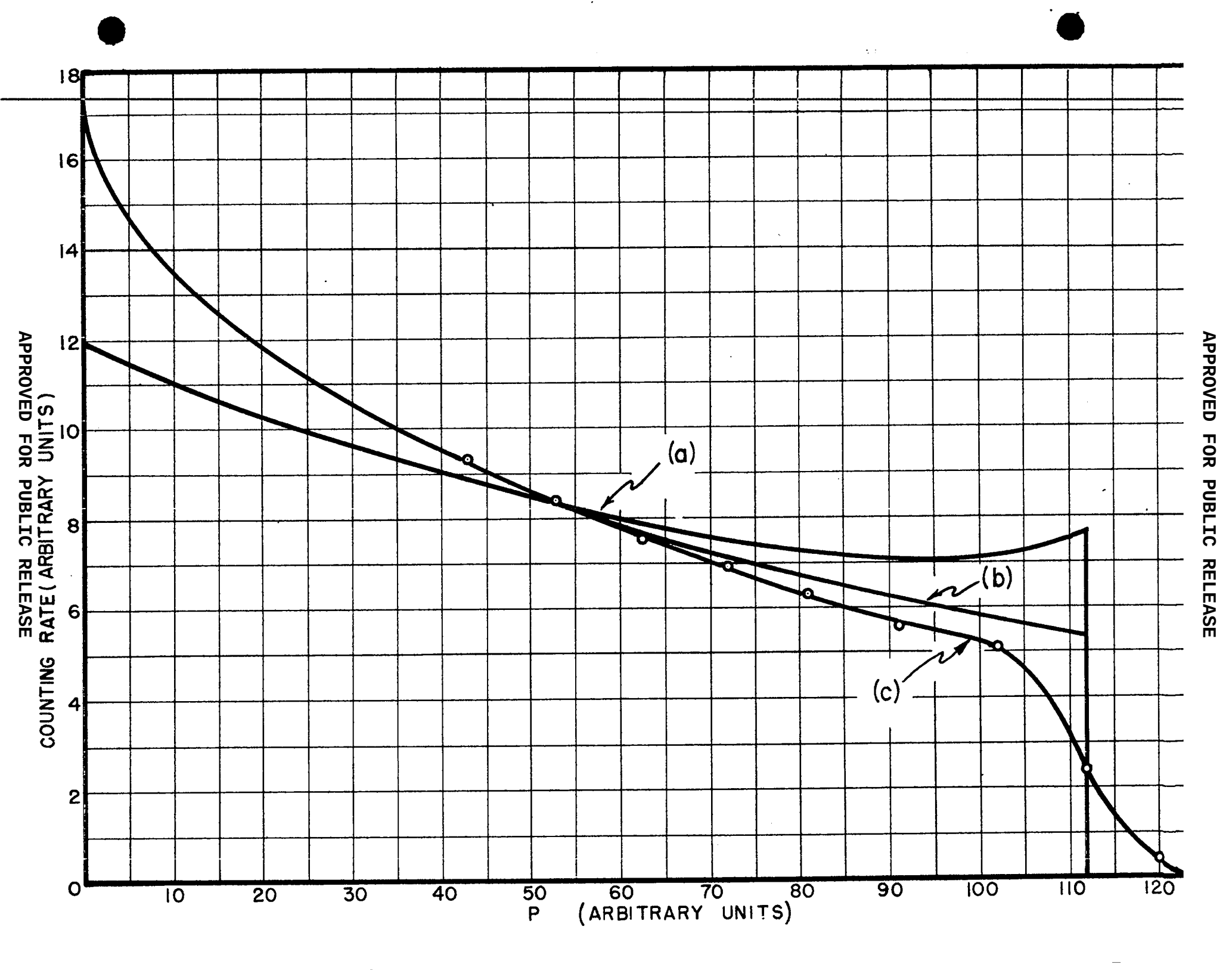
APPROVED FOR PUBLIC RELEASE
COUNTING RATE (ARBITRARY UNITS)
0
2
4
6
8
10
12
14
16
18
10
20
30
40
50
60
70
80
90
100
110
120
P (ARBITRARY UNITS)
(a)
(b)
(c)
APPROVED FOR PUBLIC RELEASE

14.15 GAS RECOIL PROPORTIONAL COUNTER

Figure 20 illustrates the construction of a chamber(similar in principle to that described in Section 14) which was used as a flux meter for neutrons of low energy (down to 0.035 million electon volt). The most interesting feature is the arrangement of the collecting electrode and of the supporting guard electrode which are so designed as to avoid any deformation of the electric field near the ends of the collecting electrode (see Section 11.5). The collecting electrode and the guard electrode both consist of sections of hypodermic needles, 0.042 inch O.D. They are mechanically connected and electrically insulated by means of glass tubes about 0.025 inch O.D., as shown in the detail in Figure 20. The electrical connection to the collecting electrode is made by means of a thin metal wire which slides through the guard electrode and is soldered to the inside of the collecting electrode.

The walls of the counter and the outer case are made of dural in order to minimize the danger of scattering and absorption of neutrons. The Kovar pieces are soldered to the dural end plates with the following technique: First, the Kovar pieces are tinned with soft solder and the dural pieces are covered with Belmont aluminum solder. Then each Kovar piece is soldered to the corresponding dural piece with aluminum solder without using any flux. The screw connection between the pieces (3) and (5) makes it possible to adjust the position of the guard electrodes supporting the collecting electrode before the last Kovar piece is soldered into place. The counter was used only at low energies (down to 0.035 million electron volt), usually with a gas filling of pure hydrogen at 1.5 centimeter Hg pressure and a gas multiplication around 50. The pulse height distribution curves obtained with monoenergetic neutrons are very similar to those obtained at the corresponding energies with the counter described in Section 14, and do not agree very well with the calculated curves.

Figure 20

Proportional counter(see Section 15)

(1) Outer dural case, grounded; 4 inches O.D., 1/16 inch wall, 13 inches long.

(2) Kovar tube, 3/8 inch O.D., it is grounded during operation.

(3) Kovar tube, 3/8 inch O.D., threaded on the inside.

(4) Glass.

(5) Brass rod, threaded on the outside.

(6) Lucite spacer ring.

(7) Dural tube, 3 inches O.D., 1/32 inch wall in the thinner section.

(8) Hypodermic needle, 0.042 inch O.D., it forms the guard electrode.

(9) Hypodermic needle, 0.042 inch O.D., 4 inches long; it forms the collecting electrode.

(10) Kovar tube, 1/16 inch wall; 2-1/4 inch O.D.

(11) Gas inlet and needle valve.

(12) Amphenol connector to the collecting electrode.

(13) Amphenol connector to the high voltage electrode.

(14) Glass spacer.

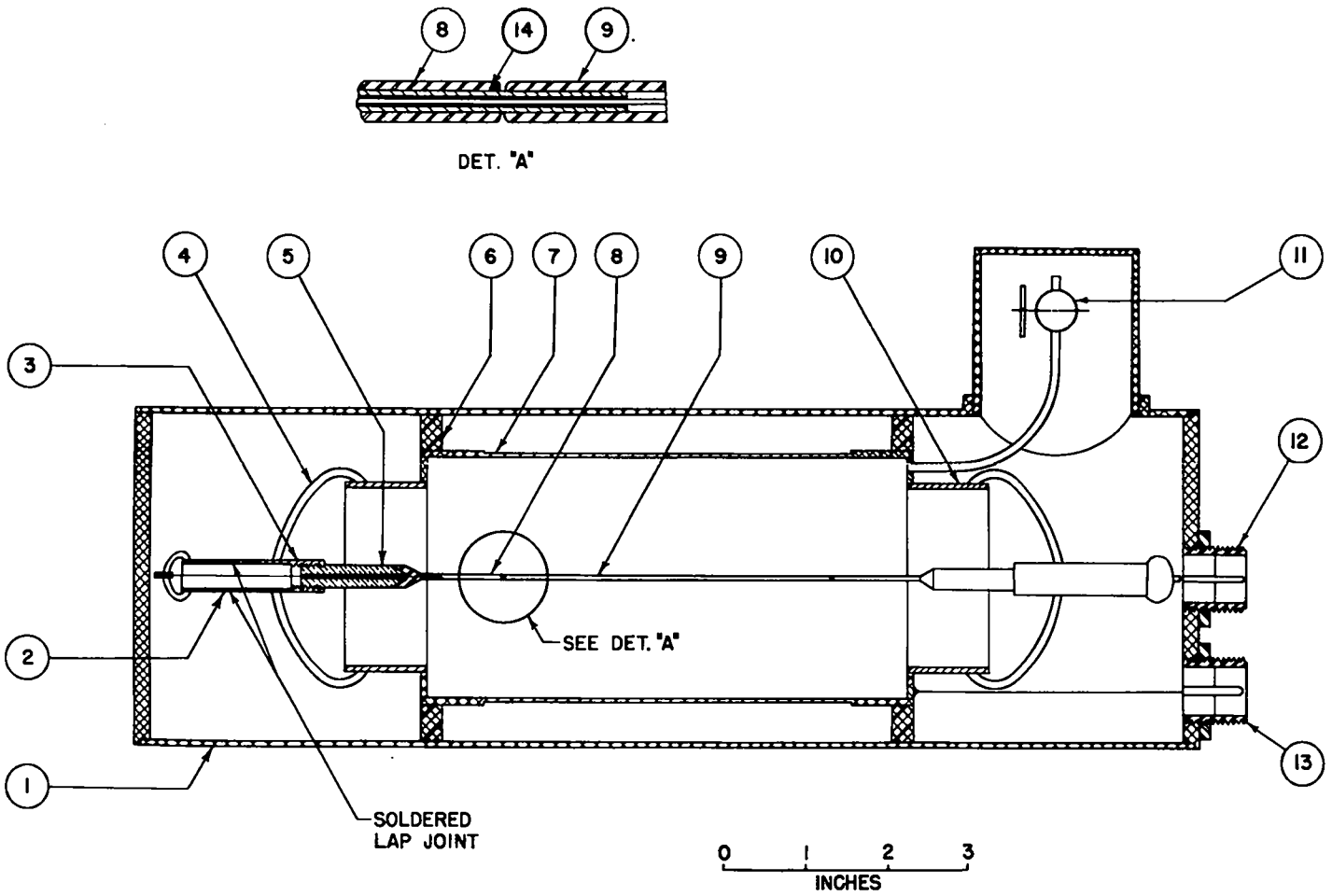

APPROVED FOR PUBLIC RELEASE

14.16 THICK RADIATOR, ELECTRON PULSE, SPHERICAL CHAMBER

This chamber, the construction of which is shown in Figure 21, was designed as a directional detector for relative flux measurements. The radiator is a thick paraffin layer deposited on a section of the removable hemispherical cap and coated with a very thin layer of graphite to make the surface conducting. The chamber is made gas tight with neoprene gaskets throughout. The inner electrode assembly is put together, then placed in position and fastened with the nut (a). The gaskets between the collecting electrode and the inner lucite insulator, and between this insulator and the guard electrode, are tightened by means of the nut (b). The gasket between the guard electrode and the outer lucite insulator is tightened by means of the nut (c). The gasket between this insulator and the brass collar is tightened by means of the nut (a). The brass disc on the stem of the collecting electrode is used to reduce the disturbing effect of recoil protons from the lucite insulators. The chamber is filled with argon and pressures up to 6 atmospheres can be used. The chamber is usually operated at a voltage of -2000 volts. A small hole in the chamber wall, covered with an aluminum foil enables one to introduce α-particles from a polonium source into the chamber for testing purposes. As already mentioned, the chamber was designed as a directional counter which detects only those neutrons which enter the chamber through the paraffin radiator. The "directionality factor", defined as the ratio between the numbers of counts recorded when the neutrons enter the chamber through the coated and the uncoated surfaces, respectively, was improved by lining the chamber with gold sheet. In this way a value for this ratio of about 100 was obtained. The counting rate, as a function of the angle of incidence of the neutrons is shown in Figure 22. In these measurements the incident neutrons had an energy of 3 million electron volts. The two curves were taken with

Figure 21

Spherical chamber (see Section 16)

APPROVED FOR PUBLIC RELEASE

Fig

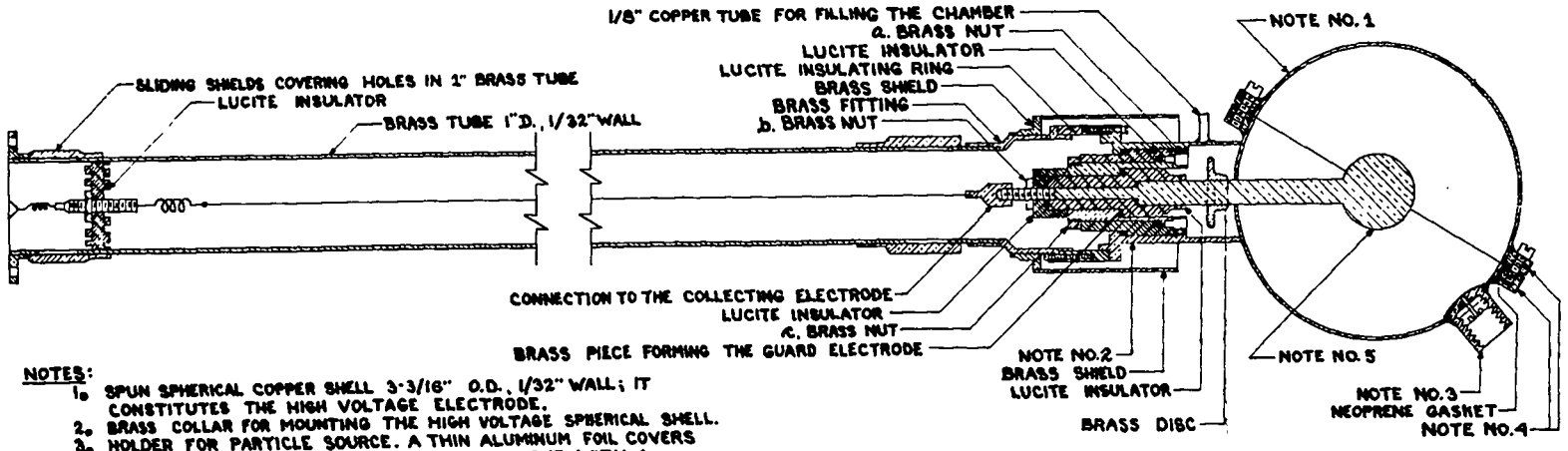

NOTES:

1. SPUN SPHERICAL COPPER SHELL 3-3/16" O.D., 1/32" WALL; IT CONSTITUTES THE HIGH VOLTAGE ELECTRODE.
2. BRASS COLLAR FOR MOUNTING THE HIGH VOLTAGE SPHERICAL SHELL.
3. HOLDER FOR PARTICLE SOURCE. A THIN ALUMINUM FOIL COVERS THE HOLE AND THIS WINDOW IS MADE GAS TIGHT WITH A NEOPRENE GASKET.
4. BRASS FLANGES, HARD SOLDERED TO THE COPPER SHELL.
5. COLLECTING ELECTRODE, MADE OF A BRASS STEM 1/4" IN DIA., TERMINATING WITH A BRASS SPHERE, 3/4" IN DIA.

Figure 22

Angular response of the chamber represented in Figure 21. The black areas represent the portion of the shell lined with paraffin. The arrow marked N represents the direction of the incoming neutrons. Neutron energy 3 million electron volts.

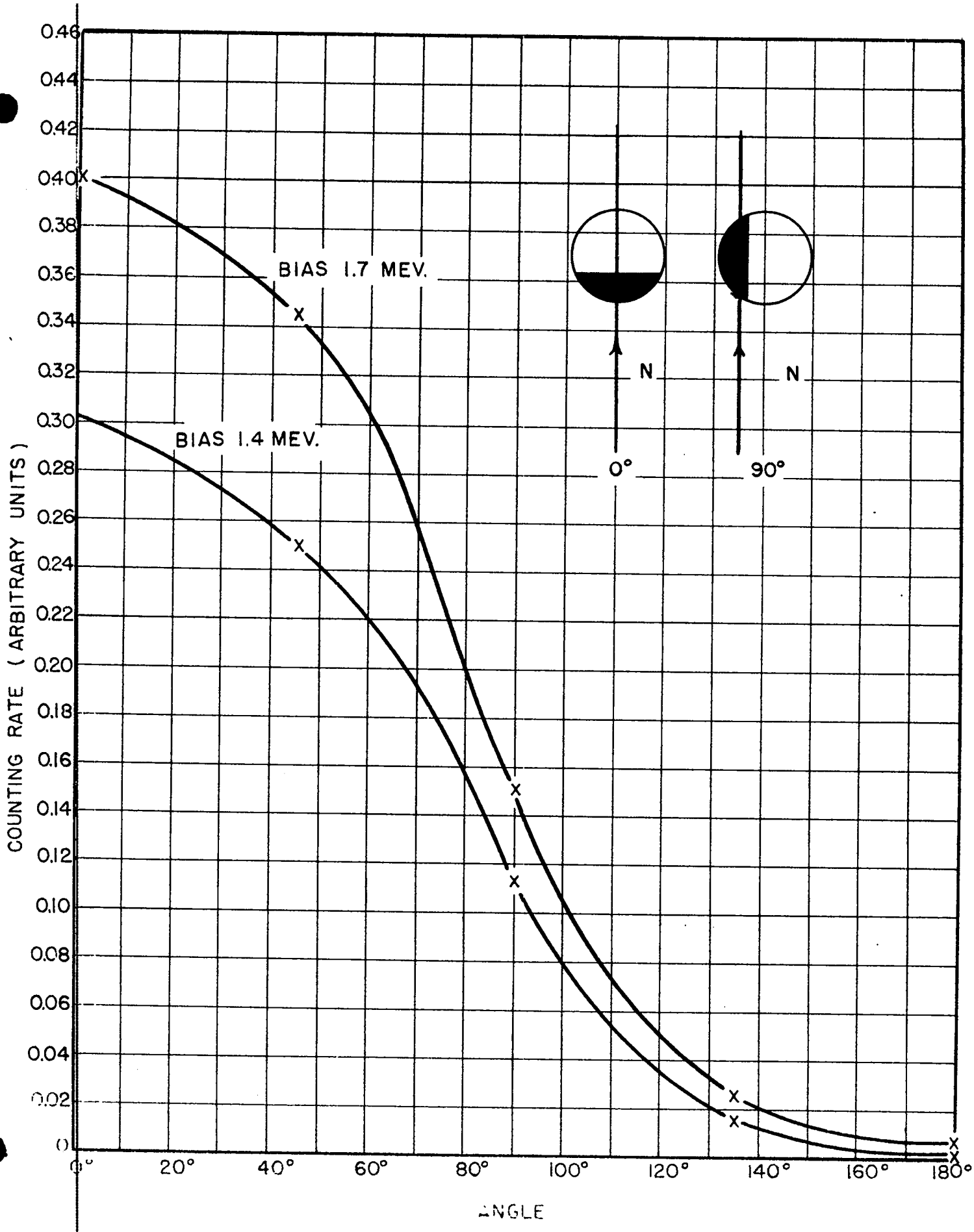

biases adjusted in such a way as to count all pulses larger than 1.4 and 1.7 million electron volts, respectively.

The dependence of the counting yield of the chamber on the bias energy was investigated and found similar to that described by Equation 28' and shown in Figure 6. A close agreement could not be expected because the assumptions under which Equation 28' was deduced (plane radiator, ion pulse chamber) are not fulfilled.

It may be noted that the chamber described was not provided with a gas purifier. Some difficulty was experienced during its operation because of a gradually increasing contamination of the gas of the chamber leading to electron attachment. This was probably caused by organic vapors slowly evolving from the lucite insulators and the neoprene gaskets.

14.17 THIN RADIATOR, PROPORTIONAL COUNTER

Figure 23 shows the construction of a counter designed as a flux meter for neutrons of low energies. Argon and krypton at pressures ranging from 12 to 170 centimeters Hg were used as gas fillings. The voltage was chosen so as to obtain gas multiplications between 5 and 50. The radiator was a layer of glycerol tristearate deposited by distillation in vacuum on a platinum foil. Its thickness varied from 60 to 390 γ per square centimeter. The counter was operated with the case grounded and the center wire at a high positive potential. The pulses were taken off the center wire by capacity coupling.

If the gas pressure is sufficiently high so that practically all recoil tracks from the radiator terminate in the gas, the yield of the counter should depend on the neutron energy E_n and the bias energy B as indicated in Figure 1.

Experiments were carried out to test this prediction and the results were in fair agreement with the theory.

Figure 23

Thin radiator proportional counter (see Section 17)

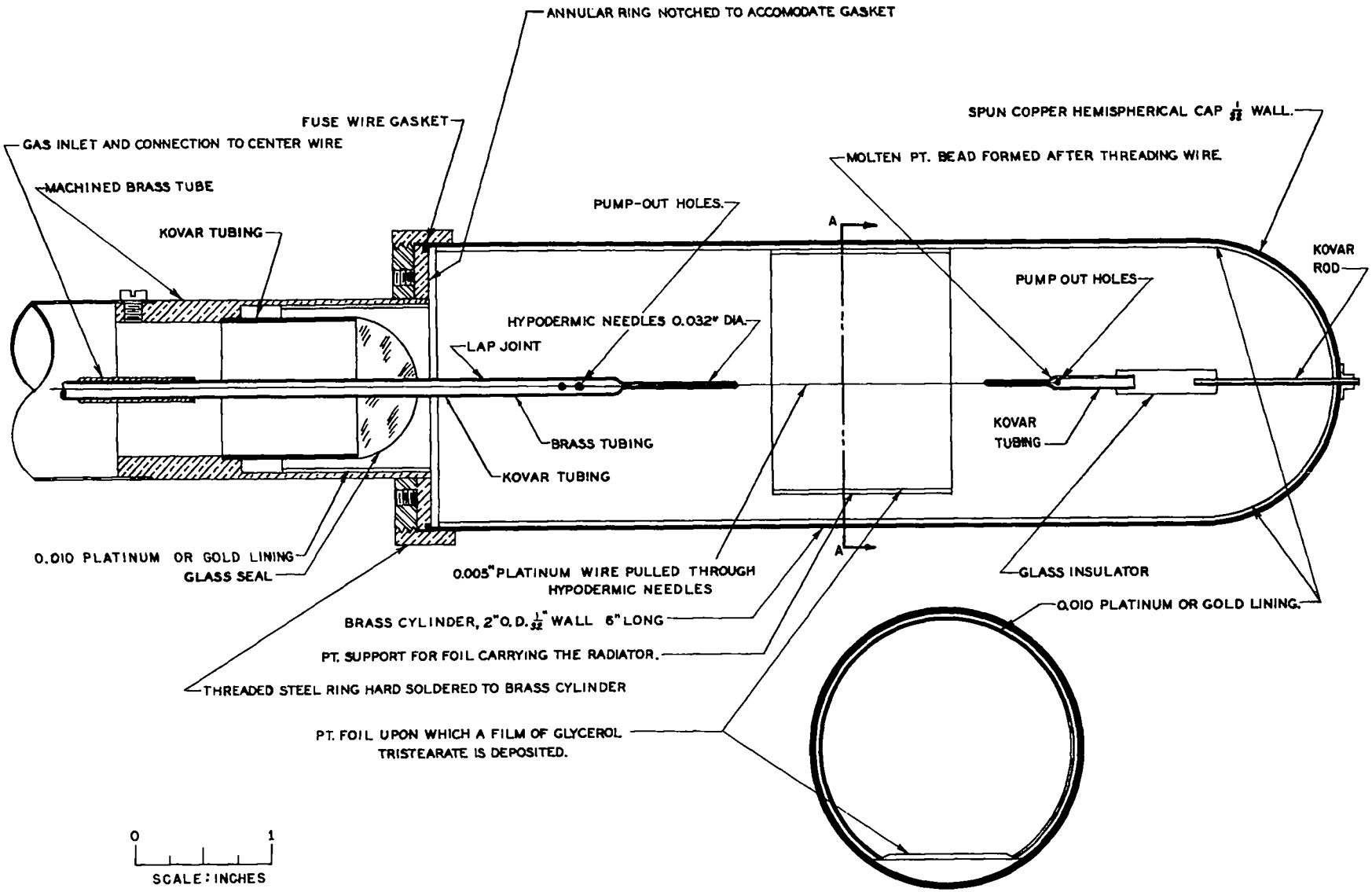

SECTION A-A

14,18 INTEGRATING GAS RECOIL CHAMBER

Figure 24 shows the construction of an integrating chamber designed at the British T. A. Project for the flux measurements of monoenergetic neutrons. The chamber is filled with ethylene ($C_2 H_4$) and the walls are coated with paraffin wax to a thickness larger than the maximum range of the recoil protons. The surface of the wax is made conducting by evaporating silver to a thickness of 0,2 milligrams per square centimeter The paraffin wax used had the composition $(C H_2)_n$, i.e., it contained carbon and hydrogen in the same proportion as the gas filling of the chamber. Under these circumstances, when the instrument is used as an integrating chamber, the wall effects are eliminated. In other words, the ionization per unit volume of the gas is the same as if the dimensions of the chambers were infinitely large compared with the range of the recoil protons. The ionization current produced by the hydrogen recoils, I_H is then given by Equation 29 which may be rewritten as follows:

$$I_H = \phi A n_H \sigma_H (E_n) \frac{E_n}{2} \frac{e}{W_o}$$

where A is the volume of the chamber, ϕ the neutron flux density, i.e., the number of neutrons per second and per square centimeter, n_H is the number of hydrogen atoms per cubic centimeter of the gas, and σ_H is the total scattering cross-section of hydrogen.

To the ionization current produced by the hydrogen recoils one has to add that produced by the carbon recoils, which has the expression:

$$I_c = \phi A n_c \sigma_c (E_n) (E)_{av.} \frac{e}{W_o}$$

where n_c is the number of carbon atoms per cubic centimeter of the gas, $\sigma_c (E_n)$ is the total scattering cross-section of carbon and $(E)_{av.}$ is the average energy

Figure 24

Integrating gas recoil ionization chamber (see Section 12). Vacuum seals on the body of the chamber made with low melting point wax.

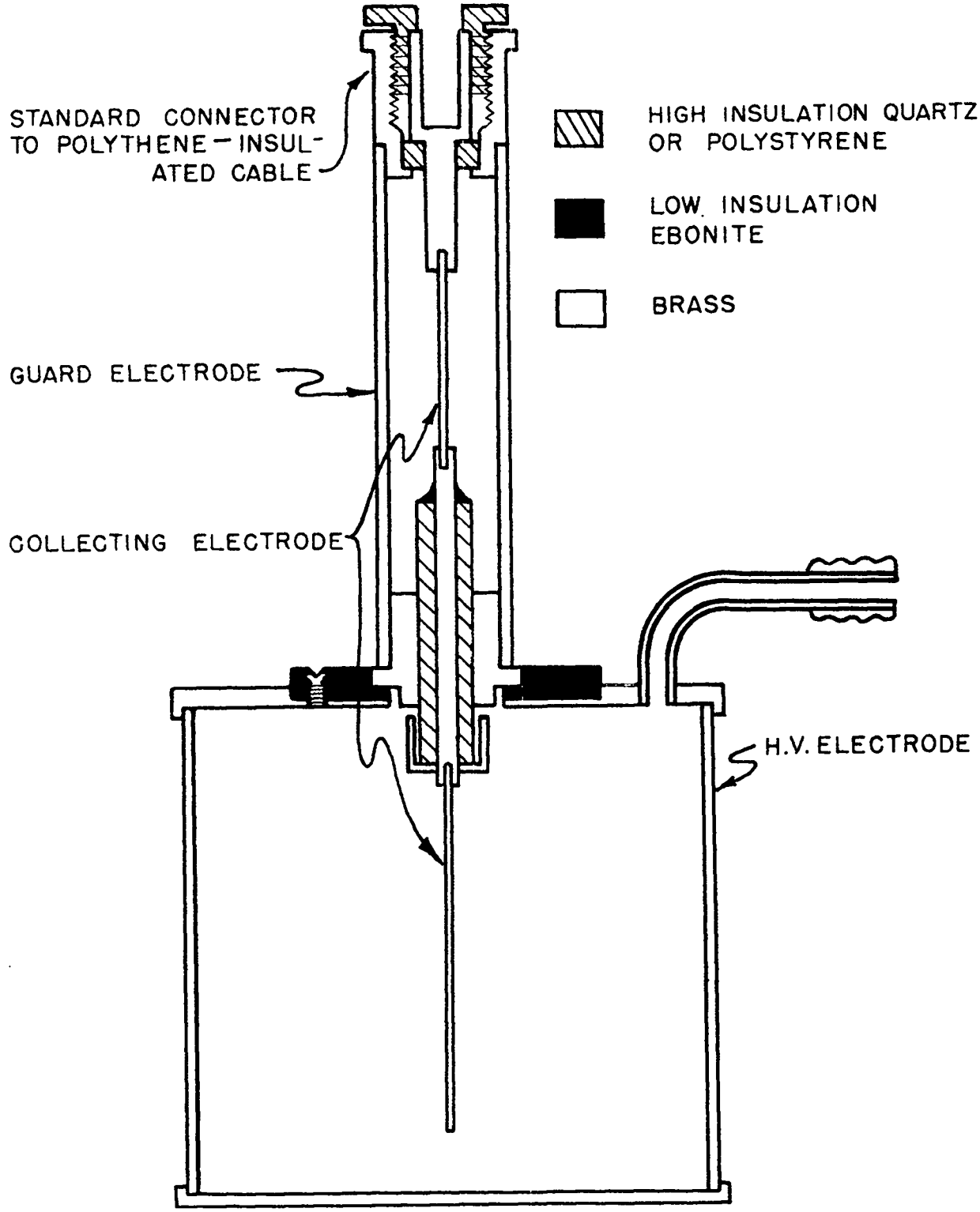

of the carbon recoils. Because of some uncertainty in the values of σ_C and $(E)_{av.}$, the relation between I_C and n is not so well known as that between I_H and n. On the other hand, I_C is small compared with I_H since the carbon cross-section is considerably smaller than that of hydrogen, so that this uncertainty does not introduce any appreciable source of error.

Very often neutrons are accompanied by γ-rays, while, with a pulse chamber, the γ-ray pulses can be biased off. This cannot be done with an integrating chamber. However, it is possible to separate the effects of neutrons from those of γ-rays by determining the ionization current simultaneously with the chamber described above and with a second identical chamber in which all hydrogen has been replaced with deuterium.

The substitution of deuterium for hydrogen in an ionization chamber does not change the sensitivity of the chamber for γ-rays (this was experimentally verified). It changes, however, its sensitivity to neutrons. Hence, the difference of ionization currents is proportional to the neutron flux.

If one assumes isotropic scattering of neutrons on deuterons in the center of gravity system, the difference of ionization currents, ΔI, is related to the neutron flux density n by the equation:

$$\Delta I = \phi A \frac{E_n}{2} \frac{e}{W_o} n \left[\sigma_H (E_n) - \frac{8}{9} \sigma_D (E_n) \right]$$

where $\sigma_D(E_n)$ is the total scattering cross-section of deuterons, n is the number of either hydrogen or deuterium atoms per cubic centimeter, and $\frac{1}{2}(\frac{8}{9} E_n)$ represents the average energy of the deuterium recoils. It may be pointed out that the assumption of isotropic scattering of neutrons on deuterons, which enters in the evaluation of the average energy, is somewhat uncertain.

14.19 COINCIDENCE PROPORTIONAL COUNTER

Figure 25 illustrates the construction of a detector used as an absolute neutron flux meter. It consists essentially of two proportional counters. The recoil protons, ejected from the paraffin radiator, are collimated by the diaphragms (2) and (3). Only those recoils are recorded which traverse both proportional counters, thus producing simultaneous pulses. The ratio of the number of recoils recorded to the total number of recoils generated in the radiator is determined by the solid angle defined by the diaphragms. The effective area of the radiator is determined by another diaphragm (1), placed directly in front of the radiator.

The radiator consists of a paraffin film evaporated on a metal disc. Tank argon, at pressures ranging from 1 to 10 centimeters Hg, was used as a gas filling. Aluminum and collodion foils of different thicknesses, mounted on two discs could be placed along the path of the recoil protons for the purpose of determining their range, from which the energy of the incident neutrons could be calculated. The discs carrying the absorbing foils can be rotated from the outside through ground joints. The thin wire rings on both sides of the absorbing foils were used to shield the two counters electrically from one another. This was found necessary because otherwise the operation of the counters was modified by the insertion of an aluminum foil between them. Measurements of the coincidence counting rate versus bias were carried out and showed the existence of flat "plateaus", indicating that all of the pulses produced by the hydrogen recoils in the proportional counters had sizes greater than a certain value, which, in turn, was well above the background noises.

It must be noted that the instrument described did not prove very reliable as an absolute neutron flux meter. However, it is likely that a satisfactory instrument based on the same principle could be built by improving the design of the counters. Multiple wire proportional counters (see Section 11.7) might prove particularly suitable in this arrangement.

Figure 25

Coincidence proportional counter (see Section 19).
Shaded areas represent hard rubber insulators.
Counters made gas tight with glyptal.

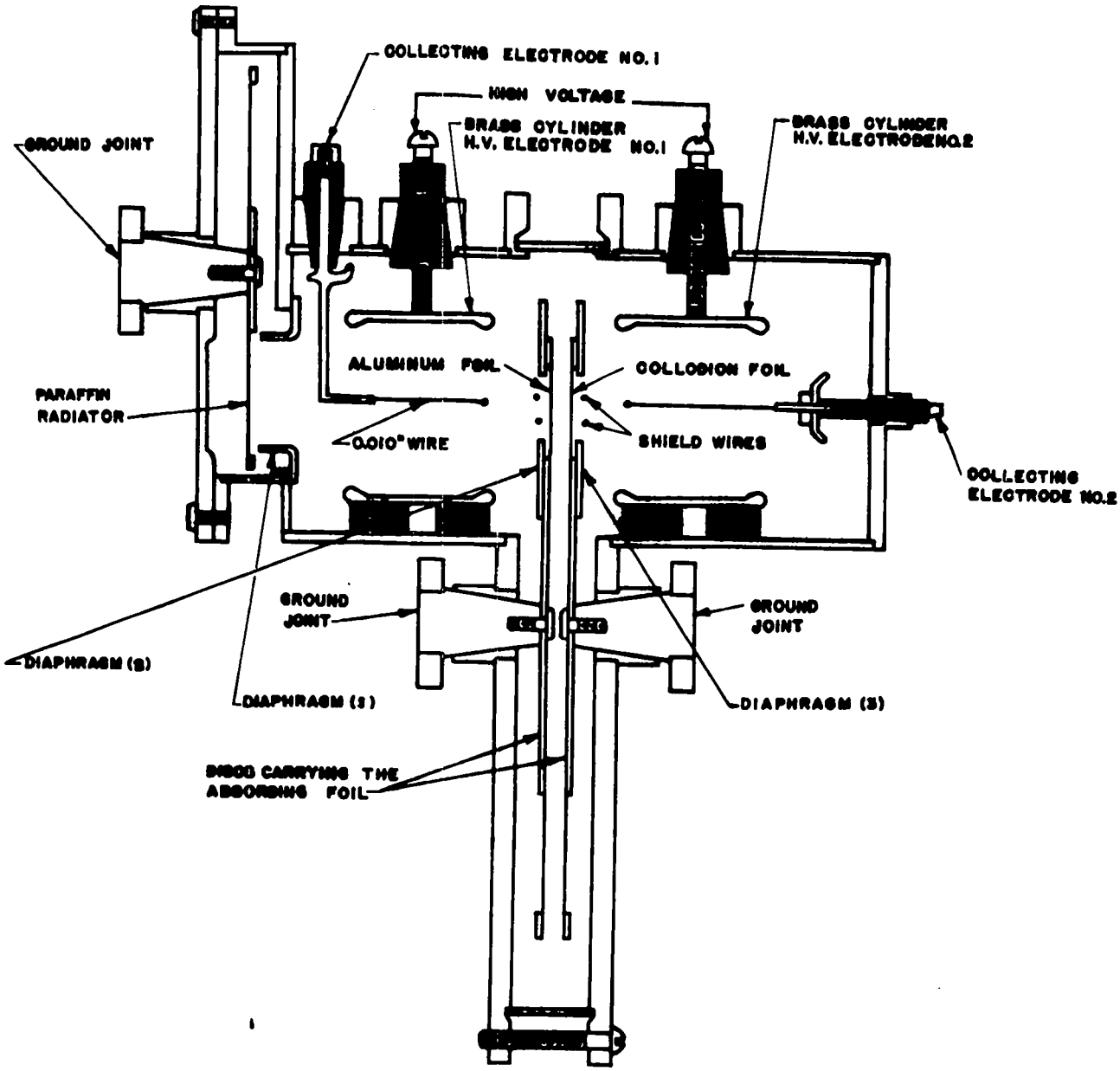

LOS ALAMOS TECHNICAL SERIES

VOLUME I

EXPERIMENTAL TECHNIQUES

PART II

CHAPTER 15

DETECTORS OF (n,α) AND (n,p) REACTIONS

by

BRUNO ROSSI AND HANS STAUB

CHAPTER 15

DETECTORS OF (n,α) AND (n,r) REACTIONS

15.1 NEUTRON SPECTROSCOPY USING (n,α) OR (n,p) REACTIONS

In principle it is possible to use the (n,α) and (n,p) reactions for measuring the energy distribution of a neutron beam. At any given neutron energy, the total energy released in the reaction is constant and depends on the neutron energy in a simple form, provided that the reaction products are emitted in the ground state (this is the case in many reactions). The total energy, which is the sum of the incident neutron energy E_n and the reaction energy Q, is divided between the two outgoing charged particles. If the reaction occurs in a gas with sufficient stopping power to prevent the escape of any of the particles from the counting volume, one obtains pulses the sizes of which are proportional to $E_n + Q$. Since Q is constant and usually well known, such an arrangement provides an almost ideal method for measuring the energy of monoenergetic neutrons for which $(E_n + Q) > 0$. For accurate measurements Q should not be too large. However, for the determination of the energy distribution of non-monoenergetic neutrons, it would be necessary to know the energy dependence of the cross section accurately. Unfortunately, this is not the case and, moreover, all reactions with sufficiently small Q exhibit pronounced resonances which make the interpretation of the experimental results even more difficult. The following is a list of reactions which have been under consideration for spectroscopic purposes.

Table 15.1-1

Reaction	Q	Remarks
1. $_3Li^6 + _0n^1 \longrightarrow _2He^4 + _1H^3$	+4.63 Mev	Resonance at E_n = .27 Mev. Q high, σ very large at $E_n = 0$.
2. $_5B^{10} + _0n^1 \longrightarrow _2He^4 + _3Li^7$	+2.34 and 2.78 Mev (See below)	No resonances, Q fairly large, σ very large at $E_n = 0$.
3. $_7N^{14} + _0n^1 \longrightarrow _1H^1 + _6C^{14}$	+0.60 Mev	Sigma shows sharp resonances at .55, .7 and 1.45 Mev
4. $_7N^{14} + _0n^1 \longrightarrow _2He^4 + _5B^{11}$	-0.28 Mev	Sigma shows resonance at 1.5 Mev

15.2 FLUX MEASUREMENTS

Extensive use has been made of (n,α) reactions for detecting slow neutrons. The reaction B(n,α) is most commonly used because the cross section is very large and furthermore known to obey the 1/v law in the low energy region ($E_n < 500$ eV). The value of the cross section for $v_n = 2200$ microseconds is $703 \pm 9 \times 10^{-24}$ cm^2 for the natural isotopic mixture of B^{10} and B^{11}, and therefore 3830×10^{-24} cm^2 for pure B^{10}. Reactions 1 and 3 in Table 15.1-1 (which, because of the positive Q value, occur also at thermal energies) have considerably lower cross section than the reaction B(n,α). In the case of reaction 1, the materials are not as easy to handle as boron. For these reasons the following sections shall be confined to the discussion of boron detectors. Such detectors have not only been used to measure small neutron flux but also to detect fast neutrons after they have been slowed down by a suitable moderator.

The B(n,α) reaction has been extensively studied by Bower, Bretscher and Gilbert.(1) The reaction is not moncenergetic but leads for thermal

(1) Proc. Cambridge Phil. Soc., 34, 290, 1938

neutrons only rarely to the ground state of Li^7. The majority of the disintegrations result in the well known excited state of Li^7 at .44 Mev. The

ranges of the particles are given as .7 centimeters for the α-particles and .4 centimeters for the Li nuclei. Since the Q value of the reaction leading to the excited state of Li is 2.34 Mev, the Li nucleus, for thermal neutrons, carries .85 Mev.

Solid boron as well as gaseous compounds can be used. In the latter case the filling consists most frequently of BF_3 which is a comparatively stable compound. However, considerable difficulties are encountered in purifying the gas sufficiently to prevent electron capture, particularly at pressures in excess of one atmosphere. Careful distillation from frozen ($-127^{\circ}C$) commercial BF_3 improves the gas considerably in this respect, apparently by removing substances which capture the electrons, such as HF. However, the best BF_3 fillings were obtained by thermal decomposition of $C_6H_5N_2BF_4$. The difficulties of purification are avoided by using thin films of solid boron coated on the electrodes of the detector and filling the chamber with an inert gas like argon or a mixture of argon and CO_2. The films can be prepared by decomposing borane (B_2C_6) on heated foils of tungsten or tantalum. The disadvantage of this type of detector as compared with the gaseous ones arises from the fact that in order to obtain high counting yields a large number of foils must be used since the range of the reaction particles is very small. For absolute measurements the use of solid films is advisable because the amount of irradiated material can be very accurately determined.[2] It may be mentioned that the use of B^{10} isotope

---

(2) Tungsten as a carrier foil has proved to be unsuitable for such measurements since boron apparently diffuses into the metal. This does not seem to occur in the case of tantalum foils.

---

obviously increases the sensitivity of both types of detectors by about a factor of 5 as compared to detectors using the natural isotopic mixture of 81.6 per cent inactive B^{11} and 18.4 per cent B^{10}.

For absolute measurements of a slow neutron flux, a knowledge of the

neutron energy is of course required since the cross section of the $B(n,\alpha)$ reaction varies rapidly with energy. Corrections have to be applied for the finite film thickness in the case of solid films and wall corrections in the case of gas filled detectors.

Let us consider first the case of a parallel plate ion pulse chamber with a solid boron film of finite thickness t deposited on the high voltage electrode. The detection efficiency F(B) (number of counts divided by the number of disintegrations) is given by the equation:

$$F(B) = 1/2 \left[1 - \frac{t}{2(R_o - R(B))} \right] \qquad (1)$$

where R_o is the range of the emitted α-particle, R(B) the range of an α-particle of energy B. Both ranges are to be measured in the material of the film (see Section A.6). In this formula, (Equation 1), it is assumed that all α-particles have the same energy, that $\left[R_o - R(B)\right] \geq t$, and that the pulses from the lithium nuclei are not counted ($B > .85$ Mev). The formula does not rigorously apply to the case of an electron pulse chamber. However, it applies approximately if the range of the α-particles in the chamber is sufficiently small and the value of B sufficiently low. If the bias energy is lower than .85 Mev so that Li pulses are also counted, the expression for the detection efficiency becomes:

$$F(B) = 1 - \frac{t}{4} \left[\frac{1}{R_{o_1} - R_1(B)} + \frac{1}{R_{o_2} - R_2(B)} \right] \qquad (2)$$

where the subscript 1 refers to the α-particle and the subscript 2 to the Li. Again this formula holds only if $\left[R_{o_2} - R_2(B)\right] \geq t$. Let us consider next a cylindrical gas filled chamber of radius b and operated as an ion pulse chamber. The computation of the exact expression for the detection efficiency is very complicated if the finite range of the Li recoil is taken into account. Furthermore, it cannot be carried out without an exact knowledge of the range energy relation of very slow Li particles. Thus it shall be assumed that the

ionization from the Li recoil is confined to a very small region around the origin of the disintegration. The contribution of the Li, in the case of thermal neutrons, shall be taken as equal to .85 Mev. This assumption is rather crude since the range of the Li recoil according to Bower, Bretscher, and Gilbert is about 4/11 of the total range of the two particles. It appears, however, from the photometric traces of cloud chamber tracks that most of the ionization of the Li recoil occurs close to the point of origin of the disintegration. Under these assumptions the detection efficiency becomes

$$F(E) = 1 - \frac{r(B)}{2b} \qquad (3)$$

where r(B) is that portion of the range of the α-particle (measured from the point of origin) which it must spend in the sensitive volume in order to produce, together with the Li recoil, a pulse equal to the bias energy. If R_o is the range of the α-particle, E(R) the energy corresponding to a certain range R, B the bias energy, and E_{Li} the energy of the Li recoil, we have:

$$B - E_{Li} = E(R_o) - E\left[R_o - r(B)\right] \qquad (4)$$

In deriving Equation 3 it is assumed that $r(B) \ll b$.

In most cases the best procedure to obtain the counting rate at zero bias energy consists in determining the number of counts as a function of the bias and extrapolating linearly to zero bias. This procedure proves to be satisfactory if the measurements extend to a sufficiently low bias.

15.3 BORON CHAMBER OF HIGH SENSITIVITY

Figure 1 shows the construction of a highly sensitive boron chamber which can be used for detecting neutrons of all energies by slowing them down in paraffin in order to increase the cross section for the B(n,α) reaction. The chamber consists of a cylindrical vessel with a central electrode supported by guard electrodes. It is embedded in a block of paraffin

Figure 1

High sensitivity boron trifluoride chamber.

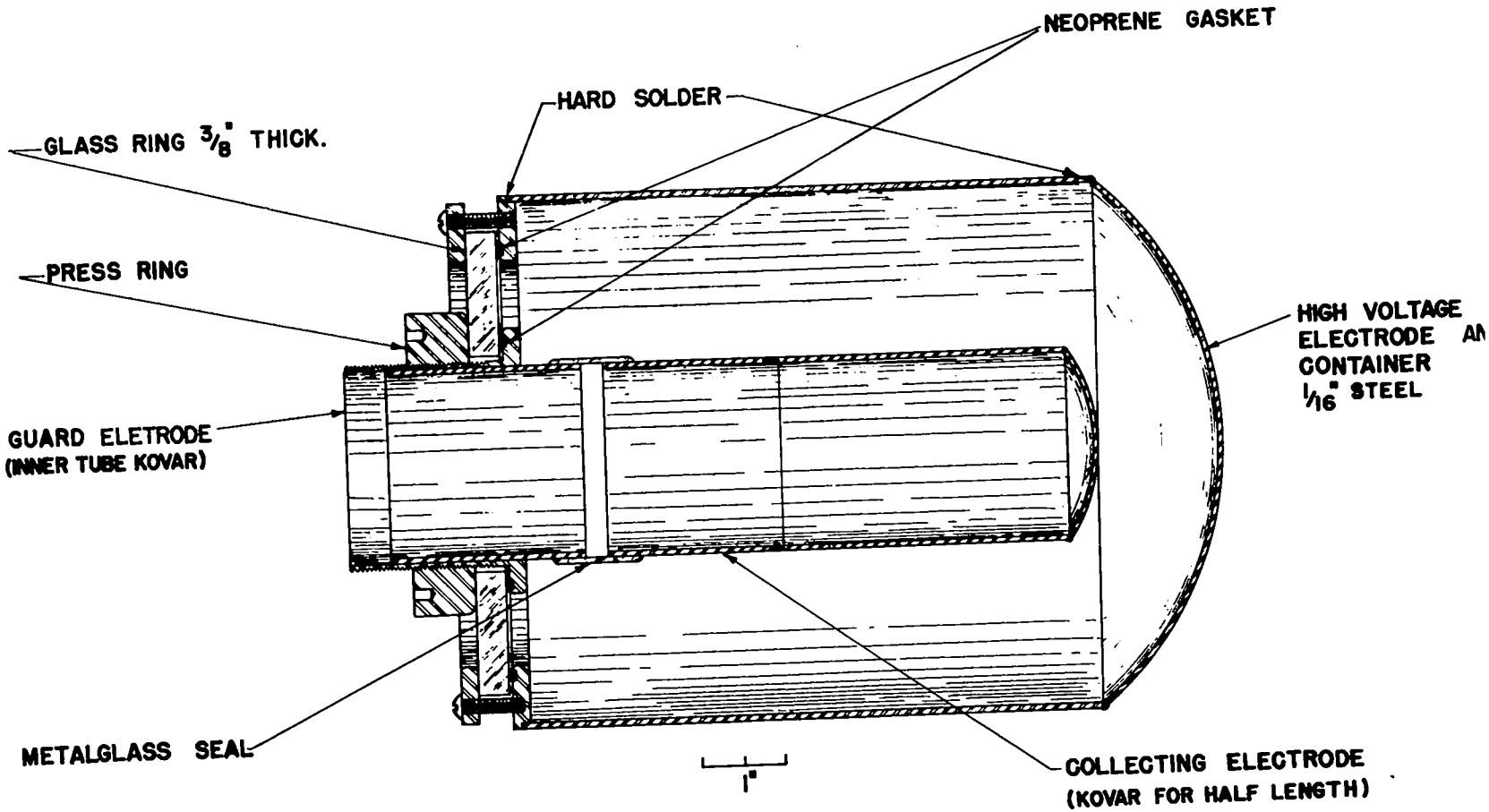

APPROVED FOR PUBLIC RELEASE

50 x 50 x 50 centimeters. The diameters of the inner and outer electrodes are 2-1/4 inches and 4-3/8 inches, respectively. The gas filling consists of BF_3, specially prepared by decomposition of $C_6 H_5 N_2 BF_4$, at a pressure of 74.6 centimeters Hg. The chamber is connected to an amplifier of .2 microsecond rise time and 20 microseconds resolving time. Figure 2 shows the dependence of the counting rate on chamber voltage. The drop of the curve below 3 kilovolts shows that a considerable fraction of electrons is captured even in as pure a gas as the one used. Figure 3 shows the bias curve at 4 kilovolts chamber voltage.

For all neutron energies the highest sensitivity is obtained if the source is placed in the cylindrical cavity of the inner electrode. However, the sensitivity is then dependent very markedly on the energy of the primary neutrons, and source strength comparisons are only possible by a careful calibration at various neutron energies. If the source is moved away from the chamber in a plane perpendicular to the axis, the sensitivity decreases (see Figure 4). The decrease is more rapid for less energetic neutrons, and there exists therefore a region (13 centimeters from axis) where the counting yield depends only slightly on the energy. From the same Figure it appears that the maximum sensitivity, defined as the number of counts divided by the number of emitted neutrons, is of the order of a few per cent, in fair agreement with an estimated value. The detector has been used for measuring the strength of very weak sources. The background is about 15 counts per minute.

15.4 BF_3 COUNTER ARRANGEMENT OF HIGH SENSITIVITY

The apparatus consists of twelve BF_3 proportional counters arranged with their axes on a cylinder of 9 inches diameter and embedded in a cylindrical block of paraffin 18 inches in diameter and 16 inches in length, with a central cylindrical opening of 5 inches diameter in which the source is placed. The counters are 2 inches in diameter and 12 inches long, and are of simple construction. The central electrode is 1 mil kovar wire supported by glass insulators. No guard electrodes are used, which makes careful cleaning and drying of the

Figure 2

Counting rate versus chamber voltage for the boron trifluoride chamber of Figure 1.

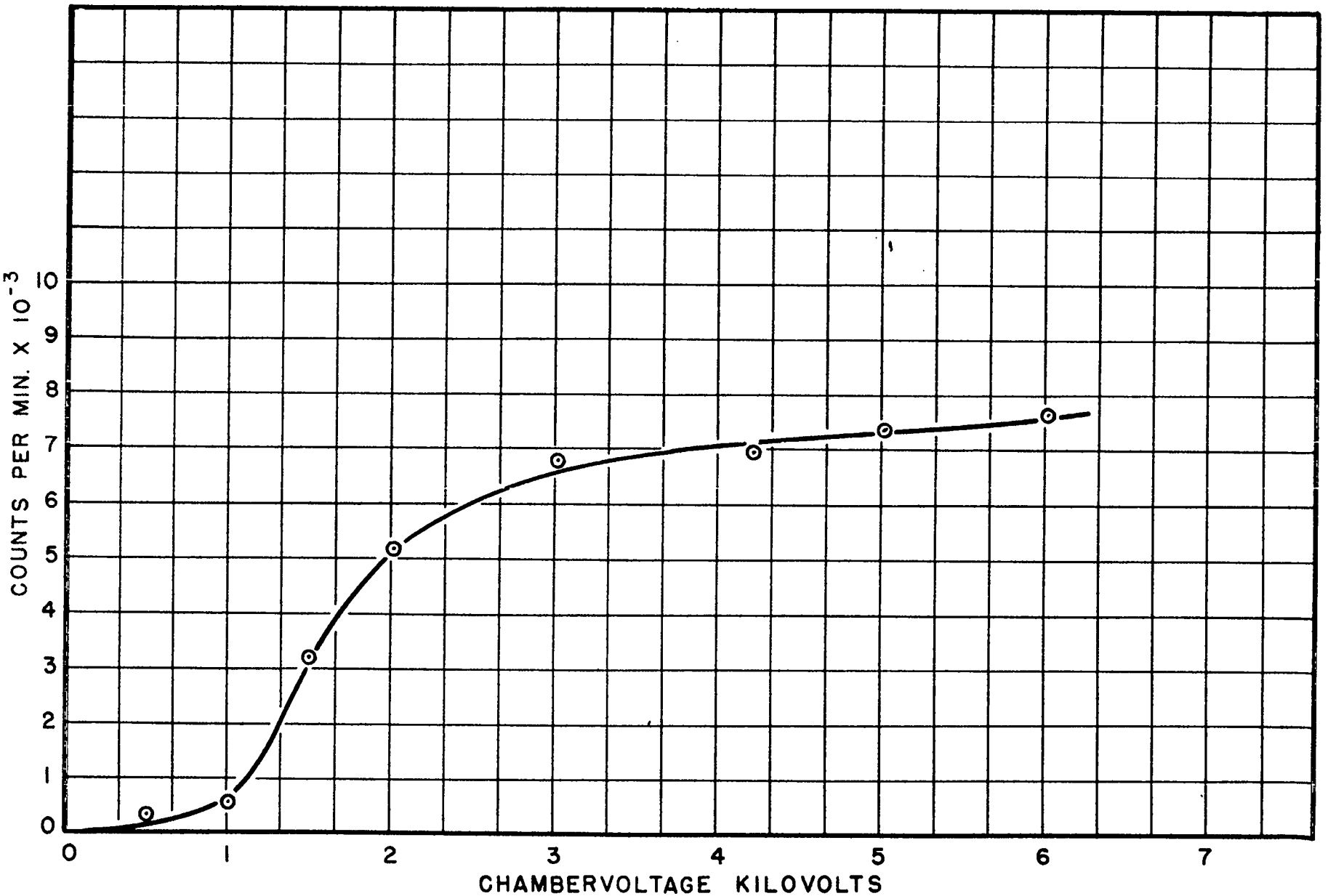

APPROVED FOR PUBLIC RELEASE

Figure 3

Counting rate versus bias for boron trifluoride chamber of Figure 1. Voltage 4000V. Pressure 746 mm Hg.

APPROVED FOR PUBLIC RELEASE

Figure 4

Sensitivity of boron trifluoride chamber (Figure 1) versus distance of source from chamber, in a plane perpendicular to the axis of the chamber. The various curves are taken with sources of different average primary neutron energies.

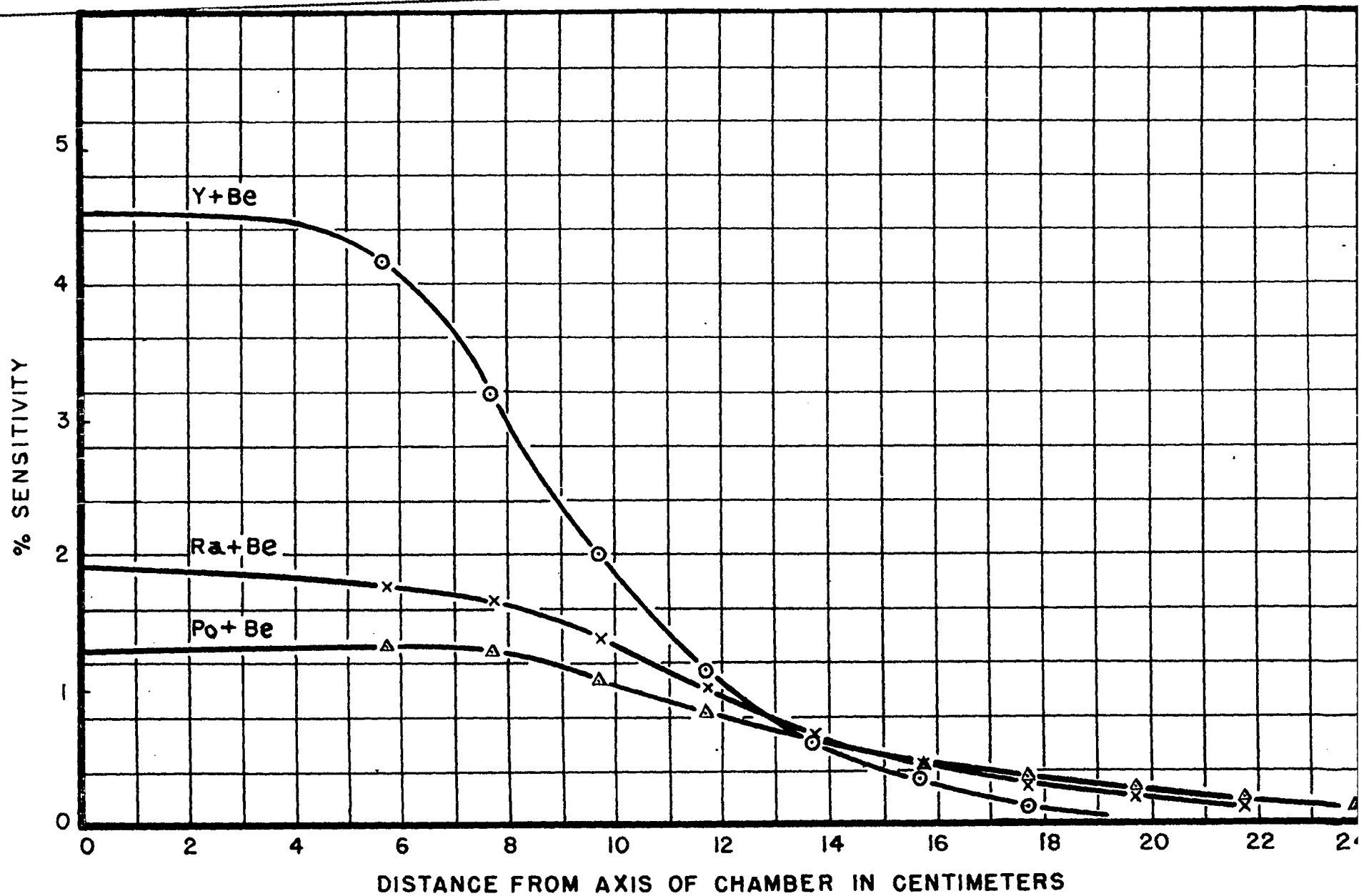

APPROVED FOR PUBLIC RELEASE

insulators necessary. The counters are filled with B^{10} enriched BF_3 containing 70 per cent B^{10} to a pressure of 600 millimeters Hg. With a Po-Be neutron source in the center of the paraffin block, the sensitivity is 13 per cent. The counters were connected in parallel and operated at -2600 volts. The resolving time of the amplifier was .5 microseconds. Figures 5 and 6 show the dependence of the counting rate on the counter voltage at fixed bias, and the dependence of counting rate on the bias at the normal counter voltage of -2600 volts. Both curves exhibit flat regions around the operating point. In addition to its very high counting yield, this arrangement has a high resolution and is therefore capable of counting at high rates without appreciable loss. At 40,000 counts per second in the twelve counters, the loss is only 5.5 per cent. This quantity was measured in the usual way by comparing the counting rates of two different sources, measured individually, with the observed counting rate when the sources were placed simultaneously in the detector. From the measured loss and the resolving time of the amplifier, it is apparent that the total resolving time of the arrangement is mainly determined by the counters.

15.5 FLAT RESPONSE COUNTERS

The detectors described in the two preceding sections have sensitivities which depend very strongly on the energy of the primary neutrons. Several attempts have been made to find an arrangement of paraffin surrounding a boron detector such that the number of boron disintegrations is proportional to the number of primary source neutrons and independent of their energies over a wide range. These detectors have been termed long boron counters or flat response counters. The theoretical treatment of the response of such an arrangement is very complicated. Qualitatively the following arguments might serve to illustrate their performance. Suppose a boron detector is embedded in a cylindrical block of paraffin. A source of neutrons is placed on the axis at a large distance from the front face of the cylinder. The

Figure 5

Counting rate versus counter voltage of high sensitivity boron trifluoride proportional counters.

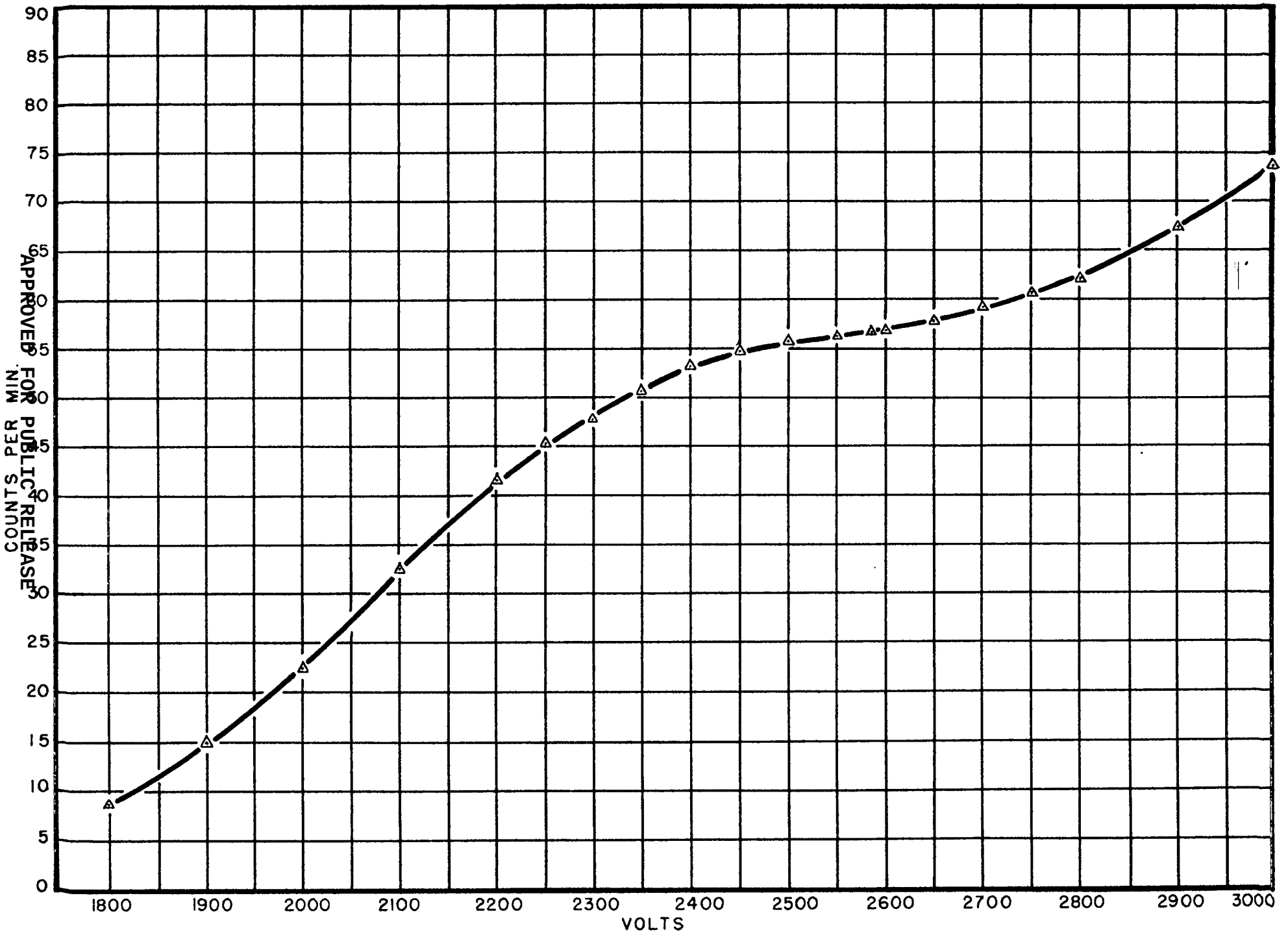

APPROVED FOR PUBLIC RELEASE

Figure 6

Counting rate versus bias at 2600 volts counter voltage of high sensitivity boron trifluoride proportional counters.

APPROVED FOR PUBLIC RELEASE

detector is assumed to extend to the front face of the block and be very long compared to the mean free path in paraffin of any neutron to be detected. Neutrons entering the paraffin will be degraded to thermal energies and diffuse into the detector where they will give rise to $B(n,\alpha)$ reactions. Due to the large cross section, the counting rate will be essentially determined by the flux of thermal neutrons. For an infinitely large slab of paraffin the efficiency would be higher for higher neutron energies since low energy neutrons penetrate only a short distance into the paraffin before being thermalized. They have therefore a better chance of escaping back through the front face (instead of passing through the boron detector) than neutrons which were originally of higher energy and are therefore thermalized at a greater distance from the front face. The reason for this is twofold. At higher energies, more collisions are required for thermalization, and the collision cross section is smaller than at low energies. In order to minimize the dependence of the efficiency on the energy, one has to limit the dimensions of the paraffin so that the thermalized fast neutrons have an increased chance to escape from the paraffin. Obviously it is not possible to accomplish this for all energies from thermal to several Mev. However, arrangements have been found which exhibit rather flat response curves over energy regions of several Mev.

Among the various constructions, two shall be described which have shown the best flat response curves. The first one (so-called 8" long counter) shown in Figure 7 consists of a paraffin cylinder of 12 inches length and 8 inches diameter. Along its axis a BF_3 proportional counter, 1 inch in diameter and 8 inches active length, is embedded. It protrudes slightly over the front face of the paraffin but is protected from direct thermal neutrons by a cadmium shield. The counter is electrically shielded by an aluminum tube. For insulation purposes the space between the counter wall and the shield is filled with ceresin wax. The central electrode of the counter consists of a kovar wire of 10 mil diameter. The counter is filled with enriched (80 per cent B^{10}) BF_3 to a pressure

Figure 7

Detail of 8 inch flat response counter.

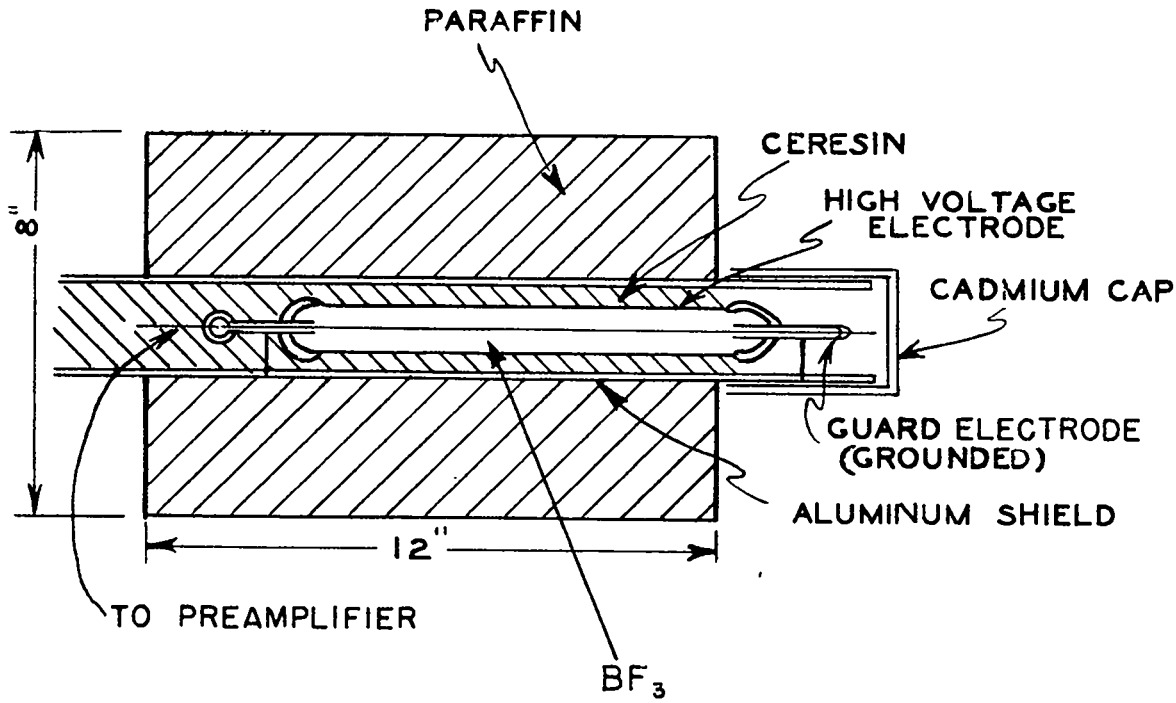

of 25 centimeters Hg. With -2700 volts applied to the wall, a gas amplification of about 10 is obtained. The sensitivity versus neutron energy is represented in Figure 8. The measurements were taken with the source of neutrons on the axis of the detector 1 meter from the front face. The arrangement was in the center of a room 20 x 15 feet, and 50 inches above the floor so as to minimize the effect of scattering and degrading of the neutrons by floors and walls. Nevertheless it is believed that 15 per cent of the counted neutrons still were scattered. The absolute sensitivity is about one count for every 10^5 neutrons emitted by a spherically symmetrical source. The most reliable points of the sensitivity curves are those taken with the Li(p,n) and D(D,n) sources. The flux of these sources was determined by U-235 fission counts. Their energies are exactly known (points at .5, 1.0, 1.5 and 3 Mev). Similarly reliable are the points at .15 Mev and .023 Mev which were taken with (γ,n) sources of known strength of (Be + Y) and (Be + Sb), respectively. For the points at .4 Mev, 2.2 Mev and 5 Mev, sources with a complex neutron spectrum were used to which a certain average energy is ascribed. These points are therefore open to some doubt. This is particularly true for the point taken with the Ra-Be source. It is furthermore estimated that the response at thermal energy of the neutrons is around 70 in the units used on Figure 8.

A considerable improvement of the response was achieved with the arrangement shown in Figure 9. Here the counter is shielded with an additional layer of paraffin separated from the inner part by a boron-carbide or boron-trioxide shield, which reduces the number of counts caused by stray neutrons to about 5 per cent when the source is again placed at 1 meter distance from the front face. The sensitivity for low energy neutrons is increased by drilling a set of holes into the front face of the paraffin cylinder. These holes give the slow energy neutrons a better chance of entering the boron detector before being reflected back through the front face. Eight holes 1 inch in diameter and 3-1/2 inches deep are drilled parallel to the axis of the paraffin cylinder with their centers on a circle of 3-1/2 inch diameter. The boron trifluoride counter

Figure 8

Sensitivity curve of 8 inch flat response counter.

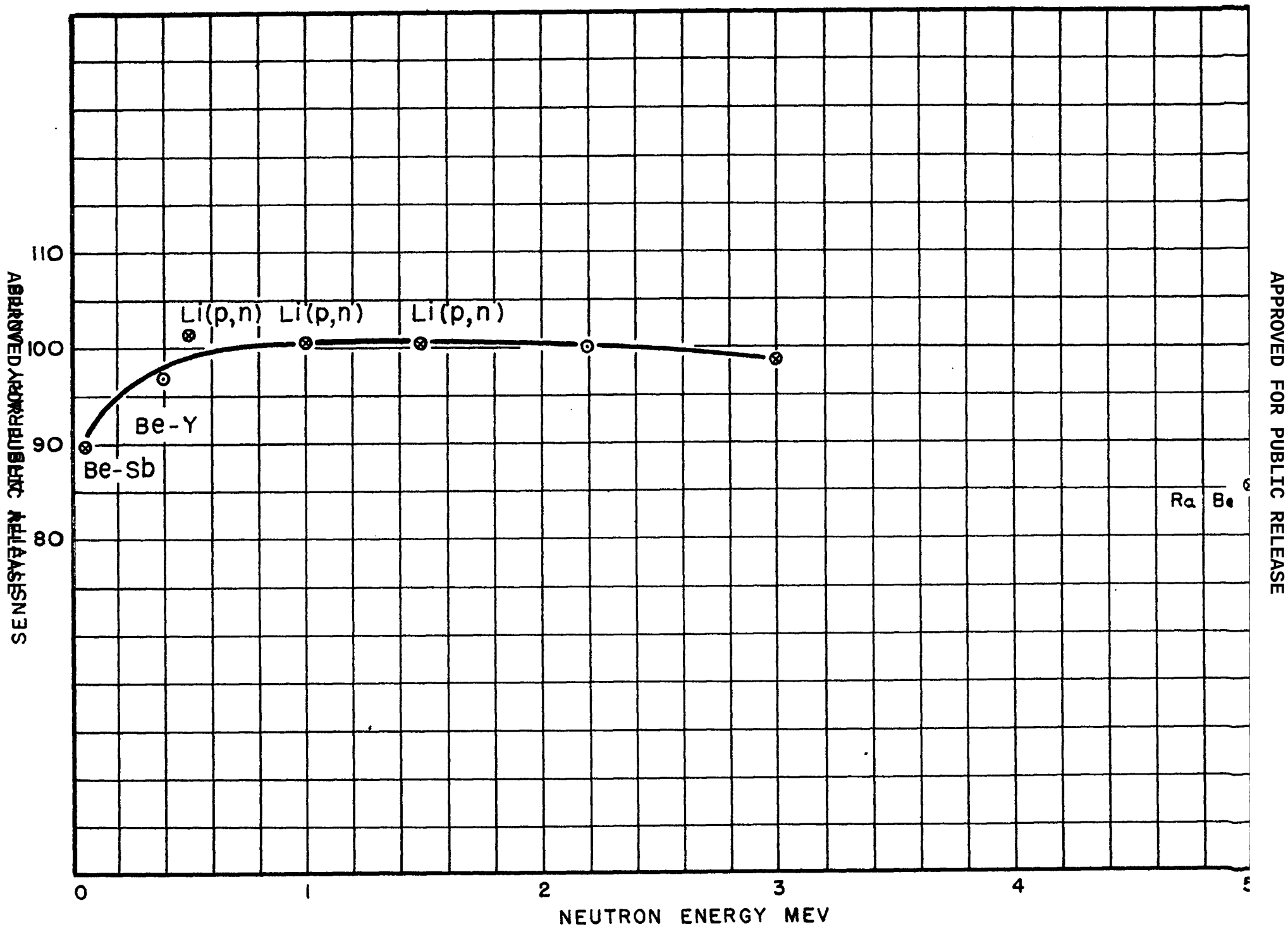

Figure 9

Detail of 15 inch shielded flat response counter.

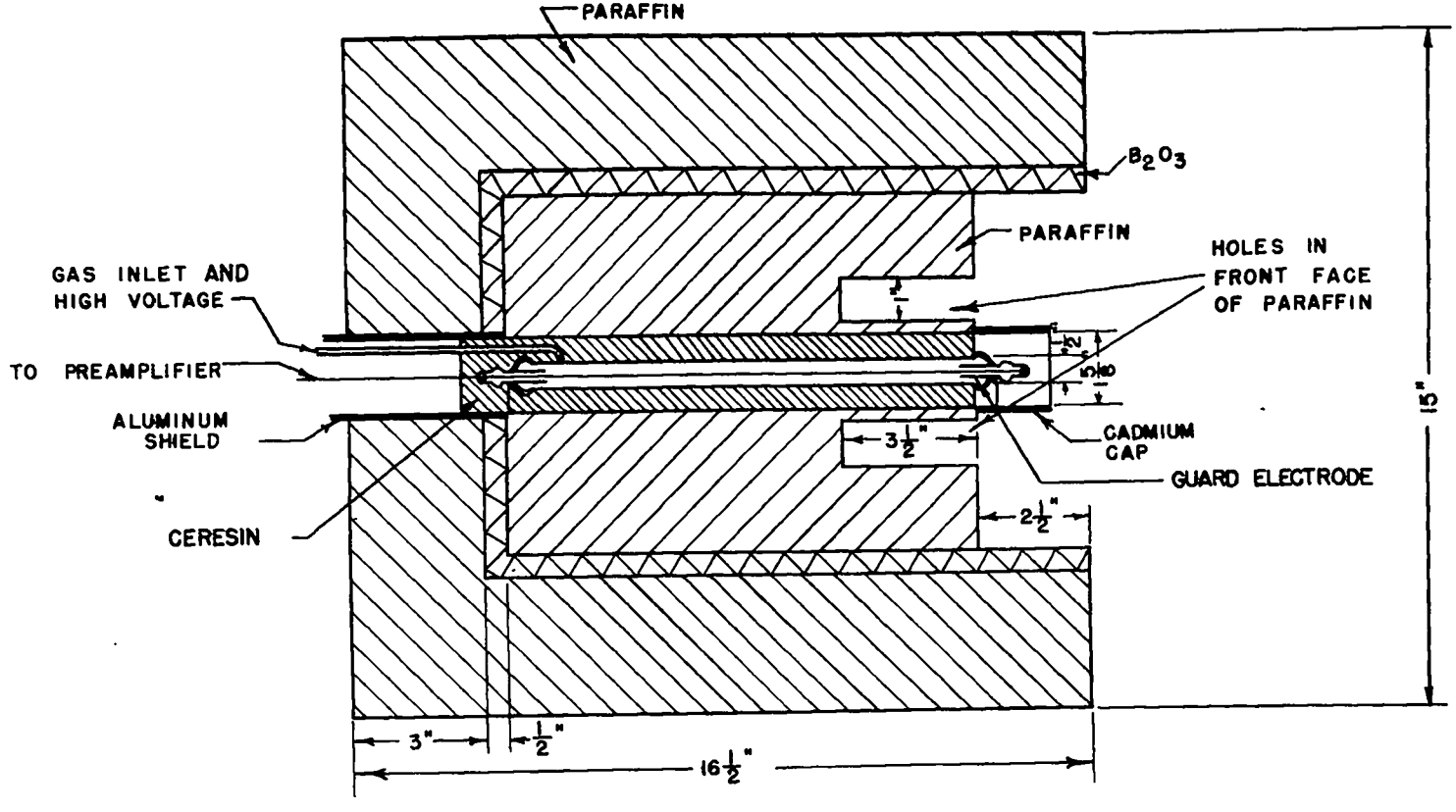

APPROVED FOR PUBLIC RELEASE

used in this arrangement has a diameter of 1/2 inch and an active length of 12 inches. It is otherwise similar to the one used in the preceding arrangement. The dependence of the sensitivity on the neutron energy is shown in Figure 10. The thermal energy point was measured with photo neutrons from (Be + Sb) degraded strongly by a layer of heavy water. The point at .023 Mev was obtained with the same source without degradation, and the point at 1.2 Mev by a Li(p,n) source, the flux of which was determined by a U-235 fission detector. These points are therefore very reliable. The points at .4 Mev, 2.2 Mev, and 5 Mev (Ra + Be) are taken with a complex neutron spectrum and are therefore somewhat questionable.

15.6 SOLID BORON RADIATOR CHAMBER

The chamber is of the parallel plate type with the boron covered foil on the negative high voltage electrode. The electrode separation is 0.4 centimeters and the diameter of the electrodes 1.6 centimeters. The chamber is filled with argon at about 3 atmospheres pressure and operates with a collecting voltage of between 100 and 200 volts. The boron is deposited on a tantalum foil by thermal decomposition of B_2C_6. The deposit has a diameter of 1.4 centimeters and has a thickness of about 25 γ/cm^2 which is considerably less than the range of both the α-particles and the Li recoils. The bias curve obtained with this chamber is shown in Figure 11. A sufficiently flat plateau is found, and the correction for finite thickness given by Equations 1 and 2 can be applied in order to determine the counting rate at zero bias.

15.7 ABSOLUTE BF_3 DETECTORS

Two detectors with gaseous boron compounds suitable for absolute flux measurements are shown in Figures 12 and 14. Their common characteristic is the accurately known volume in which the counted pulses originate.

In the cylindrical chamber (Figure 12), there exists only a small region where it is uncertain whether or not detectable pulses originate. This region is one where the collecting electrode passes from the opening of the high voltage electrode through the guard electrode. The counting volume was

Figure 10

Sensitivity of 15 inch shielded flat response counter at different neutron energies.

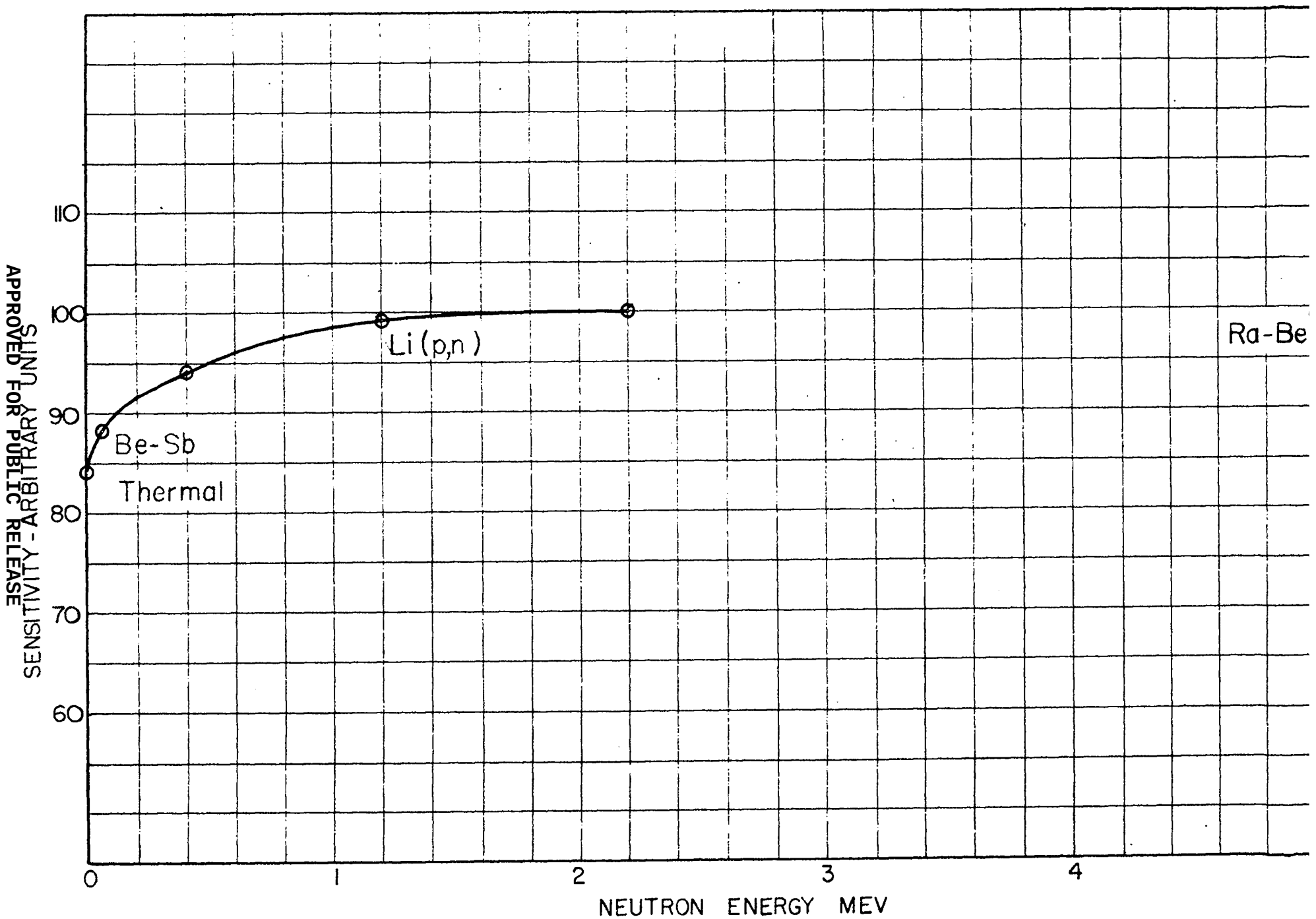

APPROVED FOR PUBLIC RELEASE

Figure 11

Bias curve of boron foil counter.

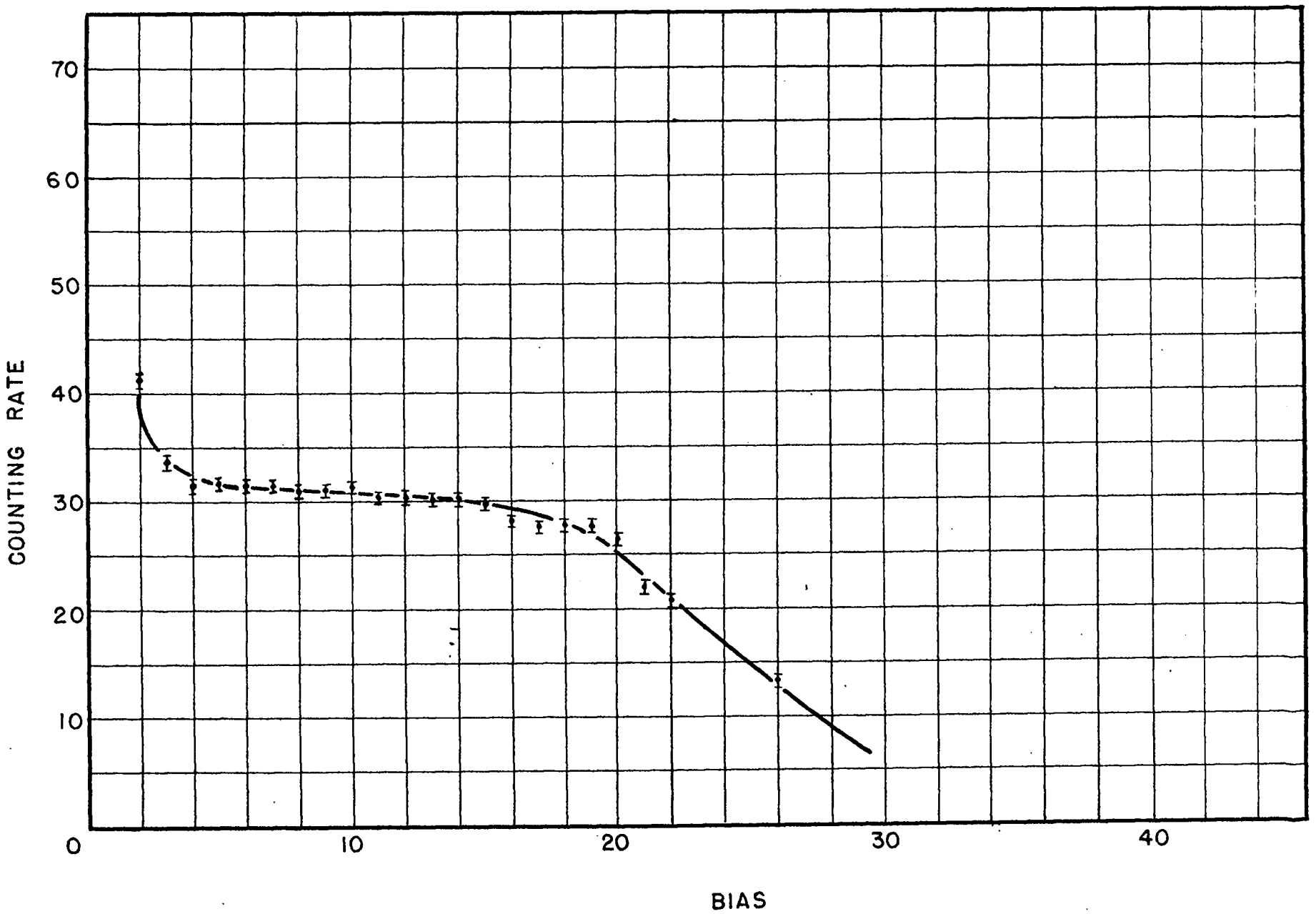

APPROVED FOR PUBLIC RELEASE

Figure 12

Definite volume boron trifluoride ionization chamber.

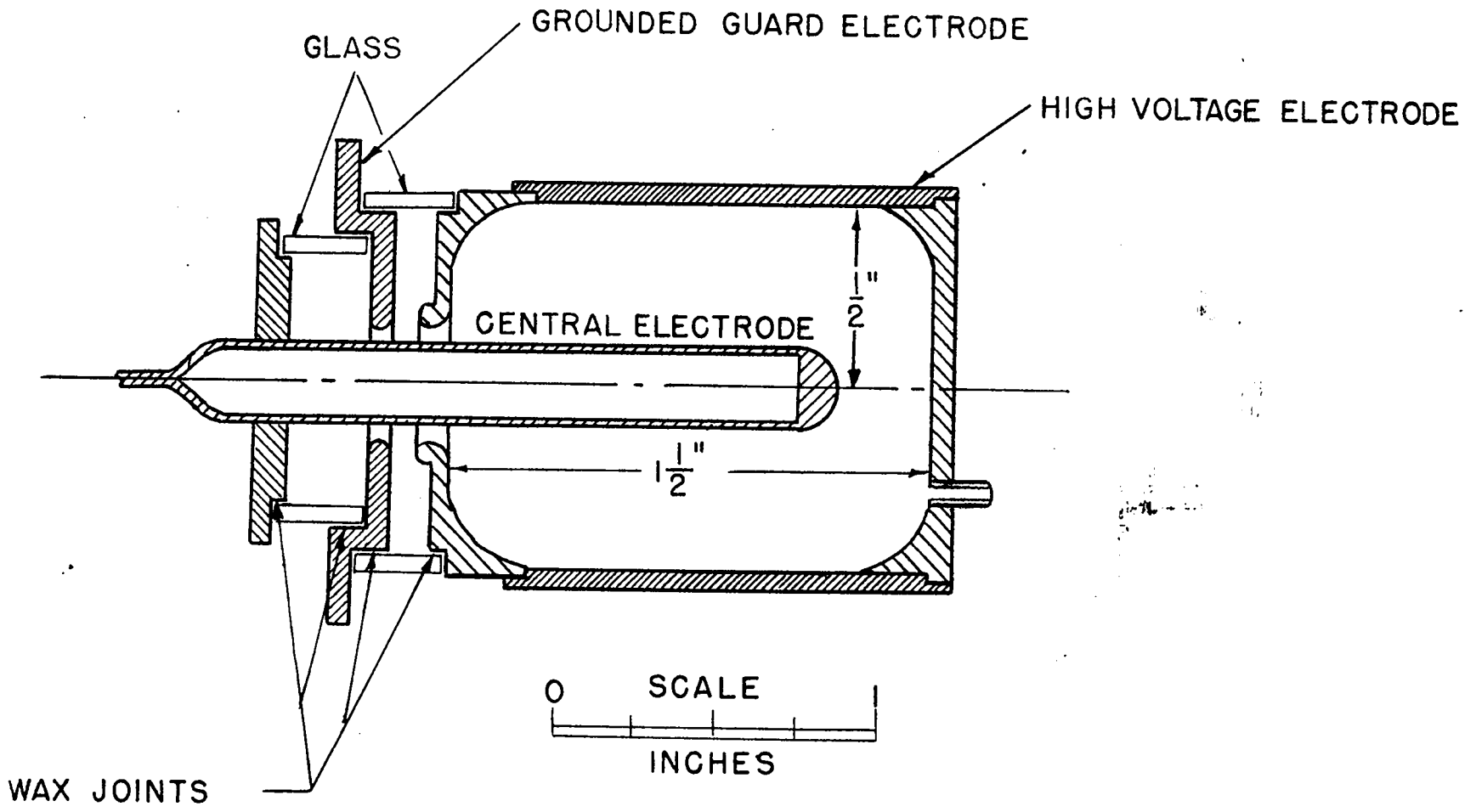

APPROVED FOR PUBLIC RELEASE

determined by filling the chamber with water. The counting rate C is related to the neutron flux density ϕ by the equation:

$$C = \phi A \sigma n \qquad (5)$$

where n is the number of B^{10} atoms per cm^3, σ the disintegration cross section, and A is the active volume. For the chamber shown in Figure 12, the counting volume is 17.86 cm^3. The volume of the uncertain region is .31 cm^3, or less than 2 per cent of the main counting volume. The corners of the counting volume are carefully rounded, a precaution which greatly reduces the wall effects. Figure 13 shows bias curves obtained with this chamber at different pressures and suitable collecting voltages. The various curves were taken with the chamber in the same neutron flux. The numbers attached to each curve give the counting rates per unit pressure at equal temperature, and it is apparent that within a small error of about 1 per cent these numbers are equal. The counting rates for zero bias were not calculated but were obtained by linear extrapolation of the observed curves. Since the slopes are quite small this procedure seems to be adequate. A calculation of the correction due to wall effects for this type of chamber would be very inaccurate.

In the proportional counter (see Figure 14), the counting volume is limited by two discs of semiconducting material carrying sufficient current to prevent accumulation of charges. The discs establish at the boundary of the counting volume an electric field which varies radially in the same manner as in the central region of the counter. In this way the usual end effects of proportional counters (see Section 11.5) are avoided.

The discs consist of soft glass, coated with "Aquadag", and metalized on the outer edge in order to insure contact with the counter wall. The central 10 mil platinum wire is fused into very small holes in the glass discs. The technique of drilling small holes into the discs is as follows: The glass plate is cemented onto a rubber diaphragm covering a vessel connected to a rubber

Figure 13

Bias curves of definite volume BF_3 ionization chamber. Curves taken at different pressures. The numbers accompanying each curve give the counting rate at unit pressure at 0°C.

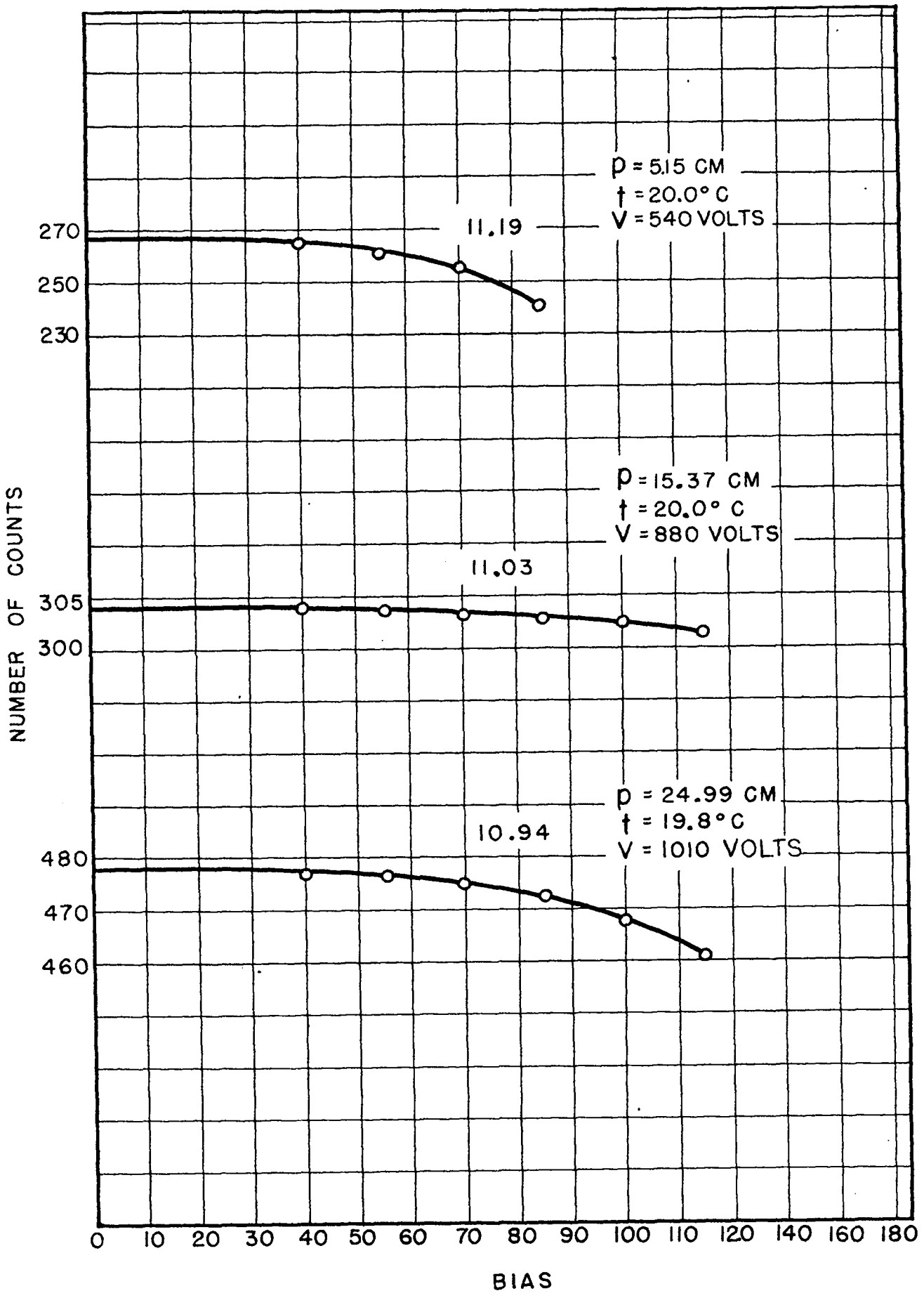

Figure 14

Definite volume boron trifluoride proportional counter.

1. Kovar-glass seal.
2. Outer shell.
3. Protecting sleeve for collecting electrode.
4. Glass beads.
5. Glass discs (edges metalized or painted with "Aquadag".)
6. Spacer
7. Inner shell.
8. Collecting electrode (.01" platinum wire).
9. Vent holes.
10. Kovar tube.

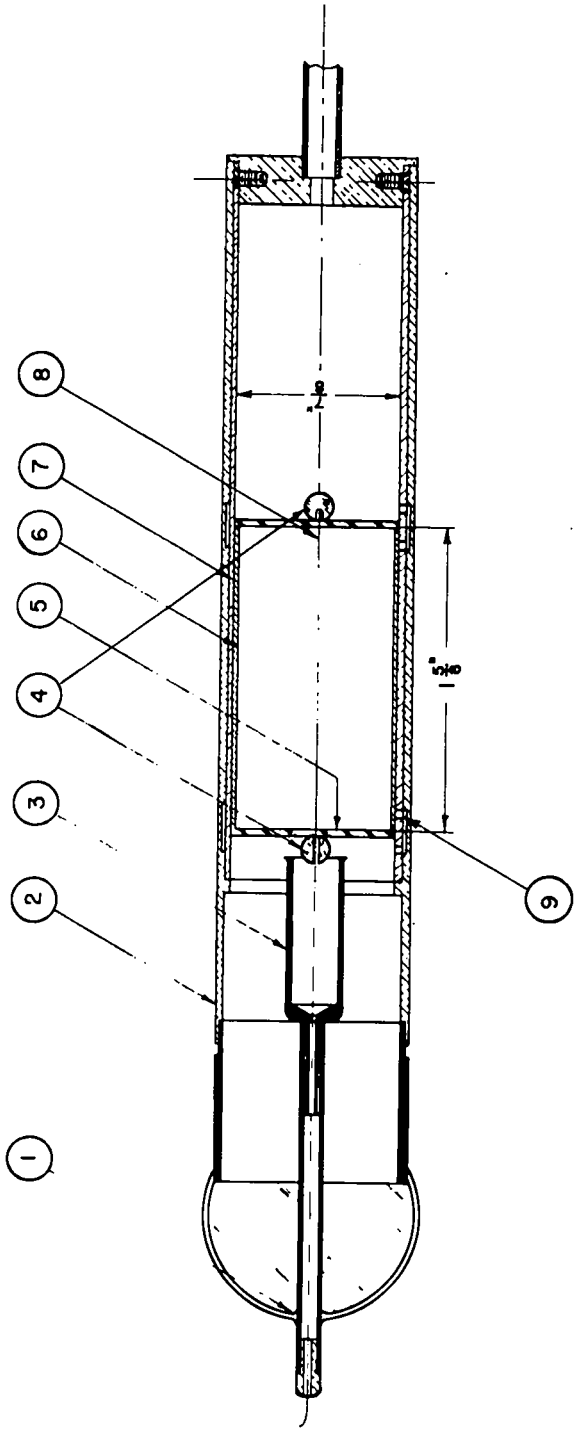

squeeze-ball. In this way the disc can be pressed gently and with uniform pressure against the drill. The latter consists of a short piece of tungsten wire, the diameter of which is slightly less than that required for the hole. It is soldered into a round piece of brass which is clamped into a chuck driven by an air turbine or a suitable high speed electric drill rotating at about 7000 rpm. Six hundred mesh carborundum with water serves as a grinding agent. With this arrangement, holes as small as 3 mil in diameter can be drilled. In order to fuse the platinum wire into the glass, the wire is threaded through the hole of the disc which is then placed into a furnace at the annealing temperature of the glass. The fusing is accomplished by passing a current of suitable strength through the wire so that the glass melts onto the wire.

By shooting α-particles radially into the counter through mica windows, it was found that the gas multiplication is very constant up to a distance of 1 millimeter from the discs. Figure 15 shows bias curves obtained at various pressures. The gas multiplication was made sufficiently high so that pulses from secondary electrons from γ-rays within the counting volume were at least as big as boron disintegration pulses outside the counting volume. The bias curves are quite flat and can easily be extrapolated to zero bias. The counting rates at zero bias per unit pressure at $0^{\circ}C$ are given with the corresponding curves. These counting rates are very closely the same. This shows that the detector can be used for absolute measurements.

Figure 15.

Bias curves of definite volume BF_3 counter. Curves taken at different pressures. The numbers accompanying each curve give the counting rate at unit pressure at 0° C.

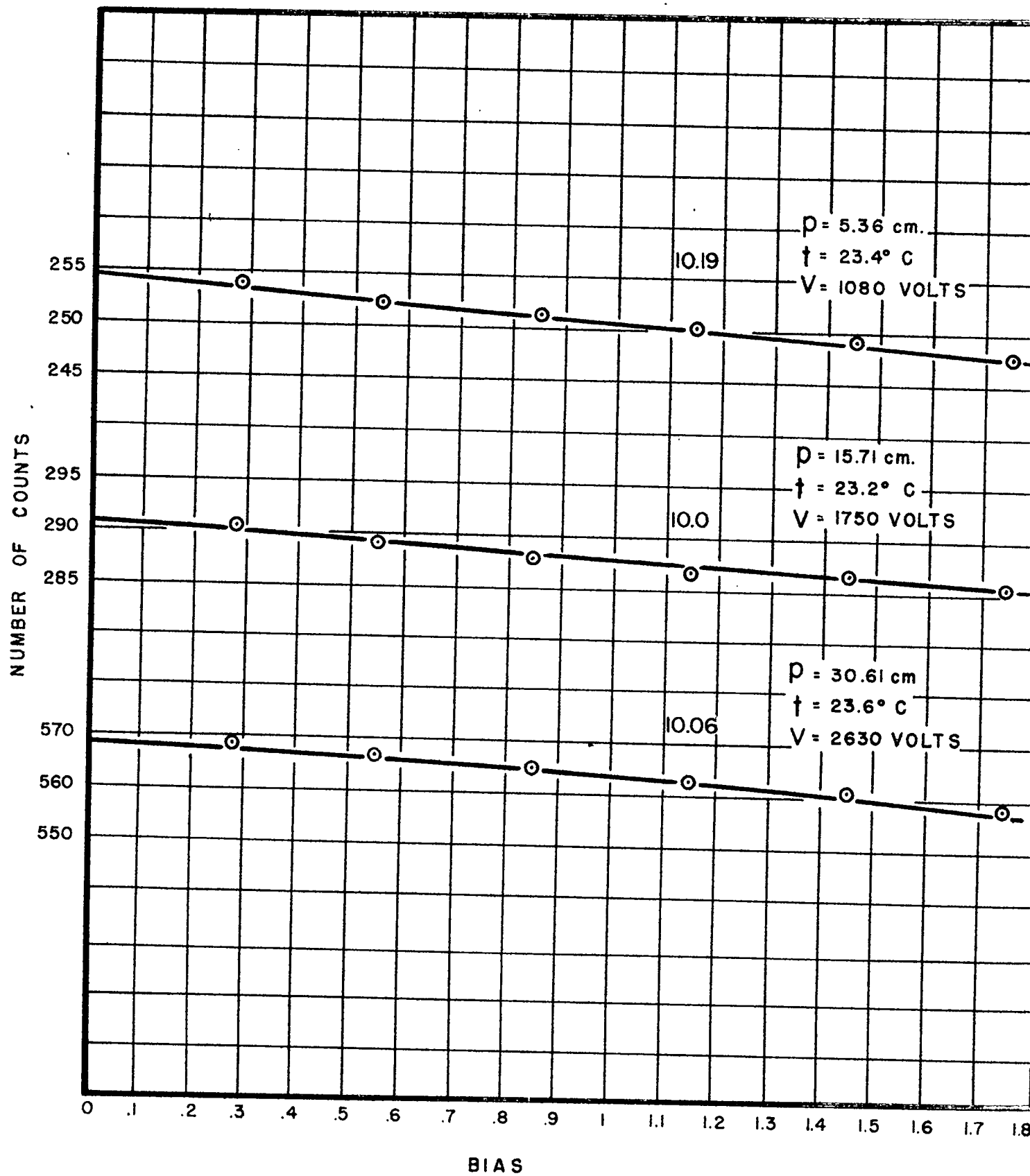

LOS ALAMOS TECHNICAL SERIES

VOLUME I

EXPERIMENTAL TECHNIQUES

PART II

CHAPTER 16

FUSION REACTIONS

by

HEINZ ROSEL AND HANS STAUB

CHAPTER 16

FISSION DETECTORS

16.1 INTRODUCTION

The main purposes for which fission detectors are used are:

(a) Measurement of the rate of fissions in a given neutron flux for the determination of the fission cross section; measurement of the rate of fissions in a material with known cross section for the determination of flux of monoenergetic neutrons. In both cases it is important to know accurately the amount of fissionable material and to count quantitatively the number of fissions occurring in the material.

(b) Relative measurements of neutron flux of sources with identical spectra. In this case it is desirable to have a detector of high counting yield, but the absolute value of this quantity does not need to be known. The various fissionable materials offer the possibility of constucting detectors with different yields for different neutron energies since the materials have different threshold energies.

(c) Investigation of the energy distribution of the fission fragments. Detectors for this purpose are very similar in construction to the ones used for the study of α-particle spectra.

In most cases the fissionable material is used in the form of thin foils. Since the mean range of the fission fragments is only about 2.1 centimeters in air it is evident that only very thin layers of material can be used for absolute.

detectors. This makes it necessary to spread the material over large areas if detectors of high counting yields are desired. The use of a gaseous fissionable compound would avoid this difficulty. Uranium-hexafluoride (UF_6) might be suitable, but unfortunately experiments in this direction have not been successful. Electron collection, which in the case of fission detectors is of prime importance (because of the necessity of achieving short resolving times; see below), could not be obtained in this gas. Moreover, the highly corrosive nature of UF_6 causes difficulties with common insulators.

The fission pulses originating from a solid deposit of fissionable material show, of course, a wide spread in energies ranging from zero to about 110 Mev. This is partly due to the natural spread of about 40 and 110 Mev, and partly due to the energy loss which the fragments undergo in passing through the fissionable material. Nevertheless it is possible to obtain bias curves which (below about half the maximum energy) show a rather flat plateau. It is also worthwhile to remember that since two fission fragments result from every fission process, the number of fission pulses observed within a solid angle of 2π is equal to the number of fissions produced in the material.

In every fission detector, the fission pulses are superimposed over a background of very numerous α-particles (see Section A.11). It is therefore important that the resolving time of a fission detector and its amplifier be made as short as possible in order to avoid piling up several α-particle pulses to a height comparable to a fission pulse. Since the α-particles have energies of around 4 Mev, whereas the fission fragments have energies of about 80 Mev, one can allow a pile-up of about five α-particles and still observe a rather large fraction of the fission pulses. This consideration usually sets an upper limit on the total amount of material which can be put into a detector. An approximate estimate of the pile-up of α-particles can be obtained from the following formula (see Section A.12):

$$C(n) = \frac{N_o}{1 + N_o \tau} \quad \frac{(N_o \tau)^{n-1}}{(n-1)!} \quad e^{-N_o \tau} \qquad (1)$$

C(n) is the number of counts per unit time containing n unresolved pulses; N_o is the true number of pulses per unit time. The pulses are assumed to be of rectangular shape of a duration τ. It may be pointed out that n pulses of height P do not necessarily give a pulse of height nP. The resulting size depends largely upon the frequency response of the amplifier, since the pulse height nP is only reached during a time $t \leqslant \tau$. It should be noted that for practical purposes this formula holds only approximately since in most cases the pulses will be of an exponential character. However, it gives the right order of magnitude if one takes τ as equal to the resolving time as defined in Section 10.3.

In many instances where it is desirable to have as much fissionable material as possible in a chamber, the pile-up of α-particles can be effectively reduced by adjusting the dimensions of the detector and the pressure of the gas so that the fission fragments spend in the sensitive volume only a fraction of their range. Since, in contrast to the behavior of α-particles, the highest energy loss per unit path length occurs for fission fragments at the beginning of the track, and since the range of the α-particles is roughly twice the range of the fission fragments, such an arrangement leads to a large increase in the relative size of fission pulses as compared to α-particle pulses. An additional improvement consists in placing over the fissionable material a plate in which a large number of suitable holes is drilled. In this way the fission fragments and α-particles are collimated to a certain extent, and are prevented from entering the chamber at small angles with respect to the electrode. Even in a shallow parallel plate chamber, most of the particles emitted at a grazing angle would have all or a large part of their path within the counting volume and therefore give an unfavorable ratio of fission to α pulse height.

Since in any fission detector, the size of the fission pulses varies

from zero to a maximum value, one will always observe only a fraction of the fissions occurring in the material. For absolute measurements of flux or cross section, it is necessary to correct for the finite thickness of the foil; i.e., the detection of efficiency, defined as the number of observed pulses divided by the number of fissions, has to be known. For a plane foil of fissionable material, arranged so that no fission fragment can escape from the counting volume without producing a detectable pulse, the detection efficiency is given by:

$$F(B) = 1 - \frac{t}{2(R_o - R(B))} \qquad (2)$$

where t is the thickness of the foil, R_o the range of the fission particles in the fissionable material, and R(B) the range of a fission particle of energy equal to the bias energy B. In deriving this relation (see Section A.6), it is assumed that all fission fragments have the same range R_o and that the thickness t of the foil is $t \ll [R_o - R(B)]$. In Figure 1 a calculated bias curve is compared with experimental data. At high bias, the experimental points deviate considerably from the curve. This is to be expected in view of the assumptions made in the calculation. In the case of a cylindrical fission chamber, carrying fissionable material on the inside of the outer electrode, an additional correction, a "wall correction", has to be applied. For an infinitely thin layer of fissionable material, the detection efficiency which takes into account particles striking the cylindrical wall is given by:

$$F(B) = 1 - \frac{r(B)}{4b} \qquad (3)$$

where b is the radius of the chamber and r(B) is that portion of the range of the particle which must be spent in the sensitive volume of the chamber in order to produce a pulse equal to the bias energy B. It is assumed that r(B) is very small compared with b. The necessary data for computing the thickness and the wall corrections are found in Section A.10, which gives stopping power and

Figure 1

Bias curve of an ion pulse chamber carrying a thin fission foil on a plane electrode. Curve calculated according to Equation 3. Crosses represent measurements using a foil of appropriate thickness.

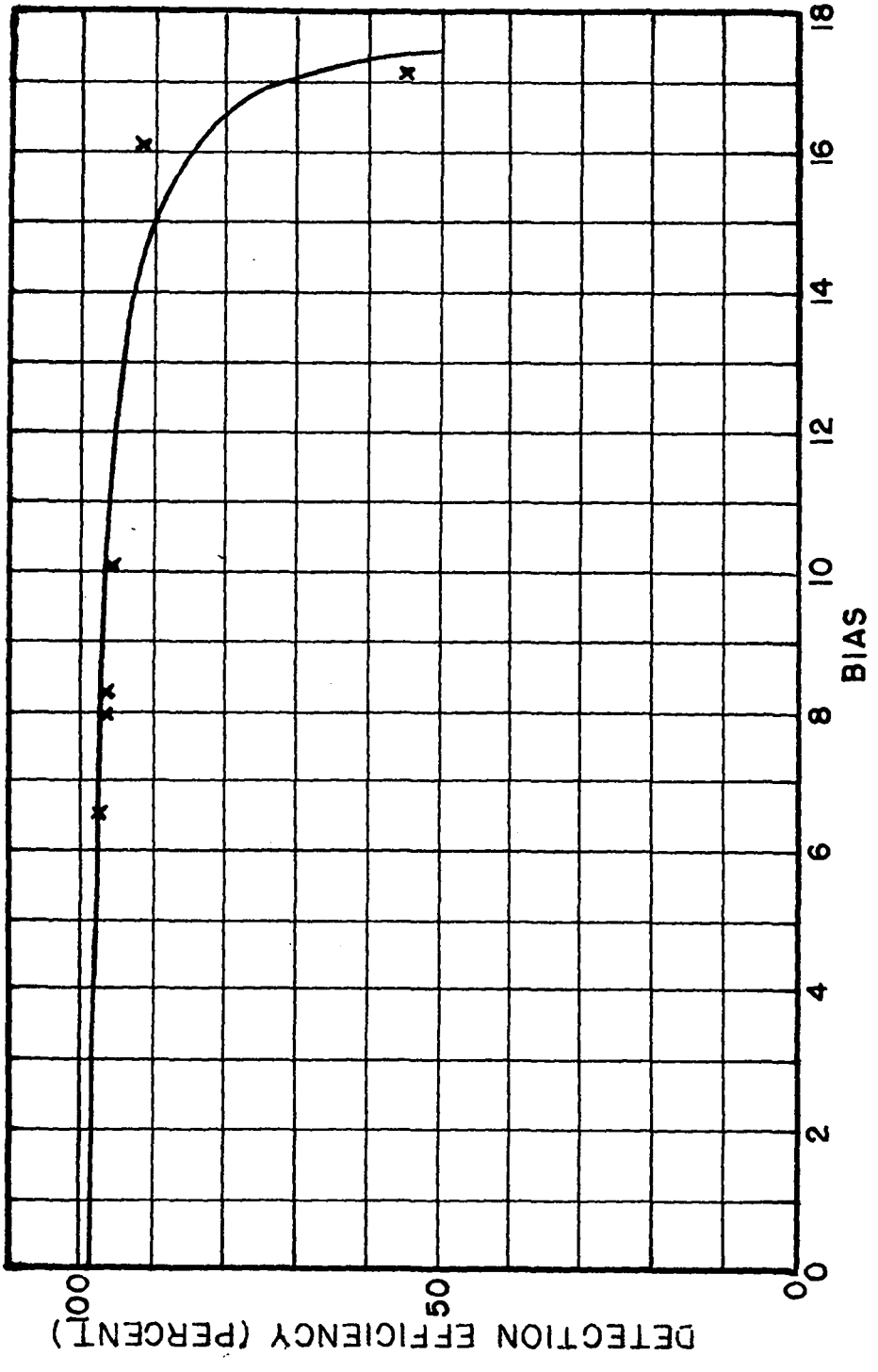

range energy relations for fission particles. If both corrections are small, the final expression for the detection efficiency is the product of Equations 2 and 3.

16.2 PARALLEL PLATE FISSION CHAMBER

A chamber suitable for the absolute measurement of the number of fissions is shown in Figure 2. It is operated at a pressure of 1.5 atm of argon or nitrogen with a collecting voltage of -300 volts at the electrode which carries the foil. The largest amount of Pu^{239} which has been used was 1.2 mg deposited on a circle of 4 cm diameter (95 γ/cm^2). With pure argon, the rise time of the pulses is of the order of 1 microsecond. The amplifier had a resolving time of .1 microsecond. This arrangement reduces the piling up of α-particles to the size of a fission pulse very effectively. No such pulse was observed over a period of weeks. Figure 3 shows a bias curve obtained with a .434 mg foil of plutonium irradiated with slow neutrons. It clearly shows a practically horizontal plateau over a considerable bias range.

16.3 SMALL FISSION CHAMBER

A chamber suitable for quantitative flux measurements and of very small dimensions is shown in Figure 4. The small dimensions are a particularly desirable feature for measurements of flux in a neutron atmosphere where the introduction of large cavities would change the neutron distribution. The volume of the chamber including the long support is only about 50 cm^3. It is filled with approximately 1 atmosphere of argon. The inner electrode serves as the high voltage electrode and as the collecting electrode, the outer electrode being grounded. The inner electrode is coupled through a small capacity to the input of the amplifier as shown schematically in Figure 4. No spurious pulses comparable in size to fission pulses were detected if the collecting voltage was kept below 250 volts. Foils containing up to 10 mg/cm^2 of U^{235} were used. The material was deposited on a 1 mil platinum

Figure 2

Parallel plate type fission chamber for absolute measurments of fission rates.

1. Gas tight cover.
2. Mounting position of sample.
3. High voltage electrode.
4. Collecting electrode.
5. Guard electrode.
6. Polystyrene insulator.
7. Gasket.
8. Collar for connection with preamplifier.
9. High voltage lead.
10. Lead to preamplifier.
11. Gas inlet.

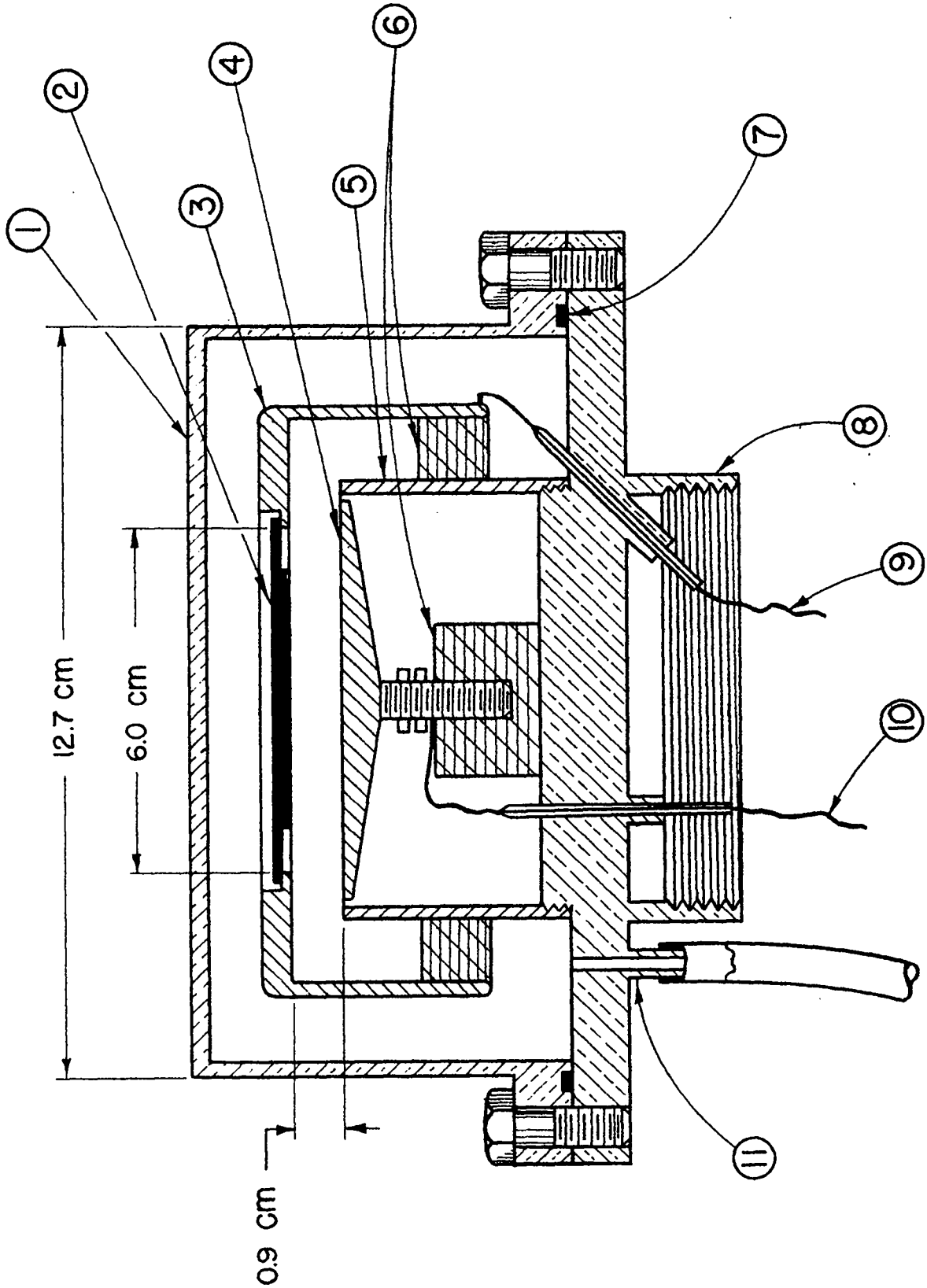

Figure 3

Fission bias curve taken with chamber shown in Figure 2.

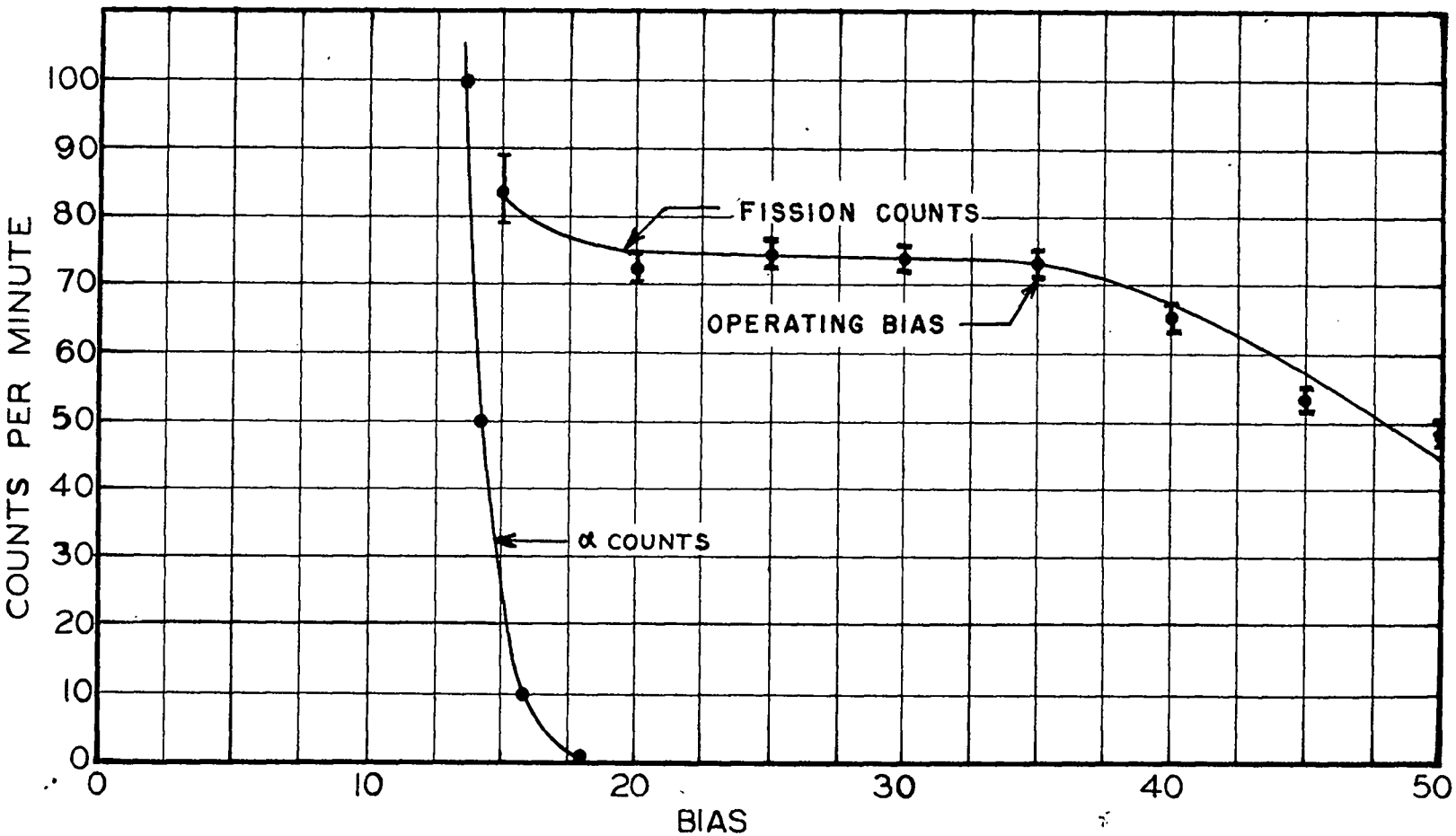

APPROVED FOR PUBLIC RELEASE

Figure 4

Small fission chamber.

1. Lucite insulator.
2. Contact spring.
3. Lead to collecting electrode (#28 wire).
4. Lucite guides.
5. Aluminum shield (.028 inch wall thickness) forming outer electrode.

The inset drawing shows the electrical connections for the case that the inner electrode served as high voltage and collecting electrode.

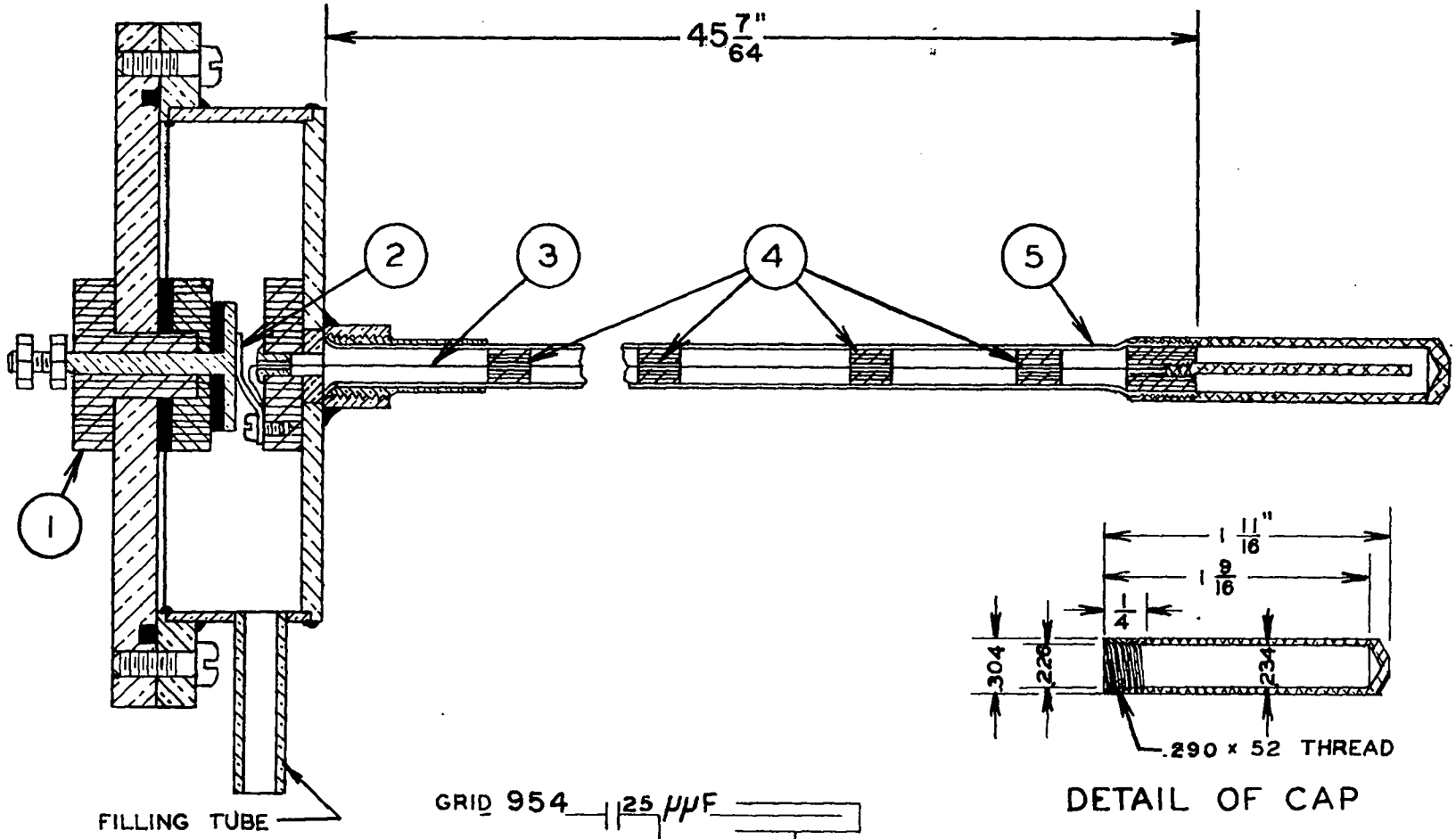

DETAIL OF CAP

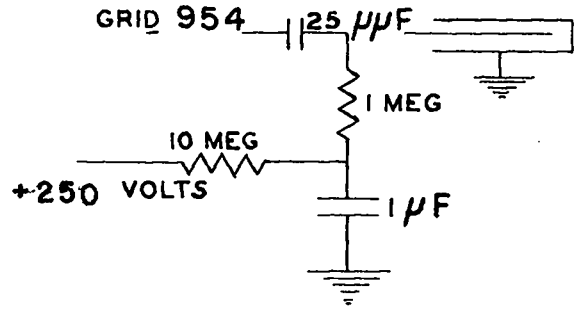

ELECTRICAL HOOKUP

APPROVED FOR PUBLIC RELEASE

foil which then was rolled into a cylinder and slipped into the chamber. The total amount of material in this case was 60 mg of U_3O_8.

16.4 FLAT FISSION CHAMBER OF HIGH COUNTING YIELD

A chamber for very large amounts of material confined to a comparatively small volume is shown in Figure 5. It was used with 750 mg of U_3O_8 on each plate (63 per cent U^{235}, 37 per cent U^{238}). The chamber was operated at pressures between 1.7 atmospheres and 3.4 atmospheres of argon with a collecting voltage of 100 to 200 volts. Since the layer of material is very thick, no plateau in the bias curve could be obtained. Using an amplifier with a square transient response and a resolving time of about 0.1 microsecond, serious trouble from piling up of α-pulses was encountered.

16.5 MULTIPLE PLATE FISSION CHAMBER OF HIGH COUNTING YIELD

In this chamber, shown in Figure 6, a very large amount of material is distributed over a number of electrodes. Twelve of the fourteen electrodes were covered with enriched uranium on both sizes. The two front and bottom plates were only plated on one side. The plates consisted of .8 mil aluminum foils of 20.5 centimeters diameter mounted on 1/16 inch thick aluminum rings. Alternate electrodes are connected, so that they form two sets, one set serving as a collecting electrode, the other as the high voltage electrode. With a coating of 1 mg/cm^2 of uranium, a total of 7.74 gm was deposited on the plates. The material was not highly enriched, since only .89 gm were U^{235}. The chamber was filled with argon at atmospheric pressure. No plateau in the bias curve was obtained. The chamber is therefore only suitable for relative measurements of neutron flux.

16.6 SPIRAL FISSION CHAMBER

This section describes a fission detector of very high counting yield combined with very small dimensions. It consists of two concentric spirals closely spaced and coated with fissionable material on both sides. The two

Figure 5

Flat fission chamber of high counting yield.

1. Metal glass seal.
2. 3/8" steel tubing 1/32" wall.
3. Lucite support.
4. Brass cover plate.
5. Lucite ring.
6. Lucite ring.
7. Brass bottom plate.
8. Support for foils.
9. Gas inlet.

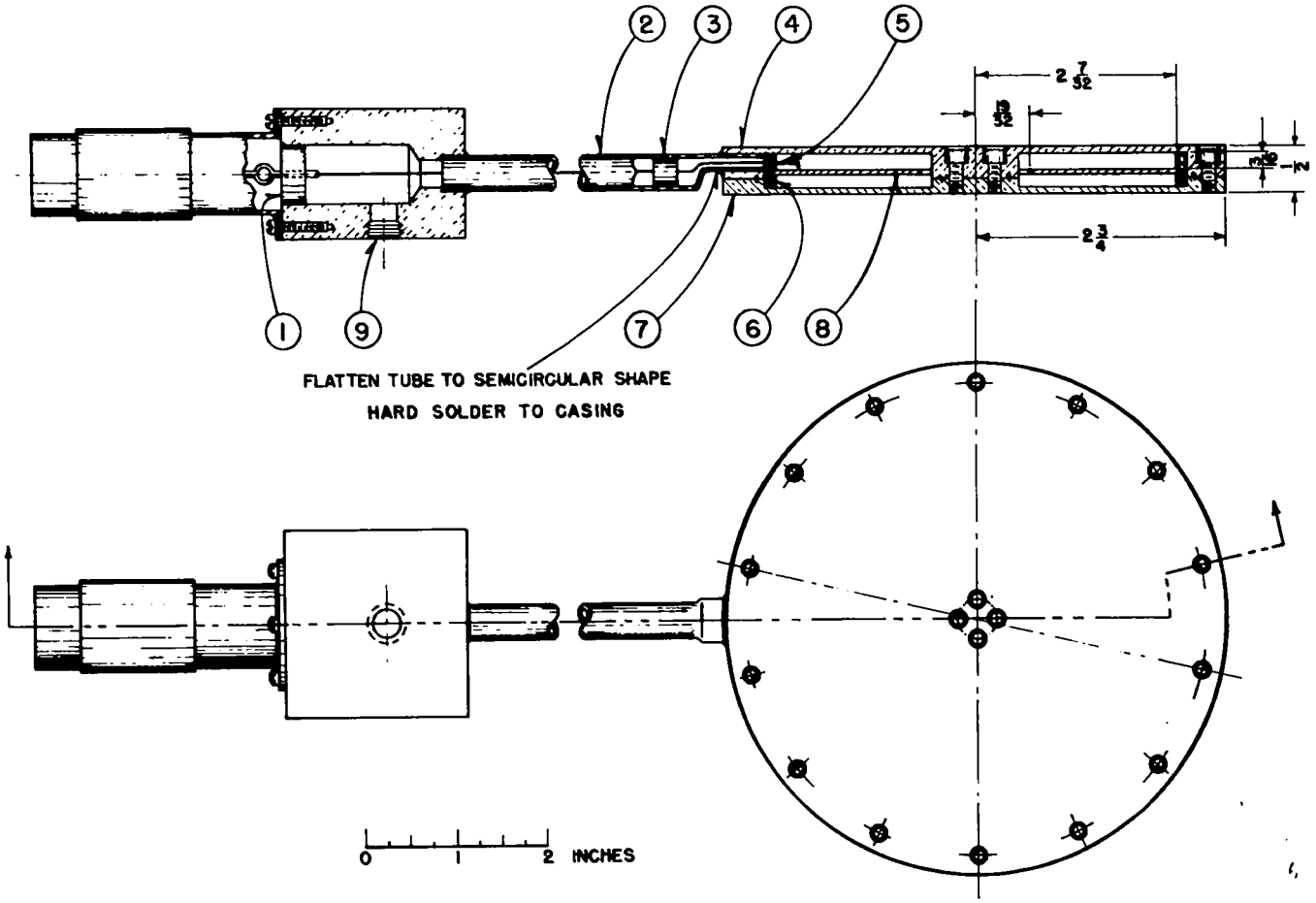

APPROVED FOR PUBLIC RELEASE

Figure 6

High counting yield chamber.

1. Lead through insulators (lucite).
2. Gas inlet.
3. Heavy second top plate to be removed after filling of chamber.
4. Aluminum rings supporting foils.
5. Supporting rod and lead.
6. Metal spacer.
7. Lucite spacers.

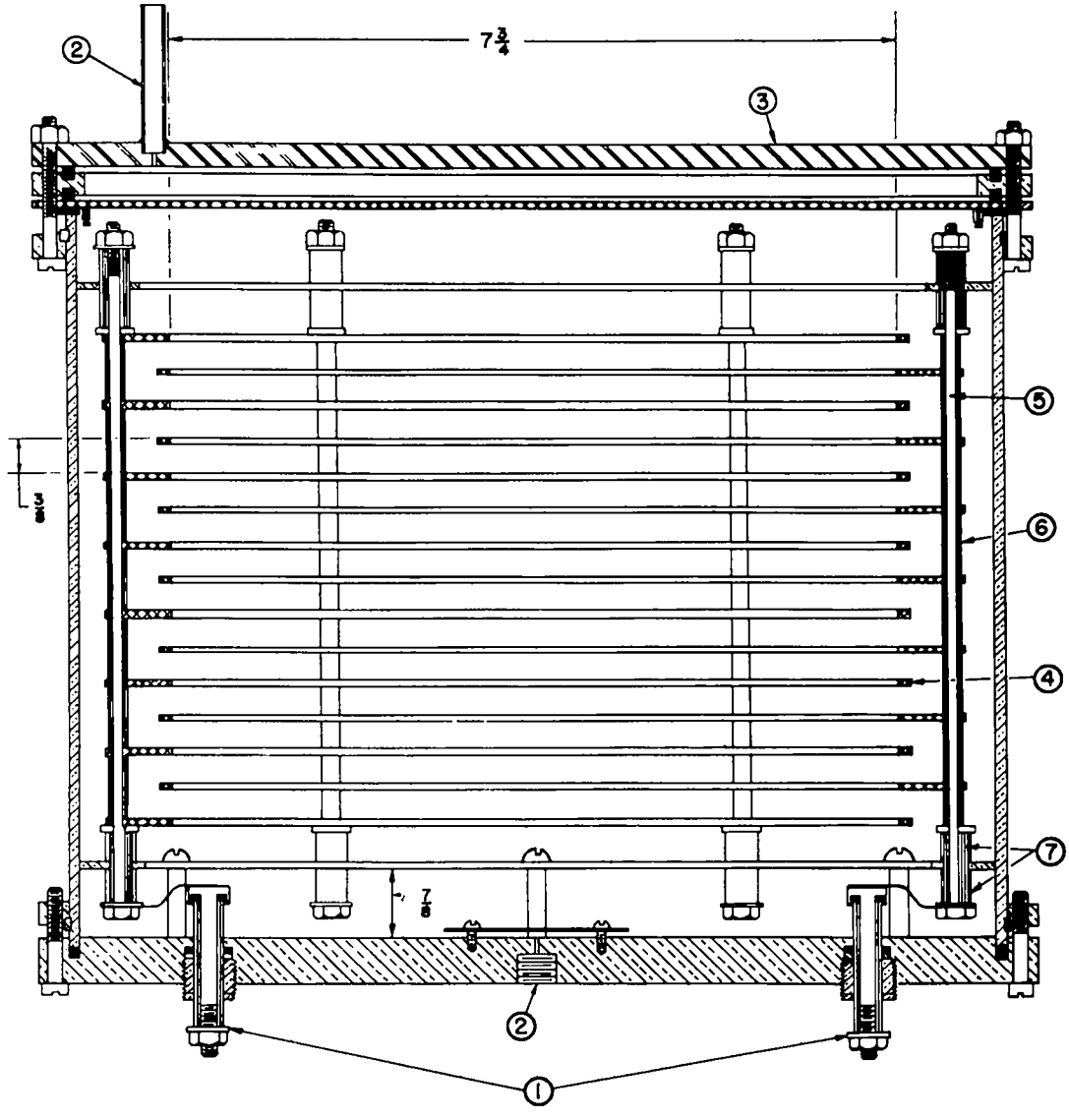

spirals represent the high voltage and collecting electrodes of the chamber. Since the preparation of the foils and the assembly of the spirals is unique, a detailed account of the procedure is given in the following paragraphs.

Preparation of foils: Uranyl nitrate is dissolved in a minimum quantity of alcohol. A solution of 1 or 2 per cent of Zapon lacquer in Zapon thinner is prepared and added to the first solution until the concentration of uranyl nitrate is about 50 mg/cc. The nitrate concentration may be much lower, but the value mentioned should not be greatly exceeded.

This solution is applied to an aluminum foil in a thin layer by means of a soft brush. The brush should not again touch any portion of the foil from which the solvent has evaporated. The foil is then baked for three or four minutes at about 550° C to burn off the Zapon lacquer and to convert the uranyl nitrate to U_3O_8. If platinum foil is used, the baking temperature may be 800 or 900° C. The higher temperature will result in more nearly complete elimination of Zapon and quantitative conversion of uranyl nitrate to U_3O_8.

When the foil has cooled, it is rolled flat between sheets of paper and the coated side is rubbed smooth with a soft tissue. Initially, the coated surface will exert considerable frictional drag on the tissue but this rapidly diminishes, without apparent removal of oxide, and a smooth, lustrous surface is produced.

A single layer of U_3O_8 applied by this method is, and apparently must be, quite thin. However, the procedure may be repeated until the desired surface density is reached. The coating is very tenacious and will withstand sharp bending of the foil.

If the foil is to be coated on both sides, as for spirals, it is advisable to paint alternately on the two sides rather than to complete the coating on one side before beginning the other.

Small areas of foil are conveniently painted, on a flat surface, by hand. Larger areas are more easily handled if the foil is wrapped around an aluminum drum which is rotated against the brush.

Aluminum foil which has been used in most of the spirals, is prepared for coating by lightly etching the surfaces in a dilute sodium hydroxide solution. It is carefully cleaned with water and alcohol and thoroughly dried before the painting is begun.

Preparation of spirals: Spirals have been wound by two methods. The first, illustrated in Figures 7 and 8, makes use of a strip of material for spacing the foils as they are wound. Ordinary sewing thread of the desired diameter is wound on a straight, stiff metal bar somewhat longer than one of the foils. The turns are wound tightly together until the width of the winding is slightly less than the width of a foil. A dilute solution of Amphenol 912 Cement and thinner or benzene (about 1 to 5), or of rubber cement and benzene (1 to 10), is now painted on the threads. After drying, the threads are cut at one end of the bar and are removed from it as a strip twice the length of the bar. In either solution the concentration of cememt should be as small as will produce a coherent strip.

The winding form in Figure 7 is a piece of $\frac{1}{4}$" metal tubing with a narrow, smooth-edged longitudinal slot a little deeper than the width of a foil. A flat-faced cylinder 1 inch in diameter and drilled with a $\frac{1}{4}$ inch hole is pushed into the tube to provide a guide surface to prevent the foils from wandering axially as they are wound. The foil ends, provided with wire leads soldered across the ends, are inserted into the slot and are bent over against the inside of the tube as shown in Figure 8. The middle of the thread strip is inserted into the slot and the spiral is formed by winding, under tension, half a turn at a time, foil and thread alternately. The fingers are used to smooth the foil and thread to aid in producing a tight, evenly spaced spiral. When the winding is completed, narrow strips of an adhesive tape may be wound around the spiral to hold it together temporarily.

Final stages in producing a spiral consist of sealing the ends in supporting and insulating material and removing the threads. By means of a force exerted on the guide cylinder, the spiral is pushed partly off

Figure 7

Method of winding spirals for spiral chamber.

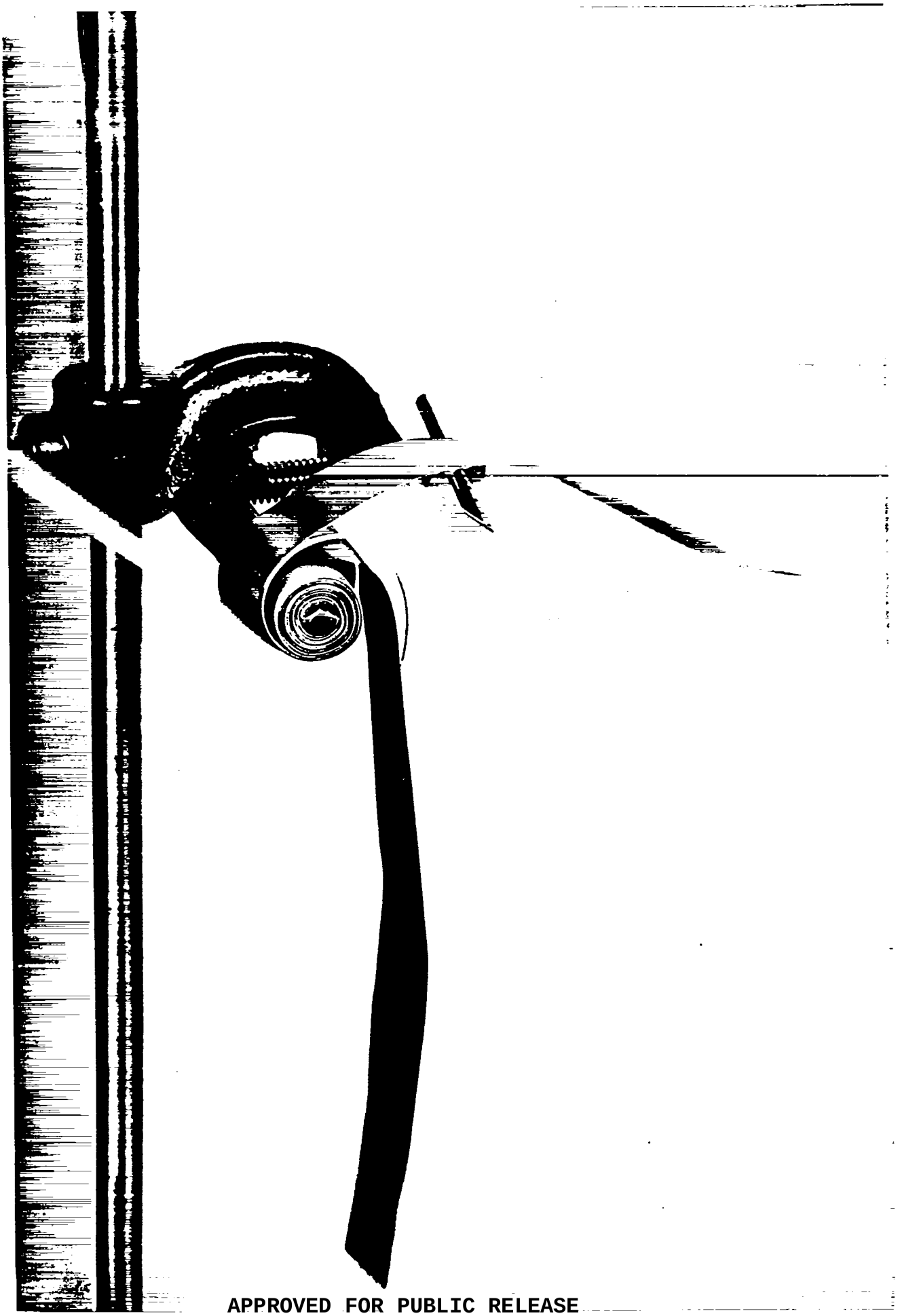

Figure 8

Fastening of ends of spirals.

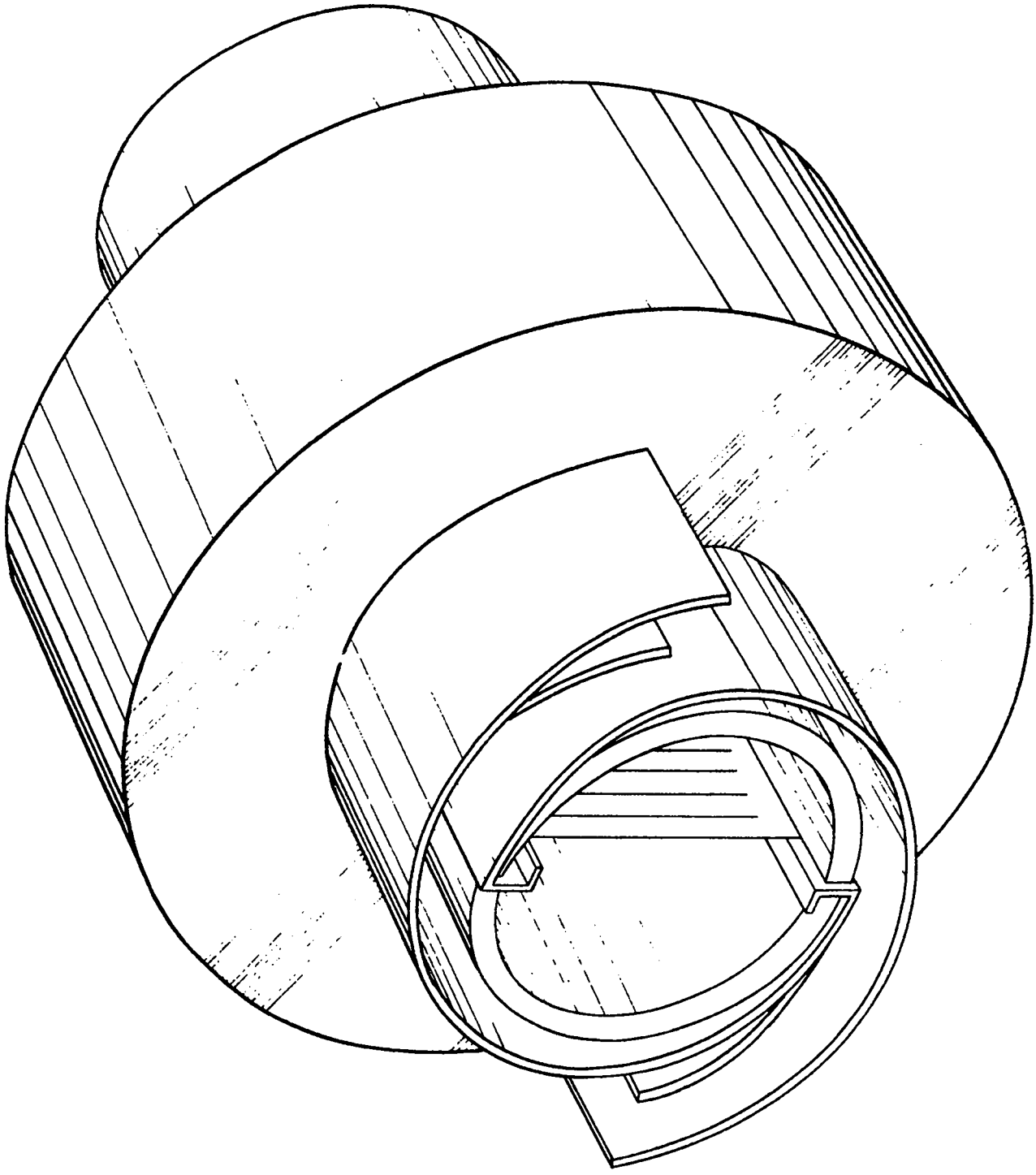

the mandrel and about a third of the threads are pulled, one at a time, from the end of the spiral. Wrinkled edges of the foils may be straightened with a scriber.

Sulphur or ordinary red sealing wax provides satisfactory support and insulation for the ends of the spiral. If sulphur is used the lead wires should be platinum or another metal which does not form a conducting sulphide. Otherwise flakes of sulphide may fall from the wires and short the foils. Ordinary "flowers of sulphur" does not seem to insulate the foils satisfactorily. Better insulating and mechanical properties are obtained by using a mixture of three parts by weight of sulphur flowers and one part of finely powdered aluminum oxide.

A small quantity of this mixture is melted to the viscous stage on a pyrex plate or in some shallow flat-bottomed vessel and is stirred to keep the aluminum oxide in suspension. The exposed end of the spiral, still on the mandrel, is carefully lowered into the molten mixture and gently rotated to aid in wetting the entire end of the spiral. Unless care is taken in adjusting the temperature, sulphur in its fluid phase will rise to a considerable height between the foils. Excess sulphur may be removed by judicious application to a heated glass surface. The central hole in the spiral must be reopened if sulphur has covered it. A heated wire may be used in removing sulphur.

Temporary support for the sealed end is provided by applying a narrow strip of adhesive tape around the spiral at this end. The tape previously applied is now gently removed and the remaining threads are pulled from the open end of the spiral as before. Tape should be reapplied to keep the outside ends of the foils in place. The wire leads are now bent back on themselves and are pulled through to the completed end of the spiral so that they will not interfere with the sealing of the remaining end.

If sealing wax is used for insulation, care is necessary in sealing the second end of the spiral to avoid softening the wax at the other end.

A set of foils used in one of these spirals is shown in Figure 9. One of the large spirals is ready for dipping while the other is completed and ready for installation in its chamber.

Should the spiral be damaged after completion, the foils may be easily salvaged. Sulphur-insulated spirals may be taken apart by pulling the two foil ends. Those employing sealing wax are placed in acetone or alcohol until the foils may be easily pulled apart. All remaining wax is then removed with clean solvent. After all visible traces of insulating material have been removed, the foils should be baked for a few minutes at about 500° C. They may then be smoothed and straightened by placing them between sheets of paper on a flat surface and drawing a smooth cylinder along the foils.

A second method of winding spirals uses only two or three threads in the winding process and these remain in the spiral, serving both to support and insulate the foils. This method is particularly adapted to the winding of very small spirals but may also be used in preparing the larger ones.

The winding mandrel consists of two lengths of 1/16" steel rods each milled to a semi-circular cross-section for about an inch of its length. These are inserted into the bearings of the apparatus shown in Figure 10 so that the milled sections overlap. Threads which have been previously soaked in dilute Amphenol cement and dried are inserted between these sections. Their spacing is determined by the grooved rods in the foreground and background of Figure 10. The ends of the foils are inserted between and on opposite sides of the threads for a little less than 1/16 inch of their length. They are carefully aligned and the small cylinders are pushed onto the split section to serve as clamps and as guides for the foils. The free ends of the foils are then placed in the clamps shown at the top and bottom of Figure 10.

Tension of the foils and threads is provided by weights and must be adjusted to the foil and thread which are used. Too much tension causes the

Figure 9

Completed spirals.

APPROVED FOR PUBLIC RELEASE

Figure 10

Second method for winding of spirals.

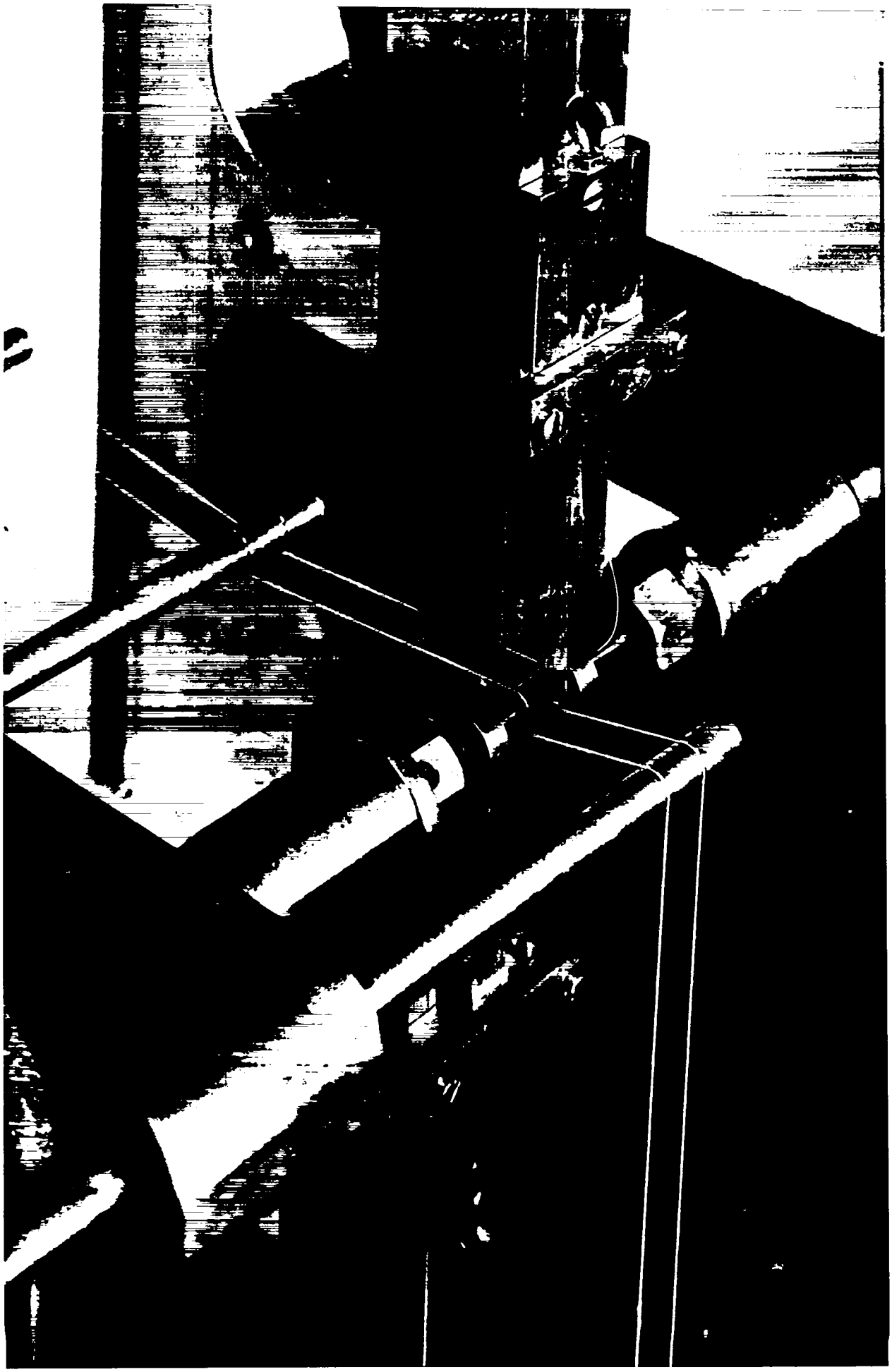

foils to be creased and the threads to wander. Too little tension produces a loose spiral which will come apart when it is removed from the machine.

In the case illustrated one lead is soldered to the inside end of one foil and one to the outside end of the other.

After the alignment has been completed, the spiral is wound by turning the shaft shown in Figure 10. When about 1 inch of foil remains unwound, the top clamp is loosened and a strip of .001 inch Amphenol polystyrene tape slightly wider than the foils and about 3 inches long is cemented to the last ½ inch of this foil. Tension on the foil is maintained manually and winding is continued until the bottom clamp must be disconnected. The threads will guide the bottom foil for the last half turn or so. When the end of the top foil has reached the spiral, a sharp razor blade is used to cut the top threads just beyond the end of the top foil. After a further half turn the other threads are similarly cut. With the guide cylinders pushed back, several layers of the Amphenol tape are applied and the end is fastened down with a small drop of Amphenol cement.

The spiral is now completed and is removed from the machine by loosening the set screws which hold the split rods in their bearings and pulling the rods from the spiral. If the spiral is shorted, the trouble will generally be found in the center of the winding. Careful probing in the 1/16 inch central hole will usually remove the distortion which shorts the foils. Small spirals produced by the above technique are shown in Figure 11.

The spirals are mounted in a suitable small container. A completed chamber is connected to the filling system at the valve which is provided and is evacuated. The entire chamber is baked until evolution of vapors is negligible. The temperature of the spiral end of the chamber will be limited, of course, by the melting or softening temperatures of the insulating material of the spiral or by the solder used in sealing the chamber. Since the spacing of the two foils is quite small (20 mils) it is necessary to operate the

Figure 11

Three spiral chambers of different sizes ready for assembly. In the foreground are two coated foils.

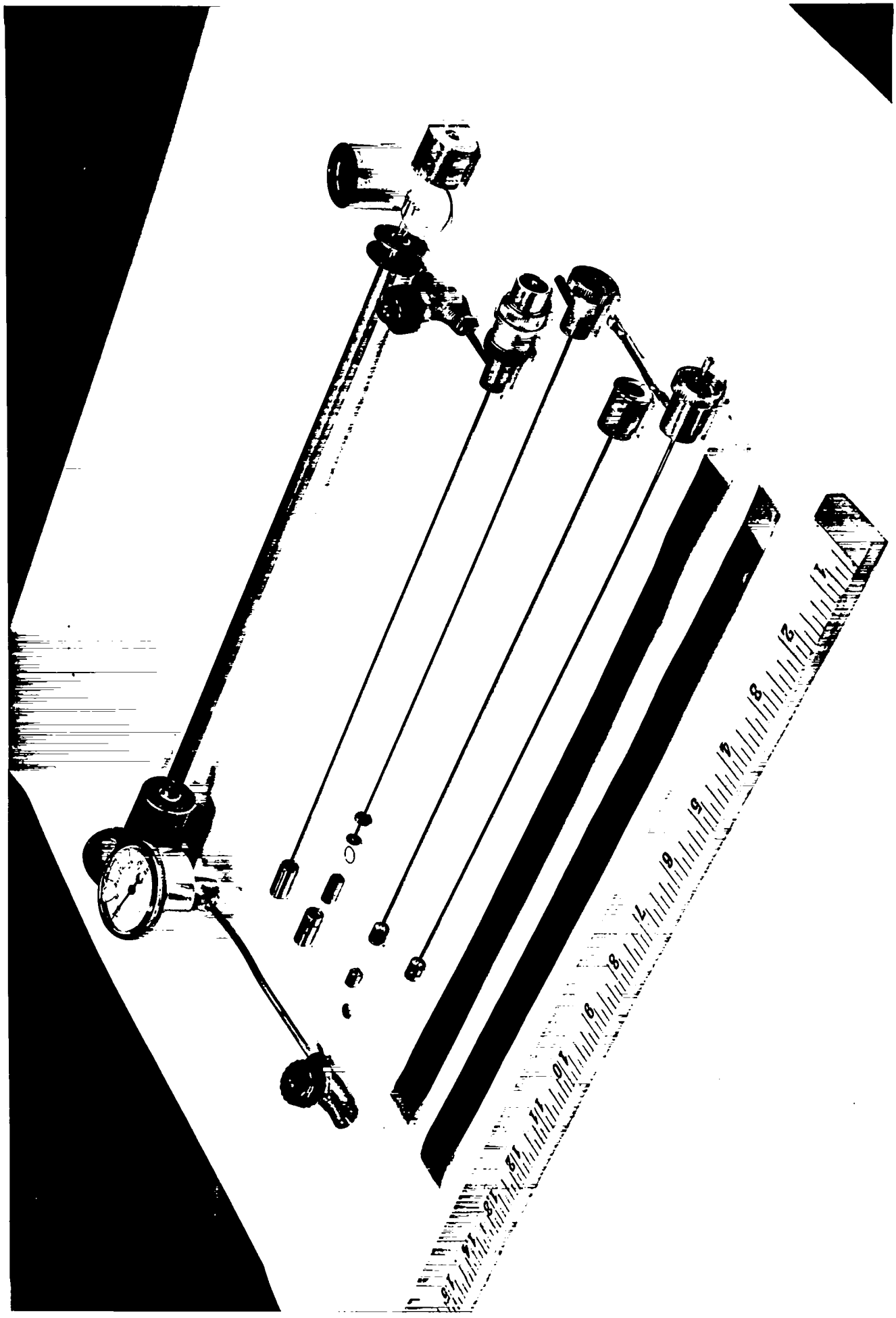

chambers at rather high pressures, from 5 to 10 atmospheres of argon for the larger type, 10 to 14 atmospheres for the smaller type. For the same reason the collecting voltage is quite low; 135 volts proved to be satisfactory for both types regardless of foil spacing.

The capacity of the spiral chambers is as high as 500 micromicrofarads. They can be operated by either grounding one foil, the other one serving as high voltage and collecting electrode, or by applying the collecting voltage to one spiral and using the other as collecting electrode. In the former case, the collecting voltage is applied through a .25 megohm resistor and the input of the amplifier coupled through a condenser of 100 to 500 micromicrofarads. The leak resistor in the first case should be about .25 megohms, and about .1 megohms in the second case. Due to the large amount of material used in these detectors, the counting bias has to be set at a comparatively high value, in order to avoid pulses from a piling up of α-pulses. Consequently the detection efficiency is somewhat low. For a background of not more than one to two counts per minute due to pile-up, the detection efficiency was found to be between 80 and 90 per cent. The amplifier used with these chambers had a resolving time of 1.5 microseconds. The rise time of the pulses is less than 0.2 microsecond. If not more than .25 mg/cm^2 of U_3O_8 are used, the bias curves show a plateau. The following table gives a list of constructions which were actually used.

Foil Spacing in mils	Diameter inches	Length inches	Useful Area in cm^2	Max. Deposit mg U
20	1	1	200	240
20	1	1	360	550
7	3/8	.3	22	35

16.7 INTEGRATING FISSION CHAMBERS

Figure 12 shows an integrating ionization chamber used for relative flux measurements in very dense slow neutron atmospheres. The ionization current can be measured diredtly with a galvanometer. The chamber is constructed in such a way that the ionization current is predominantly produced by fission

Figure 12

Integrating ionization chamber for fissions.

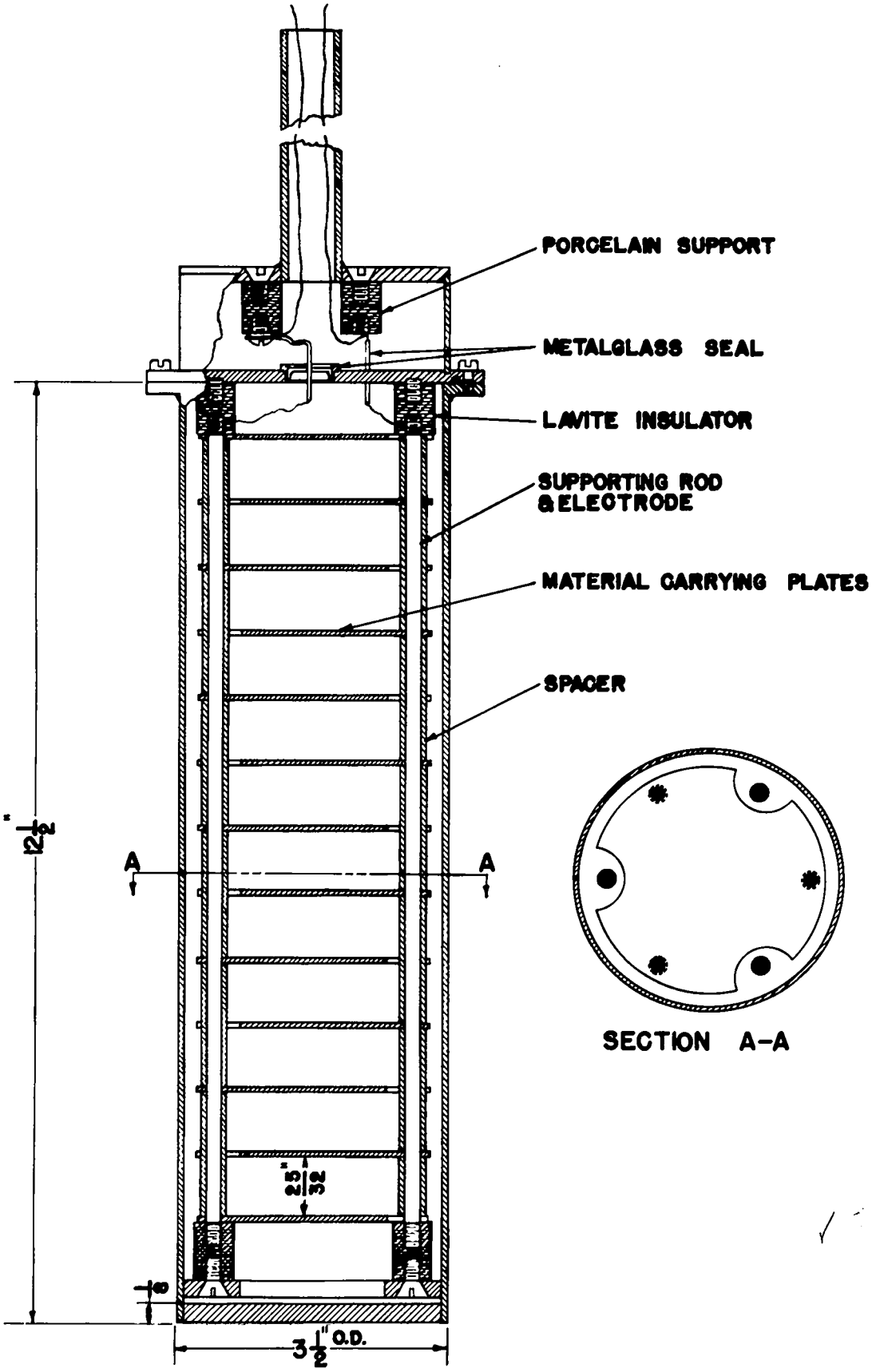

fragments and only to a small extent by δ-rays or electrons. One hundred and eighty-four mg of U^{235} (345 mg of 63.1 per cent enriched U_3O_8) are deposited in the form of nitrate on both sides of the 14 electrodes with the exception of the end plates which are coated only on one side. The plate spacing is 25/32". Alternate plates are connected to the collecting and to the high voltage leads. It was found that residual ionization due to the β activity of the chamber material, produced by previous neutron bombardment, could be greatly reduced by using ordinary cold rolled iron for the container and parts of the internal structure. The chamber is filled to a pressure of one atmosphere of argon and operated with voltages up to 1800 volts. With the maximum voltage, a linear relation between ionization current and neutron flux was found for currents up to 21 microamperes.

LOS ALAMOS TECHNICAL SERIES

VOLUME I

EXPERIMENTAL TECHNIQUES

PART II

APPENDIX

by

BRUNO ROSSI AND HANS STAUB

APPROVED FOR PUBLIC RELEASE

APPENDIX TO PART II

A.1 RANGE ENERGY RELATIONS AND STOPPING POWER

Figures 1, 2, and 3 show the range energy relations for α-particles protons, and deuterons in air at N.T.P. (760 mm Hg, 150° C) according to Livingston and Bethe. These curves were obtained by fitting theoretical expressions to experimental data. In order to obtain the range energy relation for deuterons, it should be remembered that a deuteron of energy 2E has twice the range of a proton of energy E.

Figure 4 shows the range energy relation for protons in argon according to Bethe's methods. The results were fitted to experimental values. In addition to the range energy relation, Figure 4, shows the stopping cross-section σ as a function of energy. This quantity is directly connected with the specific energy loss, $-dE/dx$, by the equation

$$\sigma = -\frac{1}{n}\frac{dE}{dx}$$

where n is the number of atoms per cm^3 (at N.T.P., $n = 2.548 \times 10^{19}$). The third curve in Figure 4 marked $\bar{x}$ gives the distance of the center of gravity of ionization of a track of energy E from the point of origin of the particle, measured along its path:

$$\bar{x}(E_o) = R(E_o) - \frac{1}{E_o}\int_0^{E_o} R(E)\,dE = \frac{1}{E_o}\int_0^{R} (-dE/dx)\,x\,dx \qquad (1)$$

Figure 5 shows the same three quantities for xenon.

Figures 6 and 7 show the range energy relations of protons in paraffin ($C_n H_{2n+2}$) and glycerol tristearate. The curves are based upon calculated values of the stopping number B in C, O, and H. The stopping number B is related to the energy loss $-dE/dx$ by the equation

$$-\frac{dE}{dx} = \frac{4\pi e^4 Z^2}{m v^2} n B \qquad (2)$$

where Ze in the charge of the incident particle, v its velocity, and m the electron mass. The expressions used for the computation of these curves are:

Figure 1

Range energy relation for α-particles. (Livingston and Bethe)

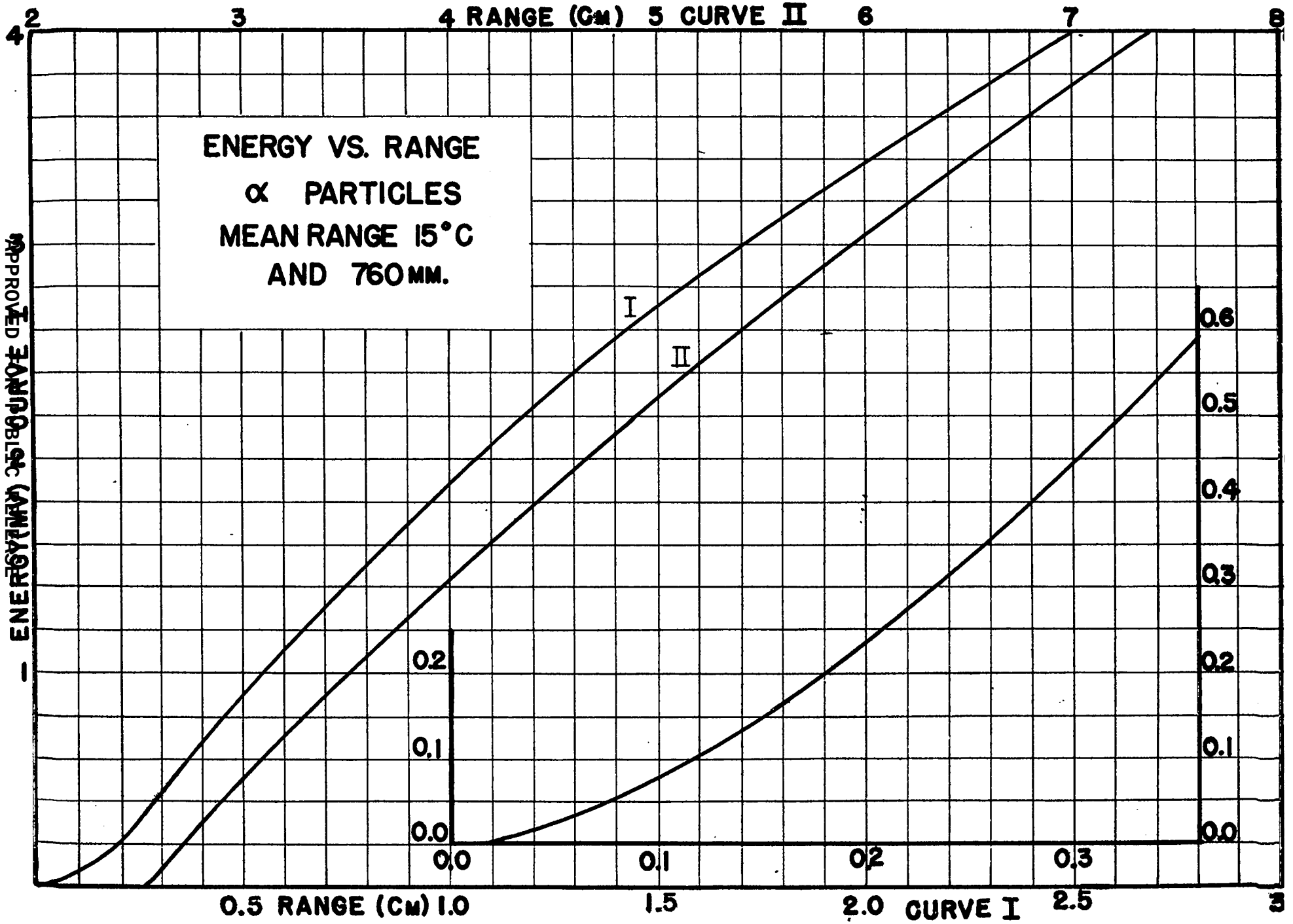

Figure 2

Range energy relation for protons and deuterons. (Livingston and Bethe)

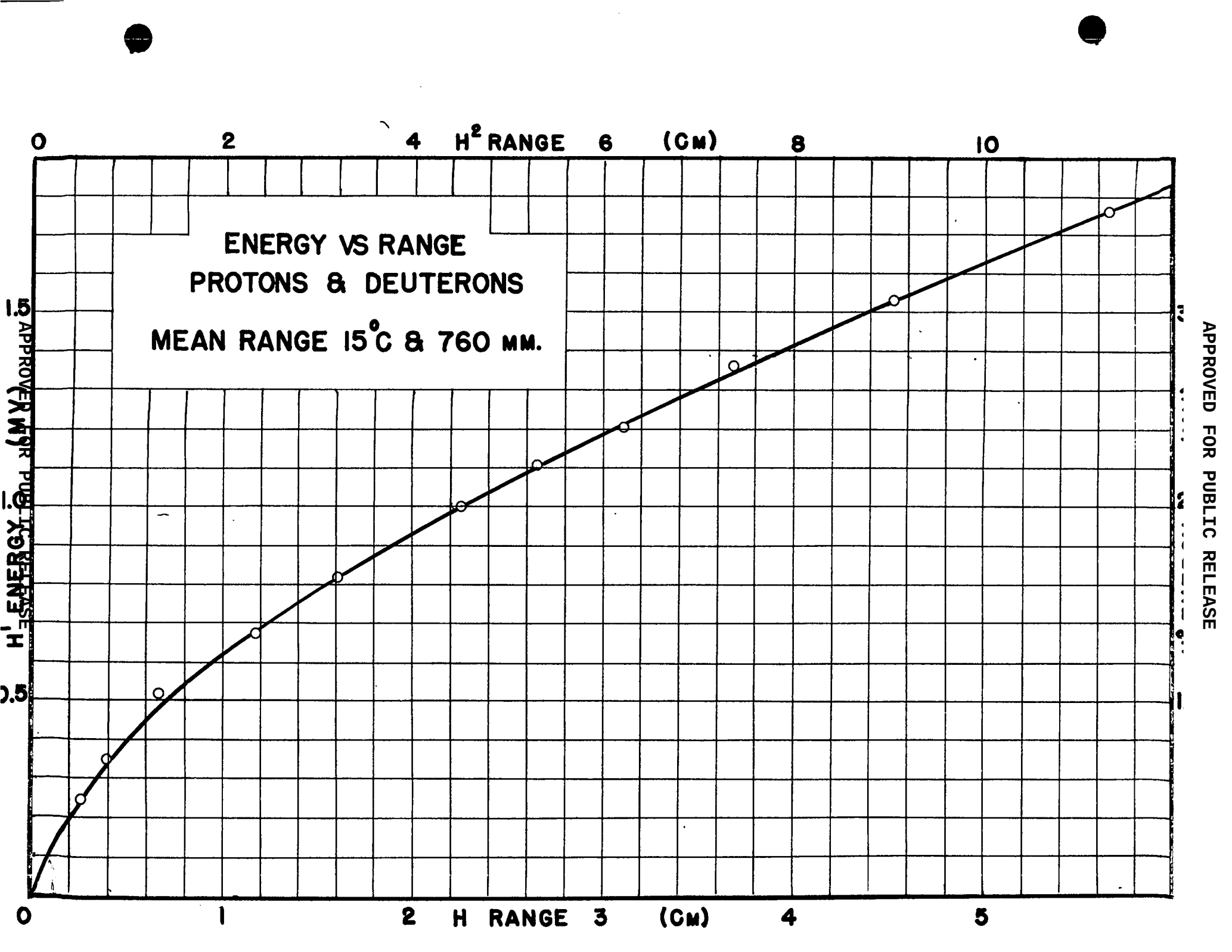

Figure 3

Range energy relation for protons. (Livingston and Bethe)

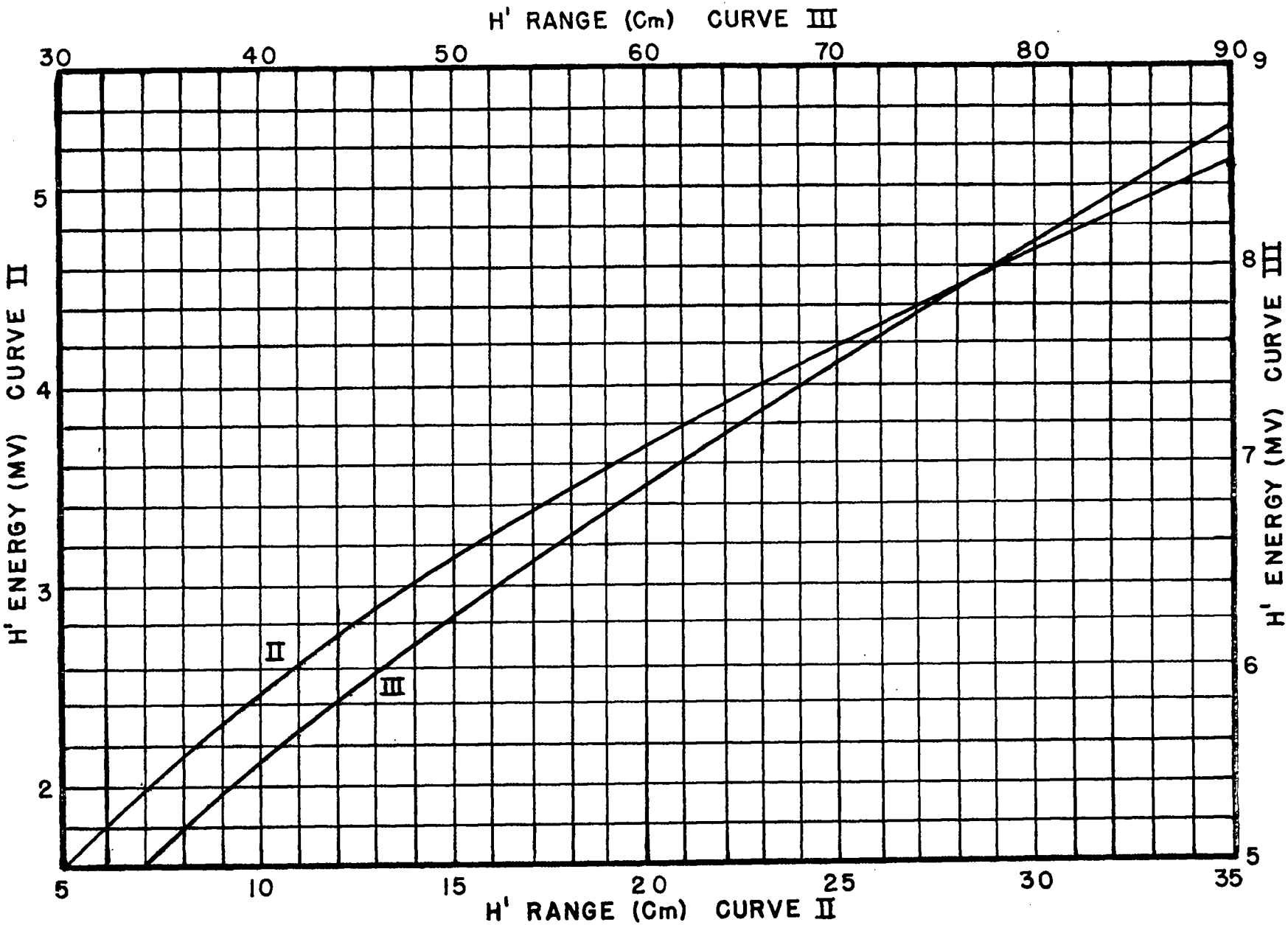

APPROVED FOR PUBLIC RELEASE

Figure 4

Range energy relation, stopping cross section and center of ionization for protons in argon (760 mm Hg; 15° C).

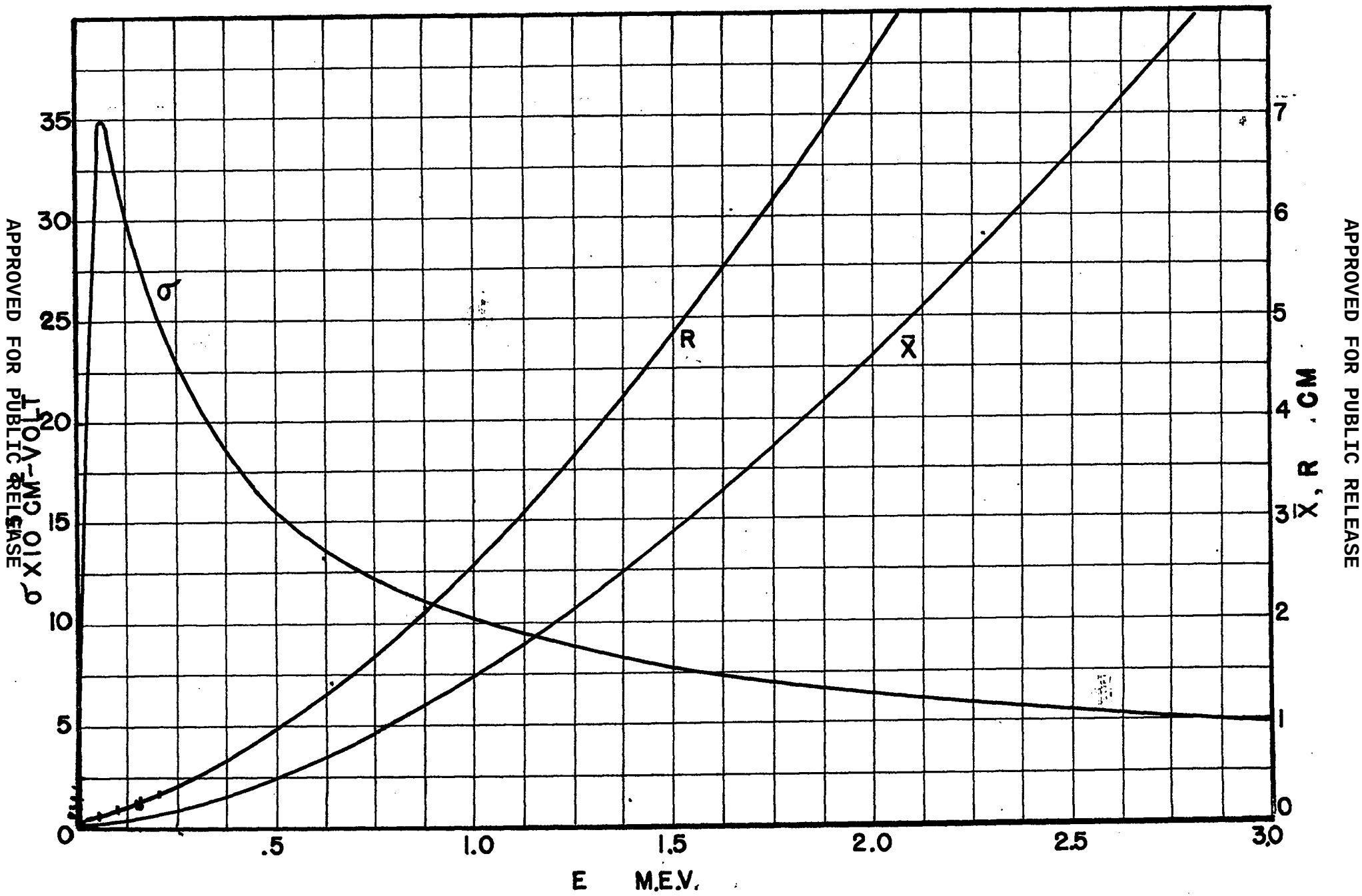

APPROVED FOR PUBLIC RELEASE

Figure 5

Range energy relation, stopping cross section and center of ionization for protons in xenon (760 mm Hg ; 15° C).

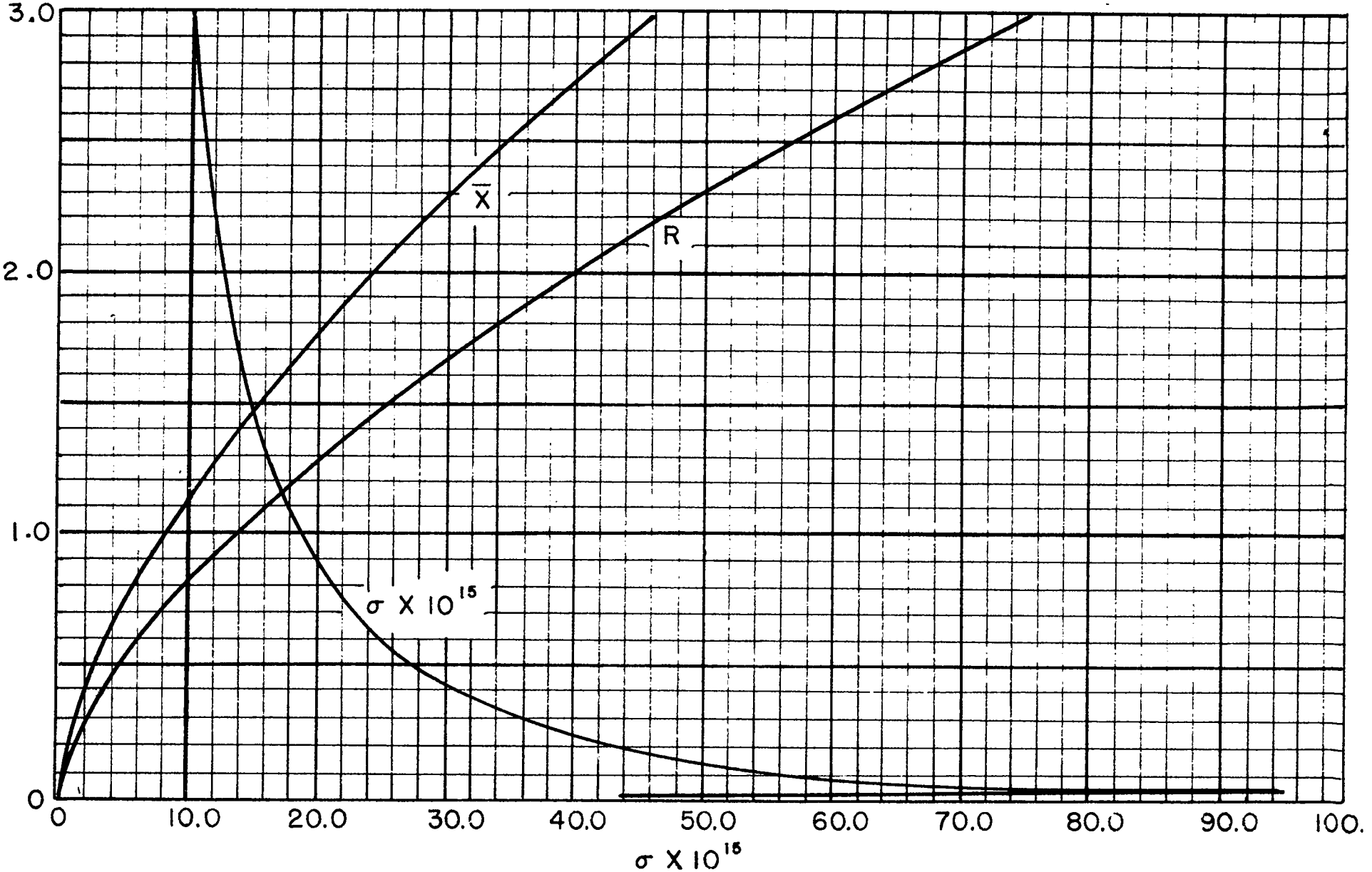

APPROVED FOR PUBLIC RELEASE

Figure 6

Range energy relation for protons in paraffin.

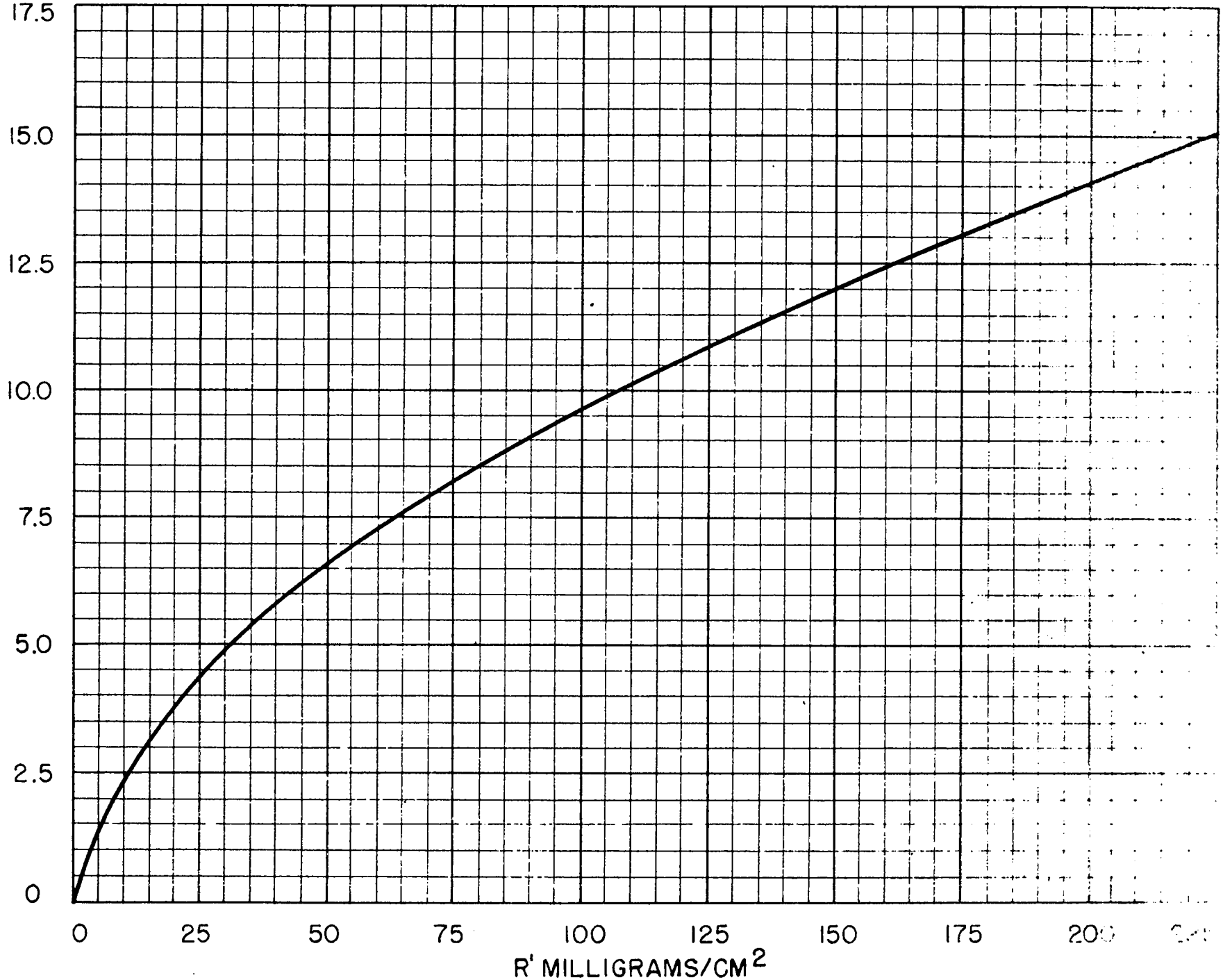

APPROVED FOR PUBLIC RELEASE

Figure 7

Range energy relation for protons in glycerol tristearate.

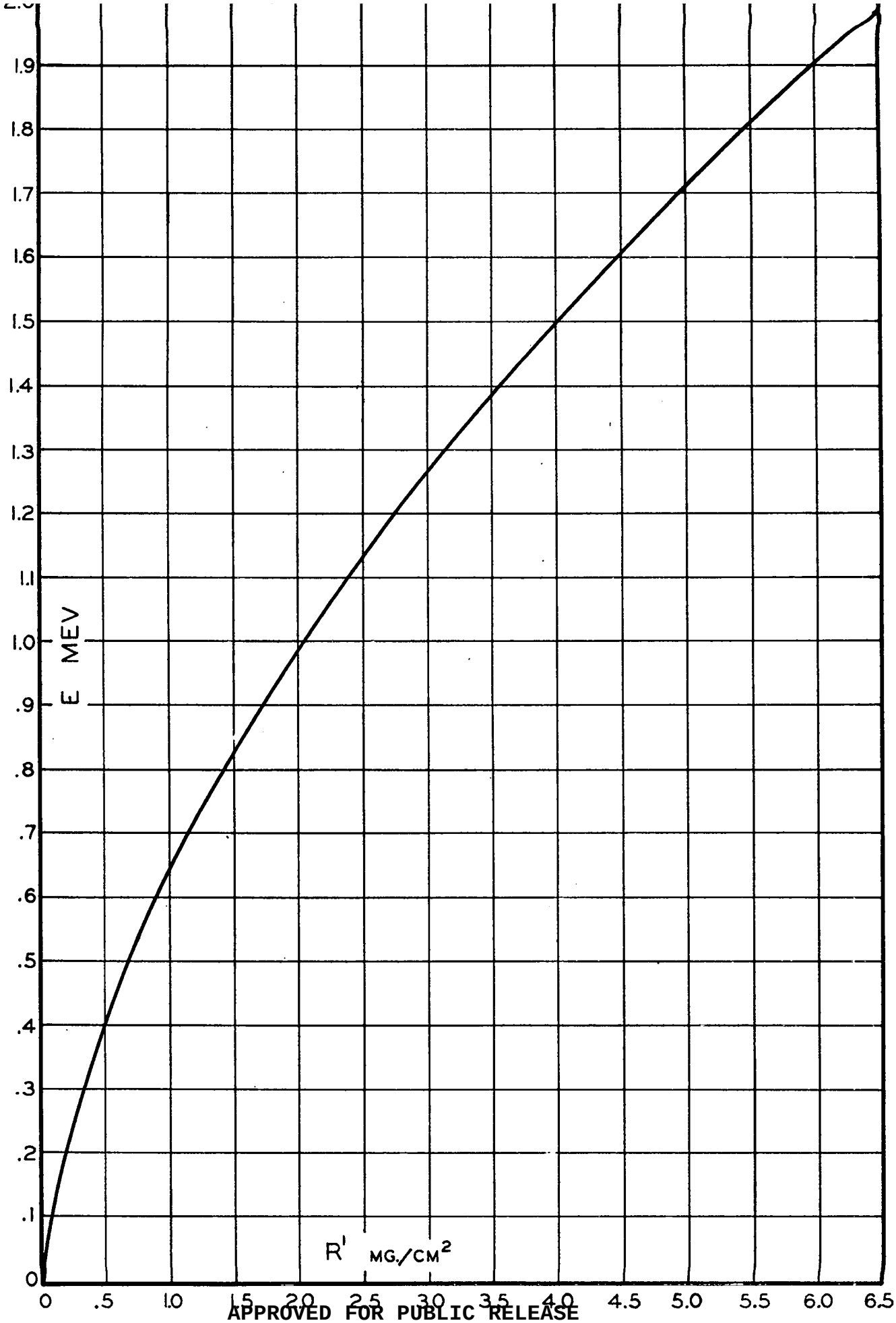

Carbon:

$$B_C = 9.4406 \log_{10} (E/.0094704) - 2.2652\, C_K(1/\eta_L) + 4.3479 \log_{10} (E/.22356) - 1.0497\, C_K(1/\eta_K) \qquad \text{for } E \geq .8$$

$$B_C = 9.4406 \log_{10} (E/.0094704) - 2.2652\, C_K(1/\eta_L) + 1.0497\, B_K(\eta_K) \qquad \text{for } .03 \leq E \leq .8$$

$$B_C = 2.2652\, B_K(\eta_L) + 1.0497\, B_K(\eta_K) \qquad \text{for } E \leq .03$$

with $\eta_K = E/.811520$ and $\eta_L = E / .034378$

Hydrogen:

$$B_H = 2.30259 \log_{10} E - .55248\, C_K(1/\eta) + 4.800 \qquad \text{for } E \geq .03$$

$$B_H = (E/1.81)\, B_K(\eta) \qquad \text{for } E \leq .03$$

with $\eta = E/ .029863$

Oxygen:

$$B_O = 18.421 \log_{10} E - 3.4199\, C_K(1/\eta_L) - C_K(1/\eta_K) + 24.741 \qquad \text{for } E \geq 1.5$$

$$B_O = 14.253 \log_{10} E - 3.4199\, C_K(1/\eta_L) + B_K(\eta_K) + 22.496 \qquad \text{for } .09 \leq E \leq 1.5$$

$$B_O = 3.4199\, B_K(\eta_L) + B_K(\eta_K) \qquad \text{for } E \leq .09$$

with $\eta_K = E / 1.4809$ and $\eta_L = E / .09036$

The functions $C_K(1/\eta)$ and $B_K(\eta)$ used in these expressions are represented in Figure 8 according to Livingston and Bethe. The energies have to be taken in Mev.

Figure 8

The functions $B_K(\eta)$ and $C_K(1/\eta)$ for the calculation of stopping numbers. (From M. S. Livingston and H. A. Bethe: Rev. Mod. Phys., 9, 245, 1937).

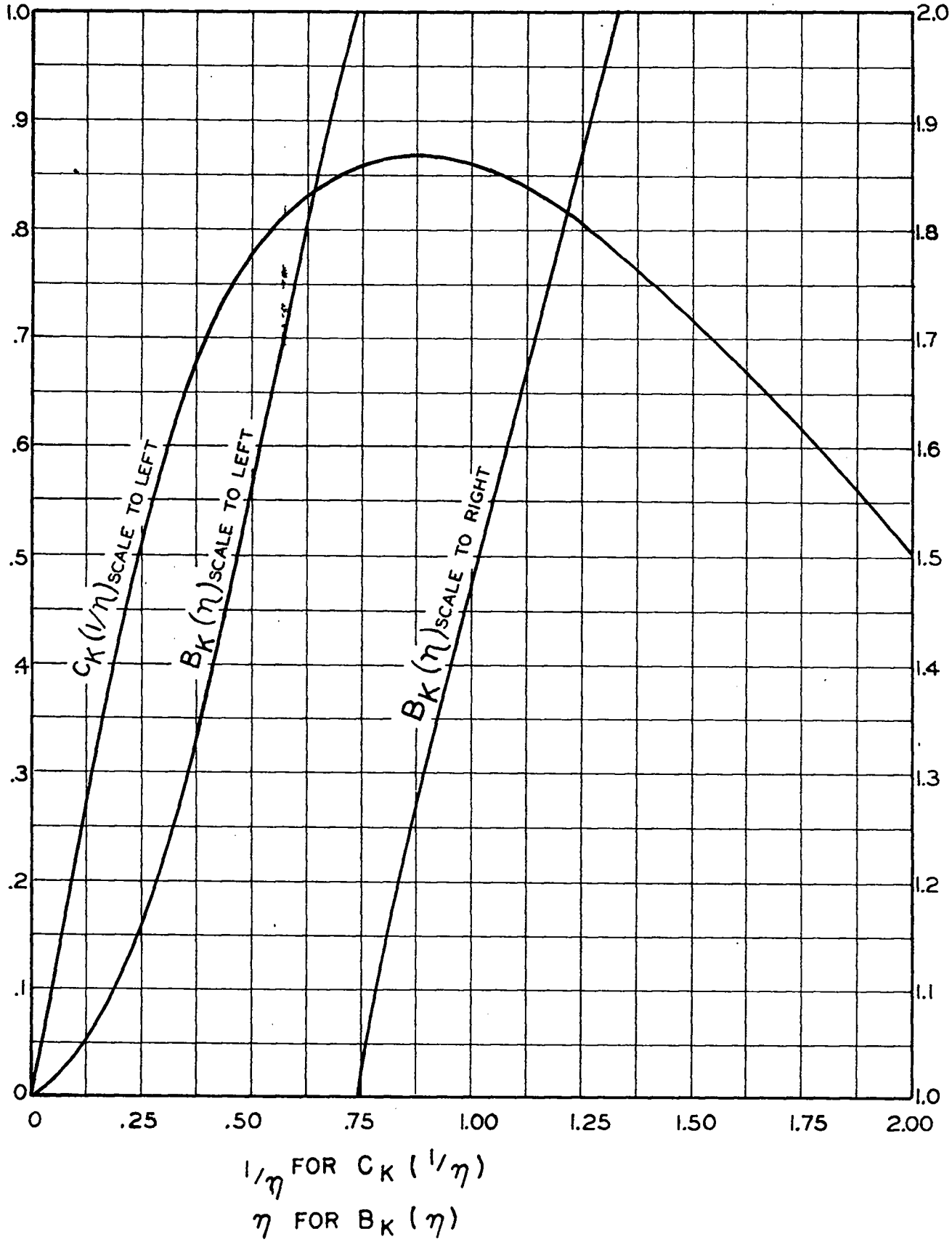

A.2 ENERGY W_o SPENT IN THE FORMATION OF ONE ION PAIR

Table A.2-1 gives the various values of W_o for different gases, particles and energies.

Table A.2-1

Gas	W_o in eV	Particle and Energy	Reference
Air	32.0	electrons .3 Mev	
Air	36.0	protons 2.5-7.5 Mev	L. H. Gray, Proc. Cambridge Phil. Soc., 40, 72, 1944
Air	35.1	α-particles 7.8 Mev	
Air	35.6	α-particles 5.3 Mev	
H_2	36.0	α-particles 5.3 Mev	
He	31.0	α-particles 5.3 Mev	
CO	34.7	α-particles 5.3 Mev	K. Schmieder Ann d. Phys., 35, 445, 1939.
CO_2	34.6	α-particles 5.3 Mev	
C_2H_4	27.6	α-particles 5.3 Mev	
C_2H_4	28.2	α-particles 5.3 Mev	
C_2H_2	27.6	α-particles 5.3 Mev	
Ne	27.8	α-particles 5.3 Mev	K. Schmieder Ann. d. Phys., 35, 445, 1939.
A	24.9	α-particles 5.3 Mev	
A	26.9	electrons 17.4 KV	D. B. Nicodemus, Thesis, Stanford University, 1946
Kr	23.0	α-particles 5.3 Mev	K. Schmieder Ann. d. Phys., 35, 445, 1939.
Xe	21.4	α-particles 1.3 Mev	R. W. Gurney Proc. Roy. Soc., A107,332,1925

A.3 RANGE OF ELECTRONS IN ALUMINUM: SPECIFIC IONIZATION OF ELECTRONS IN AIR

Curves (a) and (b) in Figure 9 show the extrapolated range of electrons in aluminum as a function of their energy. Curve (c) shows their specific ionization in ion-pairs per cm in air for N.T.P.

A.4 SCATTERING CROSS-SECTIONS OF PROTONS AND DEUTERONS FOR NEUTRONS

Figure 10 and Figure 11 show the scattering cross-sections of protons and deuterons (at rest) versus the energy of the impinging neutrons. The proton curve is the plot of a theoretical expression which fits the experimental data very well. The deuteron curve is purely experimental.

A.5 COEFFICIENTS OF ATTENUATION OF γ-RAYS IN Al, Cu, Sn, AND Pb

Figure 12 shows a plot of the coefficients of attenuation τ of γ-rays for Al, Cu, Sn, and Pb versus the energy of the quantum. For lead the three components of τ (i.e., the photoelectric, Compton, and pair production coefficient) are shown. If σ is the total cross-section per atom, and n the number of atoms per cm^3, then τ is defined as $\tau = n\sigma$.

A.6 THICKNESS CORRECTION FOR PLANE FOILS

Suppose particles of uniform range are emitted isotropically from a material layer of thickness t, one particle being emitted per disintegration. The recording device shall be biased such that every particle losing an amount of energy $E \geqslant B$ in the detector is counted. The observed number of counts C divided by the true number of disintegrations C_o is the detection efficiency F at the bias B. The number of counted particles from a layer between x and x + dx (see Figure 13) is given by

$$dC = \int_0^{\vartheta_o} 2\pi \sin\vartheta \; d\vartheta \; dx$$

where ϑ_o is that angle at which the particle, upon emerging from the foil, has just enough energy to be counted. Let the range at this energy be R(B),

Figure 9

(a)	Range of slow electrons in aluminum	Rasetti, "Elements of Nuclear Physics".
(b)	Range of fast electrons in aluminum	
(c)	Specific ionization of fast electrons in air.	Rutherford, Chadwick, and Ellis, "Radiation from Radioactive Substances"

(a)

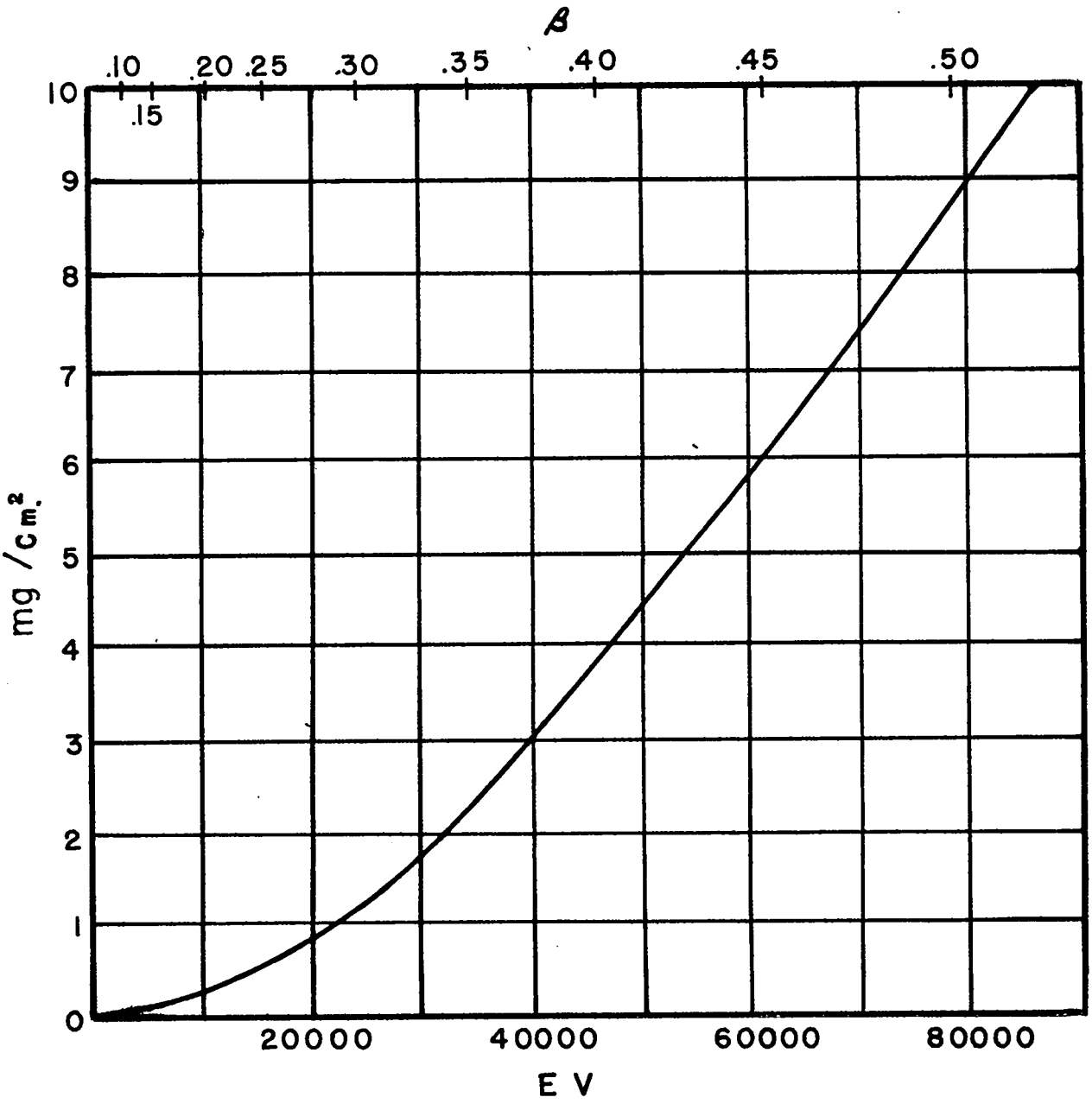

(b)

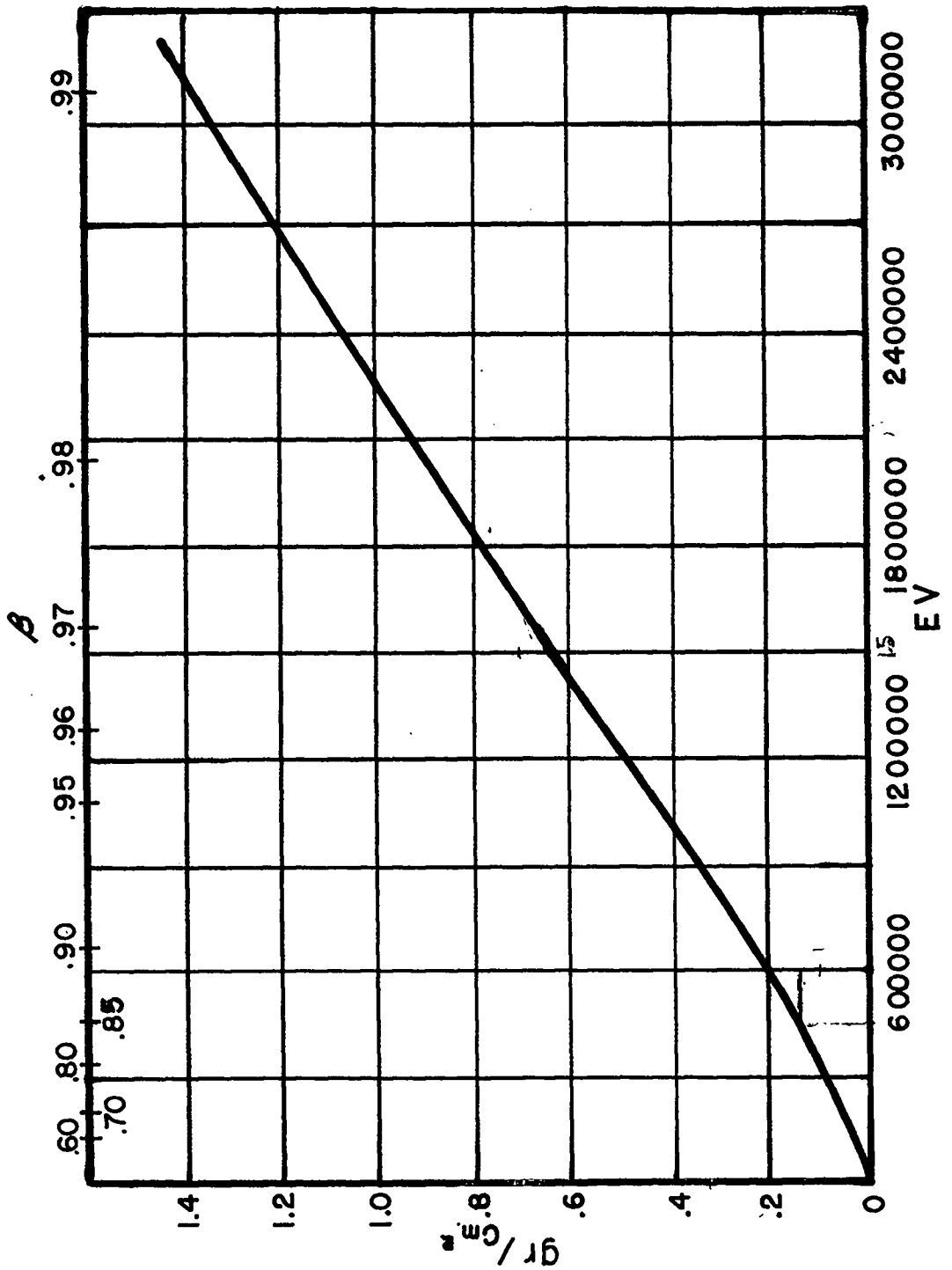

(c)

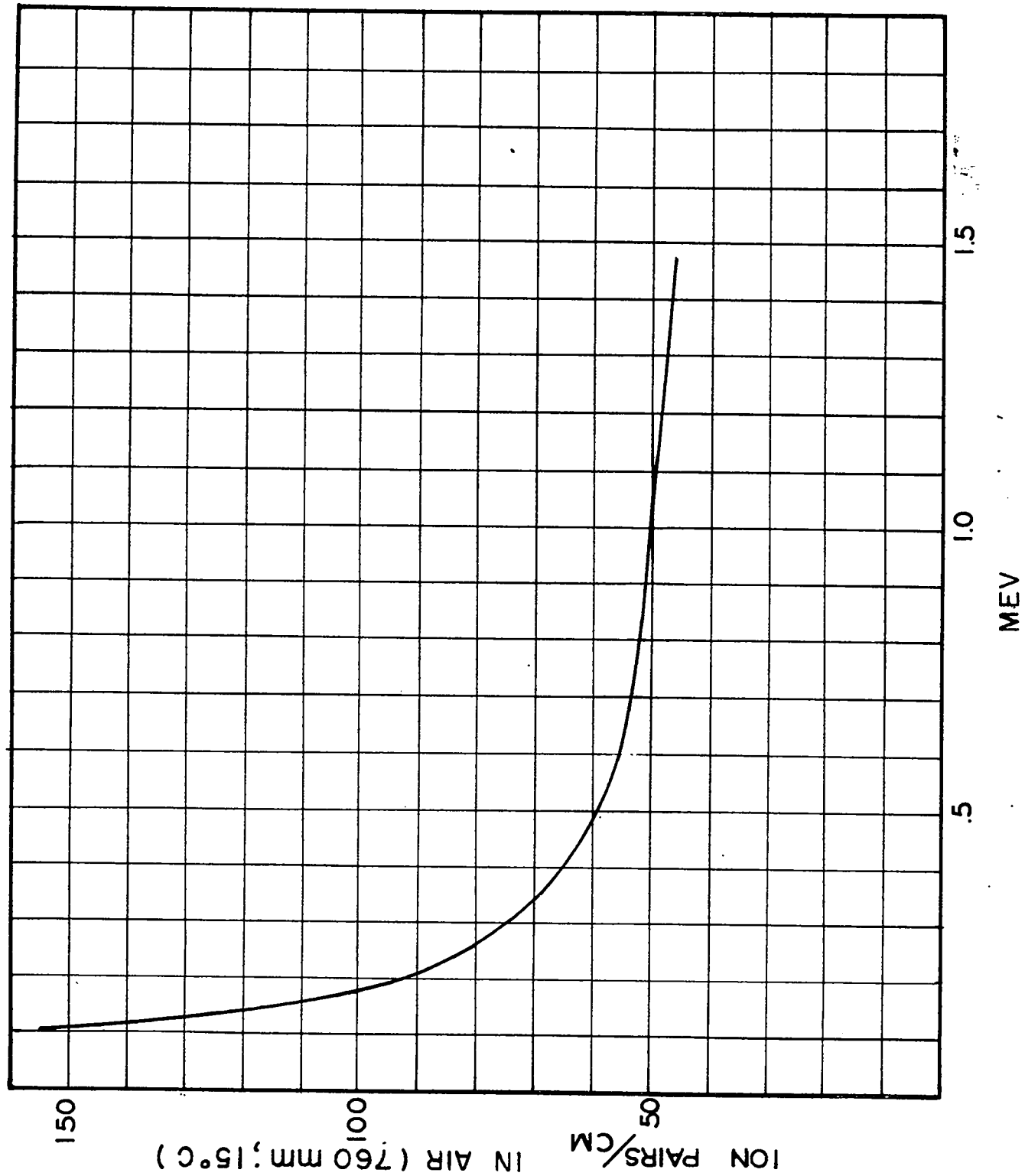

Figure 10

Neutron proton scattering cross section.

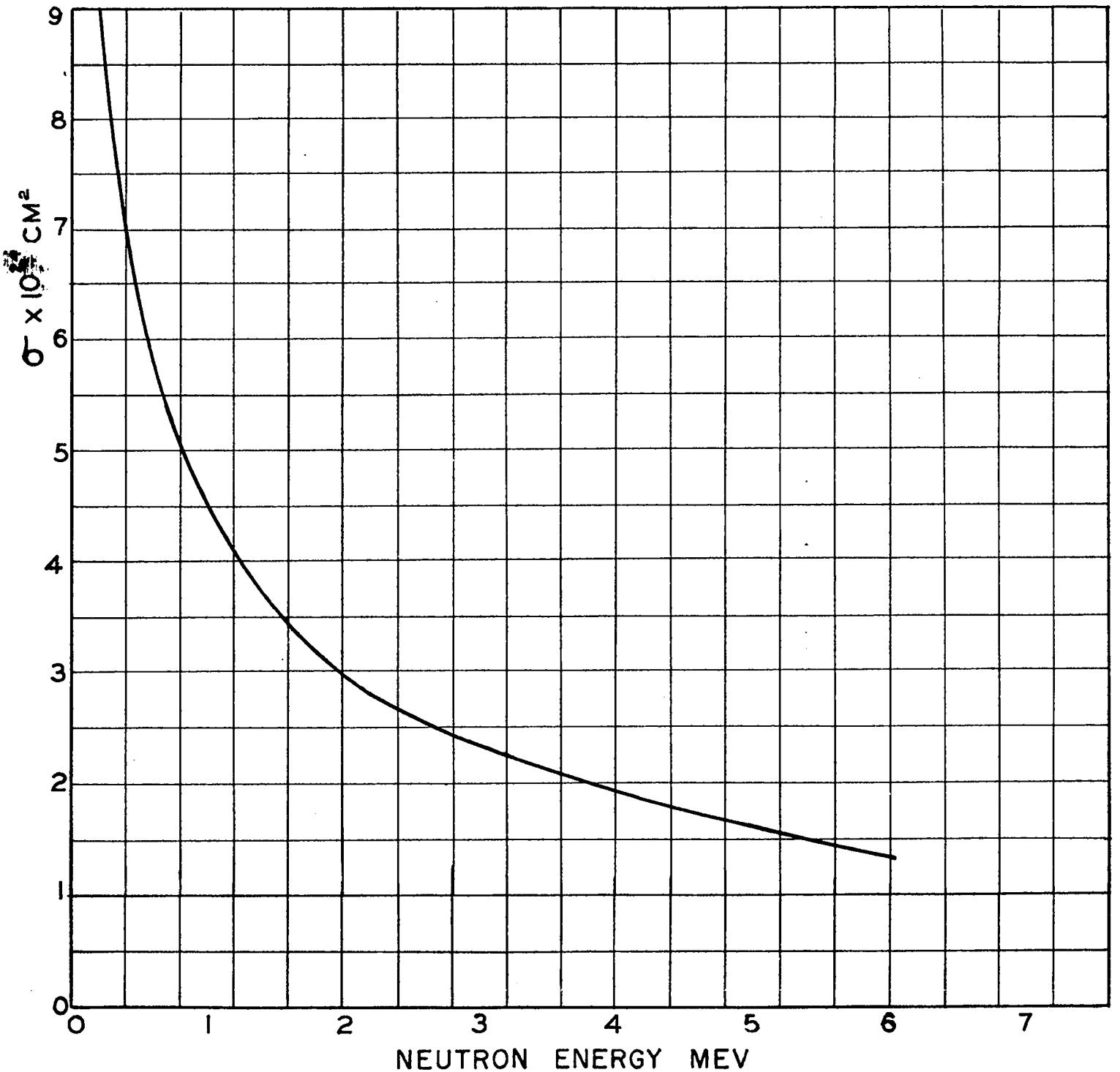

APPROVED FOR PUBLIC RELEASE

Figure 11

Neutron deuteron scattering cross section.

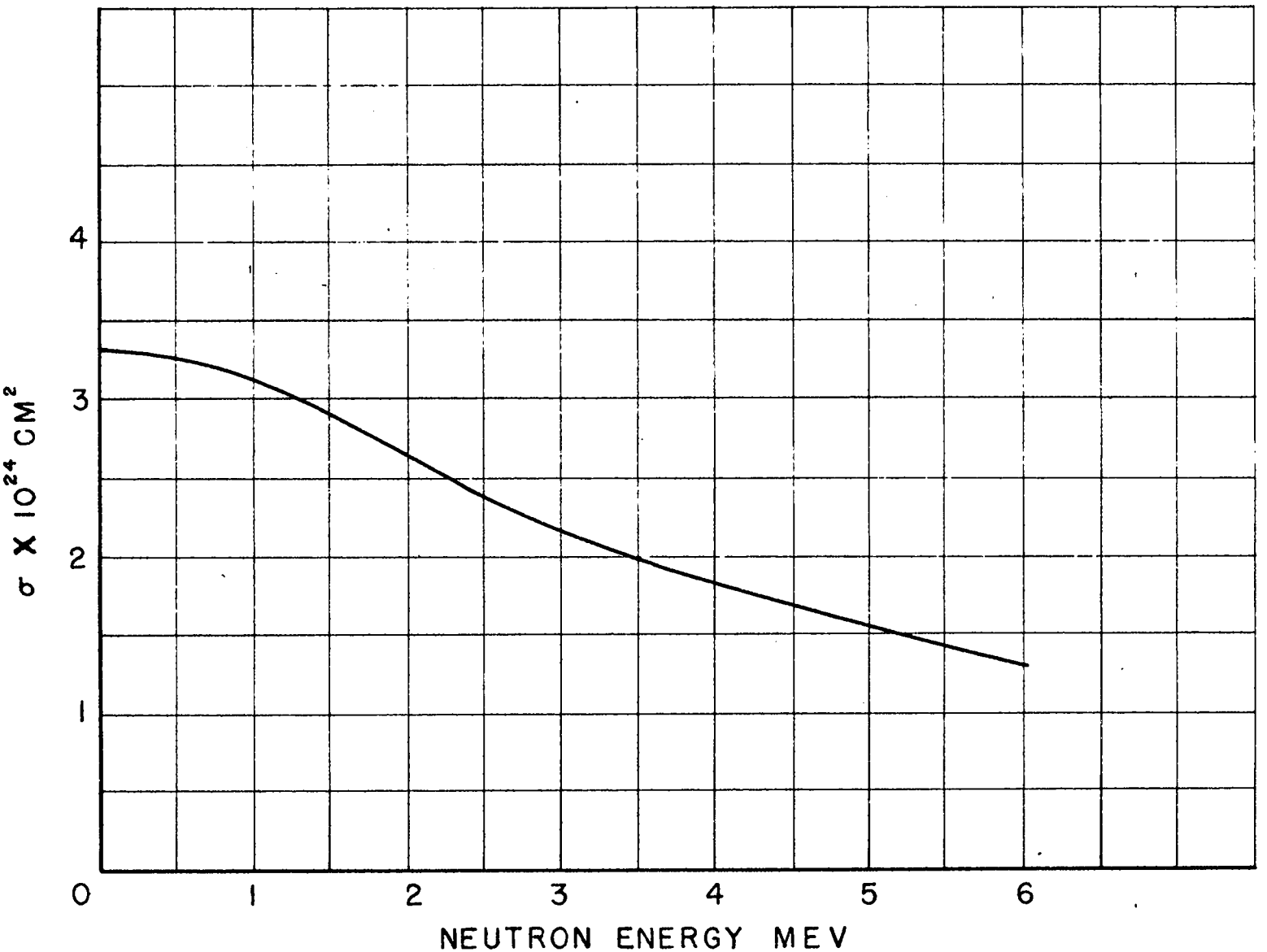

APPROVED FOR PUBLIC RELEASE

Figure 12

Attenuation coefficient for γ-rays in Pb, Sn, Cu, and Al, as a function of frequency (from Heitler, The Quantum Theory of Radiation"). The dotted curves show the three components of τ for lead.

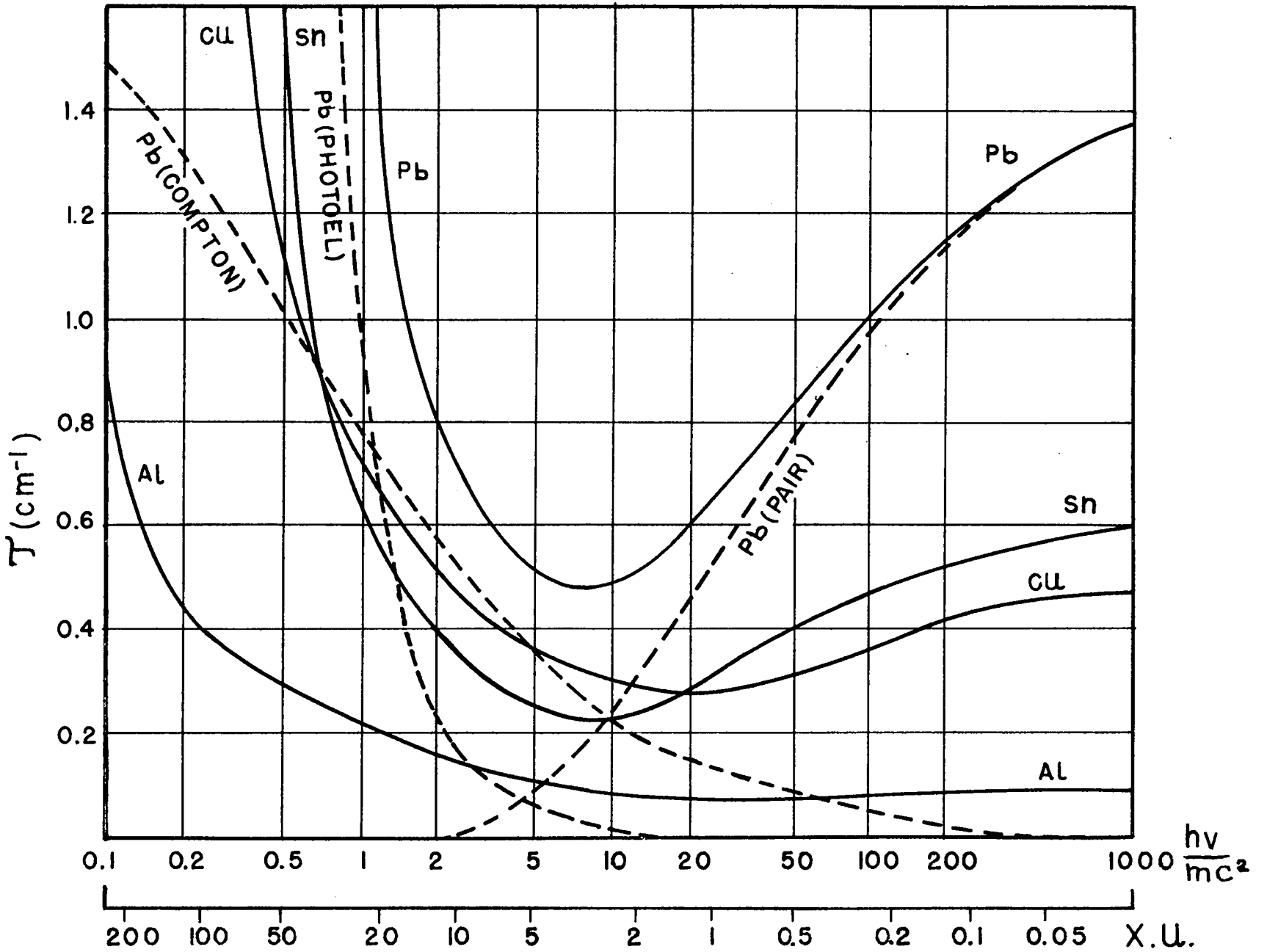

APPROVED FOR PUBLIC RELEASE

Figure 13

Thickness correction for plane foil.

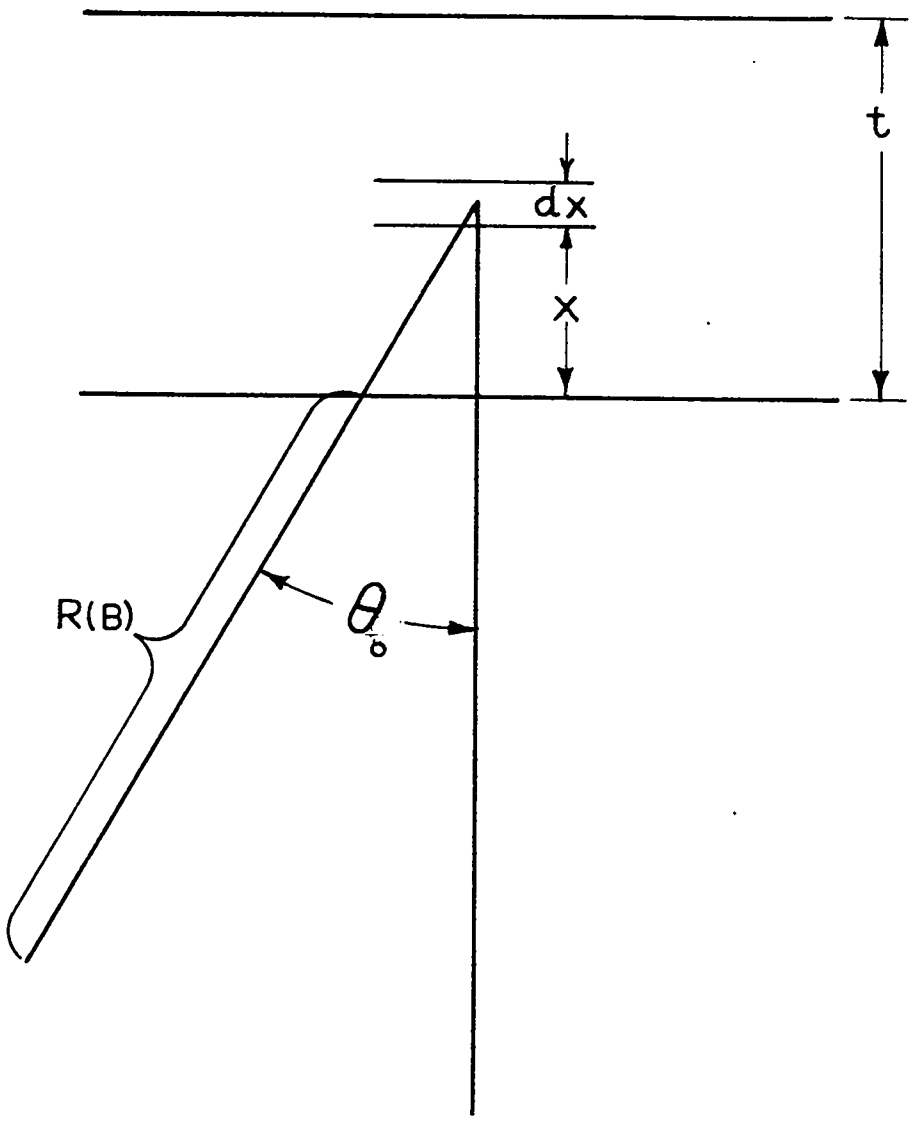
t
dx
x
R(B)
θ
o

and the original range R_o, both measured in the material of the foil. Then,

$$R(B) = R_o - \frac{x}{\cos \theta_o}$$

and the total number of counts is

$$C = 2\pi \int_0^t dx \cdot \int_0^{\theta_o} \sin\theta \, d\theta = 2\pi t \left\{ 1 - \frac{t}{2[R_o - R(B)]} \right\}$$

where $C_o = 4\pi t$,

and $$F(B) = \frac{1}{2} \left\{ 1 - \frac{t}{2[R_o - R(B)]} \right\} \qquad (3)$$

The relation is of course only valid if $x \leq [R_o - R(B)]$. It is also assumed that the pulse size is independent of the direction of the particle. Since θ_o is assumed to be rather large, the effect of electron collection may be neglected if the foil is on the negative electrode.

For low biased boron detectors, the detection efficiency will be the sum of the efficiencies for α-particles and lithium recoils as shown in Chapter 15. For fission detectors, since two fragments are emitted per disintegration, the detection efficiency is twice that given by the formula, as stated in Section 16.1. For reactions giving rise to single particles of uniform energy and for thick layers ($t \geq [R_o - R(B)]$), F is given by

$$F(B) = \frac{R_o - R(B)}{4t} \qquad (4)$$

A.7 RANGE OF LITHIUM RECOILS AND ATOMIC STOPPING POWER OF BORON.

An approximate range energy relation for Li^7 has been constructed from the photometric traces of cloud chamber tracks from $B(n,\alpha)$ disintegrations of Bower, Bratscher, and Gilbert. Within the considerable uncertainty it was found that the same energy range relation holds for Li^7 as for slow α-particles. The atomic stopping power relative to air for very slow α-particles has been estimated by interpolation to be about 0.8.

A.8 DETECTION EFFICIENCY OF CYLINDRICAL DETECTOR WITH RADIATOR

If a foil containing the emitting substance is placed on the inside of the wall of a cylindrical detector of radius b the detection efficiency is reduced because of the particles, emerging with sufficient energy under a large angle with respect to the radius, which leave the counting volume by striking the cylindrical wall surface. If this geometrical effect and the thickness effect (see Section A.6) are both small, the detection efficiency is the product of the efficiencies for each effect separately. This requires, therefore, that $r(B) \ll b$, $r(B)$ being that part of the initial range in the gas of the detector necessary to produce a measurable pulse. For an infinitely thin layer, and under the same assumptions as in Section A.6, the detection efficiency of a cylindrical detector is given by the ratio of the area of that part of the surface of a sphere of radius $r(B)$ (with its center on the cylinder of radius b) which is located inside the cylinder to the total spherical surface, $4\pi r^2(B)$ (see Figure 14).

Let us consider a polar system of coordinates with the origin on the wall of the counter, the polar axis along the radius, and the plane $\varphi = 0$ perpendicular to the axis of the cylinder. The difference f between the surface of the half sphere and its part located inside the cylinder is given by

$$f = \iint r^2 \sin\Theta \, d\Theta \, d\varphi$$

The boundary curve of the surface is given by the equations of the sphere and the cylinder

$$r = r(B)$$

$$r^2 \sin^2\Theta \cos^2\varphi + r^2 \cos^2\Theta - 2 r b \cos\Theta = 0$$

If $\cos\Theta = \mu$, then

$$f = r^2(B) \int_0^{\varphi} d\varphi \int_0^{\mu_1} d\mu$$

Figure 14

Wall correction for cylindrical foil.

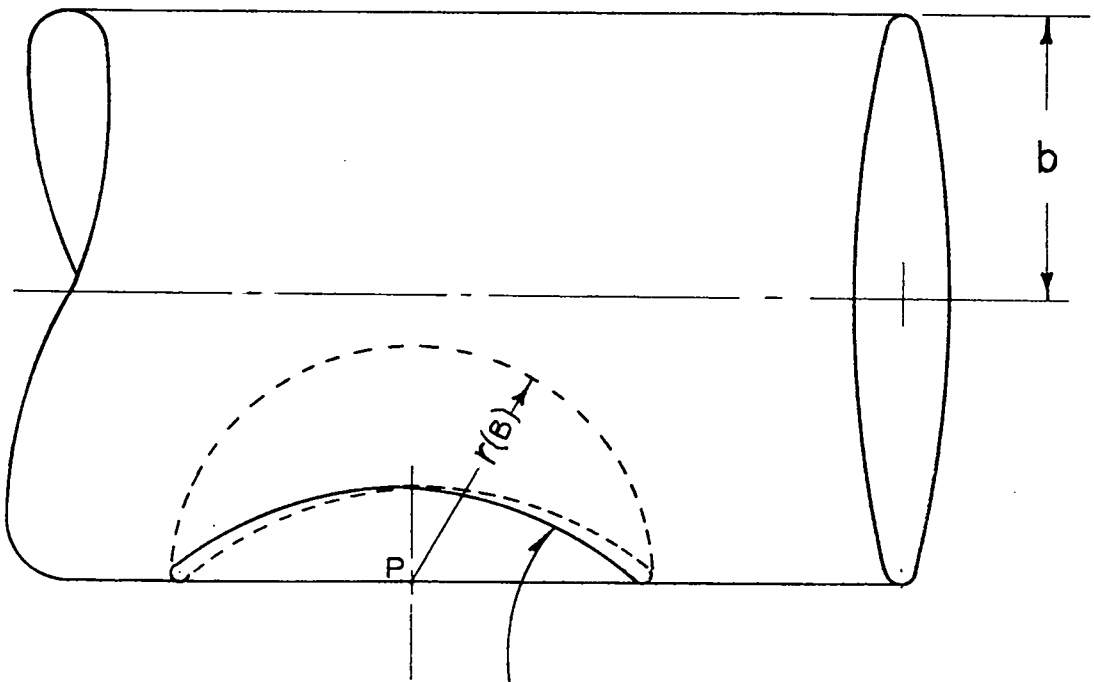

CURVE OF INTERSECTION BETWEEN SPHERE OF RADIUS $r(\beta)$ WITH CYLINDER OF RADIUS b

where μ_1 is given by the equation of the boundary curve

$$\mu_1 = \frac{1 - \sqrt{1 - [(r(B)/b) \sin\varphi \cos\varphi]^2}}{\sin^2\varphi \ (r(B)/b)}$$

Expanding μ_1 and neglecting higher than linear terms in (r(B)/b) we get

$$f = \frac{\pi}{2} \frac{r^3(E)}{b}$$

and

$$F(B) = \frac{1}{2} \left(1 - \frac{r(B)}{b} \right) \qquad (5)$$

The total detection efficiency taking the thickness of the foil into account is therefore

$$F(B)_{total} = \frac{1}{2} \left(1 - \frac{t}{2[R_c - R(B)]} \right) \left(1 - \frac{r(E)}{4b} \right) \qquad (5')$$

In the case of fissions, where two particles are emitted, the total detection efficiency is twice that given by Equation 5'.

A.9 WALL CORRECTION FOR CYLINDRICAL DETECTOR WITH VERY SMALL INNER ELECTRODE IF PARTICLES ORIGINATE IN THE GAS

If the disintegrations take place in the gas filling of a large cylindrical chamber of radius b, some particles will hit the walls before having produced a sufficient ionization to be recorded at the given bias. It shall be assumed that all the disintegration energy goes into one particle, that all particles have the same range R_o measured in the gas and small compared to b, and that they are emitted isotropically.

If cartesian coordinates are introduced (see Figure 15) with the origin at the point P, the z axis on a radius, and the y axis parallel to the axis of the cylinder, for any given direction of emission of the particle, there is a point F at a distance η from the axis C such that the particle loses an energy B equal to the bias energy before striking the wall. For particles being emitted in the direction given by the polar angles ϑ and φ, the detection efficiency is

Figure 15

Wall correction for cylindrical chamber if ionizing particles originate in gas.

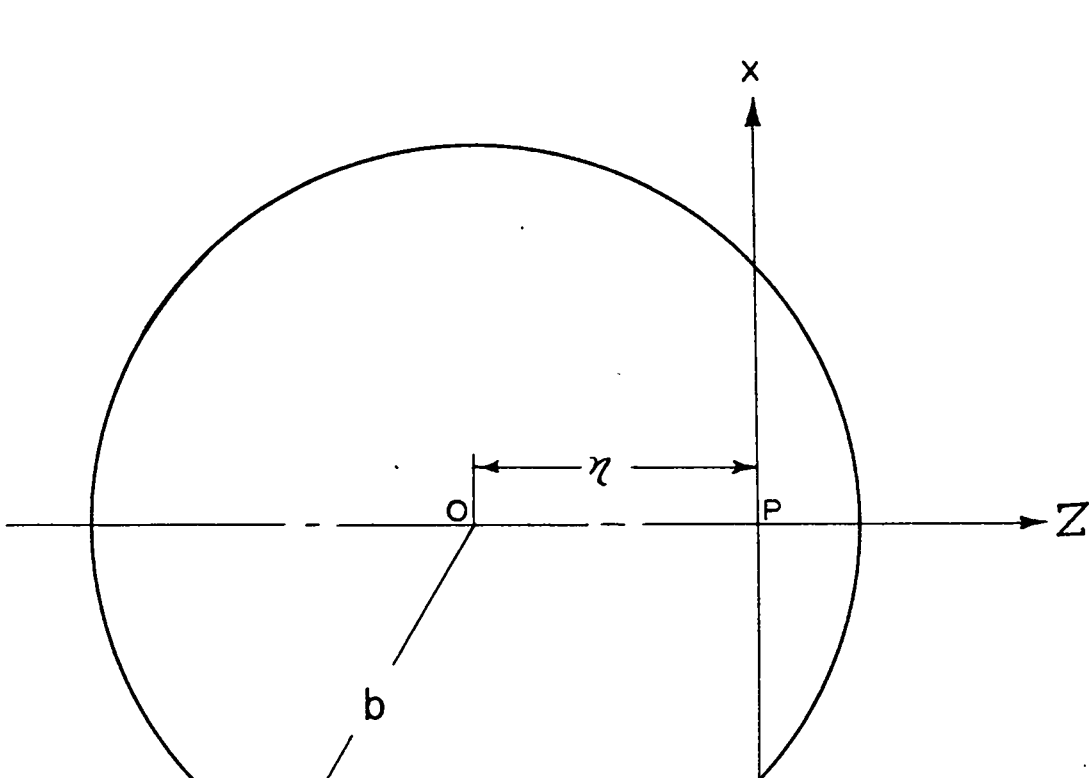

$$dF = \left(\frac{\eta(\vartheta,\varphi)}{b} \right)^2 \frac{\sin\vartheta \, d\vartheta \, d\varphi}{4\pi}$$

The equation of the cylindrical wall is

$$(r\cos\vartheta + \eta)^2 + (r\sin\vartheta\cos\varphi)^2 = b^2 \qquad (6)$$

and $\eta^2 \approx b^2 \left[1 - (2r/b) \cos\vartheta \right]$ if higher terms in (r/b) are neglected. This determines η for every given r, ϑ, and φ. Let r(B) be that portion of the initial range which has to be within the sensitive volume in order to produce a pulse of size equal to the bias energy.

$$r(B) = R_o - R(E_o - B)$$

where R_o is the original range of the particles, E_o the original energy, and B the bias energy.

In order to find the total detection efficiency, the integration has to be extended from 0 to $\vartheta_m(\varphi)$, where $\vartheta_m(\varphi)$ is given by the relation in Equation 6 with $\eta = b$. The integration over φ extends from 0 to 2π. For $\vartheta_m \leq \vartheta \leq \pi$, η remains at its maximum value b. Thus

$$F(B) = \frac{1}{4\pi} \int_0^{2\pi} d\varphi \left\{ \int_0^{\vartheta_m} (\eta^2/b^2) \sin\vartheta \, d\vartheta + \int_{\vartheta_m}^{\pi} \sin\vartheta \, d\vartheta \right\}$$

With $$\cos\vartheta_m = \frac{-b \pm \sqrt{b^2 - [r(B)\sin\varphi\cos\varphi]^2}}{r(B)\sin^2\varphi}$$

$$\approx -\frac{1}{2}\frac{r(B)}{b}\cos^2\varphi$$

Within the above approximation, F becomes

$$F = 1 - \frac{r(B)}{2b} \qquad (7)$$

A.10 RANGE ENERGY RELATION FOR FISSION FRAGMENTS: STOPPING POWER OF VARIOUS MATERIALS FOR FISSION FRAGMENTS.

The mean range of fission fragments in various materials has been computed from the measurements of Bohr, Bøggild, Brostrøm, and Lauritsen, and is shown

in Figure 16. The two curves represent averages for the two groups of fission fragments.

It was found that approximately all materials have the same stopping power for fission fragments as for α-particles of 4.5 Mev. The data for air was taken from the above reference. Values of the mean range of fission fragments and the stopping power of various materials for fission fragments are given in Table A.10-1. The values for the ranges are not considered to be very accurate except for air.

Table A.10-1

Material	Mean Range of Fission Fragments in mg/cm^2.	Atomic Stopping Power
Air	2.70	1.00
Al	3.7	1.51
Collodion	2.6	
Cu	5.2	2.40
Ag	6.1	3.08
Au	11.14	3.96
U	12.6	(4.2)
U_3O_8	10.0	

Figure 16

Range energy relation for fission fragments (Bohr, Bøggild, Brostrøm, and Lauritsen, Phys. Rev., 58, 839, 1940; also Bøggild, Brostrøm, and Lauritsen, Phys. Rev., 59, 275, 1941).

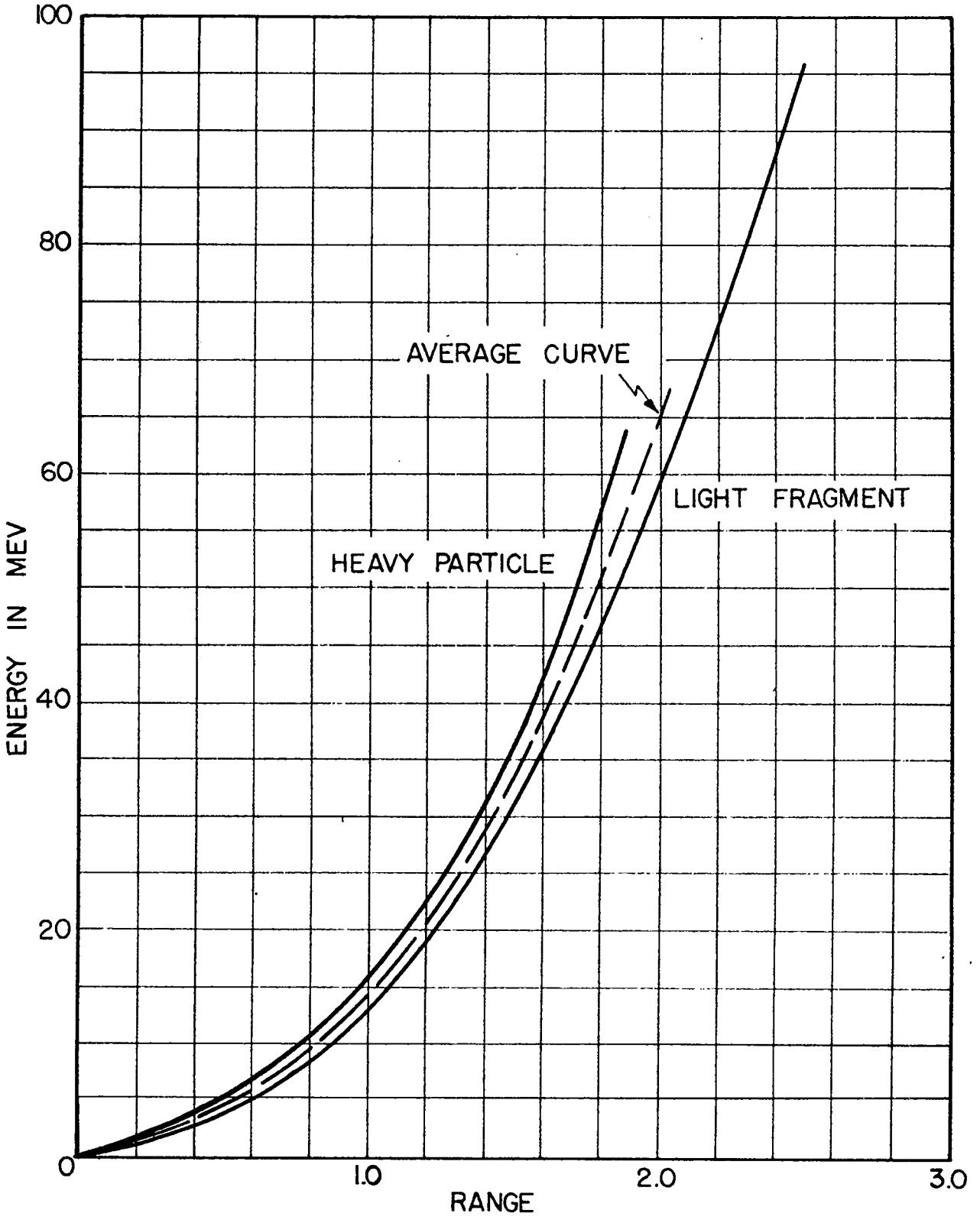

A.12 RESOLUTION AND PILING UP OF PULSES

In the following discussion of the resolution of pulses, two cases will be treated:

In the first case, it is assumed that every pulse which is counted paralyzes the detection equipment for a time τ which is large compared with the duration of the pulse. The dead time τ shall be independent of any other pulse occuring during this time. Such a situation arises, for instance, in the case of a Geiger-Mueller counter or in the cases of a thyratron triggered by a very short pulse. The probability that n-1 additional pulses occur within the time τ after a pulse is given by Poisson's formula

$$P(n-1) = \frac{(\tau n_o)^{n-1}}{(n-1)!} e^{-\tau n_o} \qquad (8)$$

where n_o is the average number of pulses per unit time. The number of counts per unit time containing n pulses is given by

$$C(n) = K \cdot P(n-1)$$

where the constant K is determined by the normalizing condition

$$n_o = \sum_1^\infty K F(n-1)\, n = K \sum F(n-1)\,(n-1+1) = K(\tau n_o + 1)$$

Thus we get for C(n)

$$C(n) = \frac{n_o}{1+\tau n_o} \cdot \frac{(\tau n_o)^{n-1}}{(n-1)!} e^{-\tau n_o} \qquad (9)$$

For the total counting rate (number of counts per unit time, irrespective of how many pulses are contained in a count) we have

$$C_o = \frac{n_o}{1+\tau n_o} \qquad (10)$$

The relative counting loss is

$$L = \frac{n_o - C_o}{n_o} = \frac{\tau n_o}{1+\tau n_o} \qquad (11)$$

A very convenient way of determining τ and therefore the counting loss consists in comparing the counting rates C_{o_1} and C_{o_2} of two sources with pulse rates n_{o_1} and n_{o_2} with the counting rate $C_{o_{12}}$ of the combined source which is given by

$$C_{o_{12}} = \frac{n_{o_1} + n_{o_2}}{1+\tau(n_{o_1}+n_{o_2})} = \frac{C_{o_1} + C_{o_2} - 2\tau C_{o_1} C_{o_2}}{1+\tau^2 C_{o_1} C_{o_2}} \qquad (12)$$

The rate of accidental coincidences G of two recording devices giving pulses of duration τ and having counting rates C_{o_1} and C_{o_2} is given by the equation:

$$G = \sum_2^\infty C_{12}(n) - \sum_2^\infty C_1(n) - \sum_2^\infty C_2(n).$$

For $(C_{o_1} + C_{o_2}) \ll 1$, one obtains, neglecting higher than linear terms:

$$G = 2\tau C_{o_1} \cdot C_{o_2} \qquad (13)$$

As a second case, consider that the dead time is not a constant, independent of subsequent counts falling within τ, but that the recording instrument records a pulse provided that the voltage of the collecting electrode has been at zero for any arbitrary short time preceding the pulse.

Again let n_o be the pulse rate. The probability that a pulse is followed by a "gap" of duration τ, (no further pulse during the time τ) is given by $e^{-\tau n_o}$. Thus the counting rate C_o (number of recorded counts per unit time) is

$$C_o = n_o \, e^{-\tau n_o}$$

The numbers of single, double and n fold counts are, respectively:

$C(1) = n_o \, e^{-2\tau n_o}$ since one requires a gap of at least τ before and after a pulse;

$C(2) = n_o \, e^{-2\tau n_o} (1 - e^{-\tau n_o})$ requiring that the pulse be followed by one other within the time τ; and

$$C(n) = n_o \, e^{-2\tau n_o} (1 - e^{-\tau n_o})^{n-1}$$

For the determination of the resolving time τ we have, using the same notation as before:

$$\tau = \frac{C_{o_1} + C_{o_2} - C_{o_{12}}}{C_{o_{12}}^2 - C_{o_1}^2 - C_{o_2}^2}$$

The piling up of square pulses of uniform height F and equal width τ is discussed below.

A pulse height n·F is produced if n pulses occur within a time τ. The counting rate of counts of height nF is therefore given by the counting rate C(n) given by Equation 9. It should be kept in mind that the height nF exists only during a time smaller than τ. Consequently, many of the multiple pulses are of very short duration. In practical cases, where the pulses usually have an exponential rise and decay, the formula gives approximate values if τ is taken as the resolving time. For an accurate treatment of practical cases, the knowledge of the complete transient response of the detecting equipment is necessary.

A.13 NUMERICAL VALUES OF THE BACK SCATTERING FUNCTION Φ FOR α- PARTICLES

(a) Relative values of Φ for various materials:

Material	$\Phi_{\text{material}} / \Phi_{\text{gold}}$
Au	1.00
Pt	.99
U_3O_8	.894
SiO_2	.19
Al	.23
Be	.10

(b) Values of Φ for gold using α-particles of 3.68 cm range (N.T.P.) at various values of R(B) in air (R(B) = the range of an α-particle whose energy is equal to the bias energy B):

R(B) cm	$\Phi \cdot 10^2$
0	9.7
.1	9.0
.2	8.5
.3	8.0
.4	7.7
.5	7.5

(c) For the variations of Φ with the range R_0 of the α-particles, one can approximately assume that

$$\Phi^2(R_0) = \Phi^2(3.68) \cdot \frac{3.68}{R_0(\text{cm})}$$

or that Φ varies approximately inversely with the square root of the range.

UNCLASSIFIED

UNCLASSIFIED

REC. FROM R.R. Davis

DATE 1-17-47

REC. ✓ F.C.